

Difficulties in Optimization of Imperfect Stiffened Cylindrical Shells

David Bushnell,* Fellow, AIAA, Retired

Charles Rankin, Associate Fellow, AIAA

Rhombus Consultants Group, Inc.

Suite B100, 1121 San Antonio Rd., Palo Alto, CA 94303

ABSTRACT

The PANDA2 computer program generates minimum-weight designs of ring and stringer stiffened flat or cylindrical composite panels subjected to multiple sets of load combinations. PANDA2 is described with emphasis on the many different stress and buckling constraints that can affect the evolution of a design during optimization cycles, on the way that imperfections are treated, on certain difficulties that imperfections may cause during optimization cycles, and on difficulties encountered during attempts to evaluate optimum designs with the use of the STAGS general purpose finite element program. Details are given on how PANDA2 determines the effect of an initial buckling modal imperfection on the load bearing capability of a ring and stringer stiffened cylindrical shell. Numerical results pertain to a metallic cylindrical shell with external T-shaped stringers and external T-shaped rings subjected to combined axial compression, external pressure and in-plane shear (torque). The maximum allowable stress is set very high so that stress constraints do not affect the evolution of the global optimum design in this example. Minimum-weight designs are determined for this shell with an initial imperfection in the form of the critical general buckling mode. Modifications to PANDA2 are described which overcome some of the difficulties associated with the determination of a global optimum design in the presence of an initial general buckling modal imperfection. Further modifications to PANDA2 are described which lead to less conservative global optimum designs than was previously the case. The optimum designs obtained by PANDA2 are evaluated by comparisons with predictions from STAGS for various finite element models generated automatically with a PANDA2 processor called STAGSUNIT. The agreement between PANDA2 and STAGS predictions for a global optimum design obtained by PANDA2 is good enough to qualify PANDA2 for the optimum design of imperfect stiffened cylindrical panels and shells under combined loads.

1.0 INTRODUCTION

The PANDA2 computer program [1-17] generates minimum-weight designs of ring and stringer stiffened flat or cylindrical composite panels subjected to multiple sets of load combinations. An example of such a structure is shown in Figs. 1-3, which are finite element models from STAGS [27-30], not PANDA2 models. Figs. 1-3 represent an externally T-ring and T-stringer stiffened cylindrical shell that has been optimized by PANDA2. Many of the results presented in this paper are derived from the configuration shown in Fig. 1, which is a finite element model of the shell specified in Column 5 of Table 8 in [16] and in Table 2 in this paper.

In this paper PANDA2 is described with emphasis on the many different stress and buckling constraints that can affect the evolution of a design during optimization cycles, on the way that imperfections are treated, on certain difficulties that imperfections may cause during optimization cycles, and on difficulties encountered during attempts to evaluate the optimum design via STAGS finite element models.

The optimizer incorporated into the PANDA2 system is called ADS, created by Vanderplaats and his colleagues many years ago [18-19]. PANDA2 uses much of the software from an earlier version, PANDA [2], and from

* Copyright © 2006 by David Bushnell. Published by the American Institute of Aeronautics and Astronautics, Inc, with permission.

BOSOR4 [20-26]. The PANDA2 system includes processors by means of which input files are automatically generated for the computer programs BOSOR4 (shells of revolution [20-26]) and STAGS (general shells [27-30]) for optimum designs previously obtained by PANDA2. Hence, optimum designs obtained by PANDA2 can easily be evaluated by executions of BOSOR4 and STAGS, especially STAGS [7,8,16]. Figures 1-3 are examples of STAGS finite element models generated by a PANDA2 processor called STAGSUNIT [7]. It is emphasized that these STAGS finite element models are NOT used within the optimization process; they are only used after PANDA2 has already obtained an optimum design.

Local and overall buckling and optimization of stiffened panels can be determined with the PANDA2 [1-17], POSTOP [31], VICONOPT [32], and PASCO [33] computer programs. These four programs are capable of obtaining optimum designs, and PANDA2, POSTOP, and VICONOPT can do so including the effect of local postbuckling of the panel skin and/or parts of the stringers.

Other contributions to the field of buckling and postbuckling of panels include works by Weaver and his colleagues [34-36], Hilburger, et al[37], Baruch and Singer [38], the creators of the STAGS general purpose program, Almroth, Rankin, Brogan, and Riks [27-30], Arbocz and his colleagues [39-41], Stein [42], Leissa [43], Arnold and Parekh [44], Starnes, Knight, and Rouse [45], Spier [46,47], Khot and Bauld [48,49], Zhang and Matthews [50], Gurdal and his colleagues [51-56], Haftka and his colleagues [57,58], Librescu and his colleagues [59-61], Sridharan and his colleagues [62,63], Hyer and his colleagues [64-66], Nemeth, Hilburger, and Starnes and colleagues [67-70], Elishakoff and his colleagues [71-73], Weller and his colleagues [74-77], Chamis and Abumeri [78] and Noor, Starnes, and Peters [79], to identify but a few in a vast literature.

2.0 PURPOSES OF THIS PAPER

The purposes of this paper are:

1. to describe briefly what the PANDA2 system consists of,
2. to identify the many different models used in PANDA2,
3. to identify the many different stress and buckling constraints several of which may effect the evolution of a design during optimization cycles,
4. to identify several "knockdown" factors used in PANDA2, not only for imperfection sensitivity but also to compensate for the inherent unconservativeness of some of the approximate models used by PANDA2 (for example "smearing" stiffeners [38]),
5. to emphasize that initial imperfections in stiffened shells give rise to redistribution of stress between skin and stiffener segments that dramatically affects stress and buckling constraints,
6. to list the ways in which the PANDA2 predictions lead to conservative optimum designs,
7. to describe how the effect of imperfections is handled in PANDA2,
8. to identify some difficulties encountered in connection with the optimization of imperfect shells,
9. to describe certain modifications to PANDA2 that overcome some of these difficulties and that lead to less conservative designs than previous versions,
10. to provide comparisons of PANDA2 predictions with results from BOSOR4 [20-26] and STAGS [27-30] for a shell optimized by PANDA2.

3.0 DESCRIPTION OF PANDA2

PANDA2 is a computer program for the minimum weight design of stiffened, composite, flat or cylindrical, perfect or imperfect panels and shells subjected to multiple sets of combined in-plane loads, normal pressure, and temperature. For most configurations the panels can be locally postbuckled [3,8,9,11,15,80].

3.1 PANDA2 Processors and Types of Analysis

As described in [1] and [16], the PANDA2 system consists of several processors, BEGIN, SETUP, DECIDE, MAINSETUP, PANDAOPT, CHOOSEPLOT, CHANGE, STAGSUNIT, PANEL, PANEL2, etc. The functions of these processors are as follows:

BEGIN - User establishes starting design, material properties, prebuckling and buckling boundary conditions.

SETUP - System sets up BOSOR4-type templates for stiffness and load-geometric matrices.

DECIDE - User chooses decision variables and bounds and sets up equality (linking) and inequality constraints.

MAINSETUP - User chooses analysis type, loading, solution strategies, imperfection amplitudes, factors of safety, etc.

PANDAOPT - Analysis type is performed (e.g. optimization).

CHOOSEPLOT - User chooses what to plot.

DIPLOT - The system obtains plots (postscript files).

CHANGE - User changes selected variables and constants.

AUTOCHANGE - A new starting design is automatically generated in a random manner [5].

SUPEROPT - An attempt is made to find a global optimum design [5,16], Fig. 34.

PANEL - A BOSOR4 input file is generated for inter-ring buckling of panel skin and stringers, with stringers modeled as flexible shell branches, Figs. 6,7.

PANEL2 - A BOSOR4 input file is generated for inter-ring and general buckling of the panel skin with smeared stringers and rings modeled as flexible shell branches [6], Figs. 9, 10, 11.

STAGSMODEL - An input file for STAGS [27-30] is generated (one finite element unit, only stringers are permitted) [8,9].

STAGSUNIT - Input files, *.bin and *.inp, for STAGS are generated (multiple shell units. Both stringers and rings are permitted) [7,16], Figs. 1-3.

CLEANPAN - Delete all files except files containing the user-provided input data for BEGIN, DECIDE, MAINSETUP, CHANGE, PANEL, PANEL2, STAGSMODEL, STAGSUNIT, CHOOSEPLOT.

3.2 PANDA2 can be run in five modes:

1. Optimization (See Fig. 34)
2. Simple analysis of a fixed design
3. Test simulation (monotonically increasing loading on a fixed design) [4,8,9]
4. Design sensitivity (one decision variable increases over a user-provided range while all others are held constant);

See Figs. 24-26)

5. Load-interaction curves (N_x, N_y) or (N_x, N_{xy}) or (N_y, N_{xy}) (Fig. 15 of [7]).

4.0 OVERVIEW OF MODELS USED IN PANDA2

PANDA2 computes stress and buckling loads from several different models as follows:

1. Discretized single-module skin-stringer (Figs.20,22 of [1]) and Figs. 4 and 5 here: The cross section of a stringer and panel skin of width equal to the stringer spacing is discretized as shown in Figs. 4 and 5. Variation of unknowns u, v, w in the axial direction is trigonometric with m axial halfwaves. This one-dimensional discretization is analogous to that used in BOSOR4 [20,22] for shells of revolution.

- (a) This model is for the axial length of shell between rings.
- (b) This model can be used for local postbuckling analysis as shown in Figs. 23 of [1] and Fig. 10 of [11] and in [8,9]. The local postbuckling theory [3] is an extension of that of Koiter described in [80].
- (c) Buckling load factors can be checked by a BOSOR4 model [20-26] generated by the PANDA2 processor called PANEL. (See Items 112c,d, 270, 319 in [17] and Fig. 21 in [1]. See Figs. 6 and 7 here.)

2. Discretized single-module "skin"-ring (Fig.30 of [6] and Figs. 8 and 9 here): The cross section of a ring and panel skin with "smeared" stringers [38] of axial length equal to the ring spacing is discretized. Variation of unknowns u, v, w , in the circumferential direction is trigonometric with n circumferential halfwaves. This one-dimensional discretization is the same as that used in BOSOR4 [20,22] for shells of revolution.

- (a) This model involves discretized skin-with-smeared-stringers combined with a discretized ring cross section.
- (b) Buckling load factors can be checked by a BOSOR4 model [20-26] generated by the PANDA2 processor called PANEL2. (See Item 463 in [17] and Fig.33 of [6]. See Figs. 10 and 11 here.)
- (c) This model is used to determine a knockdown factor that compensates for the inherent unconservativeness of models with "smeared" rings. See Items 509, 511, 522, 532, 605 in ...panda2/doc/panda2.news [17] and Item no. 6 in Section 9.0 and Fig. 8 here.

3. PANDA-type closed form buckling formulas [2] for shell skin and segments of stringers and segments of rings:

- (a) This model involves an elaborate search over (m, n, s) space, in which m = number of axial halfwaves, n = number of circumferential halfwaves and s =slope of the buckling nodal lines (assumed straight [48,49]. See Items 415 and 443 in [17].)
- (b) Donnell theory or Sanders theory [5, Item 410 in 17] or Marlowe theory [Item 411 in 17] can be selected by the user.
- (c) This model is used to compute knockdown factors for stiffened or unstiffened cylindrical panels and shells with local, inter-ring, and general buckling modal imperfection shapes with user-specified amplitudes [4].
- (d) This model is used to get a knockdown factor to compensate for the fact that the in-plane shear load N_{xy} and shell wall anisotropy equals zero in all BOSOR4-type (discretized) models.
- (e) This model is used for buckling of stiffener segments such as shown in Figs. 5 and 6 of [2].
- (f) This model is used for the buckling of sandwich wall face sheets attached to an elastic foundation that represents the core of the sandwich wall [10].
- (g) This model is used for many of the buckling modes that exist in panels with major stiffeners and substiffeners

between the major stiffeners [16].

4. Sandwich wall failure modes unique to sandwich walls [10]:

- (a) face sheet wrinkling
- (b) face sheet dimpling
- (c) core crimping
- (d) stiffener-web-bending-induced face sheet pull-off
- (e) stiffener-web-bending-induced core crushing
- (f) amplification-of-initial-face-sheet-waviness-induced face sheet pull-off
- (g) amplification-of-initial-face-sheet-waviness-induced core crushing
- (h) hexagonal core face sheet pull-off
- (i) transverse shear core failure
- (j) core tension failure.

5. Models involving solution by double trigonometric series expansions [6]:

- (a) local buckling between adjacent major stiffeners
- (b) general buckling of a "patch" involving N x M major stiffener bays
- (c) inter-ring buckling of a "patch" involving N major stringer bays
- (d) local, "general", and inter-subring models in shells with substringers and subrings between major stiffeners. The "general" buckling domain is a "patch" involving N x M substiffener bays lying between adjacent major stringers and major rings [16].

6. Optimum designs obtained by PANDA2 may be checked by running a general-purpose finite element program. The PANDA2 processor called STAGSUNIT [7] generates input files, <casename>.inp and <casename>.bin for STAGS [27-30]. STAGSUNIT [7] generates valid STAGS input files for any subdomain of a shell or panel, as seen in Refs. [7, 16] and in Figs. 1-3 and Figs. 12 - 19 here.

5.0 STRESS MARGINS

PANDA2 computes the following types of margins relating to stress constraints:

----- typical margin names -----
eff.stress:matl=1,STR,Dseg=5,node=11,layer=1,z=.281; MID.;FS=1
eff.stress:matl=1,RNG,Iseg=3,at:TIP,layer=1,z=0.363;-MID.;FS=1
fibertensn:matl=1,STR,Dseg=4,node=6,layer=1,z=-0.11; ENDS;FS=1
fibercompr:matl=1,SKN,Dseg=2,node=6,layer=2,z=0.11; ENDS;FS=1
transtensn:matl=1,SKN,Dseg=2,node=6,layer=1,z=-0.11; ENDS;FS=1
transcompr:matl=1,SKN,Dseg=2,node=6,layer=2,z=0.11; ENDS;FS=1
inplnshear:matl=1,STR,Dseg=3,node=1,layer=1,z=0.083; ENDS;FS=1
fibertensn:matl=1,STR,Iseg=4,allnode,layer=1,z=-.11;-ENDS;FS=1
fibercompr:matl=1,SKN,Iseg=1,at:n=11,layer=2,z=0.11;-ENDS;FS=1
transtensn:matl=1,SKN,Iseg=2,at:n=11,layer=1,z=-.11;-ENDS;FS=1
transcompr:matl=1,STR,Iseg=4,allnode,layer=1,z=0.11;-ENDS;FS=1
inplnshear:matl=1,STR,Iseg=3,at:TIP,layer=1,z=0.0;-ENDS;FS=1

in which the following definitions apply:

"STR" = "stringer"; "RNG" = "ring"; "SKN" = "skin";
"MID" = midway between rings (midbay); "ENDS" = "at rings"
"TIP" = at the tip of a stiffener web
"Dseg" = segment numbering for discretized single module model
"Iseg" = segment numbering from "BEGIN" (See *.BEG file)

"z" = distance from reference surface (thickness coordinate)
 "node" = nodal point in discretized single module model
 "allnode" = "at all nodes" [IQUICK=1 (non-discretized) model]
 "layer" = layer number in the segment wall
 "FS" = factor of safety
 "eff.stress" = von Mises effective stress
 "fibertensn" = tensile stress in the direction of the fibers
 "fibercompr" = compressive stress along the fibers
 "transtensn" = tension stress normal to the fibers
 "transcompr" = compressive stress normal to the fibers
 "inplnshear" = in-plane shear stress

Stresses in the category denoted "Iseg" (non-discretized model) are computed in SUBROUTINE STRCON for both positive and negative amplitudes of a buckling modal imperfection. Stresses in the category denoted "Dseg" (discretized model) are computed in SUBROUTINE STRTHK and include the effect of local postbuckling of the panel skin between adjacent stringers. See Figs. 12-14 in [11] and [8,9].

6.0 REDISTRIBUTION OF STRESS BETWEEN SKIN AND STIFFENERS CAUSED BY PREBUCKLING BENDING OF AN IMPERFECT SHELL

In computing the various stress constraints, PANDA2 includes the effect of redistribution of stress resultants between panel skin and stiffener segments caused by bending of an initially imperfect shell subjected to its design load. For example, in the optimized imperfect stiffened cylindrical shell identified in Tables 1 and 2, this prebuckling bending gives rise to additional compressive stress resultants as follows (units are lb/in in this paper):

Additional resultants (Nx,Ny) in the panel skin from global and inter-ring bending of an imperfect panel:

Additional axial resultant, dNx = -1.4357E+03
 Additional hoop resultant, dNy = -2.3231E+04
 Additional in-plane shear resultant, dNxy= 0.0000E+00

Additional axial resultants dNx along the webs and flanges of stringers from global and inter-ring bending of an imperfect panel:

Additional Nx in base of stringer, dNx = -1.4357E+03
 Additional Nx at webtip of stringer, dNx = -2.5133E+03
 Additional Nx in flange of stringer, dNx = -1.8180E+03

Additional axial resultants dNx along the webs and flanges of rings from global and inter-ring bending of an imperfect panel:

Additional Nx in base of ring, dNx = -2.5529E+04
 Additional Nx at webtip of ring, dNx = -9.7624E+04
 Additional Nx in flange of ring, dNx = -6.4280E+04

7.0 BUCKLING MARGINS FROM VARIOUS MODELS

7.1 Buckling margins from discretized single module skin-stringer model

This model is used only for inter-ring buckling phenomena. The types of buckling margins obtained with this model are as follows:

----- typical margin names -----
 Local buckling from discrete model-1.,M=5 axial halfwaves;FS=1
 long-wave local buckling, discrete model(m=1 axial halfwav);FS
 Local buckling from Koiter theory,M=5 axial halfwaves;FS=1.0
 Bending-torsion buckling; M=1 ;FS=1.0

$(m=1 \text{ lateral-torsional buckling load factor})/(FS)-1; FS=1.0$
 local wide-column bucking, discrete model($m=1$ axial halfwave)
 stringer popoff margin:(allowable/actual)-1, web 1 MID.;FS=1.
 stringer popoff margin:(allowable/actual)-1, web 2 MID.;FS=1.
 Wide column panel buckling load factor)/(F.S.) - 1; FS=1.0
 Funny hat buckling load factor)/(F.S.) -1; FS=1.0
 $-.05 + (\text{eig}(\text{high}-\text{axial}-m) - \text{eig}(\text{low}-\text{axial}-m)) / \text{eig}(\text{high}-m); FS=1.0$

Typical local buckling modes are shown in Fig.22a of [1] and Figs. 4 and 5 here. A typical wide column panel buckling mode is shown in [1], Fig. 22c. Stringer popoff is explained in the discussion associated with Figs. 6 and 7 of [1]. Bending-torsion buckling and lateral-torsional buckling modes are modes in which the tip of the stringer deforms more than the panel skin midway between adjacent stringers, such as in Fig. 4. The "Funny hat" buckling mode applies only to hat-stiffened panels and is discussed in Item 123(u) of [17]; See Fig. 21(b) in [1]. The last margin listed above attempts to keep buckling modes with high numbers of axial halfwaves m non-critical compared to those with low numbers of axial halfwaves.

In computing the various buckling load factors, PANDA2 includes the effect of redistribution of stress resultants between panel skin and stiffener segments caused by bending of an initially imperfect shell subjected to its design load. For example, see the listing for dN_x , dN_y , dN_{xy} in panel skin and stringer segments and ring segments given in the short Section 6.0.

7.2 Buckling margins from discretized single module "skin"-ring model

This model is used only for ring-stiffened cylindrical shells and panels. The model is analogous to the discretized single module skin-stringer model just described. "Skin" is in quotes because it consists of the actual skin of the cylindrical shell plus smeared stringers [38]. The ring cross section is discretized (branched shell model), with the plane of the ring web lying in the horizontal plane of symmetry of the entire discretized "skin"-ring module. Examples of this model and typical buckling modes are shown in Fig. 30 of [6] and Figs. 8 and 9 here. Margins from this model are of the following types:

----- typical margin names -----

Inter-ring buckng, discrete model, $n=37$ circ.halfwaves;FS=1.0
 Ring sidesway buk., discrete model, $n=4$ circ.halfwaves;FS=1.0
 Ring web buckling, discrete model, $n=??$ circ.halfwaves;FS=1.0
 Ring flange buckling,discrete model, $n=54$ circ.halfwaves;FS=1.0
 Hi-n Inter-ring buc.,discrete model, $n=??$ circ.halfwaves;FS=1.0
 Hi-n Ring sidesway, discrete model, $n=??$ circ.halfwaves;FS=1.0
 Hi-n Ring web buckl.,discrete model, $n=27$ circ.halfwaves;FS=1.0
 Hi-n Ring flang buckl.discret model, $n=67$ circ.halfwaves;FS=1.0
 Lo-n Inter-ring buc.,discrete model, $n=??$ circ.halfwaves;FS=1.0
 Lo-n Ring sidesway, discrete model, $n=7$ circ.halfwaves;FS=1.0
 Lo-n Ring web buck., discrete model, $n=??$ circ.halfwaves;FS=1.0
 Lo-n Ring flng buck.,discrete model, $n=??$ circ.halfwaves;FS=1.0

In computing the various buckling load factors, PANDA2 includes the effect of redistribution of stress resultants between panel skin and stiffener segments caused by bending of an initially imperfect shell subjected to its design load. For example, see the listing for dN_x , dN_y , dN_{xy} in panel skin and stringer segments and ring segments given in the short Section 6.0.

7.3 Buckling margins computed from many non-discretized models

Buckling load factors are computed from PANDA-type theory [2] and possibly also from the "alternative" buckling

theory where the buckling mode is expanded in a double-trigonometric series as described in [6]. Stiffener rolling, referred to below, is shown in Fig.6 (a-c) on p. 546 of [2]. If the panel is of sandwich wall construction, then [10] applies. If the panel has both stiffeners and substiffeners, then [16] applies. A very large eigenvalue, such as 1.E+17, indicates that buckling does not occur because the loading is tensile and there is no in-plane shear (positive N_x , N_y ; $N_{xy} = 0.0$).

If the panel is stiffened by both rings and stringers, then the following computations are performed:

1. Local buckling of the panel skin between adjacent stringers and rings:
 - (a) with the use of PANDA-type (closed form) theory [2]
 - (b) with the use of double-trigonometric series expansions [6] over a "patch" which spans the stringer spacing and is equal to or shorter than the ring spacing. The axial length of the "patch" is determined by iteration until a minimum buckling load factor is found.
2. Inter-ring buckling of panel skin with smeared stringers between adjacent rings:
 - (a) with the use of PANDA-type (closed form) theory [2] (stringers smeared; rings replaced by simple support)
 - (b) with the use of PANDA-type theory for a panel of the same geometry except that it is flat (huge radius R)
 - (c) with the use of double-trigonometric series expansions [6] over a "patch" that spans the ring spacing and that includes up to 6 stringer spacings with discrete stringers.

NOTE: Results from 2(a,b) may be superseded by results from a discretized module model in which there is one ring attached to a length of cylindrical skin-with-smeared-stringers equal to the ring spacing, with symmetry boundary conditions applied to the top and bottom of the cylindrical part of the model. See Fig. 30 of Ref.[6] and Fig. 9 here. If 2(a,b) have been superseded, a message such as the following will appear in the output file called *.OPM in which "*" signifies the user-supplied name of the case:

"Simple-support inter-ring buckling with smeared stringers is not recorded as a margin because this type of buckling has been superseded by the results from the discretized inter-ring module model, for which inter-ring buckling load factors have been computed in the range from $n = 1$ to $n = 118$ circumferential halfwaves. The critical simple-support inter-ring buckling model has 34 circumferential half waves, which lies within this range."

3. General buckling of panel skin with smeared stringers and smeared rings [38]:
 - (a) with the use of PANDA-type (closed form) theory [2] (stringers and rings both smeared)
 - (b) with the use of double-trigonometric series expansions [6] over a "patch" that may include up to six stringer spacings (seven stringers) and up to five ring spacings (six rings) with discrete stringers and discrete rings.
4. Inter-ring buckling with ring rolling, smeared stringers; PANDA-type theory [2] only.(May be superseded as with 2a,b)
5. Buckling between stringers with smeared rings including stringer rolling; PANDA-type theory [2] only.
6. Low-axial-wave stringer rolling without skin participation; PANDA-type theory [2] only.
7. High-axial-wave stringer rolling without skin participation; PANDA-type theory [2] only.
8. Low-circumferential-wave ring rolling without skin participation; PANDA-type theory [2]. (May be superseded as with 2a,b).
9. High-circumferential-wave ring rolling without skin participation. (May be superseded as with 2a,b).
10. Axisymmetric rolling of ring without participation of skin.
11. Stringer web buckling from PANDA-type theory [2] only.
12. Ring web buckling from PANDA-type theory [2] only.

13. For hat or truss-core stiffened configurations:
 - (a) hat base or truss core lower skin buckling
 - (b) hat crown or truss core upper skin buckling

7.4 Special cases

Special behavioral constraints are computed for sandwich wall construction if applicable [10]. For each panel module segment:

1. Local buckling of sandwich segment (from VINSON [82])
2. For both upper and lower face sheets of sandwich wall [10]:
 - (a) Face sheet wrinkling from BUSHNELL theory (PANDA-type with the sandwich core represented by an elastic foundation [10])
 - (b) Face sheet wrinkling from VINSON theory [83]
 - (c) Face sheet wrinkling from HOFF theory [84]
 - (d) Face sheet dimpling (local buckling of face sheet with wavelength equal to honeycomb cell diameter).
3. Failure modes that involve the sandwich core and interaction of the core with face sheets [10]:
 - (a) Core crimping (from VINSON [85])
 - (b) Stringer-web-bending-induced face sheet pull-off
 - (c) Stringer-web-bending-induced core crushing
 - (d) Ring-web-bending-induced face sheet pull-off
 - (e) Ring-web-bending-induced core crushing
 - (f) Amplification-of-initial-face-sheet-waviness induced face sheet pull-off
 - (g) Amplification-of-initial-face-sheet-waviness induced core crushing
 - (h) hexagonal-core face sheet pull-off, if applicable
 - (i) Length-direction (x-z) transverse shear core failure
 - (j) Width-direction (y-z) transverse shear core failure
 - (k) core tension failure.

7.5 Buckling modes involving substiffeners [16], if applicable:

1. For isogrid substiffening: buckling of triangular piece of subskin between adjacent substiffeners including rolling of the subisogrid members along the three edges [12, 16].
2. Buckling of subring as wide column with linearly varying width-wise web compression from subring tip to subring root.
3. Local subskin buckling between adjacent substiffeners including substiffener rolling along the 4 edges of the domain (PANDA-type theory [2]). This calculation is analogous to that for local buckling; see 1(a) in Subsection 7.3.
4. Buckling of substringer simply supported along root, no participation of the panel skin (ENDBUK-like coding, Item 600 in [17]).
5. Buckling of subring simply supported along root, no participation of the panel skin (ENDBUK-like coding).
6. Buckling of "patch" with use of double-trigonometric series expansion [6] over domain including up to 6 substringer spacings and 5 subring spacings with discrete substringers and discrete subrings. (The margin contains the string "altsoln4"). This calculation is analogous to the model 3(b) for general instability listed in Subsection 7.3.
7. Buckling of "patch" with use of double-trigonometric series expansion [6] over domain between adjacent substringers and subrings, with rolling of substiffeners included along the four edges. (The margin contains the

string "altsoln5"). This calculation is analogous to the model 1(b) for local buckling listed in Subsection 7.3.

8. Buckling between subrings with smeared substringers, subring rolling included. This calculation is analogous to the models 2(a) and 4 for inter-ring buckling [2] listed in Subsection 7.3.

9. Buckling of "patch" with use of double-trigonometric series expansion [6] over domain between adjacent subrings, with rolling of subrings included. The domain includes up to six substringer spacings and the substringers are discrete. (The margin contains the string "altsol6"). This calculation is analogous to the model 2(c) for inter-ring buckling listed in Subsection 7.3.

10. Buckling between substringers with smeared subrings from PANDA-type theory [2]. Substringer rolling is included. This calculation is analogous to model 5 listed in Subsection 7.3.

11. Models involving rolling of substringers and subrings without participation of the panel skin [2]:

- (a) low-m rolling of substringer
- (b) high-m rolling of substringer
- (c) low-m rolling of subring
- (d) high-m rolling of subring
- (e) axisymmetric rolling of subring.

Models 11(a)-(e) are analogous to Models 6 - 10 listed in Subsection 7.3 for stringer and ring rolling [2].

7.6 Buckling margins generated from non-discretized models of shell

Buckling load factors corresponding to buckling margins of the following types are computed for non-discretized models by PANDA2:

----- typical margin names -----
buck.(SAND);simp-support local buck.; M=1;N=1;slope=0.09;FS=1.
buck.(SAND);simp-support smear rings; M=272;N=1;slope=0.;FS=1.
buck.(SAND);simp-support general buck;M=1;N=3;slope=3.4427;FS=
buck.(SAND);rolling with local buck.; M=1;N=1;slope=6.57;FS=1.
buck.(SAND);rolling with smear rings;M=110;N=1;slope=0.01;FS=1
buck.(SAND);rolling only of stringers;M=12;N=0;slope=0.;FS=1.6
buck.(SAND);hiwave roll. of stringers;M=92;N=0;slope=0.;FS=1.2
buck.(SAND); STRINGERS: web buckling;M=7;N=1;slope=0.;FS=1.0
buck.(SAND); RINGS: web buckling;M=1;N=1;slope=0.186;FS=1

in which "SAND" = "Sanders shell theory", (M,N,slope)=buckling mode (axial halfwaves, circumferential halfwaves, slope of nodal lines) and "FS" = "factor of safety".

If the user seeks additional buckling solutions [6], the following additional buckling margins are computed:

----- typical margin names -----
buck.(SAND);simp-support local buck.; (0.95*altsol);FS=0.999
buck.(SAND);simp-support inter-ring; (1.00*altsol);FS=0.999
buck.(SAND);simp-support general buck;(0.85*altsol);FS=0.999

in which the string "altsol" indicates that the margins were computed with use of double trigonometric series expansions [6].

In the presence of substiffeners [16] SUBROUTINE BUCPAN computes the following additional buckling margins:

----- typical margin names -----
buck.(SAND);rolling with skin buckl.;M=1;N=1;slope=0.175;FS=1.
buckling:simp-support of substring.M=1;FS=1.
buckling:simp-support of subrings N=1;FS=1.
buckling:simp-support altsoln4 intermajorpatch; FS=0.999
buckling:simp-support altsoln5 skin+edgsubroll; FS=0.999
buck.(SAND);rolling with smear substr;M=1;N=1;slope=14.3;FS=1.
buckling:simp-support altsoln6 inter-subring ; FS=0.999
buck.(SAND);rolling with smear subrng;M=43;N=1;slope=0.02;FS=1
buck.(SAND);rolling only of substring;M=29;N=0;slope=0.;FS=1.6
buck.(SAND);hiwave roll. of substring;M=31;N=0;slope=0.;FS=1.6
buck.(SAND);rolling only of subrings; M=0;N=3;slope=0.;FS=1.6
Local subtriangular skin buckling load factor – 1; FS = 0.999

If one or more of the panel module segments is of sandwich wall construction [10], SUBROUTINE GENSTB in PANDA2 computes the following additional margins (also see above for yet more behavioral constraints relating to sandwich walls):

----- typical margin names -----
localbuck (VINSON);strng Iseg1 ;MID; local buck.; M=5;FS=1.1
Face1 wavelength/celldiam;STR;Iseg=1 ;Matl=2 ;MIDLNGTH;FS=1.
Core crushing margin;STR;Iseg=1 ;Matl 2 ;MIDLNGTH;FS=1.
Length-direction sandwich core shear;STR;Iseg=1 ;Matl 2 ;MIDLNGTH;FS=1.
Width-direction sandwich core shear;STR;Iseg=1 ;Matl 2 ;MIDLNGTH;FS=1.

If the stiffeners form an isogrid pattern (ISOGRID=1)[12], then there are additional margins pertaining to buckling of the isogrid members and the triangular piece of skin between them:

----- typical margin names -----
buck.(SAND);rolling only of isogrid3 ;M=1;N=0;slope=0.;FS=1.6
buck.(SAND);hiwave roll. of isogrid3 ;M=5;N=0;slope=0.;FS=1.2
buck.(SAND); ISOGRID : web buckling;M=4;N=1;slope=0.;FS=1.0
Local triangular skin buckling load factor – 1; FS = 1.1

in which "isogrid3" means "the 3rd set of isogrid members". (There are three sets of equally spaced isogrid members, the three sets forming equilateral triangles).

If the panel is a truss-core sandwich, Ref.[5], Fig.9, there are additional margins, as follows:

----- typical margin names -----
buck.(DONL); STRINGERS:lower skin; M=69;N=1;slope=0.723;FS=1.0
buck.(DONL); STRINGERS:webbuckling;M=35;N=1;slope=-0.356;FS=1.
buck.(DONL); STRINGERS:upper skin; M=19;N=1;slope=0.2281;FS=1.
0.45*(Stringer spacing, b)/(Stringer base width, b2) - 1;FS=1.
(Str. base width, b2)/(0.2*(Str. spacing, b)) - 1; FS=1.0

in which "DONL" means "Donnell shell theory" and "webbuckling" indicates the most critical truss core web.

If the panel is hat-stiffened, as in Figs.19,20 in [1], there are additional margins, as follows:

----- typical margin names -----
buck.(DONL); STRINGERS: under hat; M=18;N=1;slope=0.01;FS=1.0
buck.(DONL); STRINGERS: crown of hat;M=23;N=1;slope=0.;FS=1.0

7.7 Buckling margins from non-discretized models of stiffeners

Buckling load factors are computed for the various segments of the stringers and rings. In the subroutine that computes the buckling loads there is a double loop: outer loop over $K = 1,2$ (1=stringers; 2=rings); inner loop over $I = I\text{START}, I\text{END}$, the segment number within the stiffener. The buckling modes are of the type shown in Fig. 5 in [2]. Examples of corresponding buckling margins are:

----- typical margin names -----
buckling margin stringer Iseg.3. Local halfwaves=7. MID.;FS=1.
buckling margin stringer Iseg.4. Local halfwaves=7. MID.;FS=1.
buckling stringer Isegs.3+4 together.M=7 ;C=0.; MID.;FS=1.4
buckling stringer Iseg 4 as beam on foundation.M=221;MID.;FS=3
buckling margin ring Iseg.3. Local halfwaves=1. MID.;FS=1.
buckling ring Iseg 4 as beam on foundation.M=114;MID.;FS=3

in which "Iseg" is the stiffener segment number used in the prompts to the user during the interactive BEGIN execution, "MID" means "midway between rings" and "FS" = "factor of safety".

In computing the various buckling load factors, PANDA2 includes the effect of redistribution of stress resultants between panel skin and stiffener segments caused by bending of an initially imperfect shell subjected to its design load. For example, see the listing for dN_x , dN_y , dN_{xy} in panel skin and stringer segments and ring segments given in the short Section 6.0.

The various stiffener buckling margins just listed are computed as follows:

- (a) buckling of "interior" stiffener segments (stiffener segments attached to other structure along both long edges): computed in SUBROUTINE WEBBUK, called by SUBROUTINE CRIPPL. Linear variation of axial compression from web root to web tip is accounted for. See Items 120d and 121 in [17].
- (b) buckling of "end" stiffener segments (stiffener segments attached to other structure along only one long edge): computed in SUBROUTINE ENDBUK, called by SUBROUTINE CRIPPL. See Item 121 in [17].
- (c) buckling of web and outstanding flange together ("Isegs.3+4 together"): computed in SUBROUTINE CRIPP2. The axial load in the stiffener web in this calculation is the average of that at the web root and that at the web tip. See Items 30 and 516 in [17].
- (d) buckling of outstanding flange as beam on an elastic foundation. The elastic foundation is the web. Computed in SUBROUTINE CRIPP3. (See Item 383 in [17]).

In addition, for truss-core sandwich walls the wide column width-wise buckling of segments of the truss core and face sheets are computed. In the case of isogrid stiffening, the rolling of isogrid members assumed to be hinged along their roots is computed in SUBROUTINE EIGISO. (See [12] and Item no. 122 in [17].

If the stiffeners form an isogrid pattern [12] there exist stiffener buckling margins of the following type:

----- typical margin names -----
buckling margin isogr1 web. Local halfwaves=4 .MID.;FS=1.0
buckling margin isogr2 web. Local halfwaves=4 .MID.;FS=1.0
buckling margin isogr3 web. Local halfwaves=4 .MID.;FS=1.0
buckling margin isogr3 flange. Local halfwaves=3.MID.;FS=1.0
buckling isogr3 Isegs.3+4 together.M=4 ;C=0.; MID.;FS=1.4
buckling isogr3 stiff.no.J=3 ;panel MID.;M=1 ;FS=1.2

in which "isogr1", "isogr2", "isogr3" mean "isogrid members1, 2, 3, respectively. (There are three sets of equally spaced isogrid stiffeners that form equilateral triangles).

If the panel is truss-core sandwich, as in Fig.9 of [5], there are additional margins, as follows:

----- typical margin names -----
buckling marg. stringer Iseg.(width-wise wide col.)MID.;FS=1.0
buckling marg. stringer Iseg.(width-wise wide col.)MID.;FS=1.0
buckling marg. stringer Iseg.(width-wise wide col.)NOPO;FS=1.0
buckling marg. stringer Iseg.(width-wise wide col.)NOPO;FS=1.0

in which Iseg = segment numbering as in "BEGIN"; "MID." = "midway between rings" (midbay); "NOPO" = "no postbuckling".

8.0 TYPES OF "KNOCKDOWN" USED IN PANDA2

The local, inter-ring, and general buckling load factors are knocked down to account for the following:

- (a) Imperfection sensitivity
- (b) Inherent unconservativeness of smearing stringers (if there are smeared stringers in the model)
- (c) Inherent unconservativeness of smearing rings (if there are smeared rings in the model)
- (d) Transverse shear deformation (t.s.d.) effects
- (e) Ratio of buckling loads from ARBOCZ/PANDA2 theories, if that ratio is less than 1.0. (See Item No. 14 in Section 9.0 for an explanation of ARBOCZ/PANDA2 theories).

9.0 CONSERVATIVENESS OF PANDA2 ANALYSES

Designs generated by PANDA2 tend to be conservative because:

1. In several instances there is more than one model of a particular phenomenon. {Example: general buckling from PANDA-type (closed form) theory [2] and general buckling from double trigonometric series expansion [6].} PANDA2 retains the margins from both models so that the design that evolves during optimization cycles will be feasible with respect to both models.
2. For imperfect shells the imperfection sensitivity knockdown factors generated from the PANDA-type theory [4] are applied to the double-trigonometric series "patch" models [6] even if the "patch" models yield buckling modes that do not resemble the corresponding buckling modes (local, inter-ring, general) from PANDA-type (closed form) theory.
3. Knockdown factors are applied to the double-trigonometric series expansion models [6] to compensate for possible truncation error. For example, in the case of the general buckling "patch" model, a rather conservative knockdown factor 0.85 is applied to the buckling load factor (in addition to the knockdown factor for imperfection sensitivity) in order to compensate for truncation of the double trigonometric series expansions.
4. For imperfect cylindrical panels and shells subjected to pure axial compression or predominantly axial compression, [specifically: $\text{SQRT}(N_x^2 + N_y^2)/\text{ABS}(N_z) > 10$], a factor of 4.0 is applied to the initial amplitude of the imperfection specified by the user. This is done because hyperbolic growth of the imperfection amplitude is assumed to hold [4] as the applied load approaches the design load. This assumption is only valid if the buckling eigenvalues are well separated, as is true for axially compressed columns or externally pressurized cylindrical shells. For axially compressed, very thin monocoque cylindrical shells there exists a cluster of eigenvalues in the neighborhood of the "classical" buckling load, with the result that the initial imperfection grows more slowly than hyperbolically for low loads and more steeply than hyperbolically for high loads. The factor of 4.0 compensates for the approximation of hyperbolic growth of the buckling modal imperfection amplitude; most likely it compensates

conservatively.

5. In panels and shells with both stringers and rings, the stringers and rings are allowed to deform "through eachother" where they intersect. That is, they do not support eachother in any way where they intersect.

6. The knockdown factor to compensate for the unconservativeness of smearing rings is quite conservative, since it is computed with the use of a discretized "skin"-ring single module model with symmetry conditions applied at top and bottom, which simulates an infinitely long cylindrical shell. (See leftmost image, bottom row in Fig. 30 of [6] and Fig. 8 here). The "smeared ring" knockdown factor is the ratio:

$$\frac{\text{(buckling load factor from the discretized module model)}}{\text{(buckling load factor of a ring with the same cross-section)}}$$

computed for the critical number of circumferential waves determined from a PANDA-type model [2] with smeared stiffeners and an axial length equal to the user-specified length. The "ring" referred to in the string, "buckling load factor of a ring with the same cross-section", has a circumferential bending stiffness EI that includes the actual T-shaped ring plus an axial length of skin with smeared stringers equal to the ring spacing, that is, a ring with cross section such as that shown in Fig. 8. The knockdown factor is less than 1.0 primarily because the cross section of the discretized module model can deform whereas the ring cross section is assumed not to deform. With the print option NPRINT set equal to 2 by the user, PANDA2 prints out the following information in the *.OPM file:

"Derivation of knockdown factor RNGKNZ for smearing rings..."

Buckling load factor for circumferential waves $n+dn = FNARCQ = 2.9922$
from discrete "skin"-ring model [6], Fig. 8 here: $EIGR = 2.7921E+00$

Buckling load factor for "skin"-ring module from the simple formula for a ring with bending stiffness EI:
 $p_{crit} = [(n+dn)^{**2}-1]*EI/r^{**3}/p = EIGRNG = 3.6051E+00$

Knockdown ratio for "smeared" ring model of general buckling,
 $RNGKNZ = EIGR/EIGRNG = 7.7449E-01$

(NOTE: See the PANDA2 modification described in Item 1 of Subsection 17.1).

7. The knockdown factor for transverse shear deformation (t.s.d.) is on the conservative side. (See Fig. 25 on p.527 of [1]).

8. The buckling load factor for the outstanding flanges of stringers and rings, computed in SUBROUTINE ENDBUK (called by SUBROUTINE CRIPPL, which is called by SUBROUTINE STFEIG) is conservative because it is based on the assumption that the outstanding flange is simply supported where it joins the web tip.

9. The buckling load factor for the web and outstanding flange of a stiffener buckling together (stiffener segment 3+4 buckling) is conservative because it is assumed that the web root is simply supported where it joins the panel skin.

10. The buckling load factor of an outstanding flange acting as a beam on an elastic foundation is conservative because of the factor of safety of 3.0 applied to that kind of failure. (NOTE: See the PANDA2 modification described in Item 2 of Subsection 17.1).

11. The buckling load factor of a stringer and/or ring rolling without participation of the panel skin is conservative because of the factor of safety, F.S.=1.6, applied to that kind of failure. (For a picture of this kind of buckling see Fig. 6b, p. 546 of [2]). (NOTE: See the PANDA2 modification described in Item 3 of Subsection 17.1).

12. The knockdown factor to compensate for the unconservativeness of smearing stringers is usually conservative.

13. For panels stiffened by stringers and/or rings with cross sections that have outstanding flanges (not blades), the buckling load factors computed with use of the double trigonometric series expansions [6] will usually be conservative because the edges of the "altsol patch" are assumed to be simply supported rather than supported by a

stiffener.

14. The "knockdown" factor for imperfection sensitivity is often made smaller by multiplication by a ratio, (ARBOCZ/PANDA2), which is either unity or less than unity. In the ratio, (ARBOCZ/PANDA2):

ARBOCZ = buckling load of perfect shell from ARBOCZ theory (see [5,39])

PANDA2 = buckling load of perfect shell from PANDA-type (closed form) theory (see [2]).

15. PANDA2 computes a "knockdown" factor for imperfection sensitivity by iteratively computing an effective circumferential radius of curvature as described in Sections 11.0 and 14.0. The effective radius of the imperfect shell is larger than the nominal radius of the perfect shell because it corresponds to the local circumferential radius of curvature at the point on the shell surface where there is a maximum inward lobe of the general buckling modal imperfection pattern. Although this maximum circumferential radius of curvature is local, varying along the circumference because of the circumferential waviness of the general buckling modal imperfection shape, in PANDA2 it is assumed that the maximum circumferential radius of curvature of the imperfect shell is UNIFORM over the entire circumference of the panel. This is almost certainly a conservative model. See Section 14.0 for a more complete discussion of how imperfection sensitivity is handled in PANDA2. It is emphasized here that the theory used in PANDA2 is NOT the very conservative asymptotic "classical" imperfection sensitivity theory by Koiter.

10.0 BUCKLING OF THE PERFECT SHELL: AN EXAMPLE

The following discussion is based on an optimized imperfect externally T-stringer and T-ring stiffened cylindrical shell. The optimized configuration of this shell is that listed in Column 5 of Table 8 of Ref.[16]. Table 1 here lists data pertaining to this shell and Table 2 lists the dimensions of the optimum design derived in [16]. Figures 1 – 19 display this shell and some of its buckling behavior. Note from Table 1 that the maximum allowable stress is set very high (10^6 psi). This is done so that stress constraints do not affect the evolution of the design during optimization cycles.

The shell was optimized with a general buckling modal imperfection and with the use of two load sets. The applied loads are the same in both load sets. Only the sign of the general buckling modal imperfection is changed from Load set 1 to Load set 2, as follows:

Load Set 1: general buckling modal imperfection has amplitude, $W_{imp} = +1.0$ inch.

Load Set 2: general buckling modal imperfection has amplitude, $W_{imp} = -1.0$ inch.

10.1 Various buckling modes and comparisons with STAGS and BOSOR4

Listed in Table 3 are the margins corresponding to conditions midway between rings for the configuration identified in Table 2 and with the amplitude of the general buckling modal imperfection set equal to zero. Figures 12 and 13 show general buckling load factors and mode shapes predicted by a STAGS model of the perfect shell; Figs. 14 and 15 show the combined "long-axial-wave bending-torsion"/inter-ring buckling load factor and mode shape predicted by STAGS for a 3x9 bay subdomain of the shell; Fig. 17 shows the local buckling load factor and mode shape predicted by STAGS for a 1x3 bay subdomain. The predictions of local, inter-ring, and general buckling from BOSOR4 models with in-plane shear $N_{xy} = 0$ are displayed in Figs. 6, 7 and 10, respectively. Margin 23 in Table 3 corresponds to a user-specified inequality constraint ensuring that the stringer web height will be less than 20 times the stringer web thickness. (" $V(i)$ " = ith variable listed in Table 2). Margin 24 in Table 3 is analogous to Margin 23: the ring web height will be less than 20 times the ring web thickness.

A summary of results from PANDA2, BOSOR4, and STAGS for the perfect shell is listed in Table 4. Note that a buckling load factor is given by:

$$(\text{buckling load factor}) = (\text{margin} + 1.0) * (\text{factor of safety}).$$

10.2 Philosophy encoded in PANDA2

As seen from Table 4, PANDA2 has many margins relating to "local buckling" and "inter-ring" buckling. As demonstrated especially from the STAGS predictions shown in Figs. 14-17, the actual buckling modes are often combinations of skin and stiffener buckling. They are too complicated to predict exactly with the use of the relatively simple models encoded in PANDA2.

PANDA2 attempts to arrive at reasonable (mildly conservative) optimum designs by dividing a very complex problem into many relatively simple problems. For example, local buckling in this particular case is represented in PANDA2 by six different models, leading to Margins 1, 8, 9, 10, 12, and 18 in Table 3. Similarly, inter-ring buckling in this particular case is represented by five different models, leading to Margins 2, 4, 5, 13, and 17 in Table 3. PANDA2 has been developed over the years with the philosophy that the use of many approximate models will lead to optimum designs that are reasonable and for which no complicated "combined" mode of failure will inadvertently be missed. The computer times required to arrive at reasonable "global" optimum designs are not outrageous because each of the many PANDA2 models has few degrees of freedom compared to finite element models such as those displayed for the STAGS models shown in Figs. 1 - 3. Most of the computer time in PANDA2 runs is spent on the "altsol" models [6] in which each displacement component (u, v, w) is expressed as a double trigonometric series expansion with up to 121 terms (11×11) per displacement component. These models have up to 305 degrees of freedom with non-banded stiffness matrices.

For any design some of the PANDA2 models are unconservative because they cannot reproduce complex behavior such as that shown in Figs. 14 - 17. For example, the "inter-ring buckling, discrete model" (Margin no. 5 in Table 3) has smeared stringers [38]. Therefore, it cannot reproduce the stringer deformation behavior exhibited in Figs. 14-17. However, compensating models correspond to Margins 8, 9, and 17, all of which are conservative estimates of buckling in which the cross section of a stringer deforms.

10.3 Some comments on the PANDA2 results listed in Tables 3 and 4:

1. Margin 5 is unconservative because the stringers are "smeared" [38] and their cross sections therefore cannot deform as shown in Figs. 4-7 and Figs. 14-17.
2. Margin 8 is conservative because the stringer "Iseg.4" (outstanding flange) is assumed to be simply supported where it is attached to the outer tip of the stringer web.
3. Margin 9 is conservative because the root of the web of the stringer is assumed to be simply supported where it meets the panel skin.
4. Margin 10 is conservative because of the large factor of safety (3.0).
5. Margin 13 is conservative because simple support is assumed where the ring webs intersect the panel skin and the rings are ignored. (With the rings included Margin 13 increases from 0.172 to 0.286).
6. Margin 14 is conservative primarily because the "knockdown" factor to compensate for "smearing" rings [38] is conservative.
7. Margin 15 is conservative because of the "knockdown" factor 0.85 used to compensate for truncation error in the double trigonometric series expansions of the "altsol" model [6].
8. Margin 17 is conservative because of the factor of safety 1.6.
9. The remaining PANDA2 margins listed in Table 4 (Margins 1, 12, 18 for local buckling and Margins 2 and 4 for inter-ring buckling) are not especially conservative or unconservative.

10.4 Some comments on the BOSOR4 and STAGS results listed in Table 4:

1. The BOSOR4 results listed for local buckling are unconservative because the presence of in-plane shear loading N_{xy} is neglected. (BOSOR4 cannot handle shells with in-plane shear loading). Also, the effects of transverse shear deformation (t.s.d.) are not included in BOSOR4.
2. The BOSOR4 result for inter-ring buckling (buckling load factor = 2.354) is unconservative because the stringers are "smeared" [38] in the model and their cross sections therefore cannot deform as displayed in Figs. 4-7 and Figs. 14-17.
3. The BOSOR4 result for general buckling (buckling load factor = 1.916) is unconservative because in-plane shear loading N_{xy} is neglected and the stringers are "smeared" [38].
4. The BOSOR4 result for general buckling (buckling load factor = 2.784) is unconservative because, for this model, the critical buckling mode has two circumferential waves, not three. Corresponding to $n=2$ the buckling load factor is 1.132 for this model, much too conservative. This model is NOT used in PANDA2 to estimate general buckling. It is used instead, with $n = 3$ in this particular case, to determine the "knockdown" to compensate for the unconservativeness of "smearing" rings as described in Item no. 6 of Section 9.0.

Since PANDA2 uses BOSOR4 software for the single module discretized models, why does the PANDA2 prediction for local buckling listed in Table 4 differ so much from the BOSOR4 prediction (buckling load factor 1.790 for PANDA2 vs 1.939 for BOSOR4)? The answer can be seen from Table 5, in which is listed output from PANDA2 for buckling of the single module discretized skin-stringer model similar to that shown in Fig. 5. The number of axial halfwaves is between rings, and the variation of buckling modal displacements u,v,w in the axial direction (normal to the plane of the paper in Fig. 5) is trigonometric with M axial halfwaves. PANDA2 searches over M for a minimum buckling load factor. After this minimum has been found, corresponding to 8 axial halfwaves between rings in this case, PANDA2 applies two knockdown factors, "KSTAR" for the effect of transverse shear deformation (t.s.d) and "KNOCK" to compensate for the neglect of in-plane shear loading N_{xy} and neglect of anisotropy in the discretized BOSOR4-type model. The final local buckling load factor is 1.788 according to PANDA2, which is in very good agreement with that from STAGS (Fig. 17). The critical buckling load factor before "knockdown", 1.946 in Table 5, is in good agreement with the BOSOR4 prediction of 1.939 listed in Table 4 and shown in Fig. 5. The small difference between 1.946 (PANDA2) and 1.939 (BOSOR4) is a result of the following:

- (1) In the discretized module model for local buckling in PANDA2 the panel skin is assumed to be flat.
- (2) A somewhat sparser discretization is used in the PANDA2 model than that displayed for the BOSOR4 model shown in Fig. 5.

10.5 General buckling models

Table 6 provides an example of how the general buckling margin no. 14 in Table 3 is derived by PANDA2 for the perfect shell. First (Part 1) an exhaustive search over (m,n,s) space is conducted. $\{(m,n,s) = (\text{axial halfwaves, circumferential halfwaves, slope of buckling nodal lines})$; see Items 415 and 443 in [17] for details about the search}. Note that this search reveals two rather close eigenvalues, 2.17 for the mode, $(m,n,s)=(1,3,.274)$, and 2.28 for the very different mode, $(m,n,s)=(6,0,.473)$. These two modes are approximately those displayed by the STAGS models with "smeared" stiffeners in Figs. 18 and 19, respectively. More will be written later concerning the effect of close but dissimilar general buckling modes on what may happen during design iterations for shells with an initial general buckling modal imperfection.

Part 2 of Table 6 demonstrates how the buckling load factor and mode shape (slope of buckling nodal lines) are refined and how the buckling load factor is "knocked down" to account for transverse shear deformation (t.s.d.) and to compensate for "smearing" the stringers. In Part 3 the buckling load factor is further "knocked down" by the ratio (ARBÖCZ/PANDA2) = 0.91845 (explained above in Item no. 14 of Section 9.0) and by a factor to compensate for "smearing" the rings (derived in Item no. 6 of Section 9.0). A comparison of the buckling load factors per given by

the STAGS models in Figs. 12 and 18 reveals that the "smeared" ring knockdown factor, 0.7745, used by PANDA2, is conservative in this case. The ratio of the eigenvalues obtained by STAGS and printed in Figs. 12 and 18 is $1.6491/1.8240 = 0.9041$. The STAGS model in Fig. 12 has both rings and stringers modeled as shell branches, whereas the STAGS model in Fig. 18 has both rings and stringers "smeared" [38]. Therefore, the ratio 0.9041 should account (approximately) for smearing BOTH rings and stringers. In the PANDA2 model the equivalent ratio would be

$$("knockdown" \text{ for smeared stringers} \times "knockdown" \text{ for smeared rings}) = (0.9378 \times 0.7745) = 0.7263,$$

indeed a conservative estimate compared to the ratio 0.9041 derived from the two STAGS models. (NOTE: The "smeared" ring knockdown factor is now computed as described in Item 1 of Section 17.1, which leads to a less conservative knockdown factor than 0.7745 in this case).

Part 4 in Table 6 lists the final buckling load factor from PANDA2, 1.3818. The corresponding margin is:

$$(\text{buckling load factor})/(\text{factor of safety}) - 1 = 1.3818/0.999 - 1 = 0.383$$

listed as Margin No. 14 in Table 3. (The rather strange factor of safety, 0.999, is used in this example because PANDA2 automatically increases the factor of safety from the user's input to 1.1 if the user specifies a value between 1.0 and 1.1, including 1.0. PANDA2 does this to avoid very large constraint gradients sometimes encountered with factors of safety of 1.0.)

Table 7 is analogous to Table 6. Its purpose is to provide an example of how the general buckling margin no. 15 in Table 3 is derived for the perfect shell. In these computations the buckling modal displacements over a NUMSTR-stringer by NUMRNG-ring "patch" are expressed in double-trigonometric series expansions of the buckling modal displacements, u, v, w , the coefficients of which are the unknowns of the eigenvalue problem [6]. The purpose of including this model in PANDA2 is to capture buckling modes of the type shown in Fig. 16 of [6] and Figs. 20 - 22 of [7] more accurately than can be obtained with the simple PANDA-type closed form solution [2] such as represented by Margin no. 14 in Table 3.

Part 1 of Table 7 is an introduction. Part 2 gives the eigenvalues, EIGODD, EIGEVN. The critical buckling load factor is the smallest of EIGODD and EIGEVN. As explained in Item No. 438 of [17]:

"Advantage is taken of the fact that, provided the anisotropic B16 and B26 terms in the 6×6 integrated constitutive matrix of the shell wall are not significant, the total system of equations $A^*x = \lambda B^*x$ can be split into two smaller systems of equations of approximately half the total rank each. In one of the subsystems $m + n$ is odd (m = number of axial halfwaves; n = number of circumferential halfwaves) and in the other $m + n$ is even. The alternative solution is obtained much faster and requires less storage if the split into $m+n=odd$ and $m+n=even$ subsystems can be introduced."

Part 3 of Table 7 lists the eigenvector, that is, the coefficients of the (M, N) terms in the double trigonometric series for w . In this case careful inspection of the (M, N) matrix reveals that the buckling mode of the "patch" is actually a form of local buckling resembling the mode shape shown in Fig. 17 of [7]. The only significant (M, N) terms correspond to six circumferential halfwaves over the "patch". There are 7 equally spaced stringers in the "patch" (NUMSTR=7 in Part 1), including the two stringers that run along the two straight edges of the "patch". Therefore, there are six stringer bays in the "patch". Virtually all of the buckling occurs between adjacent stringers with negligible overall bending of the stringers. (The stringers do rotate about their web roots, however). Regardless of the "local" characteristic of this "general" buckling mode, PANDA2 treats this model as general buckling, applying "knockdown" factors meant for general buckling. Hence, this "altsol" model is usually conservative.

There is at present no logic in the "altsol" section of PANDA2 to scan the mode and change the "knockdown" strategy based on results from the scan. Based on the scan it would often be difficult to determine whether the mode is a local mode or a mode in which there is some stringer and/or ring bending. The buckling mode from STAGS shown in Fig. 14 is an example. It appears at first as though the stringers are only rolling about the roots of their webs. However, Fig. 15, which shows the same buckling mode as viewed from one end of the panel (with the rings deleted from the view), demonstrates that some of the stringers are bending; there are only five circumferential

halfwaves in the panel skin, whereas there are nine stringer bays in the STAGS model. If the stringers are numbered starting from the bottom of the figure, Stringers 1, 3, 5, 6, 8 and 10 are essentially rotating about their web roots, whereas Stringers 2, 4, 7, and 9 experience significant axial bending. Figures 20 - 22 of [7] provide another example. From Fig. 20 of [7] one would conclude that the buckling mode is entirely inter-ring. However, Fig. 22 of [7] clearly demonstrates that at least one ring experiences some overall bending, not just rolling about its web root, as would be the case for a true inter-ring buckling mode.

Part 4 of Table 7 shows how the buckling load factor, 1.6834, is "knocked down". In this particular case involving a perfect shell the only significant "knockdown" factor is 0.85, the purpose of which is to compensate for possible unconservativeness of truncating the double trigonometric series expansions. The (ARBOCZ/PANDA2) factor, 0.91845, is counteracted by the "2nd modifying factor", 1.0888, because the "patch" used in this model is judged by PANDA2 to be shallow. Therefore the ARBOCZ solution [5,39] does not apply because the ARBOCZ theory applies to complete cylindrical shells, not shallow panels.

The final result appears in Part 5 of Table 7 and the corresponding margin is Margin No. 15 in Table 3.

11.0 HOW IMPERFECTION SENSITIVITY IS HANDLED IN PANDA2

PANDA2 can optimize imperfect stiffened panels and shells [4]. Imperfections are assumed to be in the shapes of the general, inter-ring, and local buckling modes obtained from the "PANDA-type" model [2]. One section of PANDA2 applies to ring and stringer stiffened panels with a GENERAL buckling modal imperfection, that is, an imperfection shape that is determined from a model in which the rings and stringers are smeared out. The following discussion applies to that particular section of PANDA2, which is called PART 1 in SUBROUTINE STRIMP. Analogous discussions pertaining to inter-ring (PART 2 in STRIMP) and local (PART 3 in STRIMP) buckling modal imperfections could have been written.

11.1 Two major effects of a general buckling modal imperfection

A **general** buckling modal imperfection in a **stiffened** shell has two major effects:

1. The imperfect stiffened panel or shell bends as soon as any loading is applied. This bending causes significant redistribution of stresses between the panel skin and the various stiffener parts, thus affecting significantly many local and inter-ring buckling and stress constraints. See the short Section 6.0 for an example of how the stress resultants in the various segments of a T-ring and T-stringer stiffened cylindrical shell are changed due to prebuckling bending that occurs when a general buckling modal imperfection exists.
2. The "effective" circumferential curvature of an imperfect cylindrical panel or shell depends on the amplitude of the initial imperfection, on the circumferential wavelength of the critical buckling mode of the perfect and of the imperfect shell, and on the amount that the initial imperfection grows as the loading increases from zero to the design load. The "effective" circumferential radius of curvature of the imperfect and loaded shell is larger than its nominal radius of curvature because the larger "effective" radius corresponds to the maximum local radius of the cylindrical shell with a typical inward circumferential lobe of the initial and subsequently load-amplified buckling modal imperfection.

In PANDA2 this larger local "effective" radius of curvature is assumed to be the governing UNIFORM radius in the buckling equations pertaining to the imperfect shell; the imperfect shell is replaced by a new perfect cylindrical shell with the larger radius. By means of this device a complicated nonlinear collapse analysis is converted into a simple bifurcation buckling problem - a linear eigenvalue problem. For each type of buckling modal imperfection (general, inter-ring, local) PANDA2 computes a "knockdown" factor based on the ratio:

$$\frac{\text{(buckling load factor: panel with its "effective" radius)}}{\text{(buckling load factor: panel with its nominal radius)}}$$

11.2 Computation of "imperfection sensitivity" in PANDA2

In the "imperfection sensitivity" calculations, which occur in SUBROUTINE STRIMP, PANDA2 does the following (with the use of Donnell shell theory):

1. Computes the buckling load factor for a PERFECT panel from PANDA-type theory [2].
2. Computes the buckling load factor for a PERFECT panel from ARBOCZ theory. Equations are from Ref. [39], in particular, Equation No. (3.61) in that report. This ARBOCZ theory is also described briefly in [5].
3. Computes the buckling load factor for an IMPERFECT panel from ARBOCZ theory.
4. Computes the buckling load factor for an IMPERFECT panel from PANDA-type theory [2]. This is done iteratively since the "effective" circumferential radius of curvature of the imperfect panel depends on the buckling load factor that is being computed.
5. Decides (partly depending on user-provided input) on whether to use the buckling mode of the PERFECT shell or the buckling mode of the IMPERFECT shell as the imperfection shape. (See Table 13).
6. Possibly changes the amplitude of the initial imperfection. (See Table 13).
7. Computes the curvature changes and twist, W_{xx} , W_{yy} , W_{xy} , generated because of prebuckling bending of the imperfect shell as it is loaded by the design load.
8. Presents a summary of "knockdown" factors to be used in connection with local, inter-ring, and general buckling of the stiffened shell.

For more information on the behavior of imperfect stiffened shells, please see [4, 7, 16] and the following items in [17]: 377, 456, 525, 553, 564, 594, and 596. Also, more details are provided in Section 14.0.

12.0 MARGINS FOR THE IMPERFECT OPTIMIZED SHELL

The results given so far (except for those in the short Section 6.0 entitled "REDISTRIBUTION OF STRESS BETWEEN SKIN AND STIFFENERS..." are all for a PERFECT shell. However, the shell depicted in Figs. 1 - 19 and for which results are listed in Tables 1 – 7 was optimized including a general buckling modal imperfection [4] with amplitudes $W_{imp} = +1.0$ inch (Load Set 1) and $W_{imp} = -1.0$ inch (Load Set 2).

Listed in Table 8 are the margins for the IMPERFECT shell. Whereas none of the margins listed in Table 3 is critical because that table applies to the same design with the imperfection amplitude set equal to zero, many of the margins for the imperfect shell are critical: (Margins 6, 9, 13, 16, 17, 19 in Part 1; Margins 5, 8, 12, 16, 18 in Part 2; Margins 1, 2, 4, 5, 12, 13, 14, 15, 16, 21 in Part 3; Margins 1, 2, 4, 6, 13, 14 in Part 4). One might expect such a condition at an optimum design.

Note that there are two slightly negative margins, Margin 19 of Part 1 and Margin 16 of Part 2. PANDA2 accepts a design as "FEASIBLE" provided that no margin is less than -0.01. PANDA2 accepts a design as "ALMOST FEASIBLE" provided that no margin is less than -0.05. In SUPEROPT runs (attempts to find a global optimum design) PANDA2 always accepts "ALMOST FEASIBLE" designs.

13.0 SOME RESULTS OF PANDA2 COMPUTATIONS INVOLVING AN IMPERFECTION

Listed in Table 9 are data pertaining to the effects of the initial buckling modal imperfection. Note from Part 1 of Table 9 that the only significant buckling modal imperfection in this case is the general buckling modal imperfection, which has a user-supplied amplitude of 1.0 inch.

The results listed in Part 2 of Table 9 are very important. Although there are no initial local or inter-ring buckling modal imperfections, the local and inter-ring buckling load factors are significantly reduced from those for the perfect shell because of the redistribution of stress between skin and stiffeners during prebuckling bending of the shell with the general buckling modal imperfection. The redistribution of stress resultants dN_x , dN_y , dN_{xy} in this case is listed above in the short Section 6.0.

There is no effect of stress redistribution on general buckling, of course, because the overall stress resultants over the entire wall (panel skin plus smeared stiffeners) are unaffected by inextensional prebuckling bending of the imperfect shell; they are the applied stress resultants, $N_x(1)$, $N_y(1)$, $N_{xy}(1)$ and pressure $p(1)$ listed in Table 1.

In Part 3 of Table 9 are listed the "knockdown" factors and buckling modes from PANDA-type theory [2] for local, inter-ring, and general buckling. These "knockdown" factors do NOT include the effect of stress redistribution discussed in the previous paragraphs. That effect is included in the part of PANDA2 in which the PREBUCKLED stress state of the imperfect shell is computed. The "knockdown" factors for local and inter-ring buckling are unity and very close to unity because the user in this case specified "zero" (actually a very small number) for the amplitudes of local and inter-ring buckling modal imperfections. Note that the "knockdown" factor for general buckling is fairly large, 0.858, indicating only a mild sensitivity to a general buckling modal imperfection according to the PANDA-type theory [2,4].

Part 4 of Table 9 lists the curvature changes and twist, W_{xx} , W_{yy} , W_{xy} caused by local, inter-ring, and general buckling modal imperfections when the imperfect shell is subjected to the design load combination listed in Table 1. These are the quantities that determine how the stresses are redistributed among panel skin and stiffener segments as the imperfect shell bends during prebuckling loading. It is emphasized that W_{xx} , W_{yy} , W_{xy} depend strongly on the buckling mode shapes. Only the curvature changes and twist from prebuckling growth of the GENERAL buckling modal imperfection are non-zero here because the user has specified "zero" for the amplitudes of the LOCAL and INTER-RING buckling modal imperfections in this particular case.

Part 5 of Table 9 summarizes the "knockdown" factors from PANDA2 theory [2] and from ARBOCZ theory [5,39]. Note that for general buckling,

1. The ARBOCZ theory gives lower buckling loads than the PANDA2 theory for the PERFECT shell (ARBOCZ/PANDA2 = 0.91845 for general buckling).
2. The ARBOCZ theory gives a smaller "knockdown" factor than the PANDA2 theory for general buckling, 0.74576 for ARBOCZ compared to 0.85791 for PANDA2.
3. The "knockdown" factor to be used for general buckling of the imperfect shell is the lowest of that from PANDA2 and ARBOCZ theories. Hence, the "knockdown" factor to be used in the PANDA2 computations of general buckling of the imperfect shell is $0.91845 \times 0.74576 = 0.68494$ in this case.

The most significant results in Table 9 are printed in boldface. To summarize: Part 2 represents the effect of stress redistribution between panel skin and stiffener parts. Part 3 represents the effect of the increased effective radius of the imperfect shell over the nominal value for the perfect shell. These results demonstrate that for a **stiffened** shell the effect of an initial general buckling modal imperfection is very different from that for a **monocoque** shell. For a **stiffened** shell the effect of the geometry change (increase in effective radius) is relatively small, leading to a knockdown factor of 0.858 for general buckling of the imperfect shell, which represents only mild imperfection sensitivity. The important effect in this particular case is the redistribution of stress in the imperfect shell as it bends under the design load. In contrast, for a monocoque shell the important (and only) effect is the effect of the geometry change; stress redistribution plays no role.

14.0 DETAILS ABOUT HOW PANDA2 FINDS BUCKLING LOADS OF IMPERFECT SHELLS

The information in this section, most of which is listed in Table 10, appears in PANDA2's output file, *.OPM, if the

user selects the "verbose" mode, NPRINT = 2, in the MAINSETUP processor (*.OPT input file). Table 10 contains 6 parts:

Part 1 Some definitions

Part 2 Some notes about the verbose output

Part 3 PANDA-type general buckling analysis [2] of the perfect panel

Part 4 ARBOCZ general buckling analysis [5] of the perfect panel

Part 5 ARBOCZ general buckling analysis [5] of the imperfect panel

Part 6 PANDA-type general buckling analysis [2,4] of the imperfect panel

Part 7 Last iteration: PANDA-type general buckling analysis [2,4] of the imperfect panel

Some comments with regard to Table 10 are:

1. The entire Table 10 applies only to the section of PANDA2 concerned with imperfection sensitivity in the presence of a GENERAL buckling modal imperfection. Only general buckling load factors are included in Table 10. Both stringers and rings are "smeared" [38] in the structural model used in this section of PANDA2 (PART 1 of SUBROUTINE STRIMP).

2. Analogous verbose output exists for inter-ring and for local buckling. The logic is the same for those modes as for general buckling of the perfect and imperfect shells. The only difference is the extent of the domain which buckles and the loading experienced by the domain which buckles. For inter-ring buckling the domain includes a shell with axial length equal to the ring spacing and circumferential arc length equal to the circumferential arc length of the panel. The stringers are "smeared" [38] in the model. The loading is the part of the applied loading, N_x , N_y , N_{xy} , that is borne by the inter-ring portion of the stiffened shell. For local buckling the domain includes a shell with axial length equal to the ring spacing and circumferential arc length equal to the stringer spacing and there are no stringers or rings. The loading is the part of the applied loading, N_x , N_y , N_{xy} , that is borne by the panel skin.

3. Computations are performed for both PANDA-type theory [2] and ARBOCZ theory [5,39] in order to produce a conservative estimate of imperfection sensitivity. In the PANDA-type theory the effect of the imperfection is to increase the effective circumferential radius of curvature, which occurs where the general buckling mode has a maximum inward circumferential lobe. This increase in effective uniform radius of the cylindrical shell depends on the loading and leads to a reduced buckling load factor, of course. In the part of the ARBOCZ theory used in PANDA2 {Eq.(19) in [5]} the imperfection is assumed to be axisymmetric and the effect of the imperfection is to produce bands of increased hoop compression where the axial lobes of the axisymmetric imperfection are inward (as in Koiter's special theory [81]). The bands of increased hoop compression give rise to a significant "knockdown" factor for general instability, as is demonstrated for monocoque cylindrical shells under pure axial compression by Fig. 262 on p. 297 of [23].

4. There are many special features in the computations developed over many years during the development and refinement of PANDA2:

(a) the extensive search over the buckling modal space (m,n,s) to avoid missing critical eigenvalues. (See the beginning of Part 2 of Table 10 and Items 415 and 443 of [17]).

(b) the use of "fractional" wavenumbers to smooth the buckling constraints with respect to small changes in the design of the shell. (See Parts 2, 3 and 7 of Table 10).

(c) the special emphasis on multiple minima of eigenvalues in (m,n,s) space. (See Parts 2 and 3 of Table 10).

(d) the development of a mild "knockdown" factor, EIGRAT, based on two different assumptions with regard to buckling modes (Fig. 9 of [2]). (See Part 3 of Table 10).

(e) the "knockdown" factors for transverse shear deformation (t.s.d.) and to compensate for "smearing" the stringers and to compensate for "smearing" the rings. (See Parts 3 and 7 of Table 10).

(f) the iterative scheme to arrive at the effective radius of the imperfect cylindrical shell and the corresponding

critical buckling mode. (See Parts 6 and 7 of Table 10).

5. In Parts 6 and 7 of Table 10 notice the significant change in critical buckling mode from an $(m,n,s) = (1,3,0.473)$ mode ($EIGMNC(critical) = 2.14$ at Iteration No. 1) to an $(m,n,s) = (5,3,0.0)$ mode ($EIGMNC(critical) = 1.97$ at Iteration No. 5). The critical mode at Iteration No. 1, in which $(m,n) = (1,3)$, resembles the buckling modes from the STAGS models shown in Figs. 12 and 18. The critical mode from Iteration No. 5, in which $(m,n) = (5,3)$, resembles the buckling mode from STAGS shown in Fig. 13. This change in the critical buckling mode for general buckling of the imperfect shell has a dramatic effect on the buckling margins, as will be seen. At Iteration No. 5 (Part 7 of Table 10) the eigenvalues (buckling load factors) corresponding to the two modes $(m,n,s) = (1,3,0.473)$ and $(5,3,0.0)$ are very close: 2.06 and 1.97, respectively. One can easily imagine that a slightly different design would lead to results in which the $(1,3,0.473)$ mode is critical rather than the $(5,3,0.0)$ mode. Such a result would have a dramatic influence on many of the margins because the buckling mode shape has a profound influence on the prebuckling changes in curvature and twist, W_{xx} , W_{yy} , W_{xy} , in the imperfect shell as deformed under the design load. The changes in curvature and twist, W_{xx} , W_{yy} , W_{xy} , determine how the stresses get redistributed between the panel skin and stiffener parts.

15.0 DIFFICULTIES IN OPTIMIZATION OF IMPERFECT STIFFENED CYLINDRICAL SHELLS

15.1 "Oscillating" general buckling modal imperfection shapes from cycle to cycle

Table 11 lists selected output from PANDA2. Parts 1 - 3 are from the section of PANDA2 related to imperfection sensitivity and deformation of the stiffened shell with a general buckling modal imperfection in the form of the critical mode, $(m,n,s) = (5,3,0.0)$. This mode is determined as listed in Parts 6 and 7 of Table 10. The dimensions of the stiffened shell are as listed in Table 2.

Perhaps the most important quantities in Table 11 are the curvature changes and twist, called W_{xx9} , W_{yy9} , W_{xy9} at the end of Part 3 of Table 11. These are the quantities that determine how the prebuckling stresses of the imperfect shell are redistributed among panel skin and stiffener segments as the imperfect shell bends under the design load. (In the presence of an inter-ring buckling modal imperfection the curvature changes and twist are called W_{xx8} , W_{yy8} , W_{xy8} , and in the presence of a local buckling modal imperfection they are called W_{xx7} , W_{yy7} , and W_{xy7} in PANDA2's verbose output).

The margins for Load case 1 (positive general buckling modal imperfection amplitude), Subcase 1 (midway between rings), $W_{imp} = +1.0$ inch, are listed in Part 4 of Table 11. Many of them are significantly negative, indicating an UNFEASIBLE design. Why are the margins so different from those listed in Part 1 of Table 8, which indicates a FEASIBLE design for the same configuration, imperfection amplitude, and loading? They are different because the $(m,n) = (5,3)$ buckling mode was chosen by PANDA2 as the general buckling modal imperfection shape rather than the mode shape $(m,n) = (1,3)$ with its much longer axial halfwave length, to which the margins in Part 1 of Table 8 correspond. PANDA2 chose differently in the Table 11 case than in the Table 8 case because, in the MAINSETUP interactive session, the user provided different input:

Strategy (1), the strategy leading to the results in Table 11:

n \$ Do you want PANDA2 to change imperfection amplitudes?

Strategy (2), the strategy leading to the results in Table 8:

y \$ Do you want PANDA2 to change imperfection amplitudes?
300.0 \$ Axial halfwavelength of typical general buckling mode, AXLWAV(1)

More explanation appears below and in Table 13 concerning the different strategies, (1) and (2), used by PANDA2 depending on these different input data from the PANDA2 user.

With the user's choice of Strategy (2), PANDA2, in this particular example, obtains the results listed in Table 12.

The margins have been omitted from this table to save space; they are the same as those listed in Part 1 of Table 8. The same design is FEASIBLE with this much milder $(m,n) = (1,3)$ buckling modal imperfection shape because the axial halfwavelength of the $(1,3)$ mode is five times longer than that of the much more harmful $(5,3)$ mode. Notice that the axial curvature change W_{xx9} and twist W_{xy9} are much greater for the $(5,3)$ mode (Table 11) than for the $(1,3)$ mode (Table 12). Of course this is due to the higher value of axial halfwaves m in the $(m,n) = (5,3)$ mode. The circumferential curvature change W_{yy9} , depending most strongly on the number of circumferential halfwaves n , is affected much less by the difference in mode shapes because the number of circumferential halfwaves, $n=3$, happens to be the same in both cases in this particular example.

Figure 20 give plots of selected margins for 11 design iterations starting from the optimized design (Iteration zero) listed in Table 2 for the case in which Strategy (1) is chosen by the PANDA2 user. Most of the margins "oscillate" wildly because the critical general buckling mode shape "oscillates" between the $(m,n) = (5,3)$ and $(1,3)$ buckling modal imperfection shapes from design iteration to iteration. In the *.OPM output file PANDA2 prints the following warning to the user whenever such "oscillations" occur:

```
*** WARNING *** WARNING *** WARNING ***
CONVERGENCE TO AN OPTIMUM DESIGN IS DIFFICULT BE-
CAUSE SOME MARGINS OSCILLATE FROM ITERATION TO
ITERATION BECAUSE THE NUMBER OF AXIAL HALFWAVES
IN THE GENERAL BUCKLING MODE OSCILLATES FROM
m = 1 TO m > 1 DURING DESIGN ITERATIONS:
m for the last 5 iterations = 5 5 1 5 1
** END WARNING *** END WARNING *** END WARNING **
```

This particular warning message corresponds to Iterations 7 - 11 in Fig. 20. This type of "oscillation" makes it very difficult to find a "global" optimum design.

As described above in connection with Strategy (1) and Strategy (2), the user may elect to allow PANDA2 to change the user-specified amplitude of the initial buckling modal imperfection. The relevant section of the PROMPT.DAT file, which contains prompts and explanatory "help" paragraphs that elicit responses from the user for each input datum, now reads as listed in Table 13.

Figure 21 shows the same margins for the case when the user follows Strategy (2) instead of Strategy (1), that is, he/she responds as follows during the MAINSETUP interactive session:

```
y $ Do you want PANDA2 to change imperfection amplitudes?
300.0 $ Axial halfwavelength of typical general buckling mode, AXLWAV(1)
```

The behavior of the margins is much smoother.

Figure 22 displays the behavior of the objective function with use of the two strategies. It is much more likely that a good "global" optimum design will be determined with the use of Strategy (2). Also, the final optimum design will not be overly conservative because the general buckling modal imperfection shapes with short axial wavelengths, which are unlikely to exist in actual fabricated shells, will most probably be "filtered" out during optimization cycles.

15.2 "Oscillating" slope of nodal lines of general buckling modal imperfection

Near the end of Part 2 of Table 10 appear the following lines:

```
***** Multiple Minima Eigenvalues vs Slope for Mode (M,N)= 1 3 *****
Normalized ratio, (eig2-eig1)/abs(eig2-eig1)= -1.0000E+00 for iteration no. 1
I,SLOPE,EIGENVALUE= 1 4.7076E-01 2.2526E+00
I,SLOPE,EIGENVALUE= 2 1.9665E+00 2.2476E+00
*****
```

For the optimized design in this case, corresponding to general buckling with $(m,n) = (1,3)$ (axial,circumferential) halfwaves, there are two very different nodal line slopes with almost equal eigenvalues (buckling load factors). Figure 23 shows a plot of buckling load factor vs general buckling nodal line slope for the optimized configuration listed in Table 2. The reader can imagine that with designs slightly different from the optimum design, the general buckling mode shape changes abruptly. At one design cycle a mode shape with a nodal line slope near 0.50 is critical whereas at the next design cycle a mode shape with a nodal line slope near 2.0 is critical. Abrupt changes such as this give rise to abrupt changes in the curvature changes and twist, W_{xx} , W_{yy} , W_{xy} , of the imperfect shell as it bends under the design load. As with the abruptly different axial and circumferential wavenumbers (m,n) from design cycle to cycle discussed previously, abrupt changes in slope of the buckling nodal lines for given (m,n) from design cycle to cycle also make it very difficult to find a "global" optimum design.

Figure 24 is a "design sensitivity" plot which exhibits a sharp change in many of the margins caused by an abrupt change in slope of the nodal lines of the critical general buckling mode with (m,n) fixed at $(1,3)$ (axial, circumferential) halfwaves. One can well imagine that discontinuities of this sort make it very difficult to find a "global" optimum design.

After much thought, it was decided to modify PANDA2 as described in Item 620 of [17], part of which is quoted here:

"*****IMPORTANT CHANGE ***** IMPORTANT CHANGE *****"

Because of the unavoidable "discontinuous" behavior described in news ITEM NO. 617 [see Fig. 24 in this paper], I decided to make a major change in the model of behavior of shells and panels with initial buckling modal imperfections. The "discontinuous" behavior makes it very difficult and time consuming to find "global" optimum designs because several of the design margins jump around with small changes in decision variables. The unavoidable jagged behavior is caused, in many of the cases explored, by abrupt significant changes in slope of the buckling nodal lines with tiny changes in some of the decision variables. (See Tables 617.2, 3, 5 in ITEM NO. 617). In two cases explored here, "testax4" and "testax3" (See ITEM NO. 600 for geometry, material properties, loading, etc.) the modification described next completely eliminates the "discontinuous" behavior and produces without difficulty optimum designs that weigh less than those previously found and that are confirmed to be safe designs through comparisons of PANDA2 predictions with predictions from the STAGS computer program.

"Briefly, the modification is this: The buckling modal imperfections are assumed to have the classical 'checkerboard' configuration, that is, the slopes of the nodal lines in the imperfection shapes for general, inter-ring, and local buckling modal imperfections are assumed to be zero. This assumption seems to be a reasonable one, especially since it is well known that the behavior of a cylindrical shell under pure in-plane shear loading, N_{xy} , (a loading that produces non-zero slope of buckling nodal lines) is not very sensitive to initial imperfections.

"Although the modification is a very significant one from a philosophical point of view, it was very easy to implement in PANDA2: Wherever SUBROUTINE CURIMP (in which W_{xx} , W_{yy} , W_{xy} are computed) is called in SUBROUTINE STRIMP, the argument for the value of the slope of the buckling modal nodal lines, CSLOPU, is replaced by zero.

"*****"

Figure 25 shows the result of this change. Comparison of Fig. 25 with Fig. 24 reveals that:

1. The discontinuity of the margins at ring height $H(RNG)$ equal approximately to 8.1 inches (Fig. 24) has been eliminated.
2. Many of the buckling margins have been raised somewhat even for $6.5 < H(RNG) < 8.0$ inches. (See Margins 9 and 19, for examples). They have been raised because the effect of slope of buckling nodal lines on the prebuckling bending and twist, W_{xx} , W_{yy} , W_{xy} , is now neglected.

Figure 26 shows design margins vs $H(RNG)$ for load set 2: imperfection amplitude, $W_{imp} = -1.0$ inch rather than $+1.0$ inch. Note especially that Margins 1 and 2 are now critical at the design configuration, $H(RNG) = 7.977$ inches, whereas with $W_{imp} = +1.0$ inch they were not critical. With $W_{imp} = -1.0$ inch there never was any discontinuity such as that shown in Fig. 24, which applies to Load Set 1 ($W_{imp} = +1.0$ inch).

16.0 EVALUATION OF OPTIMIZED DESIGNS WITH STAGS

The PANDA2 processor called STAGSUNIT [7] produces input files, *.bin and *.inp, for the STAGS computer program [27-30]. Figures 1-3 and 12 - 19 are examples of STAGS models generated by STAGSUNIT. STAGSUNIT was designed in such a way that subdomains of a panel or shell can be analyzed by STAGS for which the behavior is reasonably close to that of the subdomain as embedded in the entire shell (except for shells with significant in-plane shear loading N_{xy} combined with general buckling modal imperfections). Figures 2 and 3 are subdomains of the shell shown in Fig. 1. It is emphasized that STAGS is not used within optimization cycles. It is used only to evaluate an optimum design previously obtained by PANDA2.

Various strategies required to obtain good results with STAGS in cases involving significant nonlinear behavior are discussed in [3,7,8,9,11,16]. Some of the difficulties encountered are described there.

16.1 How to use STAGS for the analysis of imperfect shells

In order to use STAGS to evaluate a shell with a general buckling modal imperfection, one must:

1. Obtain an optimum design with PANDA2 via multiple executions of SUPEROPT.
2. Use STAGSUNIT to generate input files, *.bin and *.inp, for STAGS operating in its linear bifurcation buckling mode (STAGS analysis type index INDIC=1).
3. Run STAGS multiple times in its linear bifurcation buckling branch with various "eigenvalue shifts" in order to find one or more general buckling modes.
4. Edit the *.bin and *.inp files (or run STAGSUNIT again with different input) to prepare for a nonlinear static equilibrium run with STAGS (STAGS analysis type index INDIC=3). Include at least one buckling modal imperfection in the *.inp file.
5. Run the nonlinear static (INDIC=3) STAGS case and inspect the results after execution.
6. Multiple nonlinear static STAGS runs are usually required to obtain a collapse load. With each run it may be necessary to add one or more nonlinear bifurcation buckling modes as additional imperfection shapes in order to "trigger" collapse [8,9]. (See Subsection 18.5 for an example).
7. It may be necessary to follow Step 6 with a series of nonlinear dynamic STAGS runs [11] in order to determine the maximum load-bearing capability of a shell. This step is used in the STAGS analysis of the re-optimized "testax3" case, as described in Section 18.0.

16.2 Difficulty finding general buckling modes with numerically large STAGS models

When PANDA2 optimizes a stiffened cylindrical shell with a general buckling modal imperfection, it often happens that for the optimum design the general buckling load factor of the perfect shell is higher than many of the buckling load factors corresponding to various kinds of local buckling, such as local buckling of the panel skin between stiffeners and various local buckling modes of the stiffener cross sections. With STAGS models of the optimized design it may be very tedious to find the relatively rare eigenvalues that correspond to general buckling modes because they are hidden in a "haystack" of eigenvalues that correspond to local buckling. This phenomenon is described in [7, 16]. (See Figs. 23 and 24 of [16] for a good example). In order to use STAGS to evaluate an optimum design previously obtained by PANDA2 for a globally imperfect cylindrical shell, one must first find at least one general buckling mode with the STAGS model to use as an initial imperfection shape.

Figure 27 shows one of the many local buckling modes (Mode 275 in this case) that interfere with the acquisition of

a general buckling mode such as that shown in Fig. 13 (Mode 336). In order to find general buckling mode shapes one must often make many, many linear buckling STAGS runs with the use of different initial "eigenvalue shifts", a tedious process indeed. In cases involving stiffened shells it is very helpful first to obtain general buckling modes and eigenvalues from models in which one or both sets of stiffeners (stringers and rings) are "smeared out". (STAGSUNIT can do this). Then one has a good idea what value to assign to the initial "eigenvalue shift" in numerically large models in which the stiffeners are modeled as shell branches. Figure 28 shows the general buckling mode in a model in which the stringers are "smeared out" and the rings are shell branches. Note that in this case the eigenvalue, $p_{cr} = 1.6516$, is very close to that for a similar model in which both the stringers and the rings are modeled as shell branches (Fig. 12: $p_{cr} = 1.6491$).

16.3 Use of a subdomain to obtain approximate behavior from STAGS models

A "converged" model of the type shown in Fig. 1 has too many degrees of freedom for the STAGS analysis of complete cylindrical shells with dimensions such as those listed in Table 2. By "converged" is meant a model with a dense enough finite element mesh to capture with reasonable accuracy local buckling behavior of the stiffener cross sections. A dense mesh is needed over the stiffeners because the globally imperfect shell bends under the design load in such a way as to cause "early" local buckling of the stiffener cross sections. Figures 26 and 28 of [4] demonstrate this phenomenon.

In the cases explored in this paper the in-plane shear loading N_{xy} is fairly small compared to the axial compression N_x . Since it is well known that buckling loads of imperfect cylindrical shells under pure in-plane shear N_{xy} are not very sensitive to initial imperfections, it is thought that a reasonably good evaluation of the imperfect optimum design obtained by PANDA2 can be accomplished via STAGS models in which N_{xy} is set equal to zero. With $N_{xy} = 0$ and with an orthotropic shell (isotropic or orthotropic skin plus smeared stringers and rings), the general buckling modes have a "checkerboard" pattern (buckling nodal lines are oriented axially and circumferentially). Therefore, there are many planes of antisymmetry (axially oriented buckling nodal lines) of general buckling displacement around the circumference. In particular, for the optimum designs obtained here, for which the critical general buckling mode has three circumferential waves, with $N_{xy} = 0$ there exist six axially oriented buckling nodal lines spaced at intervals of 60 degrees. Therefore, we can analyze a subdomain of the complete cylindrical shell of length equal to the length of the cylindrical shell and spanning only 60 degrees of circumference. For this subdomain it is feasible to have a finite element mesh that is dense enough in the panel skin and stiffeners to capture with reasonable accuracy local buckling of the panel skin and stiffener cross sections.

Figure 29 shows general buckling of a 60-degree STAGS model in which the stringers are "smeared out" and the rings are shell branches. The general buckling mode has one half wave over the length and one half wave over the 60 degrees of circumference, which is equivalent to three full waves over the complete (360 deg.) circumference of the cylindrical shell. Note that the buckling load factor, $p_{cr} = 1.6823$, is reasonably close to $p_{cr} = 1.6516$ for the "full" model which includes N_{xy} (Fig. 28). The analogous model in which all the stiffeners are modeled as shell branches has the lowest general buckling load factor (mode 58) with $p_{cr} = 1.6544$, as displayed in Fig. 30. Plus and minus imperfections of the shape shown in Fig. 30 with amplitude W_{imp} equal to one inch are used in two nonlinear STAGS analyses to obtain the results shown in Fig. 31. According to STAGS the imperfect shell collapses at a load factor of about 1.22, about 22 per cent higher than the design load, load factor $PA = 1.0$.

Figures 32 and 33 show the distribution of normal displacement w at collapse for outward ($W_{imp} = +1.0$, Fig. 32) and inward ($W_{imp} = -1.0$, Fig. 33) general buckling modal imperfections.

17.0 PANDA2 WAS MODIFIED TO PRODUCE LESS CONSERVATIVE DESIGNS

From Fig. 31 it is seen that PANDA2 yields an optimum design (Table 2) that is rather conservative. According to PANDA2, the optimized shell fails at a load factor close to the design load, $PA = 1.0$. (See the margins listed in Table 8). In contrast, STAGS predicts failure of the same shell at $PA = 1.22$. Can PANDA2 be made less conservative while avoiding the danger of generating under-designed optima?

17.1 Modifications to make PANDA2 less conservative

The modifications are described in Items 633 and 634 of [17]. They are:

1. The "knockdown" factor RNGKNZ to compensate for the unconservativeness of smearing rings according to the theory of [38] is now computed in a way that yields lower values when the rings are spaced farther apart than an axisymmetric axial bending "boundary layer" length BLL and higher values when the rings are spaced closer together than half the axial distance BLL. "BLL" stands for "Boundary Layer Length". For an isotropic monocoque cylindrical shell, $BLL = 2.73 * \sqrt{(\text{radius} \times \text{thickness})}$. For an orthotropic cylindrical shell, such as a shell with isotropic or orthotropic skin with smeared stringers, $BLL = 2.73 * \sqrt{(\text{radius} \times (\text{effective thickness}))}$, in which

$$(\text{effective thickness}) = \sqrt{C44n * 12 / C22}$$

where $C44n$ is the axial bending stiffness about the neutral axis for axial bending of the shell skin plus smeared stringers and $C22$ is the circumferential extensional stiffness of the same shell wall. For ring spacing between BLL and $0.5 * BLL$, a quantity RNGFCT that varies linearly between zero and unity is computed. If the ring spacing is greater than BLL then RNGFCT equals zero; if the ring spacing is less than $0.5 * BLL$ then RNGFCT equals unity.

As written previously, PANDA2 computes a ratio, RATIO, as follows:

Buckling load factor for circ. waves $n+dn = FNARCQ = 2.9922$
from discrete "skin"-ring model [6], Fig. 8 here: $EIGR = 2.7921E+00$

Buckling load factor for "skin"-ring module from the simple formula for a ring with bending stiffness EI:
 $\text{pcrit} = [(n+dn)^{**2}-1] * EI / r^{**3} / p = EIGRNG = 3.6051E+00$

Knockdown ratio for "smeared" ring model of general buckling,
 $\text{RATIO} = EIGR / EIGRNG = 7.7449E-01$

Note that fractional circumferential waves, $n+dn = FNARCQ$ are used. The numbers just listed correspond to the optimized geometry given in Table 2. If RATIO is less than 0.9, the "knockdown" factor RNGKNZ is now given by

$$\text{RNGKNZ} = \text{RATIO} + \text{RNGFCT} * (0.9 - \text{RATIO})$$

If RATIO is greater than or equal to 0.9 then $\text{RNGKNZ} = \text{RATIO}$. For the geometry listed in Table 2 the ring spacing is less than $0.5 * BLL$. Therefore, the quantity RNGFCT = 1.0 and RNGKNZ = 0.9. This is a less conservative "knockdown" factor than that used by PANDA2 previously, $\text{RNGKNZ} = 0.77449$.

2. The factor of safety for the outstanding flange of a stiffener buckling as a beam on an elastic foundation (the web) has been reduced from 3.0 to 1.2. Hence, the margins listed in Part 1 of Table 8 for the imperfect shell with geometry given in Tables 1 and 2,

11 1.80E-01 buckling stringer Iseg 4 as beam on foundation. M=221;MID.;FS=3.0
13 6.61E-02 buckling ring Iseg 4 as beam on foundation. M=114;MID.;FS=3.0

will now be far from critical for the same design.

3. The factor of safety for stiffener rolling without participation of the panel skin has been reduced from 1.6 to 1.4. Hence, the margin listed in Part 1 of Table 8,

19 -4.77E-03 buck.(SAND);rolling only of stringers;M=12;N=0;slope=0.;FS=1.6

will no longer be critical for the same design.

17.2 Determination of a new optimum design

Figure 34 shows the objective vs design iterations for one execution of SUPEROPT. Previously [5,7,16] SUPEROPT permitted a maximum of about 275 design iterations. (See Fig. 2 in [16]). Now SUPEROPT permits about 475 design iterations. Each "spike" in the plot in Fig. 34 corresponds to a new "starting" design, which is established randomly by the AUTOCHANGE processor [5]. At iterations between 150 and about 175, between 300 and about 325, and between 430 and about 455, the "starting" design becomes the best "ALMOST FEASIBLE" design found since the beginning of the SUPEROPT run rather than being determined by AUTOCHANGE. The move limits of the decision variables for the establishment of succeeding designs in each design cycle are temporarily severely restricted until the next execution of AUTOCHANGE. At the next execution of AUTOCHANGE in the SUPEROPT process the move limits are reset to their original values. This strategy is new and is used in order to capture more reliably the local minima in the neighborhoods of the best acceptable design determined at each of the three times (approximately Iteration 160, approximately Iteration 310, and approximately Iteration 440) during the SUPEROPT process. At exactly which iteration the move limits become temporarily severely restricted depends on how many PANDAOPTs per AUTOCHANGE the user decides on (See [5]) and how many design iterations per PANDAOPT the user chooses during the MAINSETUP interactive session (*.OPT file).

The dimensions of the re-optimized design after one SUPEROPT execution are listed in Table 14. The new optimum weight of 180 degrees of the stiffened cylindrical shell is 10620 lb compared to 11510 lb listed for the old optimum design in Table 2. Table 15, which is analogous to Table 3, lists the margins obtained when the amplitude of the initial imperfection is set equal to zero. Table 16, which is analogous to Table 8, lists the margins with imperfection amplitudes $W_{imp} = +1.0$ and -1.0 inch when Strategy(2) has been used (Subsection 15.1).

18.0 STAGS MODELS OF THE NEW DESIGN

Figures 35 - 71 give results from STAGS models of the new optimum design obtained by PANDA2. The STAGS 480 finite element is used in most of the models and the 410 finite element is used in the rest.

18.1 Bifurcation buckling and nonlinear static STAGS models spanning 60 degrees

Figure 35, analogous to Fig. 29 for the old optimum design, shows the general buckling mode from a 60-degree STAGS model in which $N_{xy} = 0.0$ and the stringers have been "smeared" [38]. Note that, according to STAGS, general buckling of the perfect shell now occurs at a load factor, $p_{cr} = 1.3753$. The analogous model of the old design yields a general buckling load factor, $p_{cr} = 1.6823$ (Fig. 29).

From Table 15 the two margins for general buckling of the perfect shell according to PANDA2 are

13 4.13E-01 buck.(SAND);simp-support general buck;M=1;N=3;slope=8.9127;FS=.999
14 4.06E-01 buck.(SAND);simp-support general buck;(0.85*altsol);FS=0.999

which correspond to general buckling load factors close to 1.413 and 1.406, respectively. These predictions are reasonably close to the STAGS prediction, $p_{cr} = 1.3753$.

The general buckling mode shape shown in Fig. 35 is used as an imperfection shape in nonlinear STAGS runs with this 60-degree model with imperfection amplitudes, $W_{imp} = +1.0$ inch and $W_{imp} = -1.0$ inch. Figure 36 shows the lowest nonlinear bifurcation buckling mode for $W_{imp} = +1.0$ inch ($p_{cr} = 1.1244$), and Fig. 37 shows the lowest nonlinear bifurcation buckling mode for $w_{imp} = -1.0$ inch ($p_{cr} = 1.0872$).

With $W_{imp} = +1.0$ inch the initial imperfection resembles the shape plotted in Fig. 35. The imperfect shell bulges outward. During loading of the imperfect shell the outstanding flanges of the rings experience tension and the panel skin experiences more hoop compression than occurs for the perfect shell. Therefore, as seen in Fig. 36, nonlinear bifurcation buckling does not occur in the ring flanges and occurs instead in the panel skin with smeared stringers as an inter-ring mode with relatively short circumferential waves.

With $W_{imp} = -1.0$ inch the initial imperfection pinches inward. During loading of the imperfect shell the outstanding flanges of the rings experience compression and the panel skin experiences less hoop compression than occurs for the perfect shell. Therefore, as seen in Fig. 37, nonlinear bifurcation buckling occurs in at least one of the outstanding ring flanges before buckling of the panel skin with smeared stringers.

For $W_{imp} = +1.0$ inch the relevant margins for buckling of the imperfect shell from PANDA2 are listed in Part 3 of Table 16 as

- 1 5.28E-02 Local buckling from discrete model-1.,M=1 axial halfwaves;FS=0.99
- 2 5.48E-02 Bending-torsion buckling; M=1 ;FS=0.999
- 4 1.22E-01 (m=1 lateral-torsional buckling load factor)/(FS)-1;FS=0.999
- 5 4.27E-03 Inter-ring buckling, discrete model, n=35 circ.halfwaves;FS=0.999

(NOTE: The sign convention for positive initial imperfection amplitude in PANDA2 is opposite to that in STAGS).

Margins 1, 2, and 4 correspond to buckling of the type shown in Figs. 14 and 15; there is significant deformation of the stringer cross section. Therefore, these types of buckling cannot be predicted from a STAGS model in which the stringers are "smeared" (Fig. 36). Margin 5 corresponds to buckling of the type shown in Fig. 36.

Margins 1 - 4 correspond to buckling load factors close to $p_{cr}(PANDA2) = 1.0528, 1.0548, 1.122$, and 1.00427 , respectively. These are in reasonably good agreement with the buckling load factor from the STAGS model shown in Fig. 36: $p_{cr} = 1.1244$.

For $W_{imp} = -1.0$ inch the relevant margins for buckling of the imperfect shell from PANDA2 are listed in Part 1 of Table 16 as

- 1 2.21E-01 Local buckling from discrete model-1.,M=1 axial halfwaves;FS=0.99
- 2 2.23E-01 Bending-torsion buckling; M=1 ;FS=0.999
- 4 2.08E-01 (m=1 lateral-torsional buckling load factor)/(FS)-1;FS=0.999
- 5 -2.92E-02 Ring flang buckling,discrete model,n=65 circ.halfwaves;FS=0.999
- 6 -2.88E-02 Lo-n Ring sidesway, discrete model, n=8 circ.halfwaves;FS=0.999

As with Margins 1, 2, and 4 listed in Part 3 of Table 16, Margins 1, 2, and 4 listed in Part 1 of Table 16 correspond to buckling of the type shown in Figs. 14 and 15 and therefore cannot be predicted from a STAGS model with "smeared" stringers. Margin 5 corresponds to buckling of the type shown in Fig. 37. Margin 6 corresponds to buckling of the ring in a mode with a relatively long circumferential wavelength. This mode is not displayed by the STAGS model, perhaps because it is masked by many, many short-wavelength modes of the type shown in Fig. 37. It is possible that the long-circumferential-wavelength ring buckling mode only exists in the PANDA2 model because of the assumption in PANDA2 that the additional compression, dN_x , in the outstanding ring flange due to prebuckling circumferential bending of the shell with the general buckling modal imperfection (see Section 6.0) is uniform in the circumferential direction. According to PANDA2 the buckling load factor corresponding to a buckling mode of the type shown in Fig. 37 is approximately $p_{cr}(PANDA2) = 0.9708$, reasonably close to the STAGS prediction, $p_{cr} = 1.0872$, and conservative.

Figures 38, 39, and 40 are analogous to Figs. 35, 36, and 37, respectively. They pertain to a 60-degree STAGS model in which both stringers and rings are modeled as flexible shell branches (shell "units" in STAGS jargon). Note especially from Fig. 39 that this numerically much larger STAGS model permits deformation of the cross sections of the stringers in the buckling mode. Therefore, Margins 1, 2, and 4 in Part 3 of Table 16 can be compared to the critical nonlinear bifurcation buckling load factor, $p_{cr} = 1.0495$, from the STAGS model. There is very good agreement between the predictions of PANDA2 and STAGS for this very detailed STAGS model.

Figure 41 shows the deformation of the panel with $W_{imp} = +1.0$ inch at the critical load factor, $p_{cr} = 1.04299$. The nonlinear static STAGS analysis was unable to find any solution beyond that for Step 15. A series of nonlinear dynamic STAGS runs was therefore executed. The results of this dynamic analysis are discussed in Subsection 18.4.1.

Figure 42 shows the deformation of the panel with $W_{imp} = -1.0$ inch at the critical load factor, $p_{cr} = 1.10073$. The

nonlinear static STAGS analysis was unable to find any solution beyond that for Step 13. As with the model with $W_{imp} = +1.0$ inch, a dynamic analysis of the type described in [11] permits continuation of the nonlinear solution beyond Step 13. The results of this dynamic analysis are discussed in Subsection 18.4.2.

18.2 Bifurcation buckling and nonlinear static STAGS models spanning 360 degrees

Figures 43 and 44 show results from a 360-degree STAGS model in which the stringers are "smeared" and the in-plane shear load $N_{xy} = 20000$ lb/in is included in the model. The cylindrical shell has a general buckling modal imperfection with amplitude $W_{imp} = 1.0$ inch and with shape similar to that shown in Figs. 12 and 28, buckling mode $(m,n) = (1,3)$. The linear general buckling load factor is $p_{cr}(STAGS) = 1.4278$, which is in good agreement with the load factor from PANDA2 associated with the $(m,n) = (1,3)$ general buckling mode: $p_{cr}(PANDA2) = 1.413$. The circumferential spacing of the mesh is varied in order to capture with reasonable accuracy the short-wavelength nonlinear bifurcation buckling of the outstanding flanges of Rings 6 and 7 as displayed in Fig. 44.

The results from this 360-degree STAGS model are qualitatively similar to those for the 60-degree models displayed in Figures 35 and 37. However, note that the 60-degree model shown in Fig. 41 exhibits a significantly higher maximum **outward** normal displacement, $+w(\max) = 4.600$ inches at load factor $PA = 1.04299$, than does the 360-degree model in which $+w(\max) = 3.768$ inches at load factor $PA = 1.14573$. A small part of this difference probably arises from the fact that in the 60-degree model displayed in Fig. 41 the stringers are modeled as flexible shell branches. Most of the difference arises from the essential difference in behavior of the 60-degree model from that of the 360-degree model in the nonlinear regime of moderately large deformation. The two straight (longitudinal) edges of the 60-degree model are free to deform in the plane of the panel skin. This deformation is present to some degree at nodal lines of the general buckling modal imperfection in the 360-degree model, which occur at 60-degree intervals around the circumference of the shell. However, the in-plane circumferential deformation of each nodal line is constrained by the presence of the remaining shell structure, structure that does not exist in the 60-degree model.

It is emphasized that a similar discrepancy between the results of the 60-degree and 360-degree models does not exist for maximum **inward** displacement, $-w(\max)$. This can be seen from an inspection of Fig. 45.

18.3 Load bearing capability of the re-optimized imperfect shells: nonlinear static models

Figure 45, which pertains to the new optimum design listed in Table 14, should be compared to Fig. 31, which pertains to the old optimum design listed in Table 2. Unfortunately, in most of the STAGS models peaks in the load-deflection curves could not be determined for the new optimum design with the use of nonlinear static STAGS models because of the presence of clusters of nonlinear bifurcation buckling modes of the types shown in Figs. 39, 40 and 44. These prevented the continuation of static nonlinear solutions beyond the load steps listed in Figs. 39, 41, 42 and 43. As mentioned in Subsection 16.1, a series of dynamic STAGS analyses as described in [11] solves this problem. (See Subsection 18.4). An exception is the curve in Fig. 45 with the label containing the string, "w in stringr 11 flange, node 28379". The STAGS model and sequence of computer runs leading to this curve is described in Subsection 18.5. Another exception is the curve in Fig. 45 with the label containing the string, "w, midbay 6, stringer 1 flange, rightmost edge" (Subsection 18.5). A third exception are the curves with the labels containing the string, "w, midbay 1, stringer 14 flange". They are derived from the "compound" STAGS model described in Subsection 18.7.

Although all except four of the load-deflection curves in Fig. 45 have positive slopes at their highest load factors, indicating additional load-bearing capability, it is best at this point (before any dynamic analyses) to consider the maximum load-bearing capability from the STAGS models to be about $PA = 1.05$ (Figs. 39-42). $PA = 1.05$ is approximately the load factor at which nonlinear inter-ring bifurcation buckling of the panel skin and stringers occurs as is shown in Fig. 39 and the load factor at which the outstanding flanges of the rings buckle as shown in Fig. 40. This load factor, $PA = 1.05$, is in very good agreement with the results from PANDA2: minimum $PA = 0.9600$ corresponding to the minimum margin listed in Part 3 of Table 16:

16 -4.00E-02 buck.(SAND);simp-support general buck;(0.85*altsol);FS=0.999

Figure 46 shows prebuckling axial and circumferential stress resultants, N_x and N_y , in the panel skin and stress resultant N_x along the axes of the outstanding ring flange and outstanding stringer flange from STAGS and PANDA2 for the shell with general buckling modal imperfections with amplitudes $W_{imp} = +1.0$ and $W_{imp} = -1.0$ inch. Generally the predictions of PANDA2 are conservative compared to those of STAGS. The one exception is N_x in the stringer flange for $W_{imp} = -1.0$ inch, for which the PANDA2 prediction is slightly unconservative compared to the STAGS prediction.

18.4 Nonlinear dynamic STAGS runs

Notice that in Figs. 45 and 46 there are plotted some data points that fall along horizontal lines at various load factors. On the **right-hand** sides of Figs. 45 and 46 the horizontally oriented data points occur at load factors $PA = 1.063$ (60-degree STAGS model with $W_{imp} = +1.0$ inch, Fig. 41) and $PA = 1.118$ (360-degree STAGS model, Fig. 43). On the **left-hand** sides of Figs. 45 and 46 the horizontally oriented data points occur at load factors $PA = 1.088$ (60-degree STAGS model with $W_{imp} = -1.0$ inch, Fig. 42) and $PA = 1.118$ (360-degree STAGS model, Fig. 43). These load factors are each two per cent higher than the highest load factor attained for the nonlinear static analysis of the corresponding model with general buckling modal imperfection amplitudes, $W_{imp} = +1.0$ inch (**right-hand** sides of Figs. 45 and 46) and $W_{imp} = -1.0$ inch (**left-hand** sides of Figs. 45 and 46). Three dynamic STAGS runs were executed, one for the 60-degree STAGS model with $W_{imp} = +1.0$ inch (Fig. 41), one for the 60-degree STAGS model with $W_{imp} = -1.0$ inch (Fig. 42), and one for the 360-degree STAGS model with $W_{imp} = 1.0$ inch. The states of each of these STAGS models after completion of the dynamic runs are displayed in Figs. 47, 48 and 49, respectively. During each of the dynamic runs (STAGS analysis type index, $INDIC = 6$) the load factor PA was held constant at $PA = 1.063$, 1.088 , and 1.118 , respectively.

18.4.1 60-degree STAGS model with $W_{imp} = +1.0$ inch: The constant load factor applied in this case is 1.063, two per cent higher than the highest load factor attained ($PA = 1.042$) for the nonlinear static analysis of the 60-degree STAGS model with a general buckling modal imperfection amplitude, $W_{imp} = +1.0$ inch, and with one additional nonlinear bifurcation buckling modal imperfection with amplitude $W_{imp}(\text{skin + smeared stringers}) = 0.05$ inch, corresponding to inter-ring buckling with the mode shape displayed in Fig. 39. STAGS cannot find any solution of the dynamic model beyond time step number 220. (time = 0.020704 seconds). These results indicate that the 60-degree STAGS model with $W_{imp} = +1.0$ inch collapses at a load factor PA between 1.042 and 1.063. Figure 47 shows the state of the panel at $PA = 1.063$, time step 220. Comparison of Fig. 47 with Fig. 41 reveals that there is significant additional deformation of the stringer that runs along the longitudinal edge at the bottom of the figure. Also, the maximum outward normal displacement at time step 220 is 6.97 inches, in contrast to $+w(\max) = 4.60$ inches plotted in Fig. 41.

18.4.2 60-degree STAGS model with $W_{imp} = -1.0$ inch: The constant load factor applied in this case is 1.088, two per cent higher than the highest load factor attained ($PA = 1.067$) for the nonlinear static analysis of the 60-degree STAGS model with a general buckling modal imperfection amplitude, $W_{imp} = -1.0$ inch, and with three additional nonlinear bifurcation buckling modal imperfections, each with amplitude $W_{imp}(\text{flanges}) = 0.03$ inch, corresponding to buckling of the outstanding flanges of Rings 6, 7 and 8. The three additional buckling modal imperfection shapes resemble the nonlinear bifurcation buckling mode shown in Fig. 40. STAGS cannot find any solution of the dynamic model beyond time step number 200. (time = 0.0222156 seconds). These results indicate that the 60-degree STAGS model with $W_{imp} = -1.0$ inch and with three additional nonlinear bifurcation buckling modal imperfections with amplitude $W_{imp}(\text{flanges}) = 0.03$ inch, corresponding to buckling of the outstanding flanges of Rings 6, 7 and 8, collapses at a load factor PA between 1.067 and 1.088. The horizontally oriented string of data points on the left-hand side of Fig. 46 correspond to the stress resultant N_x along the axis of the outstanding flange of Ring No. 6. At load factor $PA = 1.088$ an N_x data point is plotted for every 20th time step. Notice that although the maximum inward normal displacement w continues to become more and more negative with time (horizontally oriented string of data points on the left-hand side of Fig. 45 at $PA = 1.088$), the horizontally oriented data points for N_x on the left-hand side of Fig. 46 at $PA = 1.088$ indicate diminishing compression in the outstanding flange of Ring No. 6 with time. This unloading is counterintuitive. It occurs for two reasons: 1. Ring No. 6 is undergoing considerable sidesway, as demonstrated in Fig. 48, and 2. the outstanding flange of Ring No. 6 has an imperfection shape similar to that shown in Fig. 40; the amplitude of this imperfection shape increases with time. The increasing waviness in the imperfect outstanding flange relieves the axial compression N_x as time increases. Figure 48 shows the state of

the panel at $PA = 1.088$, time step 200. It is obvious that the panel has failed. (Compare Fig. 48 with Fig. 42, which shows the state of the panel at the highest load factor attainable in the nonlinear static analysis).

18.4.3 360-degree STAGS model with $Wimp = 1.0$ inch: The constant load factor applied in this case is 1.118, two per cent higher than the highest load factor attained ($PA = 1.09565$) for the nonlinear static analysis of the 360-degree STAGS model with a general buckling modal imperfection amplitude, $Wimp = 1.0$ inch, and with two additional nonlinear bifurcation buckling modal imperfections, each with amplitude $Wimp(\text{flanges}) = 0.03$ inch, corresponding to buckling of the outstanding flanges of Rings 6 and 7 in the neighborhood of the circumferential station where the finite element grid is concentrated and where the imperfection is maximum inward. The two additional buckling modal imperfection shapes resemble the nonlinear bifurcation buckling mode shown in Fig. 44. STAGS cannot find any solution of the dynamic model beyond time step number 180. (time = 0.02775 seconds). These results indicate that the 360-degree STAGS model with $Wimp = 1.0$ inch and with two additional nonlinear bifurcation buckling modal imperfections with amplitude $Wimp(\text{flanges}) = 0.03$ inch, corresponding to buckling of the outstanding flanges of Rings 6 and 7, collapses at a load factor PA between 1.09565 and 1.118. The collapse load is higher for the 360-degree STAGS model than for the 60-degree STAGS models probably because the stringers are smeared out in the 360-degree model. The horizontally oriented string of data points on the left-hand side of Fig. 46 at $PA = 1.118$ correspond to the stress resultant Nx along the axis of the outstanding flange of Ring No. 6. At load factor $PA = 1.118$ an Nx data point is plotted for every 10th time step. Notice that although the maximum inward normal displacement w continues to become more and more negative with time (horizontally oriented string of data points on the left-hand side of Fig. 45 at $PA = 1.118$), the horizontally oriented data points for Nx on the left-hand side of Fig. 46 indicate diminishing compression in the outstanding flange of Ring No. 6 with time. This unloading occurs for the same reasons given near the end of Subsection 18.4.2. Figure 49 shows the state of the shell at $PA = 1.118$, time step 180. It is obvious that the cylindrical shell has failed. (Compare Fig. 49 with Fig. 43, which shows the state of the 360-degree shell at the highest load factor attainable in the nonlinear static analysis).

18.5 Nonlinear static 60-degree STAGS model with locally dense grid and $Wimp = -1.0$ inch and $+1.0$ inch

Figures 50 – 55 pertain to this subsection. The STAGS 480 finite elements are concentrated in the middle bay (Bay No. 6), especially at mid-circumference, as shown in Fig. 50. Figure 50, analogous to Fig. 38, displays the general buckling modal imperfection shape. In this section the actual imperfection shape is the negative of that in Fig. 50. The main purposes of concentrating the finite element mesh are to capture possible very local buckling of the outstanding flanges of the stringers, as depicted in Fig. 17, and to capture possible local buckling of the shell skin between adjacent stringers.

The behavior of the STAGS model was obtained during a rather long sequence of computer runs, analogous to those described in [8,9]. The computer runs required to determine the static load-bearing capability of the shell in this case are as follows:

Run No.	Purpose of the run	Buckling modal imperfections (amplitude, loadstep, mode no., run no.)	Comments, Fig. No.
1	Get linear general buckling mode.		Fig. 50
2	Determine nonlinear behavior of 60-deg. panel with general buckling modal imperfection with $Wimp = -1.0$; Obtain some nonlinear buckling modal imperfection shapes at $PA = 1.08$.	(-1.0, 0, 31, 1)	Maximum $PA = 1.08$. Got 4 additional buckling modal imperfections: Fig. 51 + 3 ring flange buckling modes of the type shown in Fig. 40.
3	Determine nonlinear behavior of panel with general buckling modal imperfection plus the four additional nonlinear buckling modal imper-	(-1.0, 0, 31, 1) (+0.03, 10, 1, 2) (+0.03, 10, 3, 2) (+0.03, 10, 5, 2)	Maximum $PA = 1.08$. Got 4 additional buckling modes of the type shown in Fig. 52 (local buckling

	fections found at Step 10 of Run 2. Obtain 4 more nonlinear buckling modal imperfections.	(+0.03, 10, 7, 2)	of stringer flanges).
4	Determine nonlinear behavior of panel with general buckling modal imperfection plus the four additional nonlinear buckling modal imperfections found at Step 10 of Run 2 plus the four additional nonlinear buckling modal imperfections found at Step 10 of Run 3. The shell has a total of 9 buckling modal imperf.	(-1.0, 0, 31, 1) (+0.03, 10, 1, 2) (+0.03, 10, 3, 2) (+0.03, 10, 5, 2) (+0.03, 10, 7, 2) (+0.01, 10, 1, 3) (+0.01, 10, 3, 3) (+0.01, 10, 6, 3) (+0.01, 10, 8, 3)	Maximum PA = 1.08. Ring 7 flange buckling Ring 6 flange buckling Ring 8 flange buckling See Fig. 51. Stringer 11 flange buckling Str. 9,10 flange + rolling Stringer 9 flange buckling See Fig. 52.
5	Determine nonlinear behavior with the same buckling modal imperf. as were used in Run 4. Starting load factor, PA = 0.987265 (Step 9).	(same 9 buckling modal imperfections as used in Run 4.)	Maximum PA = 1.08. Purpose is to refine the nonlinear analysis.
6	Determine nonlinear behavior with the same buckling modal imperf. as were used in Runs 4 & 5. Starting load factor, PA = 1.08 (Step 14). Obtain 2 more nonlinear buckling modal imperfections.	(same 9 buckling modal imperfections as used in Runs 4 and 5.)	Maximum PA = 1.08883 (Step 21). Purpose is to refine the nonlinear run and get 2 more nonlinear buckling modal imperf. (Figs 52 and 53).
7	Determine nonlinear behavior with the same buckling modal imperf. as were used in Runs 4,5,6 plus two additional nonlinear buckling modal imperfections from Run 6.	Same 9 buckling modal imperfections as used in Runs 4 and 5 and 6 plus (-0.05, 21, 1, 6) (+0.01, 21, 3, 6)	Maximum PA = 1.06156 (Step 13). The shell starts to collapse. See Fig. 53. Similar to Fig. 52.
8	Determine nonlinear behavior with the same buckling modal imperf. as were used in Run 7. Starting load factor, PA = 1.06156 (Step 13). We enter the unstable phase.	(same 11 buckling modal imperfections as used in Run 7.)	Maximum PA = 1.06156. Purpose is to refine the nonlinear analysis and continue as the shell collapses. Run terminates (max. time) at Step 25, for which PA = 1.04693.

Figures 50 – 53 show four of the buckling modes used as imperfection shapes. The others are described very briefly in the list above.

Figure 54 shows the state of the shell at the end of Run 8. The largest deformation occurs in Bay 7, unfortunately not where the nodal point density is highest, that is, in the middle of Bay 6. The largest normal displacement w is in the outstanding flange of Stringer 11 (counting from the bottom of the figure) in Bay 7, on the right-most edge of the stringer flange between Finite Element 4 and Finite element 5 to the right of Ring 7 (Nodal Point No. 28379 in the STAGS finite element model).

Figure 55 shows the normal displacement w versus load factor PA at the two nodal points, 28379 and 28383, on the opposing right-most and left-most edges of the outstanding flange of Stringer 11. The difference in w at the two nodal points is caused by a combination of rolling of Stringer 11 and local buckling of the outstanding flange of Stringer 11 in modes analogous to those shown in Figs. 14 and 17, respectively. Collapse of the shell occurs at about PA = 1.06, six per cent higher than the failure load predicted by PANDA2, which is the design load, PA = 1.0.

The curve corresponding to normal displacement w at nodal point 28379 is also plotted on the left-hand side of Fig. 45.

Nonlinear static load-deflection behavior was also determined for the refined 60-degree STAGS model shown in Fig. 50 with initial general buckling modal imperfection amplitude, $W_{imp} = +1.0$ inch. The last three curves identified in Fig. 45 were obtained from a series of three nonlinear computer runs in which there are nine buckling modal imperfections: the general buckling modal imperfection with $W_{imp} = +1.0$ plus eight nonlinear buckling modal imperfections that correspond to various modes of local buckling at load factor PA close to 1.035. The eight nonlinear buckling modal imperfections have very small amplitudes, from $W_{imp(\text{local})} = 0.01$ to $W_{imp} = 0.03$. The maximum load-carrying capability is $PA = 1.025$, just 2.5 per cent higher than the design load factor, $PA = 1.0$.

18.6 Some difficulties encountered with STAGS models

18.6.1 Failure to converge at low load factor PA: Figure 44 shows a STAGS model of a complete (360-degree) cylindrical shell in which the mesh density is varied only in the circumferential direction. Many attempts were made without success with an analogous model in which the mesh density is varied in **both** the axial and in the circumferential directions, as is done in the 60-degree model displayed in Fig. 50. With the 480 finite element, nonlinear STAGS runs exhibit failure of convergence at load factors in the neighborhood of $PA = 0.65$, a load level well below that corresponding to any type of nonlinear general or local collapse, which is approximately $PA = 1.05$. This “early” failure occurs when the “drilling” degrees of freedom are suppressed. A change in the finite element from 480 to 410 eliminates this problem but introduces another as described next.

18.6.2 Failure to converge “from above” with increasing mesh density: Usually (but not always; see Figs. 31 and 32 in [7]) STAGS models constructed with the 480 finite element “converge from above”. In other words, an increase in mesh density leads to a decrease in buckling load factors, for example. That is why the 480 finite element is used in the work described here and in [7] and [16]. An attempt was made to find the load-bearing capability of the optimized cylindrical shell (Table 14) with use of the 410 finite element and a mesh density that varies in both the axial and circumferential directions. As mentioned in the previous paragraph the “early” convergence failure of such a model is avoided with use of the 410 element rather than the 480 element. However, nonlinear buckling of the outstanding flanges of the rings, such as shown in Fig. 44, occurs where the mesh is sparse rather than where the mesh is dense. This leads to poor estimates of buckling load factors and poor representation of the corresponding local buckling modes and therefore poor estimates of the nonlinear behavior of a shell with buckling modal imperfections of the type shown in Fig. 44. In a model of the complete cylindrical shell analogous to that shown in Fig. 44 except that the mesh density is higher in Bays 5 – 7 than in Bays 1 – 4 and Bays 8 – 11, the first eight nonlinear buckling modes of the shell with a general buckling modal imperfection similar in shape to that shown in Fig. 12 correspond to buckling of the outstanding flanges of the rings at locations completely outside the region where the mesh is dense. Unfortunately, STAGS can only find about eight nonlinear bifurcation buckling eigenvalues at a given load level, as described in the next paragraph.

18.6.3 Failure of the eigenvalue extraction part of STAGS to converge when many modes are needed: The first author has found from his experience with STAGS that nonlinear bifurcation buckling load factors can be found for up to about eight buckling modes at a given load level. If the user calls for more there is usually failure of convergence for many of the modes before the maximum permitted number of iterations (22 iterations) is reached. It may often occur, especially with configurations such as the one investigated here, that many, many local nonlinear buckling modal imperfection shapes are needed in order to compute the load-bearing capability of an imperfect ring and stringer stiffened shell from static analysis. In order to reach a maximum in the load-deflection curve of an imperfect stiffened shell that previously has been optimized by PANDA2, one must introduce enough local buckling modal imperfection shapes to convert the many bifurcations that occur on the nonlinear equilibrium path into nonlinear behavior that permits nonlinear continuation up to and beyond the maximum static load attainable by the structure.

18.6.4 The general buckling modes obtained by STAGS sometimes have short-wavelength “noise”: The word “noise” is perhaps a bad choice. The short-wavelength component of the general buckling mode represents a real physical phenomenon. The buckling mode that most resembles general buckling actually has both long and short

wavelength components. The presence of the short-wavelength component or components does not usually signify a lack of convergence to a true eigenvector, but is most often actually part of the “general buckling” mode shape. The short-wavelength components commonly occur in general buckling modes of stiffened shells that have been optimized. For optimized stiffened shells long and short wavelength buckling load factors predicted from approximate theories such as those used in PANDA2 are often very close. See Tables 8 and 16, for examples. Doubtless it is this closeness that usually gives rise to the general buckling modes that are called “noisy” in this paper. Figure 39 of [7] and to some extent Fig. 30 in this paper exhibit this phenomenon. Also see Fig. 63 here. Compare Fig. 63 with Fig. 62. For an especially “noisy” general buckling mode shape, see Fig. 71. The presence of the short-wavelength “noise”, which may be a significant component of the general buckling mode, often leads to a collapse load that is less than that predicted by PANDA2 for a shell with only a general buckling modal initial imperfection. This is because “early” failure occurs in one or more of the regions where the short-wavelength “noise” in the general buckling mode shape is of especially high amplitude. The “collapsed” shapes displayed in Figs. 64 and 65 are examples.

18.6.5 Spurious Buckling modes: Figure 7 in [7] shows an example of a spurious buckling mode in a STAGS model with 410 finite elements. Figures 67 and 68 in this paper display a nonlinear buckling mode in a model with 410 finite elements that appears to be partly spurious. The overall shape of the buckling mode makes sense, but the part of it located in the region where the mesh is most dense (midway between Rings 6 and 7) has the typical “jagged” characteristic of a spurious mode. Figure 70 exhibits “hourgassing” of the 410 finite elements in a region of the shell where the stringers are smeared out. If spurious nonlinear buckling modes are not used as initial imperfections in a subsequent nonlinear analysis, does the **potentially** spurious behavior still affect convergence to a nonlinear solution? The latent spurious nonlinear buckling eigenvalues must affect the condition number of the stiffness matrix of the loaded shell. Therefore, they must make convergence more difficult.

18.6.6 Gap in a spectrum of nonlinear eigenvalues: STAGS computes eigenvalues at user-specified load factors (INDIC=4) or at the end of a nonlinear run (INDIC = 3). During this research the first author has noticed that if some of these eigenvalues are negative and some are positive there is often a significant gap in the spectrum between negative and positive eigenvalues. This gap is especially noticeable if the nonlinear eigenvalues occur as a cluster corresponding, for example, to buckling of the outstanding flanges of different rather closely spaced stringers or rings. In general it seems that if the nonlinear eigenvalue is negative it underestimates of the nonlinear buckling load factor and if it is positive it overestimates the nonlinear buckling load factor. The underestimation or overestimation is significant only if the nonlinear eigenvalues are larger than about 0.05. In ordinary engineering applications the discrepancy is not important. It has been noticeable in the present work only because we are comparing predictions from PANDA2 and STAGS, which differ in the order of ten per cent. Hence, we notice discrepancies in the order of one per cent, which represents about ten per cent of the difference in predictions between PANDA2 and STAGS.

18.7 Nonlinear 360-degree compound STAGS models with general buckling modal imperfection Wimp=1 in.

18.7.1 Compound STAGS model: A STAGS model with 480 finite elements and a general buckling modal imperfection shape are displayed in Fig. 56. Sixty degrees of the circumference is modeled with both stringers and rings as branched shell units. The remaining 300 degrees has the stringers smeared and only the rings as branched shell units. The mesh in the 60-degree portion is less dense than that shown in Fig. 50. In each of the two regions the nodal point spacing is uniform in both shell coordinate directions.

Figure 56 represents the 19th mode (the first general buckling mode). Figure 57 shows the first buckling mode, which is characterized by buckling between adjacent rings with pronounced stringer rolling. The first buckling mode is similar to that shown in Fig. 14.

It is emphasized that in this particular case the STAGS **linear buckling analysis** was executed with the index **ILIN set equal to unity** in each of the 88 shell units in the model. ILIN = 1 means that STAGS uses linear kinematic relationships. (In all previous runs ILIN was always zero). With ILIN = 1, STAGS overestimates buckling load factors associated with mode shapes with relatively short wavelengths. Setting ILIN = 1 therefore makes it somewhat less tedious to find the relatively rare, long-wavelength general buckling modes “hidden” like needles in a “haystack” of short-wavelength local modes such as that shown in Fig. 57. Setting ILIN = 1 for the linear

bifurcation buckling analysis also seems to have another beneficial effect. The general buckling modes, when found, tend to be relatively unpolluted by short-wavelength “noise”, such as is displayed in Fig. 39 of [7] and to some degree in Fig. 30 of this paper. (However, see Figs. 63 and especially Fig. 71 for counter examples!). For all **nonlinear** runs **ILIN should be reset to zero** in the input for every shell unit. With $ILIN = 1$ in the nonlinear analyses the stiffness of shells deforming in short-wavelength modes is overestimated, with the result that the collapse load is likely to be overestimated. This problem is avoided with the choice $ILIN = 0$ in nonlinear STAGS runs ($INDIC=3$).

18.7.2 Compound imperfect shell with $Wimp = -1.0$ inch: The compound STAGS model with a general buckling modal imperfection equal to the **negative** of the shape displayed in Fig. 56 was run in the STAGS nonlinear static analysis branch ($INDIC = 3$, Run 2). Figure 58 shows the eighth nonlinear bifurcation buckling mode corresponding to load step 17, at which the load factor PA is close to 1.054. This mode shape is characterized mostly by rolling of the stringers with various axial half-wavelengths. The deformation shown in Fig. 58 was introduced as an additional imperfection shape with an amplitude, $Wimp(2) = 0.05$ inch, and a new nonlinear STAGS run was initiated starting at the very small load factor $PA = 0.05$. At the completion of this run (Run 3) new potential imperfection shapes were computed. Nonlinear buckling eigenvalues 4 and 8, computed at the load factor $PA = 1.08$, correspond to buckling of the outstanding flanges of Rings 7 and 6, respectively. Figure 59 shows the nonlinear bifurcation buckling mode corresponding to buckling of Ring 7. The buckling mode corresponding to buckling of Ring 6 (counting from the left-hand side of Fig. 59) is similar in nature. Another nonlinear STAGS run (Run 4) was launched, again starting at the small load factor, $PA = 0.05$. The maximum load factor reached was $PA = 1.078$. STAGS was unable to converge for $PA > 1.078$. Therefore, a transient run of the imperfect shell [general imperfection with $Wimp(1) = -1.$ inch plus the imperfection shown in Fig. 58 with $Wimp(2) = 0.05$ inch plus two imperfections of the type shown in Fig. 59, both with amplitudes, $Wimp(3) = Wimp(4) = 0.01$ inch] was launched at a load level two per cent higher than 1.078, that is, at $PA = 1.10$. Figure 60 shows the state of the shell at the end of this transient run. The failure mode is similar to that shown in Fig. 48. Collapse occurs between load factor $PA = 1.078$ and $PA = 1.10$.

18.7.3 Compound imperfect shell with $Wimp = +1.0$ inch: For this case a sequence of nonlinear static runs of the imperfect shell, with the general buckling modal imperfection shape shown in Fig. 56 and two additional nonlinear bifurcation buckling modal imperfections similar in nature to that shown in Fig. 58, led to determination of the static collapse load at load factor, $PA = 1.0852$. Collapse occurs locally in the neighborhood of the left-hand side of the shell in Stringers 13 and 14 (counting from the lower part of the 60-degree detailed part of the compound model shown in Fig. 56). Figure 61 shows the state of Stringer 14 after collapse has occurred. Stringer 13 exhibits a similar deformation with the opposite sign. It is not shown in Fig. 61 because part of the deformed Stringer 13 overlaps the deformed Stringer 14, obscuring the local buckling phenomenon. The two curves in Fig. 45 with labels containing the string, “w, midbay 1, stringer 14 flange”, show the normal displacement of the left and right-hand sides of the outstanding flange of Stringer 14 in the middle of Bay 1 as functions of load factor PA . Compare the collapse load from this model, $PA = 1.0852$, with the static collapse load, $PA = 1.06$, from the model shown in Fig. 50 with $Wimp = -1.0$ inch, and the collapse load, $PA = 1.024$, from the same 60-degree model with $Wimp = +1.0$ inch. The 60-degree model shown in Fig. 50 is slightly conservative. However, read Subsection 18.7.4.

18.7.4 Compound model with mesh density that varies in one or two shell coordinate directions: The nodal point density in the detailed 60-degree sector of the compound model shown in Fig. 56 is not sufficient to capture very local stringer flange buckling modes of the types shown in Fig. 52. A compound model analogous to that shown in Fig. 50 is required for that. Figure 62 displays a compound model in which the mesh density in the 60-degree sector is varied only in the circumferential direction. A nonlinear run was attempted with use of the negative of the general buckling mode shown in Fig. 62 as an initial imperfection. Unfortunately, STAGS was unable to obtain a converged nonlinear equilibrium state for load factor $PA > 0.919$. No nonlinear bifurcation buckling eigenvalues were nearby at this load level and the stiffness matrix condition number was reasonably large. The problem appears to be the same as that described in Subsection 18.6.1. Analysis of the same model with use of the 410 finite element rather than the 480 finite element eliminated this problem but introduced another: a somewhat “noisy” general buckling mode shape, as shown in Fig. 63. The general buckling mode consists of the usual skewed $(m,n) = (1,3)$ pattern, but superposed on this is a pattern of short-wavelength inter-ring rolling of the stringers. Unfortunately, the amplitude of the short-wavelength rolling of the stringers is largest outside the central region where the mesh density is highest. Figure 64 shows the mode of collapse corresponding to an imperfection shape which is the negative of that shown in Fig. 63, that is, $Wimp = -1.0$ inch. Figure 65 shows the mode of collapse

corresponding to $W_{imp} = +1.0$ inch. The results displayed in Figs. 64 and 65 were obtained from transient STAGS runs following nonlinear static STAGS runs. For the negative imperfection, $W_{imp} = -1.0$ inch, collapse occurs between $PA = 0.900$ and 0.95. For the positive imperfection, $W_{imp} = +1.0$ inch, collapse occurs between $PA = 0.95$ and 1.00. The “early” collapse (compared to that from “480” models with no short-wavelength “noise” in the imperfection shape) is probably caused by the rather high-amplitude level of the stringer rolling component of the general buckling imperfection shape. Figure 66 shows a STAGS model with 410 finite elements in which the mesh density varies in both the x and y shell coordinate directions. In this model the nodal point mesh in the 60-degree sector is identical to that displayed in Fig. 50 except in the outstanding flanges of rings and stringers. Half as many nodal points occur across the widths of the flanges in the model shown in Fig. 66. The **negative** of the general buckling mode shape in Fig. 66 was used as an initial imperfection, that is, $W_{imp} = -1.0$ inch. The first nonlinear STAGS run ended at a load factor, $PA = 1.018$. Unfortunately, some of the nonlinear buckling modes computed at that load level exhibit spurious behavior, such as that displayed in Figs. 67, 68 and 70 (described in Subsection 18.6.5). A nonlinear transient run with load factor PA held constant at $PA = 1.018$ stopped after only 27 time steps, at which time the minimum permitted time step criterion in STAGS terminated the run. Figure 69 shows the state of the shell. Notice that compared to the general buckling mode shape displayed in Fig. 66, the state of the shell in Fig. 69 exhibits considerable stringer rolling in the region where the nodal point density is highest. It is unknown why there are so many cuts in the time step during the very early phase of the transient run in this case. Perhaps the latent presence of spurious modes is responsible. Perhaps there are real bifurcations on the nonlinear path corresponding to local buckling of the outstanding stringer flanges, such as that shown in Fig. 52. Because of these uncertainties it is unknown whether the load factor, $PA = 1.018$, represents a prediction of actual physical collapse of the shell or results from numerical difficulties. A final attempt to obtain a collapse load was made, this time with use of the 480 finite element. The “general” buckling mode predicted with this model is shown in Fig. 71. There is too much short-wavelength “noise” in the general buckling mode to attempt a nonlinear collapse run in this case.

19.0 CONCLUSIONS

1. The behavior of a **stiffened shell with a general buckling modal imperfection** is very different from that for a **monocoque shell**. For the example explored here the most significant effect is the **redistribution of prebuckling stress between skin and stiffener segments as the imperfect cylindrical shell bends under the design load**. The effect of increase in the effective radius of the imperfect shell is relatively mild in the case explored here (Table 9).
2. The agreement between PANDA2 and STAGS predictions for a “global” optimum design obtained by PANDA2 is good enough to qualify PANDA2 for the optimum design of imperfect stiffened cylindrical panels and shells under combined load.
3. PANDA2 has been improved as described in Sections 15.0 and 17.1 as a result of comparisons with STAGS models.
4. Two of the difficulties obtaining “global” optimum designs of imperfect stiffened cylindrical shells were overcome as described in Section 15.0. The possible difficulty of finding general buckling mode shapes from STAGS models, as described in the discussion associated with Fig. 27, still remains.
5. The use of STAGS models spanning 60 degrees appears to be a reasonably accurate substitute for a complete cylindrical shell in the examples explored here. This greatly reduced domain permits the modeling of both stringers and rings as flexible shell units rather than having to “smear” the stringers.
6. In order to continue the nonlinear equilibrium STAGS analyses beyond what is possible with static models, it is often necessary to resort to dynamic models of the type used in [11]. These dynamic models lead to reasonable upper bounds of the collapse loads.
7. At least one finite element should be introduced into STAGS that **reliably** “converges from above”. The user should be able easily to determine many more than eight nonlinear bifurcation buckling load factors and mode shapes at any given load level.
8. Some of the most complex compound STAGS models explored here (Figs. 66 and 71, for examples) cannot be

used to predict collapse because of failure of convergence to a nonlinear equilibrium state at too low a load factor (18.6.1), or a “noisy” general buckling mode shape (imperfection shape, 18.6.4), or the presence of spurious nonlinear buckling modes (18.6.5).

20.0 ACKNOWLEDGMENT

David Bushnell is indeed grateful to his friend and colleague, Frank Weiler, for the time he spent setting up the latest version of STAGS at the Lockheed Martin Advanced Technology Center, for providing directories on various workstations where large STAGS models could be run, and for his frequent assistance with many mysteries involving the computer throughout the course of the effort leading to this paper.

21.0 REFERENCES

- [1] Bushnell, D., "PANDA2 - Program for minimum weight design of stiffened, composite, locally buckled panels", COMPUTERS AND STRUCTURES, Vol. 25, No. 4, pp 469-605, 1987
- [2] Bushnell, D., "Theoretical basis of the PANDA computer program for preliminary design of stiffened panels under combined in-plane loads", COMPUTERS AND STRUCTURES, v. 27, No. 4, pp 541-563 (1987).
- [3] Bushnell, D., "Optimization of composite, stiffened, imperfect panels under combined loads for service in the postbuckling regime", Computer Methods in Applied Mechanics and Engineering, Vol. 103 (1993) 43-114
- [4] Bushnell, D. and Bushnell, W. D., "Approximate method for the optimum design of ring and stringer stiffened cylindrical panels and shells with local, inter-ring, and general buckling modal imperfections" Computers and Structures, Vol. 59, No. 3, pp 489-527 (1996)
- [5] Bushnell, D., "Recent enhancements to PANDA2" AIAA Paper 96-1337-CP, Proc. AIAA 37th Structures, Structural Dynamics and Materials Conference, pp 126-182, April, 1996.
- [6] Bushnell, D., Jiang, H., and Knight, N.F., "Additional buckling solutions in PANDA2", Proceedings 40th AIAA SDM Conference, AIAA Paper 99-1233, pp 302-345 April 1999
- [7] Bushnell, D. and Rankin, C.C., "Optimization of perfect and imperfect ring and stringer stiffened cylindrical shells with PANDA2 and evaluation the optimum designs with STAGS", AIAA Paper 2002-1408, Proc. AIAA 43rd SDM Meeting, pp 1562-1613, April 2002
- [8] Bushnell, D. and Bushnell, W.D., "Minimum-weight design of a stiffened panel via PANDA2 and evaluation of the optimized panel via STAGS", Computers and Structures, Vol. 50, No. 4, pp 569-602 (1994)
- [9] Bushnell, D. and Bushnell, W.D., "Optimum design of composite stiffened panels under combined loading", Computers and Structures, Vol. 55, pp 819-856 (1995)
- [10] Bushnell, D., "Optimum design via PANDA2 of composite sandwich panels with honeycomb or foam cores", AIAA Paper 97-1142, Proc. 38th AIAA Structures, Structural Dynamics and Materials Conference, pp 2163-2202, April, 1997
- [11] Bushnell, D., Rankin, C.C., and Riks, E., "Optimization of stiffened panels in which mode jumping is accounted for", AIAA Paper 97-1141, Proc. 38th AIAA SDM Conference, pp 2123-2162, April 1997
- [12] Bushnell, D., "Global optimum design of externally pressurized isogrid stiffened cylindrical shells with added T-rings", Int. J. Non-Linear Mechanics, Vol. 37, Nos 4-5, pp 801-831 (2002)
- [13] Bushnell, D., "Optimization of panels with riveted Z-shaped stiffeners via PANDA2", in Advances in the

Mechanics of Plates and Shells, Durban, D, Givoli, D., and Simmonds, J.G., Eds, Kluwer Academic Publishers, pp 79-102 (2001)

[14] Bushnell, D., "Truss-core sandwich design via PANDA2", Computers and Structures, Vol. 44, No. 5, pp 1091-1119 (1992)

[15] Bushnell, D., Holmes, A.M.C., Flaggs, D.L., McCormick, P.J., "Optimum design, fabrication and test of graphite- epoxy curved, stiffened, locally buckled panels loaded in axial compression", in BUCKLING OF STRUCTURES, edited by I. Elishakoff, et al, Elsevier, Amsterdam, pp 61-131, 1988

[16] Bushnell, D. and Rankin, C.C., "Optimum design of stiffened panels with substiffeners", AIAA Paper 1932, 46th AIAA Structures, Structural Dynamics and Materials Meeting, Austin, TX, April 2005

[17] Bushnell, D., .../panda2/doc/panda2.news, a continually updated file distributed with PANDA2 that contains a log of all significant modifications to PANDA2 from 1987 on.

[18] Vanderplaats, G. N., "ADS--a FORTRAN program for automated design synthesis, Version 2.01", Engineering Design Optimization, Inc, Santa Barbara, CA, January, 1987

[19] Vanderplaats, G. N. and Sugimoto, H., "A general-purpose optimization program for engineering design", Computers and Structures, Vol. 24, pp 13-21, 1986

[20] Bushnell, D., "Stress, stability and vibration of complex, branched shells of revolution", Computers & Structures, vol. 4, pp 399-435 (1974)

[21] Bushnell, D., "Buckling of Shells--Pitfall for Designers", AIAA Journal, Vol. 19, No. 9, September, 1981, pp. 1183-1226

[22] Bushnell, D., "Computerized Analysis of Shells--Governing Equations", Computers & Structures, Vol. 18, pp.471-536, 1984

[23] Bushnell, D., *Computerized Buckling Analysis of Shells*, published by Nijhoff, The Netherlands, 1985, reprinted by Kluwer Academic Publishers, 1989

[24] Bushnell, D., "BOSOR4--Program for stress, buckling, and vibration of complex shells of revolution," in STRUCTURAL MECHANICS SOFTWARE SERIES, vol. 1, Univ. Press of Virginia, pp 11-143, 1977. Also, see also, STRUCTURAL ANALYSIS SYSTEMS, Vol. 2, Editor: A. Niku-Lari, Pergamon Press, 1986, pp 25-54

[25] Bushnell, D., "Stress, buckling and vibration of prismatic shells", AIAA Journal, Vol. 9, No. 10, pp 2004-2013, Oct. 1971

[26] Bushnell, D., "Automatic optimum design of shells of revolution with application to ring-stiffened cylindrical shells with wavy walls", AIAA Paper 2000-1663, 41st AIAA Structures Meeting, Atlanta, GA, April 2000

[27] B. O. Almroth, F. A. Brogan, "The STAGS Computer Code", NASA CR-2950, NASA Langley Research Center, Hampton, VA.(1978)

[28] C. C. Rankin, P. Stehlin and F. A. Brogan, "Enhancements to the STAGS computer code", NASA CR 4000, NASA Langley Research Center, Hampton, VA, November 1986

[29] Riks, E., Rankin C. C., Brogan F. A., "On the solution of mode jumping phenomena in thin walled shell structures", First ASCE/ASM/SES Mechanics Conference, Charlottesville, VA, June 6-9, 1993, in: Computer Methods in Applied Mechanics and Engineering, Vol.136, 1996.

[30] G. A. Thurston, F. A. Brogan and P. Stehlin, "Postbuckling analysis using a general purpose code", AIAA Journal, 24, (6) (1986) pp. 1013-1020.

[31] J. N. Dickson, S. B. Biggers, and J. T. S. Wang, "Preliminary design procedure for composite panels with open-section stiffeners loaded in the post-buckling range," in: Advances in Composite Materials, A. R. Bunsell, et al, editors, Pergamon Press Ltd., Oxford, England, 1980, pp 812-825. Also see, J. N. Dickson and S. B. Biggers, "POSTOP: Postbuckled open- stiffened optimum panels, theory and capability", NASA Langley Research Center, Hampton, Va., NASA Contractor Report from NASA Contract NAS1 -15949, May 1982.

[32] Butler, R. and Williams, F. W., "Optimum design features of VICONOPT, an exact buckling program for prismatic assemblies of anisotropic plates," AIAA Paper 90-1068-CP, Proceedings 31st AIAA/ASME Structures, Structural Dynamics, and Materials Meeting, pp 1289-1299. Also see Williams, F. W., Kennedy, D., Anderson, M.S., "Analysis features of VICONOPT, an exact buckling and vibration program for prismatic assemblies of anisotropic plates,", AIAA Paper 90-0970-CP, Proceedings 31st AIAA/ASME Structures, Structural Dynamics, and Materials Meeting, pp 920-929

[33] M. S. Anderson and W. J. Stroud, "General panel sizing computer code and its application to composite structural panels," AIAA Journal, 17, (1979) pp. 892-897. Also see W. J. Stroud and M. S. Anderson, "PASCO: Structural panel analysis and sizing code, capability and analytical foundations," NASA TM-80181, NASA Langley Research Center, Hampton, Va., 1981. Also see W. J. Stroud, W. H. Greene and M. S. Anderson, "Buckling loads of stiffened panels subjected to combined longitudinal compression and shear: Results obtained with PASCO, EAL, and STAGS computer programs," NASA TP 2215, NASA Langley Research Center, Hampton, Va., January 1984.

[34] Wong, K. F. W. and Weaver, P. M., Approximate solution for the compression buckling of fully-anisotropic cylindrical shells, 45th AIAA Structures, Structural Dynamics & Materials Conference, April 2004, Palm Springs, California

[35] Weaver, P. M., On optimisation of long anisotropic flat plates subject to shear buckling loads, 45th AIAA SDM Conference, April 2004

[36] Diaconu, C. G. and Weaver, P. M., Approximate solution and optimum design for postbuckling of infinite laminated composite plates subjected to compression loading, 45th AIAA SDM Conference, April 2004

[37] Hilburger, M. W., Nemeth, M. P., Riddick, J. C., and Thornburgh, R. P., Effects of elastic edge restraints and initial prestress on the buckling response of compression-loaded composite panels, 45th AIAA SDM Conference, April 2004

[38] Baruch, M. and Singer, J., Effect of eccentricity of stiffeners on the general instability of stiffened cylindrical shells under hydrostatic pressure, Journal of Mechanical Engineering Science, 5, (1) (1963) pp.23-27.

[39] Arbocz, J., The effect of initial imperfections on shell stability - An updated review, Delft University Faculty of Aerospace Engineering Report LR-695, September 1992, especially Eq.(3.61)

[40] Arbocz, J. and Hol, J. M. A. M., On the reliability of buckling load predictions, AIAA Paper 94-1371, Proc. 35th AIAA Structures, Structural Dynamics, and Materials Conference, Hilton Head SC, 514-527 (1993).

[41] Arbocz, J. and Hol, J., Shell stability analysis in a computer aided engineering (CAE) environment, AIAA Paper 93-133, Proc. 34th AIAA Structures, Structural Dynamics, and Materials Conference, La Jolla, CA, 300-314 (1993).

[42] Stein, M, The phenomenon of change of buckling patterns in elastic structures, NASA Technical report R-39, NASA (1959)

[43] A. W. Leissa, Buckling of laminated composite plates and shell panels, AFWAL-TR-85-3069, Air Force Wright Aeronautical Laboratories, Wright-Patterson AFB, Ohio 45433, June, 1985.

[44] R. R. Arnold and J. C. Parekh, Buckling, postbuckling, and failure of flat and shallow-curved, edge-stiffened composite plates subject to combined axial compression and shear loads, Presented at 27th SDM Meeting, San

Antonio, TX., April 1986, AIAA Paper No. 86-1027-CP, 1986, Proceedings pp. 769-782.

- [45] J. H. Starnes,Jr., N. F. Knight,Jr. and M. Rouse, Postbuckling behavior of selected flat stiffened graphite- epoxy panels loaded in compression, AIAA Paper 82-0777, presented at AIAA 23rd Structures, Structural Dynamics, and Materials Conference, New Orleans, May, 1982. See also, AIAA J., 23, (8) (1985) pp.1236-1246.
- [46] E. E. Spier, On experimental versus theoretical incipient buckling of narrow graphite/epoxy plates in compression, Proc. AIAA 21st SDM Conference, AIAA Paper 80-0686-CP, May, 1980.
- [47] E. E. Spier, Local buckling, postbuckling, and crippling behavior of graphite-epoxy short thin-walled compression members, Naval Air Systems Command, Washington, D. C., NASC-N00019-80-C-0174, July 1981.
- [48] N. R. Bauld, Jr. and N. S. Khot, A numerical and experimental investigation of the buckling behavior of composite panels, Computers and Structures, 15 (1982) pp. 393-403.
- [49] N. S. Khot and N. R. Bauld, Jr., Further comparison of the numerical and experimental buckling behaviors of composite panels, Computers and Structures, 17, (1983) pp. 61-68.
- [50] Y. Zhang and F. L. Matthews, Postbuckling behavior of anisotropic laminated plates under pure shear and shear combined with compressive loading, AIAA Journal, 22, (2), (1984) pp 281-286.
- [51] Stoll, F. and Gurdal, Z., "Nonlinear analysis of compressively loaded linked-plate structures, AIAA Paper 90-0968-CP, Proceedings 31st AIAA/ASME Structures, Structural Dynamics, and Materials Meeting, pp 903-913 (1990).
- [52] Stoll, F. and Gurdal, Z., and Starnes, J. H., Jr., A method for the geometrically nonlinear analysis of compressively loaded prismatic composite structures," VIPSU Center for Composite Materials and Structures Report CCMS-91-03 (VPI-E-91-01), February, 1991
- [53] Shin, D. K., Gurdal, Z., and Griffin, O. H., Jr., Minimum weight design of laminated composite plates for postbuckling performance, AIAA Paper 91-0969-CP, Proceedings 32nd AIAA/ASME Structures, Structural Dynamics, and Materials Meeting, pp 257-266 (1991)
- [54] Ley, R.P., Gurdal, Z., and Johnson, E.R. (1993). Optimal design of imperfect, anisotropic, ring-stiffened cylinders under combined loads. AIAA Paper 93-1526-CP, Proceedings of 34th AIAA Structures, Structural Dynamics, and Materials Conference, Part 4, pp 1881-1889.
- [55] Ley, R.P., Johnson, E.R., and Gurdal, Z. (1992). Buckling of imperfect, anisotropic, ring-stiffened cylinders under combined loads. AIAA Paper 92-2232-CP, Proceedings of 33rd AIAA Structures, Structural Dynamics, and Materials Conference, Part 1, pp 86-94.
- [56] Nagendra, S., Haftka, R. T., and Gurdal, Z. (1992). Stacking sequence optimization of simply supported laminates with stability and strain constraints. AIAA Paper 92-2310-CP, Proceedings of 33rd AIAA Structures, Structural Dynamics, and Materials Conference, Part 5, pp. 2526-2535.
- [57] Le Riche, R. and Haftka, R. T. (1992). Optimization of laminate stacking sequence for buckling load maximization by genetic algorithm. AIAA Paper 92-2314-CP, Proceedings of 33rd AIAA Structures, Structural Dynamics, and Materials Conference, Part 5, pp. 2564-2575.
- [58] Lombardi, M., Haftka, R. T., and Cinquini, C. (1992). Optimization of composite plates for buckling by simulated annealing. AIAA Paper 92-2313-CP, Proceedings of 33rd AIAA Structures, Structural Dynamics, and Materials Conference, Part 5, pp. 2552-2563.
- [59] Librescu, L. and Chang, M.-Y. (1993). Effects of geometric imperfections on vibration of compressed shear deformable laminated composite curved panels. Acta Mechanica, 96, 203-224.

- [60] Librescu, L. and Souza, M. A. (1991). Postbuckling behavior of shear deformable flat panels under the complex action of thermal and in-plane mechanical loadings. AIAA Paper 91-0913-CP, Proceedings of 32nd AIAA Structures, Structural Dynamics, and Materials Conference, Part 2, pp. 917-925.
- [61] Librescu, L. and Stein, M. (1991). A geometrically nonlinear theory of transversely isotropic laminated composite plates and its use in the post-buckling analysis. *Thin-Walled Structures*, 11, 177-201.
- [62] Graves-Smith, T.R. and Sridharan, S., A finite strip method for the post-locally-buckled analysis of plate structures, *Int. J. Mech. Sci.*, Vol. 20, pp 833-843 (1978)
- [63] Peng, M-H and Sridharan, S., Optimized design of stiffened panels subject to interactive buckling, AIAA Paper 90-1067-CP, Proceedings 31st AIAA/ASME Structures, Structural Dynamics, and Materials Meeting, pp 1279-1288
- [64] Meyers, C. A. and Hyer, M. W. (1992). Thermally-induced, geometrically nonlinear response of symmetrically laminated composite plates, AIAA Paper 92-2539-CP Proceedings of 33rd AIAA Structures, Structural Dynamics, and Materials Conference, Part 2, pp. 1027-1037.
- [65] Majeed, M. A. and Hyer, M. W., Mechanical behavior of inplane-loaded unsymmetrically laminated plates, *Collected Papers in Structural Mechanics Honoring Dr. James H. Starnes, Jr.*, NASA/TM-2006-214276, compiled by Norman F. Knight, Jr., Michael P. Nemeth, and John B. Malone, pp. 289-323, February 2006
- [66] Dano, M-L. and Hyer, M., Snap through behavior of unsymmetric composite laminates, *International J. of Solids & Structures*, Vol. 39, No. 1, pp. 2101-2120 (2002)
- [67] Nemeth, M. P. (1992). Buckling behavior of long symmetrically laminated plates subjected to compression, shear, and inplane bending loads. AIAA Paper 92-2286-CP, Proceedings of 33rd AIAA Structures, Structural Dynamics, and Materials Conference, Part 2, pp. 274-282.
- [68] Hilburger, M. W. and Nemeth, M. P., Buckling and failure of compression-loaded composite cylindrical shells with reinforced cutouts, *Collected Papers in Structural Mechanics Honoring Dr. James H. Starnes, Jr.*, NASA/TM-2006-214276, compiled by Norman F. Knight, Jr., Michael P. Nemeth, and John B. Malone, pp. 363-386, February 2006
- [69] Hilburger, M. W. and Starnes, J. H., Jr., Effects of imperfections on the buckling response of compression-loaded composite shells, *International J. of Non-linear Mechanics*, Vol. 37 pp. 623-643 (2002)
- [70] Hilburger, M. W., Nemeth, M. P., and Starnes, J. H., Jr., Shell buckling design criteria based on manufacturing imperfection signatures, *NASA/TM-2004-212659*, May 2004
- [71] Li, Y. W., Elishakoff, I., and Starnes, J. H., Jr., Axial buckling of composite cylindrical shells with periodic thickness variation, *Computers & Structures*, Vol. 56, No. 1, pp. 65-74 (1995)
- [72] Li, Y. W., Elishakoff, I., Starnes, J. H., Jr., and Shinozuka, M., Prediction of natural frequency and buckling load variability due to uncertainty in material properties by convex modeling, *Fields Institute Communications*, American Mathematical Society, Vol. 9, pp. 139-154 (1996)
- [73] Elishakoff, I., Li, Y. W., and Starnes, J. H., Jr., *Nonclassical Problems in the Theory of Elastic Stability*, Cambridge University Press, New York, January 2001
- [74] Abramovich, H., Weller, T., and Bisagni, C., Buckling behavior of composite laminated stiffened panels under combined shear and axial compression, *Collected Papers in Structural Mechanics Honoring Dr. James H. Starnes, Jr.*, NASA/TM-2006-214276, compiled by Norman F. Knight, Jr., Michael P. Nemeth, and John B. Malone, pp. 213-229, February 2006
- [75] Singer, J., Arbocz, J., and Weller, T., *Buckling Experiments – Experimental Methods in Buckling of Thin-Walled Structures*, John Wiley & Sons Inc., 2002

[76] Abramovich, H., Pevsner, P., Weller, T., Pecker, N. and Ghilai, G., Axial buckling of laminated composite stringer stiffened curved panels – tests vs. FE predictions, International Conference on Buckling and Postbuckling Behavior of Composite Laminated Shell Structures, March 1-2, 2004, Hilton Queen of Sheba Hotel, Eilat, Israel

[77] Abramovich, H., Pevsner, P., Weller, T. and Bisagni, C., The behavior of laminated composite stringer stiffened curved paels under torsion moments – Tests vs. FE predictions, International Conference on Buckling and Postbuckling Behavior of Composite Laminated Shell Structures, March 1-2, 2004, Hilton Queen of Sheba Hotel, Eilat, Israel

[78] Chamis, C. C. and Abumeri, G. H., Nonlinear dynamic buckling of a composite shell, *Collected Papers in Structural Mechanics Honoring Dr. James H. Starnes, Jr.*, NASA/TM-2006-214276, compiled by Norman F. Knight, Jr., Michael P. Nemeth, and John B. Malone, pp. 457-468, February 2006

[79] Noor, A. K., Starnes, J. H., Jr., and Peters, J. M. (1992). Thermomechanical buckling and postbuckling of multilayered composite panels. AIAA Paper 92-2541-CP, Proceedings of 33rd AIAA Structures, Structural Dynamics, and Materials Conference, Part 2, pp. 1052-1068.

[80] Koiter, W. T., Het Schuifplooiveld by Grote Overschrijdingen van de Knikspanning, National Luchtvaart Laboratorium, The Netherlands, Report X295, November 1946 (in Dutch)

[81] Koiter, W. T., The effect of axisymmetric imperfections on the buckling of cylindrical shells under axial compression, Kononkl. Ned. Akad. Wetenschap. Proc., B66, pp 265-279 (1963)

[82] Vinson, J. R., Optimum design of composite honeycomb sandwich panels subjected to uniaxial compression, AIAA Journal, Vol. 24, No. 10, October 1986

[83] Vinson, J. R., Comparison of optimized sandwich panels of various constructions subjected to in-plane loads, Proceedings of the First International Conference on Sandwich Constructions, Stockholm Sweden, pp 23-49 of SANDWICH CONSTRUCTIONS I, edited by K-A Olsson and R. P. Reichard, June 1989

[84] Plantema, F. J., *Sandwich Construction*, John Wiley, 1966

[85] Vinson, J. R., Analysis and optimization of composite and metallic sandwich cylindrical shells, Proceedings of the Second International Conference on Sandwich Constructions, SANDWICH CONSTRUCTIONS II, Florida, March 1992

Table 1 Geometry, Material Properties, and Loading

=====

Geometry (cylindrical shell):
Length = 300 inches
Radius = 100 inches
External T-shaped major stringers
External T-shaped major rings

Material properties (aluminum):
Young's modulus = 10 msi
Poisson ratio = 0.3
Maximum allowable stress = 1.0 msi (set high to avoid active stress constraints)

Loading used for all cases:
-100000.0 \$ Axial Resultant (lb/in), Nx(1) Load Set A
-20000.00 \$ Hoop Resultant (lb/in), Ny(1) Load Set A
20000.00 \$ In-plane shear (lb/in), Nxy(1) Load Set A
-200.0000 \$ Uniform pressure, (psi), p(1) Load Set A
Zero loading in Load Set B

Boundary conditions:
Simple support, but free to expand radially in the prebuckling phase.

Imperfection:
General buckling modal imperfection amplitude,
Wimp= +1.0 inch and -1.0 inch.

Imperfect shells have two load cases:
Load Case 1: Wimp = +1.0 inch
Load Case 2: Wimp = -1.0 inch

=====

Table 2 Optimum design of stiffened cylindrical shell (from Table 8, col.5 of [16])

DIMENSIONS OF CURRENT DESIGN...		
VARIABLE	CURRENT	DEFINITION
NUMBER	VALUE	
1	5.7644E+00	B(STR) :stiffener spacing, b: STR seg=NA, layer=NA
2	5.7644E-01	B2(STR) :width of stringer base, b2 (must be > 0, see
3	3.8010E+00	H(STR) :height of stiffener (type H for sketch), h: S
4	2.9990E+00	W(STR) :width of outstanding flange of stiffener, w:
5	5.6240E-01	T(1) (SKN) :thickness for layer index no.(1): SKN seg=1
6	3.2390E-01	T(2) (STR) :thickness for layer index no.(2): STR seg=3
7	2.3430E-01	T(3) (STR) :thickness for layer index no.(3): STR seg=4
8	2.7273E+01	B(RNG) :stiffener spacing, b: RNG seg=NA, layer=NA
9	0.0000E+00	B2(RNG) :width of ring base, b2 (zero is allowed): RNG
10	7.9770E+00	H(RNG):height of stiffener (type H for sketch), h: R
11	6.3630E+00	W(RNG):width of outstanding flange of stiffener, w:
12	7.2520E-01	T(4) (RNG):thickness for layer index no.(4): RNG seg=3
13	4.7750E-01	T(5) (RNG):thickness for layer index no.(5): RNG seg=4

SOME DEFINITIONS:

"STR" = stringer (axial stiffener)

"RNG" = ring (circumferential stiffener)

"SKN" = panel skin

layer index no. 1 = panel skin

layer index no. 2 = stringer web

layer index no. 3 = stringer outstanding flange

layer index no. 4 = ring web

layer index no. 5 = ring outstanding flange

NOTE:

In PANDA2 the complete cylindrical shell is modeled as a panel that spans 180 degrees. In the absence of in-plane shear loading (torque, N_{xy}) the behavior of the 180-degree panel simply supported along its two straight edges is identical to that of a complete cylindrical shell. If N_{xy} is small compared to $\sqrt{N_x^2 + N_y^2}$ the panel model is good enough for preliminary design.

CURRENT VALUE OF THE OBJECTIVE FUNCTION:

1.151E+04	WEIGHT OF THE ENTIRE PANEL (180 deg. of cylindrical shell, lbs)
TOTAL WEIGHT OF SKIN	= 5.2978E+03
TOTAL WEIGHT OF SUBSTIFFENERS	= 0.0000E+00
TOTAL WEIGHT OF STRINGERS	= 3.1602E+03
TOTAL WEIGHT OF RINGS	= 3.0476E+03
SPECIFIC WEIGHT (WEIGHT/AREA) OF STIFFENED PANEL=	1.2214E-01

Table 3 Design margins for perfect optimized design in the previous table

MARGINS FOR CURRENT DESIGN: LOAD SET NO.1, SUBCASE NO.1 (midway between rings)		
MAR.	MARGIN	DEFINITION
NO.	VALUE	DEFINITION
1	7.90E-01	Local buckling from discrete model-1., M=8 axial halfwaves; FS=0.99
2	3.86E-01	Long-axial-wave bending-torsion buckling; M=1 ;FS=0.999
3	7.37E+00	eff.stress:matl=1,STR,Dseg=5,node=11,layer=1,z=-0.2812; MID.;FS=1.
4	4.53E-01	(m=1 lateral-torsional buckling load factor)/(FS)-1;FS=0.999
5	7.76E-01	Inter-ring buckling, discrete model, n=33 circ.halfwaves;FS=0.999
6	7.37E+00	eff.stress:matl=1,SKN,Iseg=1,at:n=1,layer=1,z=-0.2812;-MID.;FS=1.
7	1.32E+00	buckling margin stringer Iseg.3 . Local halfwaves=7 .MID.;FS=1.
8	1.61E-01	buckling margin stringer Iseg.4 . Local halfwaves=7 .MID.;FS=1.
9	3.58E-01	buckling stringer Isegs.3+4 together.M=7 ;C=0. ;MID.;FS=1.4
10	3.60E-01	buckling stringer Iseg 4 as beam on foundation. M=221;MID.;FS=3.
11	2.36E+02	buckling ring Iseg 4 as beam on foundation. M=114;MID.;FS=3.
12	7.98E-01	buck.(SAND);simp-support local buck.; (0.95*altsol);FS=0.999
13	1.72E-01	buck.(SAND);simp-support inter-ring; (1.00*altsol);FS=0.999
14	3.83E-01	buck.(SAND);simp-support general buck;M=1;N=3;slope=3.4427;FS=0.999
15	3.99E-01	buck.(SAND);simp-support general buck;(0.85*altsol);FS=0.999
16	1.73E+01	buck.(SAND);rolling with smear rings; M=110;N=1;slope=0.01;FS=0.999
17	1.44E-01	buck.(SAND);rolling only of stringers;M=12;N=0;slope=0.;FS=1.6
18	6.65E-01	buck.(SAND);hiwave roll. of stringers;M=92;N=0;slope=0.;FS=1.2
19	1.32E+00	buck.(SAND); STRINGERS: web buckling;M=7;N=1;slope=0.;FS=1.
20	5.23E+02	buck.(SAND); RINGS: web buckling;M=1;N=1;slope=0.;FS=1.
21	9.45E+01	(Max.allowable ave.axial strain)/(ave.axial strain) -1; FS=1.
22	2.33E+00	0.3333 *(Stringer spacing, b)/(Stringer base width, b2)-1;FS=1.
23	7.04E-01	1.-V(3)^1+20.V(6)^1-1
24	8.18E-01	1.-V(10)^1+20.V(12)^1-1

Table 4 Buckling load factors of the optimized perfect shell from PANDA2, BOSOR4, STAGS. Dimension are listed in Table 2.

PANDA2 (Table 3 margin no.)	BOSOR4 (Fig.no.) margin no.)	STAGS (Fig.no.) (Nxy=0)	
local buckling	1.790(1) 1.161(8) 1.358(9) 1.360(10) 1.798(12) 1.665(18)	1.939(5) 1.939(6)	1.781(17)
inter-ring buckling	1.386(2) 1.453(4) 1.776(5) 1.172(13) 1.144(17)	1.343(4) 1.299(7) 2.354(9)	1.341(14,15) 1.307(16)
general buckling	1.383(14) 1.399(15)	1.916(10) 2.784(8)	1.649(12) 1.824(18)

Table 5 Buckling load factors from PANDA2 for single module discretized skin-stringer model of the perfect shell. Dimensions are listed in Table 2.

BUCKLING LOAD FACTORS FROM BOSOR4-TYPE DISCRETIZED MODULE MODEL... (skin-stringer discretized module of local buckling)					
AXIAL HALF- WAVES	BUCKLING LOAD FACTOR BEFORE KNOCKDOWN	KNOCKDOWN FOR TRANSVERSE SHEAR DEFORMATION	KNOCKDOWN FOR IN-PLANE SHEAR LOADING AND/OR ANISOTROPY	BUCKLING LOAD FACTOR AFTER KNOCKDOWN	EIGOLD*KSTAR*KNOCK
M	EIGOLD	KSTAR	KNOCK		
4	2.11071E+00	1.00000E+00	9.78193E-01	2.06468E+00	
5	2.09435E+00	1.00000E+00	9.78193E-01	2.04868E+00	
6	2.00808E+00	1.00000E+00	9.78193E-01	1.96429E+00	
7	1.94999E+00	1.00000E+00	9.78193E-01	1.90747E+00	
8	1.94611E+00	1.00000E+00	9.78193E-01	1.90367E+00	
9	1.98501E+00	1.00000E+00	9.78193E-01	1.94172E+00	
8	1.94611E+00	9.39423E-01	9.78193E-01	1.78835E+00	

Table 6 General buckling from PANDA-type theory [2] and "knockdown" factors for the perfect shell. Dimensions are listed in Table 2.

general buckling: smeared stiffeners
***** Sanders theory is used in this section (ISAND=1)

Part 1 results of exhaustive search over (m,n,s) = (MWAVEX, NWAVEX, SLOPEX) space:

EIGMNC=	2.17E+00	2.17E+00	2.56E+00	2.88E+00	2.56E+00	2.17E+00	2.28E+00
SLOPEX=	2.74E-01	2.74E-01	0.00E+00	1.32E-01	0.00E+00	2.74E-01	4.73E-01
MWAVEX=	1	1	7	6	7	1	6
NWAVEX=	3	3	1	4	1	3	0

Part 2 Refinement of buckling mode shape and two "knockdowns"

Before refinement (before CALL EIG), EIGVAL,CSLOPE= 2.1704E+00 2.7372E-01
After refinement (after CALL EIG), EIGVAL,CSLOPE= 2.1702E+00 2.9047E-01

Buckling load factor before t.s.d.= 2.1702E+00 After t.s.d.= 2.0714E+00
Buckling load factor BEFORE knockdown for smeared stringers= 2.0714E+00
Buckling load factor AFTER knockdown for smeared stringers= 1.9426E+00

Part 3 More "knockdowns"

General buckling load factor before and after knockdown:
EIGGEN(before modification by 5 factors below) = 1.9426E+00
Knockdown factor from modal imperfection(s) = 9.1845E-01
Knockdown factor for smearing rings on cyl. shell = 7.7449E-01
Knockup factor to avoid twice accounting for t.s.d.= 1.0000E+00
1st modifying factor, FKNMOD=1 or 1/(EIG9X*FMDKD9) = 1.0000E+00
2nd modifying factor, EIGMR9=1 or EIGGNX/EIGGEN = 1.0000E+00
After knockdn,EIGGEN*FKNOCK(9)*(RNGKNK/SHRFCT)*FKNMOD*EIGMR9=**1.3818E+00**
in which
EIG9X lambda(ARBOCZ)/lambda(original PANDA-type theory)=9.1845E-01
lambda(ARBOCZ)=perfect panel buckling from ARBOCZ theory
lambda(PANDA) =perfect panel buckling from PANDA theory
FMDKD9 = 1 or 0.9/EIG9X = 1.0000E+00
EIGGNX = eigenvalue for perfect panel from alternate solution

Part 4 Final general buckling load factor of perfect shell

1.38180E+00 buckling load factor simp-support general buckling,
PANDA-theory; Buckling mode shape: M=1,N=3;slope=3.4427

Table 7 General buckling from "altsol" model (double trigonometric series expansion [6]) for a "patch" of the perfect shell. Dimensions are listed in Table 2.

Part 1 Introductory material

Entering ALTSOL: radius, axial, circ. dimensions of "patch"=
 1.0000E+02 1.3636E+02 3.4586E+01

GENERAL BUCKLING, **NUMSTR x NUMRNG BAY PATCH**, SMEARED SUBSTIFFENERS
 Number of discrete stringers, rings: **NUMSTR, NUMRNG= 7 6**

Here we find the buckling load factor from the "alternative solution" [6]: double trigonometric series expansions for the buckling modal displacement components, u , v , w , in contrast to the simple "one term" Rayleigh method of the original PANDA analysis leading to Eq.(57) of [2].

**** NOTE: The shell is PERFECT ****
 Imperfections are accounted for via knockdown factors generated from the original PANDA-type theory as described in [4].

NOMENCLATURE:

MNTOT = rank of the stiffness and load geometric matrices
 XMAX = axial length of panel included in the model
 YMAX = "hoop" (circumferential arc) length of model
 RADIUS = radius of curvature of the panel
 M = number of axial halfwaves
 N = number of "hoop" (circumferential) halfwaves
 Nx, Ny, Nxy = in-plane resultants in Load Set A
 Nx0, Ny0, Nxy0 = in-plane resultants in Load Set B
 t.s.d. = transverse shear deformation effect
 ISANDQ = 0=Donnell, 1=Sanders, 2=Marlowe theory

Shell theory indicator, ISANDQ= 1

critical wave no. and eigenvalue from PANDA-type analysis (with t.s.d.)=
 1 2.0714E+00 (CURVED)

High-m wavenumber and eigenvalue from PANDA-type analysis (without t.s.d.)=
 7 2.5622E+00 (CURVED)

Part 2 Results from double-trigonometric series model

XMAX, YMAX, NX, NY, NXY= 1.364E+02 3.459E+01 -6.484E+04 -1.980E+04 2.000E+04

EIGODD, EIGEVN= 1.6834E+00 1.8195E+00
 Critical buckling load factor from ALTSOL before t.s.d.= 1.6834E+00 (PERFECT)

Part 3 Buckling mode shape (M = number of axial halfwaves)

M Normal buckling modal displacement, w Trial No. 1
 number of circumferential halfwaves, N

1	2	3	4	5	6	7	8	9	10	11
1 0.000	0.000	0.000-0.001	0.000	0.409	0.000	0.000	0.000	0.000	0.000	0.000
2-0.002	0.000	0.001	0.000	0.002	0.000-0.001	0.000	0.000	0.000	0.000	0.000
3 0.000	0.000	0.000	0.000	0.000	0.000	0.000	0.000	0.000	0.000	0.000
4-0.001	0.000-0.001	0.000-0.001	0.000	0.000	0.000	0.000	0.000	0.000	0.000	0.000
5 0.000	0.000	0.000	0.000	0.000	0.000	0.000	0.000	0.000	0.000	0.000
6 0.000	0.000-0.001	0.000-0.001	0.000	0.000	0.000	0.000	0.000	0.000	0.000	0.000
7 0.000	0.000	0.000	0.000	0.000	0.000	0.000	0.000	0.000	0.000	0.000
8 0.000	0.000	0.001	0.000	0.002	0.000-0.001	0.000	0.000	0.000	0.000	0.000
9 0.000	0.000	0.000	0.000	0.000	0.202	0.000	0.000	0.000	0.000	0.000
10-0.001	0.000-0.004	0.000-0.007	0.000	0.003	0.000	0.000	0.000	0.000	0.000	0.000
11 0.000	0.000	0.000	0.000	0.000- 0.207	0.000	0.000	0.000	0.000	0.000	0.000

Maximum normal displacement harmonic w.r.t M=

4.0929E-01	1.6139E-03	1.6097E-04	9.9164E-04	4.9192E-04
9.2903E-04	1.3369E-04	1.6549E-03	2.0243E-01	7.4358E-03
2.0682E-01				

Part 4 "knockdowns"

Critical buckling load factor from ALTSOL before t.s.d.=1.6834E+00 (PERFECT)
 Critical buckling load factor from ALTSOL after t.s.d.=1.6440E+00 (PERFECT)
 Critical buckling load factor from ALTSOL after t.s.d.
 and after reduction by a factor of **8.5000E-01** to compensate for
 truncation of double trigonometric series expansion (perfect shell)=
 1.3974E+00 (CURVED) (PERFECT)

General buckling load factor before and after knockdown:
 EIGGNX(before knockdown by 2 factors below) = 1.3974E+00
 Knockdown factor from modal imperfection(s) = 9.1845E-01
 1st modifying factor(no smeared stringer knockdown)= 1.0000E+00
 2nd modifying factor,1/DENFCT=1 or 1/(EIG9X*FMDKD9) = 1.0888E+00
 After knockdown, EIGGNX*FKNOCK(9)*FKNMLT/DENFCT = **1.3974E+00**
 in which
 EIG9X = lambda(ARBOCZ)/lambda(original PANDA-type theory)= 9.1845E-01
 lambda(ARBOCZ)=perfect panel buckling from ARBOCZ theory
 lambda(PANDA) =perfect panel buckling from PANDA theory
 FMDKD9 = 1 or 0.9/EIG9X = 1.0000E+00

Part 5 final result from double-trigonometric series model

1.39743E+00 buckling load factor simple-support general buckling
 from double-trig. series expansion over "patch" (0.85*altsol)

**Table 8 Design margins for the optimized imperfect stiffened cylindrical shell,
dimensions for which are listed in Tables 1 and 2. Critical margins in boldface.**

Part 1: positive imperfection Wimp(general buckling mode) = 1.0 in. midway between rings

MARGINS FOR CURRENT DESIGN: LOAD SET NO 1, SUBCASE NO.1 (midway between rings)

MAR.	MARGIN	NO.	DEFINITION
1	Local buckling from discrete model-1.,M=1	3.73E-01	axial halfwaves;FS=0.99
2	Bending-torsion buckling; M=1 ;FS=0.999	3.75E-01	
3	eff.stress:matl=1,STR,Dseg=5,node=11,layer=1,z=0.2812; MID.;FS=1.	6.72E+00	
4	(m=1 lateral-torsional buckling load factor)/(FS)-1;FS=0.999	3.54E-01	
5	Ring flang buckling,discrete model,n=51 circ.halfwaves;FS=0.999	4.74E-01	
6	5.10E-02 Lo-n Ring sidesway, discrete model, n=8 circ.halfwaves;FS=0.999	5.10E-02	
7	eff.stress:matl=1,RNG,Iseg=3,at:TIP,layer=1,z=0.3626;-MID.;FS=1.	6.39E+00	
8	buckling margin stringer Iseg.3 . Local halfwaves=7 .MID.;FS=1.	1.09E+00	
9	buckling margin stringer Iseg.4 . Local halfwaves=7 .MID.;FS=1.	7.63E-03	
10	buckling stringer Isegs.3+4 together.M=7 ;C=0. ,MID.;FS=1.4	2.06E-01	
11	buckling stringer Iseg 4 as beam on foundation. M=221;MID.;FS=3.	1.80E-01	
12	buckling margin ring Iseg.3 . Local halfwaves=1 .MID.;FS=1.	3.00E+00	
13	buckling ring Iseg 4 as beam on foundation. M=114;MID.;FS=3.	6.61E-02	
14	buck. (SAND);simp-support local buck.; (0.95*altsol);FS=0.999	8.69E-01	
15	buck. (SAND);simp-support inter-ring; (1.00*altsol);FS=0.999	1.03E-01	
16	3.15E-02 buck. (SAND);simp-support general buck;M=1;N=3;slope=3.4427;FS=0.999	3.15E-02	
17	3.86E-03 buck. (SAND);simp-support general buck; (0.85*altsol);FS=0.999	3.86E-03	
18	1.75E+01 buck. (SAND);rolling with smear rings; M=110;N=1;slope=0.01;FS=0.999		
19	-4.77E-03 buck. (SAND);rolling only of stringers;M=12;N=0;slope=0.;FS=1.6	-4.77E-03	
20	4.47E-01 buck. (SAND);hiwave roll. of stringers;M=92;N=0;slope=0.;FS=1.2	4.47E-01	
21	1.03E+00 buck. (SAND); STRINGERS: web buckling;M=7;N=1;slope=0.;FS=1.		
22	3.27E+00 buck. (SAND); RINGS: web buckling;M=1;N=1;slope=0.1864;FS=1.		
23	9.45E+01 (Max.allowable ave.axial strain)/(ave.axial strain) -1; FS=1.		
24	2.33E+00 0.3333 *(Stringer spacing, b)/(Stringer base width, b2)-1;FS=1.		
25	7.04E-01 1.-V(3)^1+20.V(6)^1-1		
26	8.18E-01 1.-V(10)^1+20.V(12)^1-1		

Part 2: positive imperfection Wimp(general buckling mode) = 1.0 in. at ring stations

MARGINS FOR CURRENT DESIGN: LOAD SET NO 1, SUBCASE NO.2 (at ring stations)

MAR.	MARGIN	NO.	DEFINITION
1	Local buckling from discrete model-1.,M=1	3.76E-01	axial halfwaves;FS=0.99
2	Bending-torsion buckling; M=1 ;FS=1.	3.77E-01	
3	eff.stress:matl=1,STR,Dseg=5,node=11,layer=1,z=0.2812; RNGS;FS=1.	6.72E+00	
4	(m=1 lateral-torsional buckling load factor)/(FS)-1;FS=0.999	3.57E-01	
5	5.46E-02 Inter-ring bucklng, discrete model, n=37 circ.halfwaves;FS=0.999	5.46E-02	
6	eff.stress:matl=1,RNG,Iseg=4,allnode,layer=1,z=0.;;RNGS;FS=1.	6.39E+00	
7	buckling margin stringer Iseg.3 . Local halfwaves=7 .RNGS;FS=1.	1.09E+00	
8	9.79E-03 buckling margin stringer Iseg.4 . Local halfwaves=7 .RNGS;FS=1.	9.79E-03	
9	buckling stringer Isegs.3+4 together.M=7 ;C=0. ,RNGS;FS=1.4	2.08E-01	
10	buckling stringer Iseg 4 as beam on foundation. M=221;RNGS;FS=3.	1.83E-01	
11	buckling margin ring Iseg.3 . Local halfwaves=1 .RNGS;FS=1.	3.00E+00	
12	6.60E-02 buckling ring Iseg 4 as beam on foundation. M=114;RNGS;FS=3.	6.60E-02	
13	buck. (SAND);simp-support local buck.; (0.95*altsol);FS=0.999	8.68E-01	
14	buck. (SAND);rolling with smear string;M=1;N=12;slope=33.33;FS=0.999	1.01E+00	
15	buck. (SAND);rolling with smear rings; M=110;N=1;slope=0.01;FS=0.999	1.75E+01	
16	-3.06E-03 buck. (SAND);rolling only of stringers;M=12;N=0;slope=0.;FS=1.6	-3.06E-03	
17	4.50E-01 buck. (SAND);hiwave roll. of stringers;M=92;N=0;slope=0.;FS=1.2	4.50E-01	
18	9.08E-02 buck. (SAND);rolling only of rings; M=0;N=8;slope=0.;FS=1.6	9.08E-02	
19	6.23E-01 buck. (SAND);hiwave roll. of rings; M=0;N=45;slope=0.;FS=1.2		
20	buck. (SAND); STRINGERS: web buckling;M=7;N=1;slope=0.;FS=1.	1.03E+00	
21	buck. (SAND); RINGS: web buckling;M=1;N=1;slope=0.1864;FS=1.	3.27E+00	

Part 3: negative imperfection Wimp(general buckling mode) = -1.0 in. midway between rings

MARGINS FOR CURRENT DESIGN: LOAD SET NO 2, SUBCASE NO.1 (midway between rings)

MAR. MARGIN	NO. VALUE	DEFINITION
1	2.59E-02	Local buckling from discrete model-1.,M=1 axial halfwaves;FS=0.99
2	2.77E-02	Bending-torsion buckling; M=1 ;FS=0.999
3	6.85E+00	eff.stress:matl=1,SKN,Dseg=2,node=6,layer=1,z=0.2812; MID.;FS=1.
4	8.51E-02	(m=1 lateral-torsional buckling load factor)/(FS)-1;FS=0.999
5	5.46E-02	Inter-ring bucklng, discrete model, n=37 circ.halfwaves;FS=0.999
6	6.39E+00	eff.stress:matl=1,RNG,Iseg=3,at:TIP,layer=1,z=0.3626;-MID.;FS=1.
7	1.56E+00	buckling margin stringer Iseg.3 . Local halfwaves=7 .MID.;FS=1.
8	3.71E-01	buckling margin stringer Iseg.4 . Local halfwaves=7 .MID.;FS=1.
9	5.53E-01	buckling stringer Isegs.3+4 together.M=7 ;C=0. ;MID.;FS=1.4
10	6.06E-01	buckling stringer Iseg 4 as beam on foundation. M=221;MID.;FS=3.
11	3.00E+00	buckling margin ring Iseg.3 . Local halfwaves=1 .MID.;FS=1.
12	6.61E-02	buckling ring Iseg 4 as beam on foundation. M=114;MID.;FS=3.
13	4.09E-02	buck.(SAND);simp-support local buck.; (0.95*altsol);FS=0.999
14	2.69E-02	buck.(SAND);simp-support inter-ring; (1.00*altsol);FS=0.999
15	3.15E-02	buck.(SAND);simp-support general buck;M=1;N=3;slope=3.4427;FS=0.999
16	7.52E-02	buck.(SAND);simp-support general buck;(0.85*altsol);FS=0.999
17	7.39E-01	buck.(SAND);rolling with smear string;M=1;N=14;slope=33.33;FS=0.999
18	1.68E+01	buck.(SAND);rolling with smear rings; M=112;N=1;slope=0.01;FS=0.999
19	3.10E-01	buck.(SAND);rolling only of stringers;M=12;N=0;slope=0.;FS=1.6
20	9.10E-01	buck.(SAND);hiwave roll. of stringers;M=92;N=0;slope=0.;FS=1.2
21	9.09E-02	buck.(SAND);rolling only of rings; M=0;N=8;slope=0.;FS=1.6
22	6.24E-01	buck.(SAND);hiwave roll. of rings; M=0;N=45;slope=0.;FS=1.2
23	1.32E+00	buck.(SAND); STRINGERS: web buckling;M=7;N=1;slope=0.;FS=1.
24	3.27E+00	buck.(SAND); RINGS: web buckling;M=1;N=1;slope=0.1864;FS=1.

Part 4: negative imperfection Wimp(general buckling mode) = -1.0 in. at ring stations

MARGINS FOR CURRENT DESIGN: LOAD SET NO 2, SUBCASE NO.2 (at ring stations)

MAR. MARGIN	NO. VALUE	DEFINITION
1	2.66E-02	Local buckling from discrete model-1.,M=1 axial halfwaves;FS=0.99
2	2.73E-02	Bending-torsion buckling; M=1 ;FS=1.
3	6.85E+00	eff.stress:matl=1,STR,Dseg=5,node=11,layer=1,z=0.2812; RNGS;FS=1.
4	8.56E-02	(m=1 lateral-torsional buckling load factor)/(FS)-1;FS=0.999
5	4.74E-01	Ring flang buckling,discrete model,n=51 circ.halfwaves;FS=0.999
6	5.10E-02	Lo-n Ring sidesway, discrete model, n=8 circ.halfwaves;FS=0.999
7	6.39E+00	eff.stress:matl=1,RNG,Iseg=4,allnode,layer=1,z=0.;-RNGS;FS=1.
8	1.56E+00	buckling margin stringer Iseg.3 . Local halfwaves=7 .RNGS;FS=1.
9	3.75E-01	buckling margin stringer Iseg.4 . Local halfwaves=7 .RNGS;FS=1.
10	5.56E-01	buckling stringer Isegs.3+4 together.M=7 ;C=0. ;RNGS;FS=1.4
11	6.10E-01	buckling stringer Iseg 4 as beam on foundation. M=221;RNGS;FS=3.
12	3.00E+00	buckling margin ring Iseg.3 . Local halfwaves=1 .RNGS;FS=1.
13	6.60E-02	buckling ring Iseg 4 as beam on foundation. M=114;RNGS;FS=3.
14	4.08E-02	buck.(SAND);simp-support local buck.; (0.95*altsol);FS=0.999
15	1.68E+01	buck.(SAND);rolling with smear rings; M=112;N=1;slope=0.01;FS=0.999
16	3.13E-01	buck.(SAND);rolling only of stringers;M=12;N=0;slope=0.;FS=1.6
17	9.14E-01	buck.(SAND);hiwave roll. of stringers;M=92;N=0;slope=0.;FS=1.2
18	1.32E+00	buck.(SAND); STRINGERS: web buckling;M=7;N=1;slope=0.;FS=1.
19	3.27E+00	buck.(SAND); RINGS: web buckling;M=1;N=1;slope=0.1864;FS=1.

Table 9 Effect of a general buckling modal imperfection on the local, inter-ring, and general buckling load factors, prebuckling bending and twisting of the imperfect shell, and knockdown factors for imperfection sensitivity of the optimized stiffened cylindrical shell (dimensions in Table 2).

Part 1

LOCAL AND GLOBAL IMPERFECTION AMPLITUDES,
AMPLITUDE MODIFIERS THAT KEEP MAX. WALL ROTATION GENERATED
BY THE MODAL IMPERFECTION COMPONENT LESS THAN 0.1 RADIAN,
AND AMPLIFICATION FACTORS TO ACCOUNT FOR GROWTH OF THE
INITIAL IMPERFECTIONS DURING LOADING:

	USER-PROVIDED IMPERFECTION AMPLITUDE	SHELL WALL ROTATION WALRTi (rad)	AMPLITUDE MODIFIER AMPMDi	AMPLIFICATION FACTOR WYYAMP FROM LOADING
local imperfection	1.0000E-10	5.4500E-11	1.0000E+00	4.0000E+00
inter-ring imperf.	1.0000E-10	-3.8000E-11	1.0000E+00	4.0000E+00
gen. modal imperf.	1.0000E+00	3.0410E-02	1.0000E+00	3.4692E+00

Part 2

BUCKLING LOAD FACTORS OF PERFECT AND IMPERFECT GEOMETRIES.

	PERFECT PANEL, ORIGINAL STRESS DISTRIBUTION	PERFECT PANEL, REDISTRIBUTION OF PREBUCKLING RESULTANTS	IMPERFECT PANEL
local buckling	1.8904E+00	1.0998E+00	1.0997E+00
inter-ring buckling	1.7300E+00	1.0318E+00	1.0261E+00
general buckling	2.0186E+00	2.0186E+00	1.7318E+00

Part 3

KNOCKDOWN FACTORS k AND MODE SHAPES (M,N,SLOPE,i) k(axial,circ.,daxial,dcirc.,slope)
Knockdown factor for local instability= 1.00E+00 (m=1,n= 1,dm=0.0,dn=0.00,s=0.09)
Knockdown factor for inter-ring buckling=9.95E-01 (m=1,n=38,dm=0.0,dn=0.00,s=100.)
Knockdown factor for general instability=8.58E-01 (m=1,n= 3,dm=0.0,dn=.041,s=1.90)

Part 4

Local changes in curv.,twist, Wxx, Wyy, Wxy = 0.00E+00 0.00E+00 0.00E+00
Bay changes in curv.,twist, Wxx, Wyy, Wxy = 0.00E+00 0.00E+00 0.00E+00
General changes in curv.,twist, Wxx, Wyy, Wxy = -2.53E-04 -2.13E-03 -7.34E-04

Part 5

BUCKLING LOAD FACTORS AND IMPERFECTION SENSITIVITY SUMMARY
LOCAL INTER-RING GENERAL
BUCKLING BUCKLING BUCKLING
RATIOS OF BUCKLING LOADS FROM ARBOCZ THEORY TO THOSE FROM
PANDA2 THEORY FOR THE PERFECT STRUCTURE:
(ARBOCZ/PANDA2) : 8.6390E-01 9.9984E-01 **9.1845E-01**

KNOCKDOWN FACTORS FOR IMPERFECTIONS DERIVED FROM
PANDA2 THEORY VS THOSE FROM ARBOCZ 1992 UPDATE OF KOITERS
1963 SPECIAL THEORY:
FROM PANDA2 THEORY: 9.9994E-01 9.9452E-01 **8.5791E-01**
FROM ARBOCZ THEORY: 9.9973E-01 9.9631E-01 **7.4576E-01**
THE GOVERNING KNOCKDOWN FACTOR FOR EACH TYPE OF BUCKLING
(LOCAL, INTER-RING, GENERAL) IS SET EQUAL TO THE MINIMUM
KNOCKDOWN FACTOR FOR THAT TYPE OF BUCKLING, REDUCED
FURTHER BY THE RATIO (ARBOCZ/PANDA2) FOR THE PERFECT PANEL

IF THE RATIO (ARBOCZ/PANDA2) IS LESS THAN UNITY:

The ratio, (ARBOCZ/PANDA2), for local buckling of the perfect panel is being increased by the factor 1.0418E+00 because the panel between stringers is fairly shallow and therefore the ARBOCZ theory is not strictly applicable to this portion of the structure. Overly conservative results may thereby be avoided.

USED NOW IN PANDA2: 8.9975E-01 9.9435E-01 **6.8494E-01**

NOTE IF THERE IS INTERNAL PRESSURE THESE KNOCKDOWN FACTORS MAY BE CHANGED AS NOTED BELOW.

**Table 10 Output from PANDA2 in *.OPM file pertaining to imperfection sensitivity
when PANDA2 is run in "verbose output" mode (NPRINT = 2). This table
contains only output pertaining to a general buckling modal imperfection.
Dimensions of the shell are listed in Table 2.**

Part 1 Some definitions:

GENSTB = subroutine that computes PANDA-type buckling loads
 ARBOCZ = subroutine that computes ARBOCZ theory buckling loads
 t.s.d. = transverse shear deformation effect
 NX, NY, NXY=axial, hoop, in-plane shear prebuckling resultants
 ILOADS = load combination number (up to 5 load combos allowed)
 ICASE = subcase number (1 means midbay; 2 means at rings)
 LOAD SET A = "eigenvalue loads" (in load-geometric matrix)
 LOAD SET B = "constant" loads (contribute to stiffness matrix)
 Four digit label starting with 9 (9xxx) : SUBROUTINE BUCPAN
 is called from Label 9xxx in SUBROUTINE STRUCT or STRIMP
 Four digit label starting with 7 (7xxx) : SUBROUTINE GENSTB
 is called from Label 7xxx in SUBROUTINE BUCPAN
 IDESGN = 0 for current design; = 1 for perturbed design
 ISAND = 0 for Donnell shell theory; 1 for Sanders theory
 INDX = 2 for general buckling
 IFFLAT = 0 for curved (cylindrical) panel; 1 for flat panel
 EILC91 = buckling load factor for PERFECT panel
 EILLOC9 = buckling load factor for IMPERFECT panel
 WYYAMP = buckling modal imperfection is amplified by WYYAMP
 due to the applied load
 RNGKNZ = knockdown factor to compensate for unconservativeness
 of smearing rings
 R(radwav) = "effective" circumferential radius of curvature
 of the imperfect shell as loaded by the design
 load combination, NX, NY, NXY. THIS IS IMPORTANT!
 EIGVAL = eigenvalue with fractional wavenumbers and
 "fractional" slope
 EIGVLX = original eigenvalue: no "fractional" refinement
 JJ+1 = design iteration number.
 DMWAVE = fractional axial halfwaves
 DNWAVE = fractional circ. halfwaves
 MBAR = number of axial halfwaves (floating point)
 NBAR = number of circumferential halfwaves (floating point)
 MWAVEX = number of axial halfwaves (integer)
 NWAVEX = number of circumferential halfwaves (integer)
 SLOPEX = slope of buckling nodal lines (assumed to be straight)
 EIGMNC = buckling load factors (eigenvalues)
 WOGLOB = out-of-roundness +general buckling modal imperfection
 WG1 = out-of-roundness (n = 2 imperfection, prismatic)
 WG2 = general buckling modal imperfection
 WOPAN = inter-ring ("panel") buckling modal imperfection
 WOLOC = local (panel skin between stiffeners) buckling modal
 imperfection
 m,n,s = axial halfwaves, circumferential halfwaves, slope in
 the buckling mode shape
 eig1 = one eigenvalue when there are multiple minima with
 respect to (m,n,s)
 eig2 = the other eigenvalue when there are multiple minima
 (eig2-eig1)/abs(eig2-eig1) = ratio that, when its sign
 changes, tells the user that there has been an abrupt
 change in the critical buckling mode shape, which may
 give rise to very large constraint gradients.
 MWAVE = number of axial halfwaves (integer)
 NWAVE = number of circumferential halfwaves (integer)

CSLOPE = slope of buckling nodal lines (assumed to be straight)
 TEST = control for type of buckling mode, PANDA-type model:
 TEST < 1.0 means that Fig. 9(b) of [2] applies.
 TEST > 1.0 means that Fig. 9(a) of [2] applies.
 Wxx,Wyy,Wxy = changes in curvature and twist of the imperfect
 shell as loaded by the design load
 L = axial length of the buckling domain
 CIRC = circumferential arc length of the buckling domain
 Eq. (3.61) = ARBOCZ theory buckling equation; Eq.(19) of [5]

Part 2 Some notes about the verbose output

NOTE: In the following output there occur listings in the form

```

EIGMNC=2.25E+00 2.25E+00 2.57E+00 2.98E+00 2.57E+00 2.25E+00 1.00E+17
SLOPEX=4.73E-01 4.73E-01 0.00E+00 1.58E-01 0.00E+00 4.73E-01 0.00E+00
MWAVEX= 1 1 7 6 7 1 0
NWAVEX= 3 3 1 4 1 3 0
  
```

These data represent the buckling load factors, EIGMNC, and mode shapes, (SLOPEX, MWAVEX, NWAVEX), corresponding to the critical values found from **searching for minima with respect to (m,n,slope) over seven (m,n) subspaces:**
(low-m, low-n), (low-m, high-m), (high-m, low-n), (high-m, high-n), etc.
 in which (m=MWAVEX, n=NWAVEX, slope=SLOPEX) = (axial halfwaves, circumferential halfwaves, slope of buckling nodal lines).
 Please see ..doc/panda2.news Items 415 and 443 for details.

ANOTHER NOTE: In the following output there may also occur listings in the form:

```

Computation of fractional circumferential wavenumber, DNWAVE:
after knockdown factor= 9.3779E-01 for smeared stringers
Orig. crit. waves and eigenv., MBAR, NBAR, ESXNW1= 1. 3. 2.1122E+00
Decrement in circ. wavenumber, MBAR, NBAR-1, ESXNW2= 1. 2. 2.2875E+00
Increment in circ. wavenumber, MBAR, NBAR+1, ESXNW3= 1. 4. 2.2609E+00
Fractional circumferential wavenumber, DNWAVE= 4.1013E-02
  
```

"Fractional" wavenumbers, m+dm = MBAR + DMWAVE and n + dn = NBAR + DNWAVE, are used in PANDA2 in order to try to smooth the behavior with respect to buckling mode shape, (m,n,slope). The redistribution of stresses and stress resultants between panel skin and stiffener parts as an imperfect shell bends under loading depends upon the curvature changes and twist, Wxx, Wyy, Wxy, which involve the second derivatives of the mode shape and hence the products m^2, n^2, and m*n. If the critical buckling mode shape has few halfwaves (m,n), then Wxx, Wyy, Wxy change dramatically when m and/or n change by 1. This dramatic change causes a dramatic change in many of the stress and buckling constraints. Such changes give rise to very large constraint gradients and "jumpy" margins from design iteration to iteration, making it very difficult to find a "global" optimum design. The use of fractional wave numbers, DMWAVE and DNWAVE, smooths the constraints because a small change in the design leads to a correspondingly small change in MBAR + DMWAVE and NBAR + DNWAVE and thus a small change in Wxx, Wyy, Wxy at the design load.

In order to obtain a "fractional" wavenumbers, PANDA2 first computes buckling load factors for n, n-1, and n+1 with m fixed and for m, m-1, m+1 with n fixed, then uses parabolic interpolation for m,n to obtain the "fractional" wave numbers such as the quantity DNWAVE listed above. "Fractional" wave numbers are not computed unless the critical m and/or n are

at least 3. Please see ..doc/panda2.news Items 125g, 367, 412
449, and 453 for more details about "fractional" wavenumbers.

A THIRD NOTE: In the following output there may also occur listings in the form:

```
***** Multiple Minima Eigenvalues: Two different mode shapes:
[MWAVEEX(1),NWAVEEX(1)] and [MWAVEEX(3),NWAVEEX(3)] *****
Two buckling mode shapes for ILOADS,ICASE= 1 1
Axial halfwaves: first mode, MWAVEEX(1)= 1; second mode, MWAVEEX(3)= 7
Circ. halfwaves: first mode, NWAVEEX(1)= 3; second mode, NWAVEEX(3)= 1
JJ+1, eig2, eig1, (eig2-eig1)/abs(eig2-eig1)=
 1 2.5715E+00 2.2525E+00 1.0000E+00

*** Multiple Minima Eigenvalues vs Slope for Mode (M,N)= (1,3) ***
Normalized ratio, (eig2-eig1)/abs(eig2-eig1)=-1.00 for iteration 1
I,SLOPE,EIGENVALUE= 1 4.7076E-01 2.2526E+00
I,SLOPE,EIGENVALUE= 2 1.9665E+00 2.2476E+00
```

This output informs the user about potential abrupt changes in the critical general buckling mode shape with possibly very small changes in the design. The first seven lines have to do with possible abrupt changes in (m,n); the second four lines have to do with a possible abrupt change in the slope of the buckling nodal lines for given (m,n). Abrupt changes of either of these types from design iteration to iteration may cause "jumpy" margins and make it very difficult to determine a "global" optimum design. See Item 596 in panda2.news for more.

Part 3 PANDA-type general buckling analysis [2] of the PERFECT panel...

```
Buckling of PERFECT panel...
***** ENTERING GENSTB: PANDA-type buckling model *****
PANDA-type buckling theory is described in [2].
Also see Items 415 and 443 in ...panda2/doc/panda2.news.
ILABEL, ILABLY, IDESGN, ISAND, INDX, ITHRU, IROLL IFFLAT =
 7165 9150 0 0 2 1 0 0
Radius R, Axial length, A, Width B
1.000000E+02 3.000000E+02 3.141593E+02
Initial imperfections for general, panel, local buckling=
Total out-of-roundness + modal, W0GLOB = 1.0000E+00
Out-of-roundness, WG1 = 0.0000E+00
General buckling modal, WG2 = 1.0000E+00
Inter-ring buckling modal, WOPAN = 1.0000E-10
Local buckling modal, WOLOC = 1.0000E-10
**** Donnell theory is used in this section (ISAND=0)
Load Set A: Nx, Ny, Nxy= -1.0000E+05 -2.0000E+04 2.0000E+04
Load Set B: Nxo, Nyo, Nxyo= 0.0000E+00 0.0000E+00 0.0000E+00
```

The following section is entered only if TEST < 1.0 and the number of axial halfwaves is at least 3. (TEST < 1.0 means that the buckling mode from PANDA-type theory is of the type shown in Fig.9(b), p.554 of the "Theoretical basis..." paper. TEST > 1.0 means that Fig.9(a) applies.)

```
In this section a ratio, EIGRAT = EIGTST/EIGTS2, is
obtained in which EIGTST = eigenvalue with TEST > 1.0 and
EIGTS2 = eigenvalue with TEST < 1.0.
The ratio EIGRAT is always 1.0 unless EIGTST < EIGTS2.
High m range: New value of "TEST" is assigned: TEST = 1.1000E+00
*** (low-n) ***
(high-m) mode: ICHEK ISAND m n s EIGENVALUE TEST
          0 0 7 2 1.584E-01 2.526E+00 1.100E+00
EIGTST needed for EIGRAT = EIGTST/EIGTS2: EIGTST= 2.5257E+00
```

```

*** (low-n) ***
(high-m) mode: ICHEK ISAND m n s EIGENVALUE TEST
          0 0 7 2 1.000E-01 2.595E+00 9.555E-02
EIGTS2 needed for EIGRAT = EIGTST/EIGTS2: EIGTS2= 2.5949E+00
Ratio needed in ARBOCZ: EIGTST/EIGTS2= EIGRAT= 9.7335E-01

At 9150 in STRIMP, 7165 in BUCPAN, General instability, PERFECT shell:
Donnell theory is always used in this section of PANDA2
where imperfection sensitivity is being computed.
Donnell theory is always used in this section of PANDA2
EIGMNC=2.25E+00 2.25E+00 2.57E+00 2.98E+00 2.57E+00 2.25E+00 1.00E+17
SLOPEX=4.73E-01 4.73E-01 0.00E+00 1.58E-01 0.00E+00 4.73E-01 0.00E+00
MWAVEX= 1 1 7 6 7 1 0
NWAVEX= 3 3 1 4 1 3 0

***** Multiple Minima Eigenvalues: Two different mode shapes:
[MWAVEX(1),NWAVEX(1)] and [MWAVEX(3),NWAVEX(3)] *****
Two buckling mode shapes for ILOADS, ICASE= 1 2
Axial halfwaves: first mode, MWAVEX(1)= 1; second mode, MWAVEX(3)= 7
Circ. halfwaves: first mode, NWAVEX(1)= 3; second mode, NWAVEX(3)= 1
JJJ+1, eig2, eig1, (eig2-eig1)/abs(eig2-eig1)=
1 2.5715E+00 2.2525E+00 1.0000E+00

*** Multiple Minima Eigenvalues vs Slope for Mode (M,N)= (1,3) ***
Normalized ratio, (eig2-eig1)/abs(eig2-eig1)= -1.00 for iteration 1
I,SLOPE,EIGENVALUE= 1 4.7076E-01 2.2526E+00
I,SLOPE,EIGENVALUE= 2 1.9665E+00 2.2476E+00
*****
Radius of curvature computed from RADWAV, R(radwav)= 1.0000E+02
Change in curvature: ABS(1./RORIG) - ABS(1./R(radwav))= 0.0000E+00
MWAVE,NWAVE,CSLOPE,EIGVAL= 1 3 4.9209E-01 2.2523E+00
EIGVAL= 2.2523E+00 (before knockdown for smeared stringers
and before knockdown for t.s.d.
and before knockdown for smeared rings)

Computation of fractional circumferential wavenumber, DNWAVE:
after knockdown factor= 9.3779E-01 for smeared stringers
Orig. crit. waves and eigenv.,MBAR,NBAR, ESXNW1= 1. 3. 2.1122E+00
Decrement in circ. wavenumber,MBAR,NBAR-1,ESXNW2= 1. 2. 2.2875E+00
Increment in circ. wavenumber,MBAR,NBAR+1,ESXNW3= 1. 4. 2.2609E+00
Fractional circumferential wavenumber, DNWAVE= 4.1013E-02

Compare fractional waves, eigv. and original waves, eigv:
Fractional:NBAR+DNWAVE,MBAR+DMWAVE,EIGOPT= 3.0410 1.0000 2.1188
Original: NBAR, MBAR, ESXNW1= 3.0000 1.0000 2.1122
"Fractional" slope=, CSLTRY= 5.2578E-01; "Original" slope=, CSLTRS= 4.9209E-01

Final values of DMWAVE, DNWAVE on leaving GENSTB= 0.0000E+00 4.1013E-02

If EIGVAL and EIGVLX are different:
EIGVAL = eigenvalue with fractional wavenumbers and "fractional" slope
EIGVLX = original eigenvalue: no "fractional" refinement

EIGVAL,EIGVLX are eigenvalues before knockdown for smearing the stringers
and/or rings, that is, before knockdown by the factor, 9.3779E-01
EIGVAL,EIGVLX before knockdown for t.s.d.= 2.2593E+00 2.2523E+00
EIGVAL,EIGVLX after knockdown for t.s.d.= 2.1525E+00 2.1462E+00
EIGVAL,EIGVLX after knockdown for smearing stringers= 2.0186 2.0127
but before knockdown for smearing rings.
EIGRAT = EIGTST/EIGTS2 = 9.7335E-01
***** LEAVING SUBROUTINE BUCPAN: UNPERTURBED DESIGN *****
GENERAL BUCKLING EIGENV. OF PERFECT PANEL, IMOD= 0
EILC91(m,dm,n,dn,s)= 2.0186E+00(1, 0.000E+00, 3, 4.101E-02, 1.902E+00)
NOTE: The eigenvalue and mode shape just printed may not be

```

the critical one for the perfect shell; It is used only in the computation of the knockdown factor to account for initial nonaxisymmetric initial imperfections in a most conservative manner.

BUCKLING LOAD FACTOR WITHOUT FRACTIONAL WAVENUMBERS
AND INCLUDING THE FACTOR EIGTST/EIGTS2=EIGRAT= 9.7335E-01
EIGVL9(m, 0,n, 0,s)= 1.9590E+00(1, 3, 1.902E+00)
This eigenvalue is the factor EIGPAN used to
normalize the buckling load factors computed in
SUBROUTINE ARBOCZ

Part 4 ARBOCZ general buckling analysis [5] of the PERFECT panel...

General buckling: smeared stiffeners, C11= 9.5350E+06 (PERFECT PANEL)
Entering ARBOCZ. Label=9150
***** ENTERING ARBOCZ: "ARBOCZ" theory *****
THE PURPOSE IS TO FIND BUCKLING LOAD OF AN AXISYMMETRICALLY
IMPERFECT CYLINDRICAL SHELL. Equations are from Ref. [39], in
particular, see Equation No. (3.61).
NOTE: Eigenvalues are NORMALIZED by the buckling load from
the PANDA-type theory computed in SUBROUTINE GENSTB,
that is, by the load factor EIGPAN = 1.9590E+00
IN ARBOCZ: ILABEL,INDX,NPRNT,W0= 9150 2 0 0.0000E+00
NOTE: The normalizer, EIGPAN, includes knockdown for smeared
stringers, but the "ARBOCZ" eigenvalues do not yet include it.
Load Set A: Nx, Ny, Nxy= -1.0000E+05 -2.0000E+04 2.0000E+04
Load Set B: Nxo, Nyo, Nxyo= 0.0000E+00 0.0000E+00 0.0000E+00
NORMALIZED eigenvalues, EIGMNC, EIGAXY; modes, SLOPEX,MWAVEX NWAVEV
from ARBOCZ theory:
EIGMNC=1.02E+00 1.02E+00 1.15E+00 2.27E+00 1.23E+00 1.02E+00 1.00E+17
ERATIO=1.00E+00 1.00E+00 1.00E+00 1.00E+00 1.00E+00 1.00E+00 1.00E+00
SLOPEX=8.17E-01 8.17E-01 1.18E+00 3.28E-01 0.00E+00 8.17E-01 0.00E+00
MWAVEV= 1 1 1 7 1 1 0
NWAVEV= 3 3 4 6 2 3 0
IN ARBOCZ: 9150: INDX= 2: R,L,CIRC,W0= 1.00E+02 3.00E+02 3.14E+02 0.00E+00
Axisymmetric NORMALIZED eigenvalue of perfect shell, Nxcrit=1.3083E+00
Critical NORMALIZED eigenvalue with use of Eq. (3.61), EIGVAL=1.0225E+00

NORMALIZED BUCKLING LOAD FACTORS FROM ARBOCZ THEORY:
NORMALIZED buckling load factor neglecting trans.shear.def.=1.0225E+00
NORMALIZED buckling load factor including trans.shear.def.=9.7937E-01
Buckling mode shape: axial m, hoop n, slope = 1 3 8.1731E-01
Leaving ARBOCZ. Label=9150
Buckling load factor BEFORE knockdown for smeared stringers=9.7937E-01
Buckling load factor AFTER knockdown for smeared stringers=9.1845E-01

Part 5 ARBOCZ general buckling analysis [5] of the IMPERFECT panel...

General buckling: smeared stiffeners, C11= 9.5350E+06 (IMPERFECT PANEL)
Entering ARBOCZ. Label=9151
***** ENTERING ARBOCZ: "ARBOCZ" theory *****
THE PURPOSE IS TO FIND BUCKLING LOAD OF AN AXISYMMETRICALLY
IMPERFECT CYLINDRICAL SHELL.
NOTE: Eigenvalues are NORMALIZED by the buckling load from
the PANDA-type theory computed in SUBROUTINE GENSTB,
that is, by the load factor EIGPAN = 1.9590E+00
IN ARBOCZ: ILABEL,INDX,NPRNT,W0= 9151 2 0 1.0000E+00
NOTE: The normalizer, EIGPAN, includes knockdown for smeared
stringers, but the "ARBOCZ" eigenvalues do not yet include it.
Load Set A: Nx, Ny, Nxy= -1.0000E+05 -2.0000E+04 2.0000E+04
Load Set B: Nxo, Nyo, Nxyo= 0.0000E+00 0.0000E+00 0.0000E+00

NORMALIZED eigenvalues, EIGMNC, EIGAXY; modes, SLOPEX,MWAVEEX NWAVEEX from ARBOCZ theory:
EIGMNC=7.54E-01 7.75E-01 7.54E-01 9.66E-01 7.60E-01 7.54E-01 1.00E+17
ERATIO=1.00E+00 1.00E+00 1.00E+00 1.00E+00 1.00E+00 1.00E+00 1.00E+00
SLOPEX=1.90E-01 1.32E-01 1.90E-01 4.00E-02 0.00E+00 1.90E-01 0.00E+00
MWAVEX= 4 3 4 4 4 4 0
NWAVEX= 3 3 5 3 3 3 0
IN ARBOCZ: 9151: INDX= 2: R,L,CIRC,W0= 1.00E+02 3.00E+02 3.14E+02 1.00E+00
Axisymmetric NORMALIZED eigenvalue of perfect shell, Nxcrit=1.3083E+00
Critical NORMALIZED eigenvalue with use of Eq.(3.61), EIGVAL=7.5407E-01

NORMALIZED BUCKLING LOAD FACTORS FROM ARBOCZ THEORY:
NORMALIZED buckling load factor neglecting trans.shear.def.=7.5407E-01
NORMALIZED buckling load factor including trans.shear.def.=7.3038E-01
Buckling mode shape: axial m, hoop n, slope = 4 3 1.9008E-01
Leaving ARBOCZ. Label=9151
Buckling load factor BEFORE knockdown for smeared stringers=7.3038E-01
Buckling load factor AFTER knockdown for smeared stringers=6.8494E-01

GENERAL BUCKLING FROM 1992 ARBOCZ EQ. (3.61)
RATIO (LOAD FACTOR FROM ARBOCZ)/(LOAD FACTOR FROM PANDA2):
Perfect shell general buckling load(m,n,slope)=9.1845E-01(1, 3, 1.22E+00)
Imperf. shell general buckling load(m,n,slope)=6.8494E-01(4, 3, 5.26E+00)
Knockdown factor from Koiter Special Theory (K.S.T.)= 7.4576E-01
Knockdown from K.S.T. without the use of EIGMOD = 7.4576E-01

Part 6 PANDA-type general buckling analysis [2,4] of the IMPERFECT panel...

NOTE: Some output has been omitted for each iteration in this section in order to highlight the most important results.

***** ITERATION LOOP FOR IMPERFECT PANEL *****
Begin iteration loop for general buckling of the imperfect panel. The general imperfection is amplified by the factor WYYAMP, which increases from iteration to iteration.
***** ITERATION NO. 1 *****
*** BEGIN BUCPAN (IMPERF. SENSITIVITY, IMPERFECT PANEL) ***
***** Donnell theory is used in this section (ISAND=0)
EIGMNC=2.14E+00 2.14E+00 2.28E+00 2.93E+00 2.28E+00 2.14E+00 1.00E+17
SLOPEX=4.73E-01 4.73E-01 0.00E+00 2.00E-02 0.00E+00 4.73E-01 0.00E+00
MWAVEX= 1 1 6 7 6 1 0
NWAVEX= 3 3 3 5 3 3 0

Radius of curvature computed from RADWAV, R(radwav)=* 1.2171E+02 *****

***** LEAVING SUBROUTINE BUCPAN: UNPERTURBED DESIGN *****
GENERAL BUCKLING EIGENV. OF IMPERFECT PANEL, IMOD= 0
EILOC9(m,dm,n,dn,s)= 1.9243E+00(1, 0.000E+00, 3, 4.650E-02, 1.979E+00)
IMPERFECTION AMPLITUDE FACTOR, WYYAMP= 1.9817E+00
EIGEFF=RNGKNZ* (FACIM1*EILOC9 +FACIM2*EILC91)/(FACIM1+FACIM2)=1.5251E+00

***** ITERATION NO. 2 *****
*** BEGIN BUCPAN (IMPERF. SENSITIVITY, IMPERFECT PANEL) ***
***** Donnell theory is used in this section (ISAND=0)
EIGMNC=2.09E+00 2.09E+00 2.09E+00 2.69E+00 2.09E+00 2.09E+00 1.00E+17
SLOPEX=4.73E-01 4.73E-01 0.00E+00 1.00E-02 0.00E+00 4.73E-01 0.00E+00

MWAVEEX=	1	1	5	6	5	1	0
NWAVEEX=	3	3	3	5	3	3	0

Radius of curvature computed from RADWAV, R(radwav)=* 1.3539E+02 *****

***** LEAVING SUBROUTINE BUCPAN: UNPERTURBED DESIGN *****
GENERAL BUCKLING EIGENV. OF IMPERFECT PANEL, IMOD= 0
EILOC9(m,dm,n,dn,s)= 1.8606E+00(1, 0.000E+00, 3, -4.487E-02, 2.318E+00)
IMPERFECTION AMPLITUDE FACTOR, WYYAMP= 2.9044E+00
EIGEFF=RNGKNZ*(FACIM1*EILOC9 +FACIM2*EILC91)/(FACIM1+FACIM2)=**1.4971E+00**

***** ITERATION NO. 3 *****
*** BEGIN BUCPAN (IMPERF. SENSITIVITY, IMPERFECT PANEL) ***
**** Donnell theory is used in this section (ISAND=0)
EIGMNC= **2.08E+00 2.08E+00 2.07E+00 2.66E+00 2.07E+00 2.07E+00 1.00E+17**
SLOPEX= **4.73E-01 4.73E-01 0.00E+00 1.00E-02 0.00E+00 0.00E+00 0.00E+00**
MWAVEEX= **1 1 5 6 5 5 0**
NWAVEEX= **3 3 3 5 3 3 0**

Radius of curvature computed from RADWAV, R(radwav)=* 1.3719E+02 *****

***** LEAVING SUBROUTINE BUCPAN: UNPERTURBED DESIGN *****
GENERAL BUCKLING EIGENV. OF IMPERFECT PANEL, IMOD= 0
EILOC9(m,dm,n,dn,s)= 1.8228E+00(5, 3.599E-01, 3, 3.713E-01, 0.000E+00)
IMPERFECTION AMPLITUDE FACTOR, WYYAMP= 3.0118E+00
EIGEFF=RNGKNZ*(FACIM1*EILOC9 +FACIM2*EILC91)/(FACIM1+FACIM2)=**1.4795E+00**

***** ITERATION NO. 4 *****
*** BEGIN BUCPAN (IMPERF. SENSITIVITY, IMPERFECT PANEL) ***
**** Donnell theory is used in this section (ISAND=0)
EIGMNC= **2.07E+00 2.07E+00 2.04E+00 2.63E+00 2.04E+00 2.04E+00 1.00E+17**
SLOPEX= **4.73E-01 4.73E-01 0.00E+00 1.00E-02 0.00E+00 0.00E+00 0.00E+00**
MWAVEEX= **1 1 5 6 5 5 0**
NWAVEEX= **3 3 3 5 3 3 0**

Radius of curvature computed from RADWAV, R(radwav)=* 1.3928E+02 *****

***** LEAVING SUBROUTINE BUCPAN: UNPERTURBED DESIGN *****
GENERAL BUCKLING EIGENV. OF IMPERFECT PANEL, IMOD= 0
EILOC9(m,dm,n,dn,s)= 1.7983E+00(5, 3.037E-01, 3, 3.776E-01, 0.000E+00)
IMPERFECTION AMPLITUDE FACTOR, WYYAMP= 3.1336E+00
EIGEFF=RNGKNZ*(FACIM1*EILOC9 +FACIM2*EILC91)/(FACIM1+FACIM2)=**1.4677E+00**

Part 7 Last iteration:

PANDA-type general buckling analysis [2,4] of the IMPERFECT panel...

***** ITERATION NO. 5 *****
*** BEGIN BUCPAN (IMPERF. SENSITIVITY, IMPERFECT PANEL) ***
**** Donnell theory is used in this section (ISAND=0)
EIGMNC= **2.06E+00 2.06E+00 1.97E+00 2.56E+00 1.97E+00 1.97E+00 1.00E+17**
SLOPEX= **4.73E-01 4.73E-01 0.00E+00 0.00E+00 0.00E+00 0.00E+00 0.00E+00**
MWAVEEX= **1 1 5 6 5 5 0**
NWAVEEX= **3 3 3 5 3 3 0**

Radius of curvature computed from RADWAV, R(radwav)=* 1.4540E+02 *****

Change in curvature: ABS(1./Rorig) - ABS(1./R(radwav)) = 3.1223E-03
MWAVE,NWAVE,CSLOPE,EIGVAL= 5 3 0.0000E+00 1.9714E+00
The radius of curvature is modified by initial imperfections:
Orig.radius Mod.radius CURCHG WYYOUT WYYPAN WYYLOC

```

1.000E+02 1.454E+02 3.122E-03 0.000E+00 0.000E+00 0.000E+00
EIGVAL= 1.9714E+00 (before knockdown for smeared stringers
                     and before knockdown for t.s.d.
                     and before knockdown for smeared rings)

```

Computation of **fractional circumferential wavenumber, DNWAVE:**
after knockdown factor= 9.3779E-01 for smeared stringers
Orig. crit. waves and eigenv.,MBAR,NBAR, ESXNW1= 5. 3. 1.8488E+00
Decrement in circ. wavenumber,MBAR,NBAR-1,ESXNW2= 5. 2. 2.2906E+00
Increment in circ. wavenumber,MBAR,NBAR+1,ESXNW3= 5. 4. 1.9027E+00
Fractional circumferential wavenumber, DNWAVE= 3.9131E-01

Computation of **fractional number of axial halfwaves, DMWAVE:**
after knockdown factor= 9.3779E-01 for smearing stringers
Orig. crit. waves and eigenv.,MBAR,NBAR, ESXNW1= 5. 3. 1.8488E+00
Decrement in axial wavenumber,MBAR-1,NBAR,ESXNW2= 4. 3. 1.8935E+00
Increment in axial wavenumber,MBAR+1,NBAR,ESXNW3= 6. 3. 1.8721E+00
Fractional number of axial halfwaves, DMWAVE= 1.5752E-01

Compare fractional waves, eigv. and original waves, eigv:
Fractional:NBAR+DNWAVE,MBAR+DMWAVE,EIGOPT= 3.3913E+00 5.1575E+00 1.8050E+00
Original: NBAR, MBAR, ESXNW1= 3.0000E+00 5.0000E+00 1.8488E+00
"Fractional" slope=, CSLTRY= 0.0000E+00; "Original" slope=, CSLTRS= 0.0000E+00

Final values of DMWAVE, DNWAVE on leaving GENSTB= 1.5752E-01 3.9131E-01
EIGVAL,EIGVLX are eigenvalues before knockdown for smearing the stringers
and/or rings, that is, before knockdown by the factor, 9.3779E-01
EIGVAL,EIGVLX before knockdown for t.s.d.= 1.9247E+00 1.9714E+00
Buckling load factor before t.s.d.= 1.9247E+00 After t.s.d.= 1.8466E+00
EIGVAL,EIGVLX after knockdown for t.s.d.= 1.8466E+00 1.8896E+00
EIGVAL,EIGVLX after knockdown for smearing stringers= 1.7318E+00 1.7721E+00
but before knockdown for smearing rings.

EIGRAT = EIGTST/EIGTS2 = 9.9065E-01
***** LEAVING SUBROUTINE BUCPAN: UNPERTURBED DESIGN *****
GENERAL BUCKLING EIGENV. OF IMPERFECT PANEL, IMOD= 0
EILOC9(m,dm,n,dn,s)= 1.7318E+00(5, 1.575E-01, 3, 3.913E-01, 0.000E+00)
IMPERFECTION AMPLITUDE FACTOR, WYYAMP= 3.4692E+00
EIGEFF =RNGKNZ*(FACIM1*EILOC9 +FACIM2*EILC91)/(FACIM1+FACIM2)= 1.4341E+00
in which FACIM1, FACIM2, and EILC91 are given by:
FACIM1=1. / (EILOC9 - 1.) = 1.3665E+00
FACIM2=1. / (EILC91 - 1.) = 9.8173E-01
EILC91 = 2.0186E+00
RNGKNZ = 7.7449E-01
(See Item 6 in the section entitled "CONSERVATIVENESS OF PANDA2 ANALYSES"
for how the knockdown factor RNGKNZ for smearing rings is derived.)

Table 11 PANDA2 is NOT permitted to change the initial imperfection [Strategy (1)]:
Selection of buckling modal imperfection and prebuckling bending and twisting,
Wxx, Wyy, Wxy, of the imperfect shell. Dimensions are listed in Table 2.

Part 1

*** NOTE: The number of circ. halfwaves in the general buckling mode of the PERFECT panel is less than or equal to that for the IMPERFECT panel. Therefore, the IMPERFECT panel mode is used for computation of deformations Wxx, Wyy, Wxy in SUBROUTINE CURIMP.

Part 2

General buckling mode for the PERFECT panel (PANDA theory):
(m= 1, dm= 0.00E+00, n= 3, dn= 4.10E-02, slope=1.90E+00)

General buckling mode for the IMPERFECT panel (PANDA theory):
(m= 5, dm= 1.58E-01, n= 3, dn= 3.91E-01, slope=0.00E+00)

(0.1 radian)/(shell wall rotation), AMPTST = 1.8515E+00

Part 3

QUANTITIES USED FOR OVERALL BENDING OF IMPERFECT PANEL
(used for generation of WXX9,WYY9,WXY9), IMOD= 0:

Amplitude of general buckling modal imperf., WIMP= 1.0000E+00
Effective load factor for general buckling, EIGEFF= 1.4341E+00
Number of axial halfwaves in general mode, m= 5
Fractional axial halfwaves in general mode, dm= 1.5752E-01
Number of circ. halfwaves in general mode, n= 3
Fractional circ. halfwaves in general mode, dn= 3.9131E-01
Slope of nodal lines in general buckling mode, slope= 0.0000E+00
Original imperfection is increased by 1/(EIGEFF-1)= 2.3036E+00
Amplitude WAMP of prebuckling bending due to loading,
WAMP=WIMP/(EIGEFF-1.)= 2.3036E+00

***** NOTE ***** NOTE ***** NOTE *****
Prebuckling bending and twist from general imperfection growth:
Wxx9,Wyy9,Wxy9= -6.7196E-03 -2.6493E-03 -4.2193E-03

Part 4

MARGINS FOR CURRENT DESIGN: LOAD CASE NO. 1, SUBCASE NO. 1

MAR. MARGIN

NO.	VALUE	DEFINITION
1	-3.24E-01	Local buckling from discrete model-1.,M=8 axial halfwaves;FS=0.99
2	-4.32E-01	Long-axial-wave bending-torsion buckling; M=1 ;FS=0.999
3	2.06E+00	eff.stress:matl=1,STR,Dseg=4,node=11,layer=1,z=-0.1172; MID.;FS=1.
4	-4.36E-01	(m=1 lateral-torsional buckling load factor)/(FS)-1;FS=0.999
5	2.03E-01	Ring flang buckling,discrete model,n=52 circ.halfwaves;FS=0.999
6	-1.44E-01	Lo-n Ring sidesway, discrete model, n=8 circ.halfwaves;FS=0.999
7	2.21E+00	eff.stress:matl=1,STR,Iseg=4,allnode,layer=1,z=-0.1172;-MID.;FS=1.
8	1.92E-01	buckling margin stringer Iseg.3 . Local halfwaves=7 .MID.;FS=1.
9	-6.18E-01	buckling margin stringer Iseg.4 . Local halfwaves=7 .MID.;FS=1.
10	-4.15E-01	buckling stringer Isegs.3+4 together.M=7 ;C=0. ;MID.;FS=1.4
11	-5.53E-01	buckling stringer Iseg 4 as beam on foundation. M=221;MID.;FS=3.
12	2.22E+00	buckling margin ring Iseg.3 . Local halfwaves=1 .MID.;FS=1.
13	-1.42E-01	buckling ring Iseg 4 as beam on foundation. M=114;MID.;FS=3.
14	1.34E+00	buck.(SAND);simp-support local buck.; (0.95*altsol);FS=0.999
15	-4.05E-01	buck.(SAND);simp-support inter-ring; (1.00*altsol);FS=0.999

```
16 3.15E-02 buck.(SAND);simp-support general buck;M=1;N=3;slope=3.4427;FS=0.999
17 -3.19E-01 buck.(SAND);simp-support general buck;(0.85*altsol);FS=0.999
18 1.81E+01 buck.(SAND);rolling with smear rings; M=111;N=1;slope=0.;FS=0.999
19 -6.14E-01 buck.(SAND);rolling only of stringers;M=12;N=0;slope=0.;FS=1.6
20 -4.40E-01 buck.(SAND);hiwave roll. of stringers;M=92;N=0;slope=0.;FS=1.2
21 2.44E+00 buck.(SAND); RINGS: web buckling;M=1;N=1;slope=0.1864;FS=1.
22 9.45E+01 (Max.allowable ave.axial strain)/(ave.axial strain) -1; FS=1.
23 2.33E+00 0.3333 *(Stringer spacing, b)/(Stringer base width, b2)-1;FS=1.
24 7.04E-01 1.-V(3)^1+20.V(6)^1-1
25 8.18E-01 1.-V(10)^1+20.V(12)^1-1
=====
```

Table 12 PANDA2 IS permitted to change the initial imperfection [Strategy (2)]:
Selection of buckling modal imperfection and prebuckling bending and twisting,
Wxx, Wyy, Wxy, of the imperfect shell. Dimensions are listed in Table 2.

Part 1

*** NOTE: Although the number of circumfer. halfwaves in the general buckling mode of the PERFECT panel is less than or equal to that for the IMPERFECT panel, since the user has elected to allow PANDA2 to change the amplitude of the general buckling modal imperfection and since the axial wavelength of the buckling mode of the IMPERFECT shell is less than half that of the PERFECT shell, we use the PERFECT panel mode for computation of deformations Wxx, Wyy, Wxy in SUBROUTINE CURIMP.

Part 2

General buckling mode for the PERFECT panel (PANDA theory):
(m= 1, dm= 0.00E+00, n= 3, dn= 4.10E-02, slope=1.90E+00)

General buckling mode for the IMPERFECT panel (PANDA theory):
(m= 5, dm= 1.58E-01, n= 3, dn= 3.91E-01, slope=0.00E+00)

(0.1 radian)/(shell wall rotation), AMPTST = 3.2884E+00

Part 3

QUANTITIES USED FOR OVERALL BENDING OF IMPERFECT PANEL
(used for generation of WXX9,WYY9,WXY9), IMOD= 0:
Amplitude of general buckling modal imperf., WIMP= 1.0000E+00
Effective load factor for general buckling, EIGEFF= 1.4341E+00
Number of axial halfwaves in general mode, m= 1
Fractional axial halfwaves in general mode, dm= 0.0000E+00
Number of circ. halfwaves in general mode, n= 3
Fractional circ. halfwaves in general mode, dn= 4.1013E-02
Slope of nodal lines in general buckling mode, slope= 1.9019E+00
Original imperfection is increased by 1/(EIGEFF-1)= 2.3036E+00
Amplitude of prebuckling bending due to loading,
Amplitude WAMP of prebuckling bending due to loading,
WAMP=WIMP/(EIGEFF-1.)= 2.3036E+00

***** NOTE ***** NOTE ***** NOTE *****
Prebuckling bending and twist from general imperfection growth:
Wxx9,Wyy9,Wxy9= -2.5262E-04 -2.1303E-03 -7.3359E-04

Table 13 New entries in PANDA2 prompting file, PROMPT.DAT, pertaining to Strategy (1) vs Strategy (2) with regard to the modeling of initial buckling modal imperfections in PANDA2

352.1 Do you want PANDA2 to change imperfection amplitudes (see H(elp))?

352.2

Default is "Y". If you answer "Y" then PANDA2 may automatically reduce the amplitude of one or more of the buckling modal imperfections that it judges to be larger than that which would be easily detectable by the most casual inspection and therefore greater than that represented by a reasonable tolerance. It was necessary to allow PANDA2 to do this in order:

(a) to try to avoid extreme oscillations of design margins from design iteration to iteration, and

(b) to avoid production of optimum designs that are too conservative.

Since the initial buckling modal imperfections have the unknown shapes of the local, inter-ring, and general buckling modes, the user cannot know ahead of time whether or not a given imperfection amplitude is too large. An imperfection of given amplitude is easier to detect if it has a shape that has short axial and circumferential wavelengths than if it has long wavelengths because it is the wall out-of-plane rotations that are most likely to be detected. These out-of-plane rotations increase inversely with the critical buckling modal wavelengths. The user does not know in advance what the various wavelengths of the critical buckling modes are.

If you answer "Y", PANDA2 will take the following three steps

STRATEGY (2) :

Step 1. Use the critical buckling mode shape,
 $(m, n, \text{slope}) = (\text{axial halfwaves}, \text{circ. halfwaves}, \text{nodal line slope})$
 corresponding to the PERFECT rather than the IMPERFECT geometry
 if the axial halfwavelength of the critical buckling mode of the
 IMPERFECT geometry is less than or equal to half the user-
 specified axial halfwavelength of the imperfection.

**Step 2. Change the amplitude of whatever imperfection results
 from Step 1 by the factor (ratio):**
 $(\text{axial halfwavelength of the critical buckling mode}) /$
 $(\text{user-specified axial halfwavelength of the imperfection})$

**Step 3. Reduce the buckling modal imperfection amplitude remaining
 after Steps 1 and 2 if it leads to an out-of-plane wall rotation
 that is greater than 0.1 radian. If this happens a warning such as
 the following (which happens to apply only to the local buckling
 modal imperfection) will be printed in the *.OPM file:**

```
***** WARNING ***** WARNING ***** WARNING *****
THE CIRCUMFERENTIAL HALFWAVELENGTH OF THE LOCAL IMPERFECTION
Wimp(local), WHICH HAS THE SAME FORM AS THE LOCAL BUCKLING
MODE, IS SHORT, WHILE ITS AMPLITUDE IS RATHER HIGH:
Circumferential halfwavelength of Wimp(local), Wlength=2.97E+01
Present amplitude of the local imperfection, Wimp(local)=1.67E+00
PLEASE CONSIDER REDUCING Wimp(local). YOUR DESIGN MAY BE TOO
CONSERVATIVE.
***** END WARNING ***** END WARNING *****
```

The following material printed in the *.OPM file informs the user by what factor the user-supplied imperfection amplitude was reduced in this case in order to keep the maximum out-of-plane wall rotation less than 0.1 rad:

LOCAL AND GLOBAL IMPERFECTION AMPLITUDES,
AMPLITUDE MODIFIERS THAT KEEP MAX. WALL ROTATION GENERATED
BY THE MODAL IMPERFECTION COMPONENT LESS THAN 0.1 RADIAN,
AND AMPLIFICATION FACTORS TO ACCOUNT FOR GROWTH OF THE
INITIAL IMPERFECTIONS DURING LOADING:

USER-PROVIDED IMPERFECTION AMPLITUDE	AMPLITUDE MODIFIER AMPMDi	AMPLIFICATION FACTOR WYYAMP FROM LOADING
local imperfection 1.6750E+00	5.4998E-01	1.0182E+00

In the above case the local buckling modal imperfection amplitude actually used by PANDA2 is $1.675 \times 0.54998 = 0.92122$.

You may, however, want to answer the question "N". For example, if you wish to use PANDA2 to evaluate a damaged panel with a known (probably rather large) initial imperfection, you will not want PANDA2 to "take charge" and automatically modify the imperfection amplitude as it did in the above example.

365.0

PANDA2 will next ask you to provide an axial halfwavelength of the general buckling modal imperfection. For axially stiffened panels or panels under external pressure or flat panels, please use the axial length of the panel. PANDA2 uses the axial half-wavelength you give here to change your given amplitude of the general buckling modal imperfection if the axial halfwavelength of the general buckling mode of the perfect shell turns out to be different from that you will next provide here (imperfection amplitude becomes smaller if the axial halfwavelength of the critical buckling mode of the perfect shell is shorter than that you provide here and larger if it is longer than that you will provide here). The purpose of this strategy is to prevent wild swings in margins corresponding to small changes in design caused by abruptly different critical general buckling mode shapes. Please see ITEM NO. 525 in the file ...panda2/doc/panda2.news for more.

366.1 Axial halfwavelength of typical general buckling mode, AXLWAV
366.2

For flat panels or axially stiffened panels, or panels with significant external pressure, use the axial length of the panel.

For laminated composite cylindrical panels you might also use the axial length of the panel, even if the panel is unstiffened.

Table 14 Optimum design of stiffened cylindrical shell after modification of PANDA2

DIMENSIONS OF CURRENT DESIGN...		
VARIABLE	CURRENT	
NUMBER	VALUE	DEFINITION
1	5.8178E+00	B(STR) :stiffener spacing, b: STR seg=NA, layer=NA
2	5.8178E-01	B2(STR) :width of stringer base, b2 (must be > 0, see
3	3.6633E+00	H(STR) :height of stiffener (type H for sketch), h: S
4	2.8610E+00	W(STR) :width of outstanding flange of stiffener, w:
5	5.6639E-01	T(1)(SKN) :thickness for layer index no.(1): SKN seg=1
6	2.8154E-01	T(2)(STR) :thickness for layer index no.(2): STR seg=3
7	2.2753E-01	T(3)(STR) :thickness for layer index no.(3): STR seg=4
8	2.7273E+01	B(RNG) :stiffener spacing, b: RNG seg=NA, layer=NA
9	0.0000E+00	B2(RNG) :width of ring base, b2 (zero is allowed): RNG
10	7.8659E+00	H(RNG) :height of stiffener (type H for sketch), h: R
11	6.2330E+00	W(RNG) :width of outstanding flange of stiffener, w:
12	6.5922E-01	T(4)(RNG) :thickness for layer index no.(4): RNG seg=3
13	3.5912E-01	T(5)(RNG) :thickness for layer index no.(5): RNG seg=4

CURRENT VALUE OF THE OBJECTIVE FUNCTION:	
1.062E+04	WEIGHT OF THE ENTIRE PANEL (180 deg. of cylindrical shell, lbs)
TOTAL WEIGHT OF SKIN	= 5.3354E+03
TOTAL WEIGHT OF SUBSTIFFENERS	= 0.0000E+00
TOTAL WEIGHT OF STRINGERS	= 2.7240E+03
TOTAL WEIGHT OF RINGS	= 2.5642E+03
SPECIFIC WEIGHT (WEIGHT/AREA) OF STIFFENED PANEL=	1.1278E-01

Table 15 Design margins for perfect optimized design listed in Table 14

MARGINS FOR CURRENT DESIGN: LOAD SET NO.1, SUBCASE NO.1 (midway between rings)		
MAR.	MARGIN	DEFINITION
NO.	VALUE	DEFINITION
1	5.86E-01	Local buckling from discrete model-1., M=8 axial halfwaves; FS=0.999
2	2.57E-01	Long-axial-wave bending-torsion buckling; M=1 ;FS=0.999
3	7.10E+00	eff.stress:matl=1,STR,Dseg=5,node=11,layer=1,z=0.2832; MID.;FS=1.
4	3.14E-01	(m=1 lateral-torsional buckling load factor)/(FS)-1;FS=0.999
5	5.52E-01	Inter-ring bucklng, discrete model, n=30 circ.halfwaves;FS=0.999
6	7.10E+00	eff.stress:matl=1,SKN,Iseg=1,at:n=1,layer=1,z=0.2832;-MID.;FS=1.
7	8.30E-01	buckling margin stringer Iseg.3 . Local halfwaves=7 .MID.;FS=1.
8	1.23E-01	buckling margin stringer Iseg.4 . Local halfwaves=7 .MID.;FS=1.
9	1.14E-01	buckling stringer Isegs.3+4 together.M=7 ;C=0. ;MID.;FS=1.4
10	2.13E+00	buckling stringer Iseg 4 as beam on foundation. M=223;MID.;FS=1.2
11	7.39E-01	buck.(SAND);simp-support local buck.; (0.95*altsol);FS=0.999
12	1.67E-01	buck.(SAND);simp-support inter-ring; (1.00*altsol);FS=0.999
13	4.13E-01	buck.(SAND);simp-support general buck;M=1;N=3;slope=8.9127;FS=0.999
14	4.06E-01	buck.(SAND);simp-support general buck;(0.85*altsol);FS=0.999
15	1.59E+01	buck.(SAND);rolling with smear rings; M=112;N=1;slope=0.01;FS=0.999
16	9.46E-02	buck.(SAND);rolling only of stringers;M=12;N=0;slope=0.;FS=1.4
17	4.33E-01	buck.(SAND);hiwave roll. of stringers;M=89;N=0;slope=0.;FS=1.2
18	4.31E+02	buck.(SAND);rolling only axisym.rings;M=0;N=0;slope=0.;FS=1.4
19	8.30E-01	buck.(SAND); STRINGERS: web buckling;M=7;N=1;slope=0.;FS=1.
20	2.99E+04	buck.(SAND); RINGS: web buckling;M=1;N=6;slope=0.;FS=1.
21	9.00E+01	(Max.allowable ave.axial strain)/(ave.axial strain) -1; FS=1.
22	2.33E+00	0.3333 *(Stringer spacing, b)/(Stringer base width, b2)-1;FS=1.
23	5.37E-01	1.-V(3)^1+20.V(6)^1-1
24	6.76E-01	1.-V(10)^1+20.V(12)^1-1

Table 16 Design margins for the optimized imperfect stiffened cylindrical shell, dimensions for which are listed in Tables 1 and 14. Critical margins are printed in boldface

Part 1: positive imperfection Wimp(general buckling mode) = 1.0 in. midway between rings

MARGINS FOR CURRENT DESIGN: LOAD SET NO 1, SUBCASE NO.1 (midway between rings)			
MAR. MARGIN	NO. VALUE	DEFINITION	
1	2.21E-01	Local buckling from discrete model-1., M=1	axial halfwaves;FS=0.99
2	2.23E-01	Bending-torsion buckling; M=1 ;FS=0.999	
3	6.61E+00	eff.stress:matl=1,SKN,Dseg=2,node=6,layer=1,z=0.2832; MID.;FS=1.	
4	2.08E-01	(m=1 lateral-torsional buckling load factor)/(FS)-1;FS=0.999	
5	-2.92E-02	Ring flang buckling,discrete model,n=65	circ.halfwaves;FS=0.999
6	-2.88E-02	Lo-n Ring sidesway, discrete model, n=8	circ.halfwaves;FS=0.999
7	6.27E+00	eff.stress:matl=1,RNG,Iseg=3,at:TIP,layer=1,z=0.3296;-MID.;FS=1.	
8	6.72E-01	buckling margin stringer Iseg.3 . Local halfwaves=7 .MID.;FS=1.	
9	-8.27E-03	buckling margin stringer Iseg.4 . Local halfwaves=7 .MID.;FS=1.	
10	4.63E-03	buckling stringer Isegs.3+4 together.M=7 ;C=0. ;MID.;FS=1.4	
11	1.77E+00	buckling stringer Iseg 4 as beam on foundation. M=223;MID.;FS=1.2	
12	2.42E+00	buckling margin ring Iseg.3 . Local halfwaves=1 .MID.;FS=1.	
13	1.27E+00	buckling ring Iseg 4 as beam on foundation. M=139;MID.;FS=1.2	
14	7.91E-01	buck. (SAND);simp-support local buck.; (0.95*altsol);FS=0.999	
15	9.73E-02	buck. (SAND);simp-support inter-ring; (1.00*altsol);FS=0.999	
16	1.21E-02	buck. (SAND);simp-support general buck;M=1;N=3;slope=8.9127;FS=0.999	
17	-2.27E-02	buck. (SAND);simp-support general buck;(0.85*altsol);FS=0.999	
18	1.60E+01	buck. (SAND);rolling with smear rings; M=112;N=1;slope=0.01;FS=0.999	
19	-3.14E-02	buck. (SAND);rolling only of stringers;M=12;N=0;slope=0.;FS=1.4	
20	2.68E-01	buck. (SAND);hiwave roll. of stringers;M=89;N=0;slope=0.;FS=1.2	
21	6.26E-01	buck. (SAND); STRINGERS: web buckling;M=7;N=1;slope=0.;FS=1.	
22	2.64E+00	buck. (SAND); RINGS: web buckling;M=1;N=1;slope=0.1749;FS=1.	
23	9.00E+01	(Max.allowable ave.axial strain)/(ave.axial strain) -1; FS=1.	
24	2.33E+00	0.3333 *(Stringer spacing, b)/(Stringer base width, b2)-1;FS=1.	
25	5.37E-01	1.-V(3)^1+20.V(6)^1-1	
26	6.76E-01	1.-V(10)^1+20.V(12)^1-1	

Part 2: positive imperfection Wimp(general buckling mode) = 1.0 in. at ring stations

MARGINS FOR CURRENT DESIGN: LOAD SET NO 1, SUBCASE NO.2 (at ring stations)

MAR. MARGIN	NO. VALUE	DEFINITION
1	2.18E-01	Local buckling from discrete model-1., M=1
2	2.19E-01	Bending-torsion buckling; M=1 ;FS=1.
3	6.61E+00	eff.stress:matl=1,STR,Dseg=5,node=11,layer=1,z=0.2832; RNGS;FS=1.
4	2.06E-01	(m=1 lateral-torsional buckling load factor)/(FS)-1;FS=0.999
5	4.27E-03	Inter-ring buckng, discrete model, n=35
6	6.27E+00	eff.stress:matl=1,RNG,Iseg=4,allnode,layer=1,z=0.;-RNGS;FS=1.
7	6.70E-01	buckling margin stringer Iseg.3 . Local halfwaves=7 .RNGS;FS=1.
8	-1.01E-02	buckling margin stringer Iseg.4 . Local halfwaves=7 .RNGS;FS=1.
9	3.38E-03	buckling stringer Isegs.3+4 together.M=7 ;C=0. ;RNGS;FS=1.4
10	1.76E+00	buckling stringer Iseg 4 as beam on foundation. M=223;RNGS;FS=1.2
11	2.42E+00	buckling margin ring Iseg.3 . Local halfwaves=1 .RNGS;FS=1.
12	1.27E+00	buckling ring Iseg 4 as beam on foundation. M=139;RNGS;FS=1.2
13	7.92E-01	buck. (SAND);simp-support local buck.; (0.95*altsol);FS=0.999
14	7.50E-01	buck. (SAND);rolling with smear string;M=1;N=13;slope=33.33;FS=0.999
15	1.60E+01	buck. (SAND);rolling with smear rings; M=112;N=1;slope=0.01;FS=0.999
16	-3.29E-02	buck. (SAND);rolling only of stringers;M=12;N=0;slope=0.;FS=1.4
17	2.66E-01	buck. (SAND);hiwave roll. of stringers;M=89;N=0;slope=0.;FS=1.2
18	1.95E-01	buck. (SAND);rolling only of rings; M=0;N=8;slope=0.;FS=1.4
19	3.35E-01	buck. (SAND);hiwave roll. of rings; M=0;N=50;slope=0.;FS=1.2
20	6.25E-01	buck. (SAND); STRINGERS: web buckling;M=7;N=1;slope=0.;FS=1.
21	2.65E+00	buck. (SAND); RINGS: web buckling;M=1;N=1;slope=0.1749;FS=1.
22	9.01E+01	(Max.allowable ave.axial strain)/(ave.axial strain) -1; FS=1.

Part 3: negative imperfection Wimp(general buckling mode) = -1.0 in. midway between rings

MARGINS FOR CURRENT DESIGN: LOAD SET NO 2, SUBCASE NO.1 (midway between rings)

NO.	VALUE	DEFINITION
1	5.28E-02	Local buckling from discrete model-1.,M=1 axial halfwaves;FS=0.99
2	5.48E-02	Bending-torsion buckling; M=1 ;FS=0.999
3	6.78E+00	eff.stress:matl=1,STR,Dseg=5,node=11,layer=1,z=0.2832; MID.;FS=1.
4	1.22E-01	(m=1 lateral-torsional buckling load factor)/(FS)-1;FS=0.999
5	4.27E-03	Inter-ring bucklng, discrete model, n=35 circ.halfwaves;FS=0.999
6	6.27E+00	eff.stress:matl=1,RNG,Iseg=3,at:TIP,layer=1,z=0.3296;-MID.;FS=1.
7	9.98E-01	buckling margin stringer Iseg.3 . Local halfwaves=7 .MID.;FS=1.
8	2.94E-01	buckling margin stringer Iseg.4 . Local halfwaves=7 .MID.;FS=1.
9	2.51E-01	buckling stringer Isegs.3+4 together.M=7 ;C=0. ;MID.;FS=1.4
10	2.61E+00	buckling stringer Iseg 4 as beam on foundation. M=223;MID.;FS=1.2
11	2.42E+00	buckling margin ring Iseg.3 . Local halfwaves=1 .MID.;FS=1.
12	1.27E+00	buckling ring Iseg 4 as beam on foundation. M=139;MID.;FS=1.2
13	1.15E-01	buck.(SAND);simp-support local buck.; (0.95*altsol);FS=0.999
14	-1.88E-02	buck.(SAND);simp-support inter-ring; (1.00*altsol);FS=0.999
15	1.21E-02	buck.(SAND);simp-support general buck;M=1;N=3;slope=8.9127;FS=0.999
16	-4.00E-02	buck.(SAND);simp-support general buck;(0.85*altsol);FS=0.999
17	5.26E-01	buck.(SAND);rolling with smear string;M=1;N=15;slope=33.33;FS=0.999
18	1.56E+01	buck.(SAND);rolling with smear rings; M=110;N=1;slope=0.01;FS=0.999
19	2.31E-01	buck.(SAND);rolling only of stringers;M=12;N=0;slope=0.;FS=1.4
20	6.14E-01	buck.(SAND);hiwave roll. of stringers;M=89;N=0;slope=0.;FS=1.2
21	1.95E-01	buck.(SAND);rolling only of rings; M=0;N=8;slope=0.;FS=1.4
22	3.35E-01	buck.(SAND);hiwave roll. of rings; M=0;N=50;slope=0.;FS=1.2
23	8.30E-01	buck.(SAND); STRINGERS: web buckling;M=7;N=1;slope=0.;FS=1.
24	2.64E+00	buck.(SAND); RINGS: web buckling;M=1;N=1;slope=0.1749;FS=1.
25	9.00E+01	(Max.allowable ave.axial strain)/(ave.axial strain) -1; FS=1.

Part 4: negative imperfection Wimp(general buckling mode) = -1.0 in. at ring stations

MARGINS FOR CURRENT DESIGN: LOAD SET NO 2, SUBCASE NO.2 (at ring stations)

NO.	VALUE	DEFINITION
1	5.19E-02	Local buckling from discrete model-1.,M=1 axial halfwaves;FS=0.99
2	5.29E-02	Bending-torsion buckling; M=1 ;FS=1.
3	6.79E+00	eff.stress:matl=1,STR,Dseg=5,node=11,layer=1,z=0.2832; RNGS;FS=1.
4	1.21E-01	(m=1 lateral-torsional buckling load factor)/(FS)-1;FS=0.999
5	-2.91E-02	Ring flang buckling,discrete model,n=65 circ.halfwaves;FS=0.999
6	-2.88E-02	Lo-n Ring sidesway, discrete model, n=8 circ.halfwaves;FS=0.999
7	6.27E+00	eff.stress:matl=1,RNG,Iseg=4,allnode,layer=1,z=0.;;-RNGS;FS=1.
8	9.96E-01	buckling margin stringer Iseg.3 . Local halfwaves=7 .RNGS;FS=1.
9	2.90E-01	buckling margin stringer Iseg.4 . Local halfwaves=7 .RNGS;FS=1.
10	2.49E-01	buckling stringer Isegs.3+4 together.M=7 ;C=0. ;RNGS;FS=1.4
11	2.60E+00	buckling stringer Iseg 4 as beam on foundation. M=223;RNGS;FS=1.2
12	2.42E+00	buckling margin ring Iseg.3 . Local halfwaves=1 .RNGS;FS=1.
13	1.27E+00	buckling ring Iseg 4 as beam on foundation. M=139;RNGS;FS=1.2
14	1.16E-01	buck.(SAND);simp-support local buck.; (0.95*altsol);FS=0.999
15	1.56E+01	buck.(SAND);rolling with smear rings; M=110;N=1;slope=0.01;FS=0.999
16	2.29E-01	buck.(SAND);rolling only of stringers;M=12;N=0;slope=0.;FS=1.4
17	6.11E-01	buck.(SAND);hiwave roll. of stringers;M=89;N=0;slope=0.;FS=1.2
18	8.27E-01	buck.(SAND); STRINGERS: web buckling;M=7;N=1;slope=0.;FS=1.
19	2.65E+00	buck.(SAND); RINGS: web buckling;M=1;N=1;slope=0.1749;FS=1.

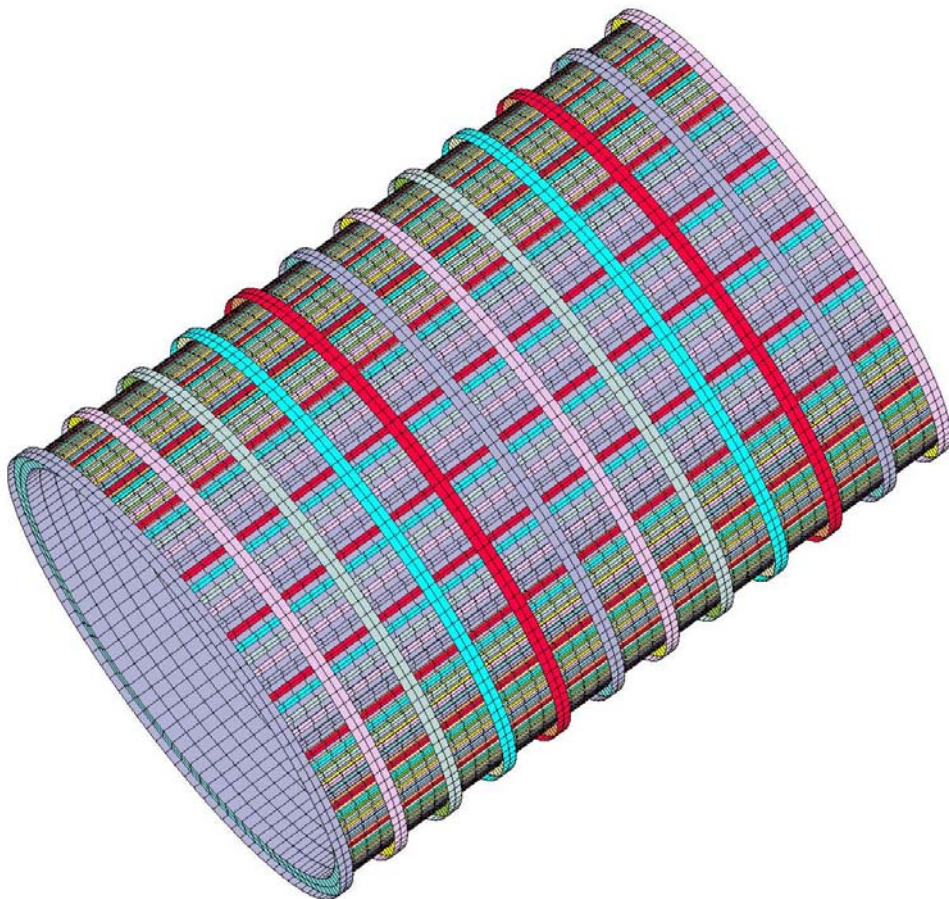
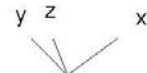


FIG. 1 STAGS model by STAGSUNIT; Entire cylindrical shell.
Case name = "testax3". The optimized shell configuration is listed in Table 2

Θ_x -35.84
 Θ_y -13.14
 Θ_z 35.63



| 6.247E+01 |

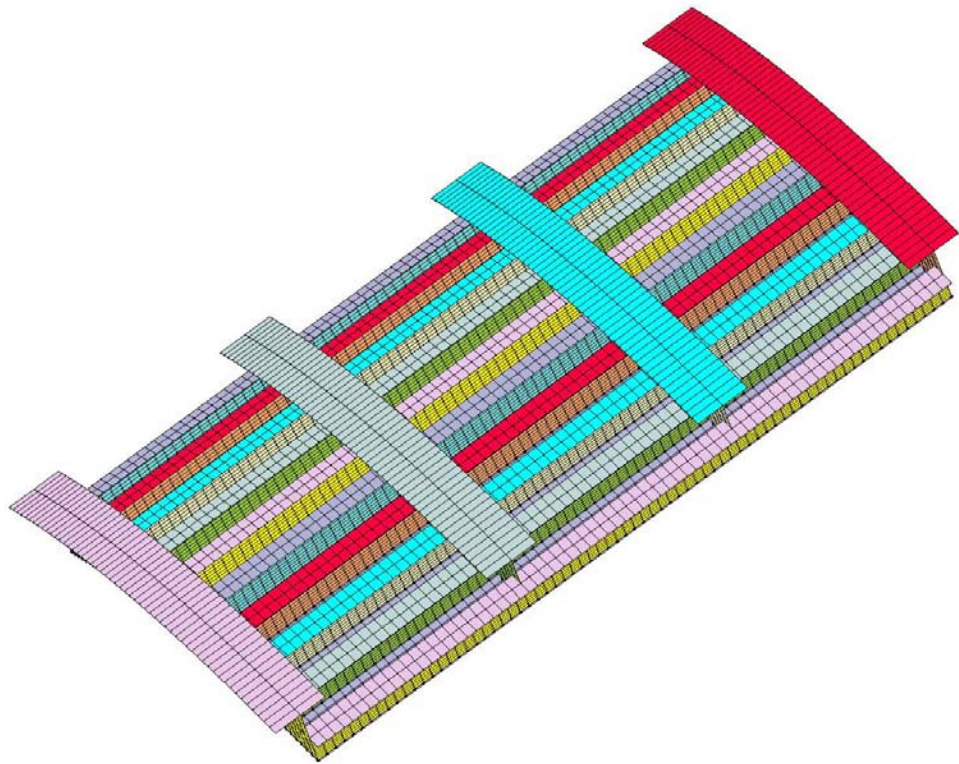


FIG. 2 STAGS model by STAGSUNIT; 3 ring bays x 9 stringer bays.
testax3: The optimized shell configuration is listed in Table 2

$\Theta_x -35.84$
 $\Theta_y -13.14$
 $\Theta_z 35.63$

y z
V

| 1.617E+01 |

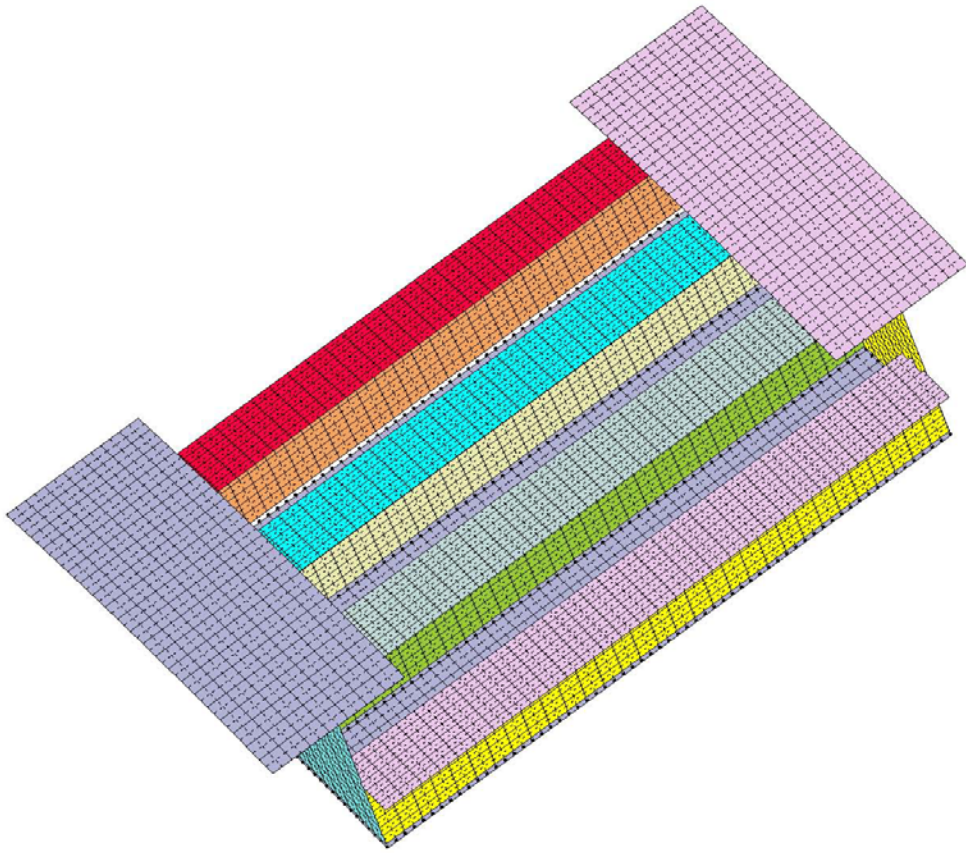


FIG 3 STAGS model by STAGSUNIT; 1 ring bay x 3 stringer bays.
testax3: The optimized shell configuration is listed in Table 2

Θ_x -35.84
 Θ_y -13.14
 Θ_z 35.63

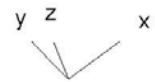


FIG. 4 testax3: Single discretized skin-stringer module; Table 2
Axial Station - inches; m=1 axial halfwaves; buckling load factor = 1.343

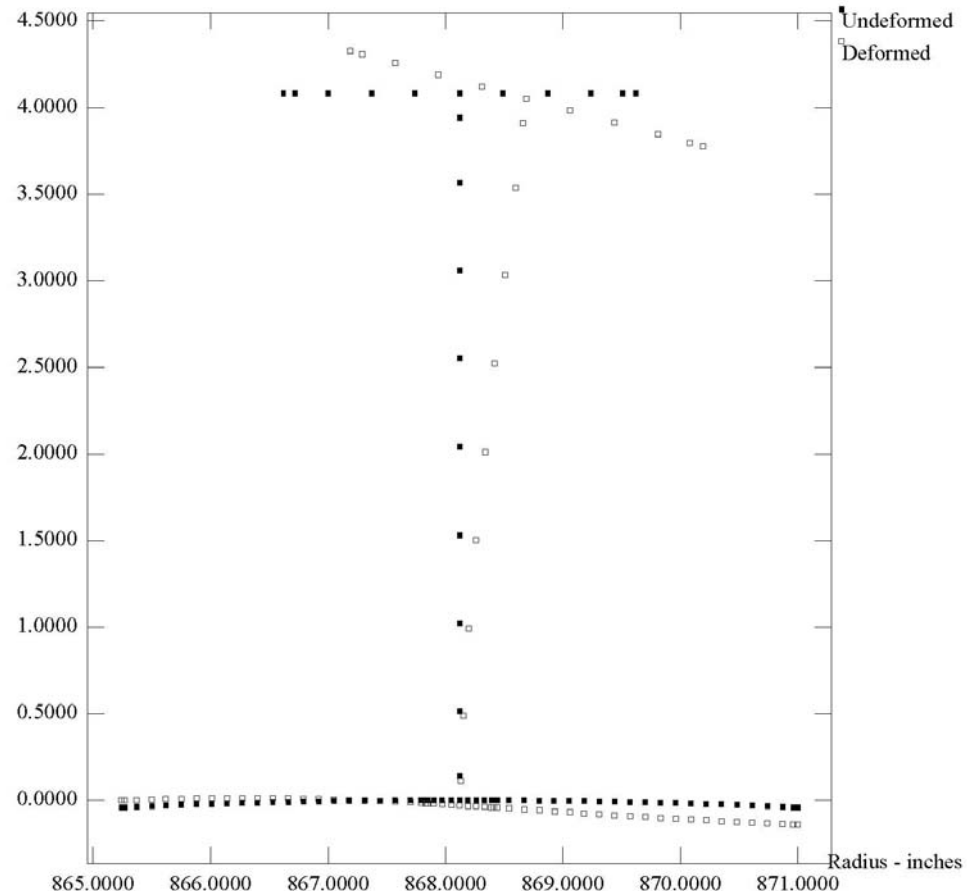
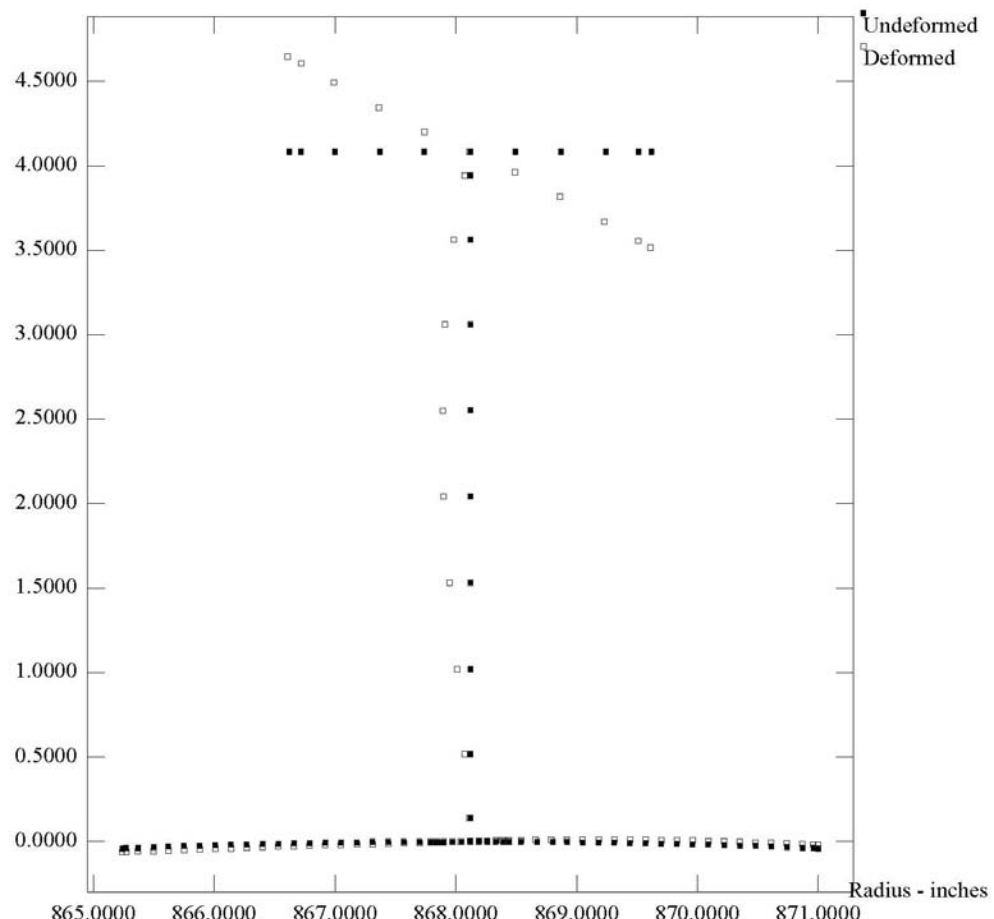
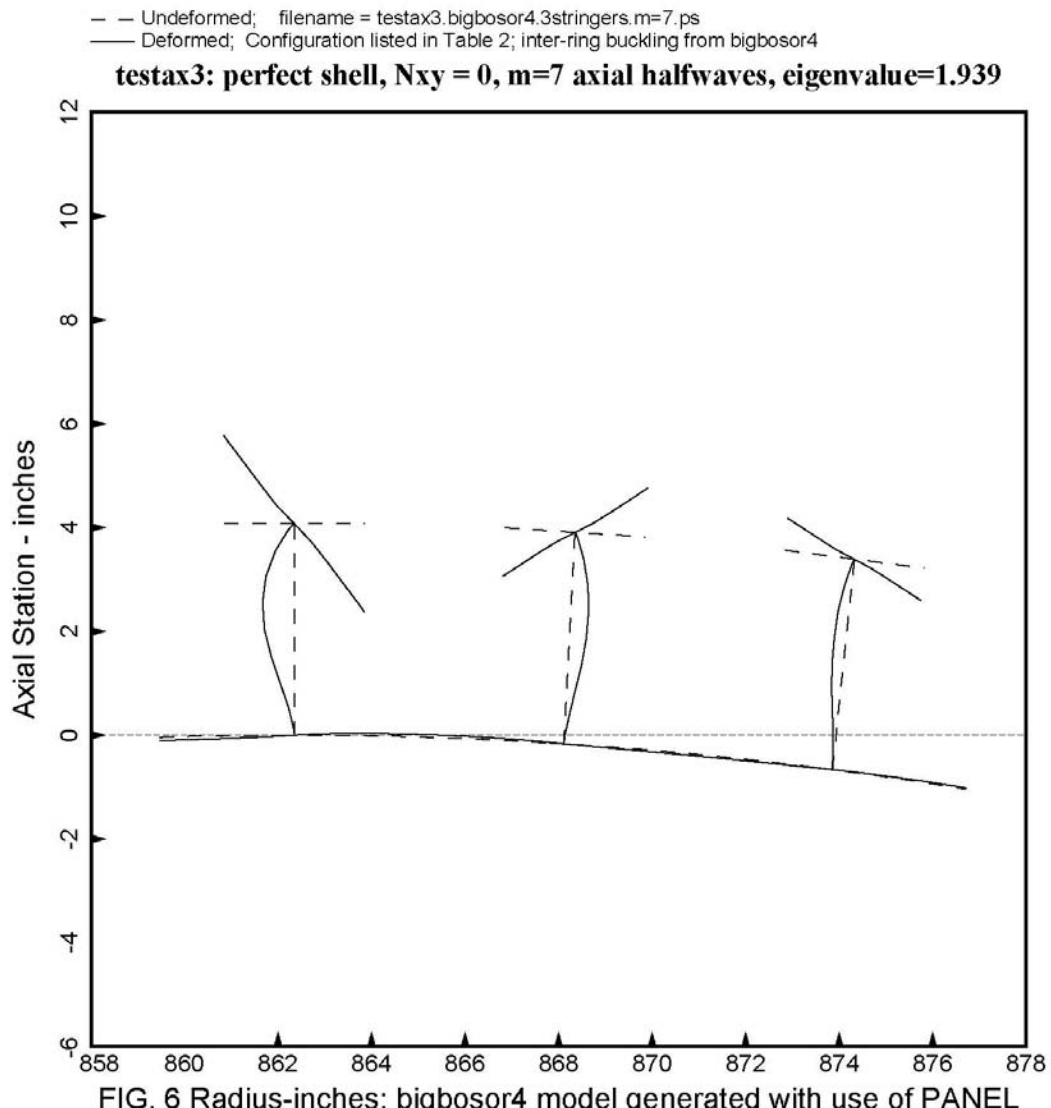


FIG. 5 testax3: single discretized skin-stringer module, Table 2

Axial Station - inches; $m=7$ axial halfwaves; buckling load factor = 1.939





-- Undeformed; filename = testax3.bigbosor4.10stringers.m=1.ps
— Deformed; Configuration listed in Table 2; inter-ring buckling from bigbosor4

testax3: perfect shell, $N_{xy} = 0$, $m=1$ axial halfwaves, eigenvalue=1.299

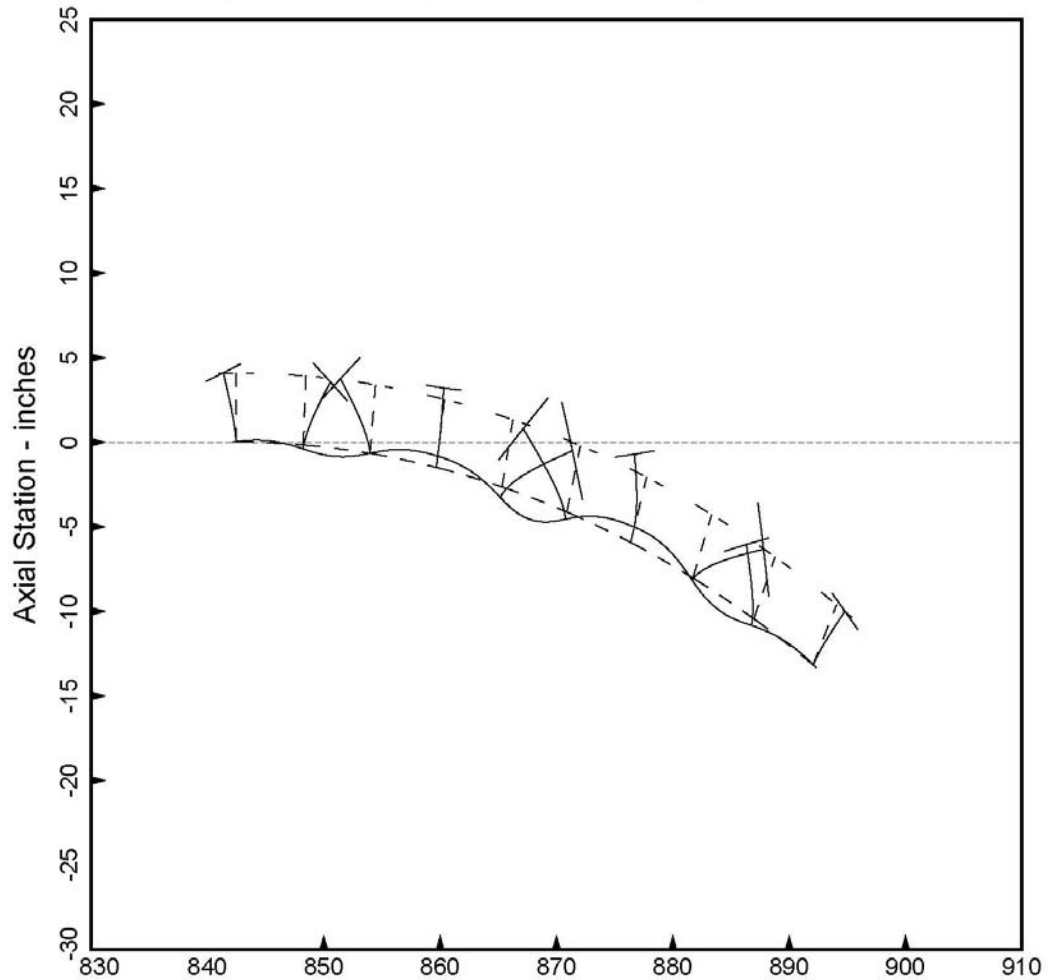


FIG. 7 Radius-inches; bigbosor4 model generated with use of PANEL

— — Undeformed; Table 2 configuration; filename= testax3.bigbosor4.1ring.n=3.ps
— Deformed; single-module skin-with-smeared-stringers/ring model

testax3: perfect shell, $N_{xy} = 0$, $n=3$ circ. waves, eigenvalue=2.7836

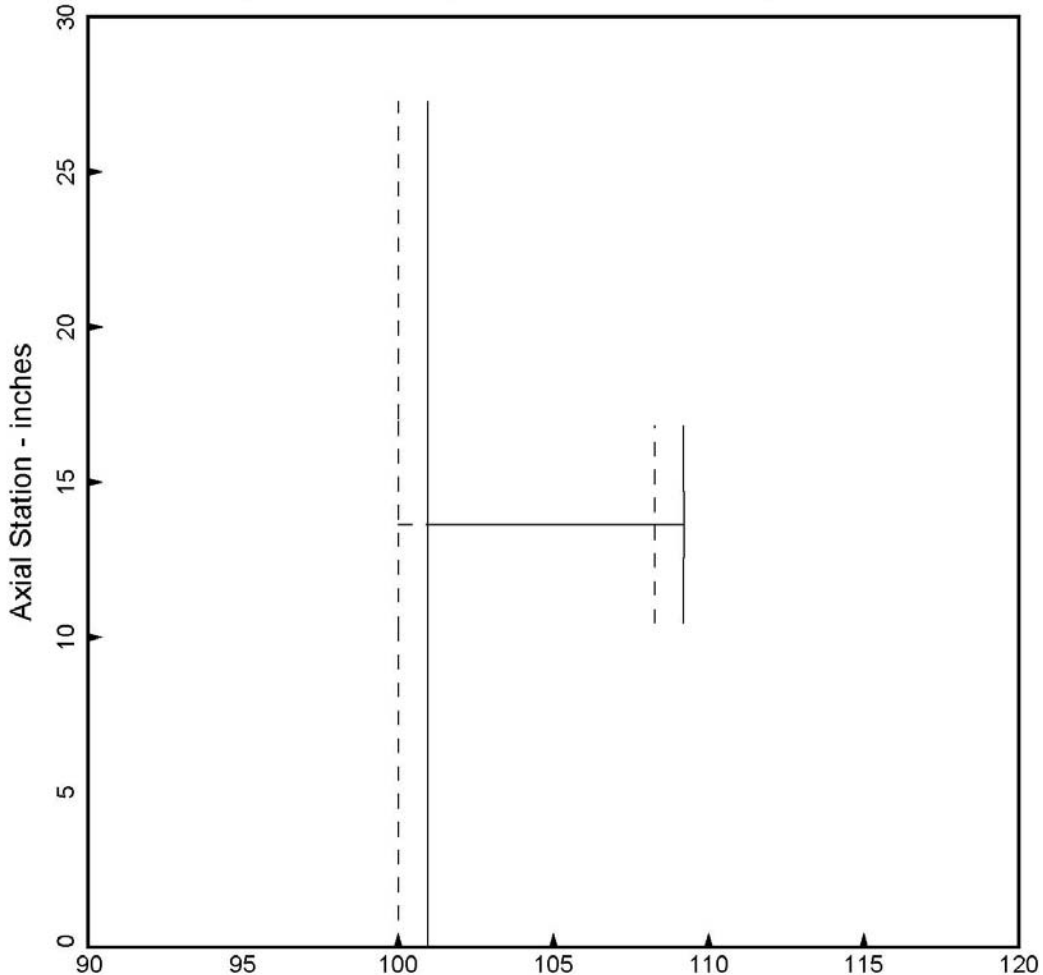


FIG. 8 Radius-inches; This model is used for smeared ring knockdown

-- Undeformed; Table 2 configuration; filename= testax3.bigbosor4.1ring.n=33.ps
— Deformed; single-module skin-with-smeared-stringers/ring model

testax3: perfect shell, $N_{xy} = 0$, $n=33$ circ. waves, eigenvalue=2.3537

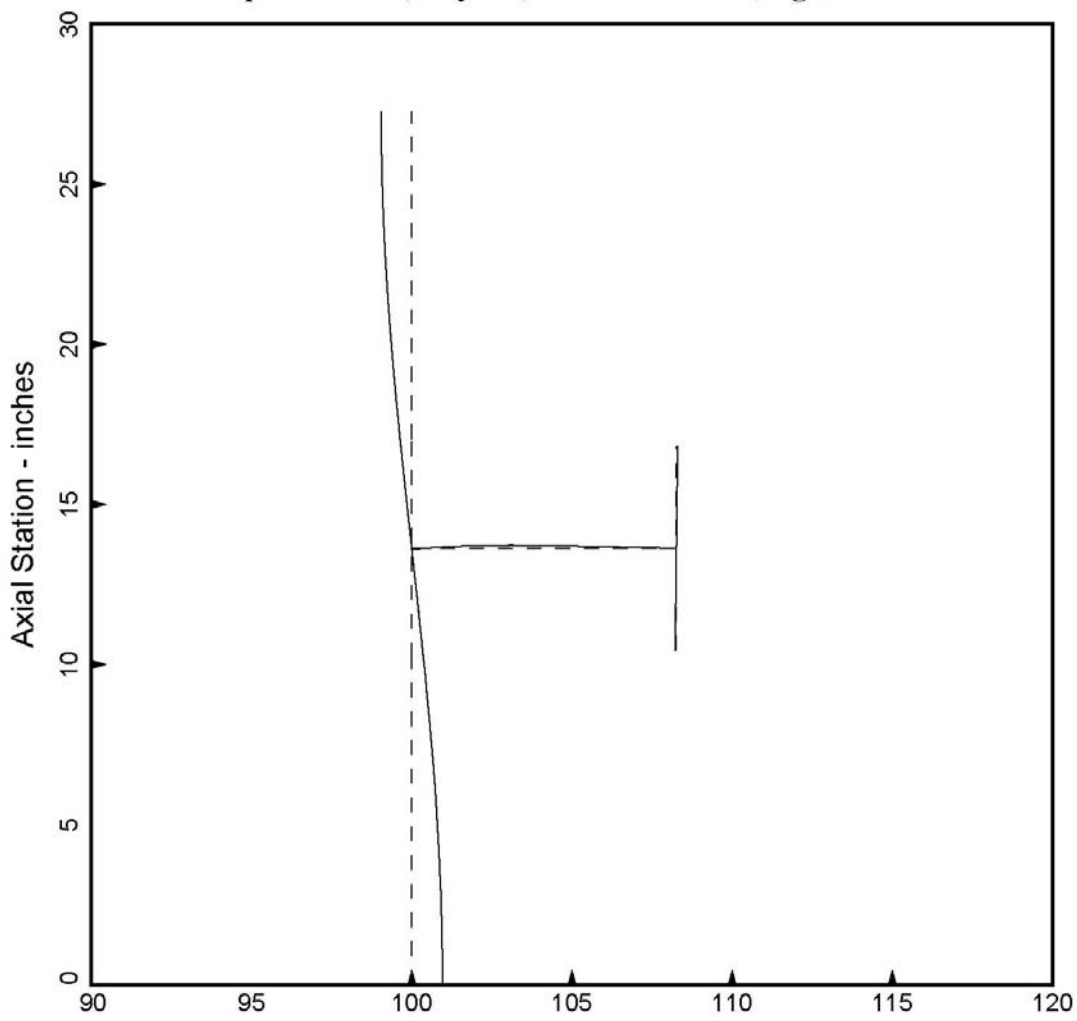
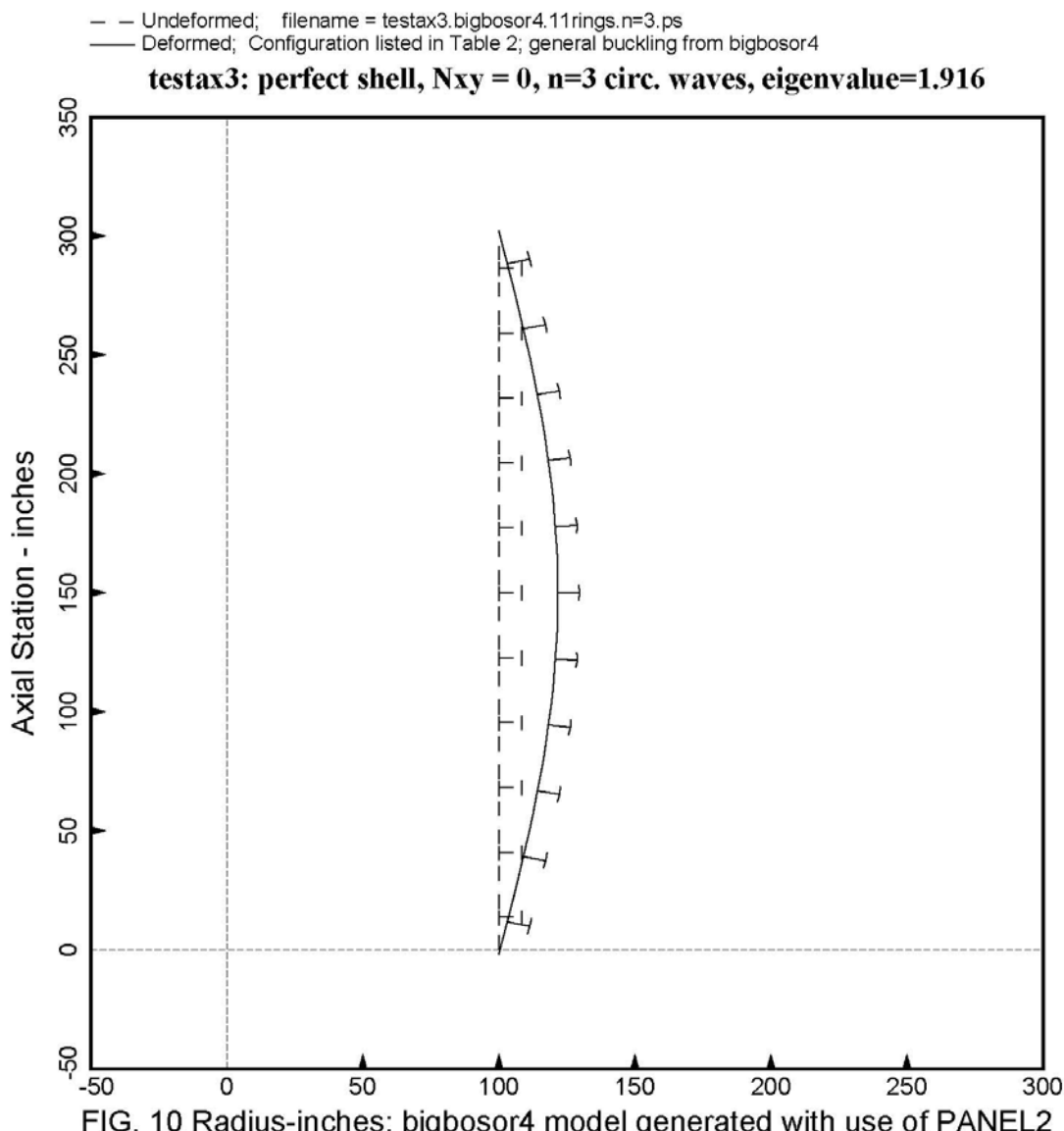


FIG. 9 Radius-inches; This model is used for "skin"-ring buckling



-- Undeformed; filename = testax3.bigbosor4.11rings.n=4.ps
— Deformed; Configuration listed in Table 2; general buckling from bigbosor4

testax3: perfect shell, $N_{xy} = 0$, $n=4$ circ. waves, eigenvalue=2.369

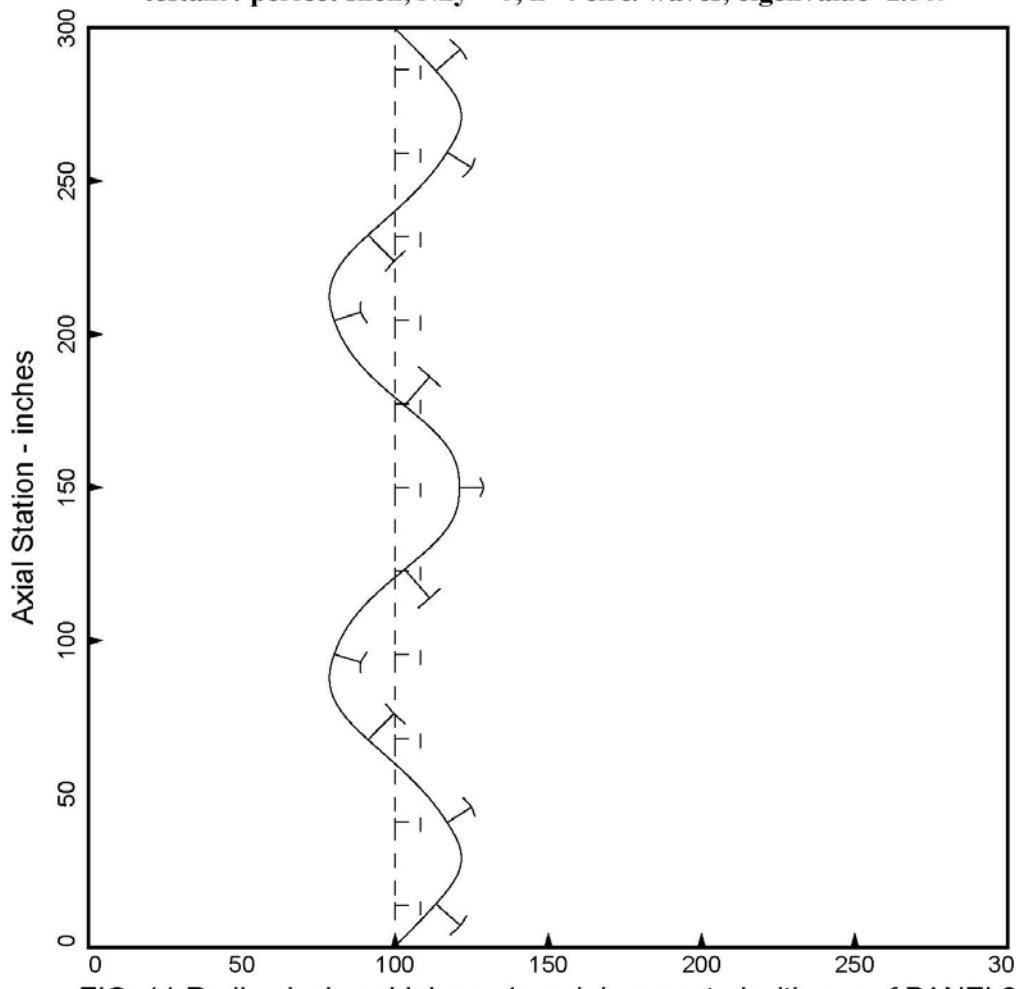
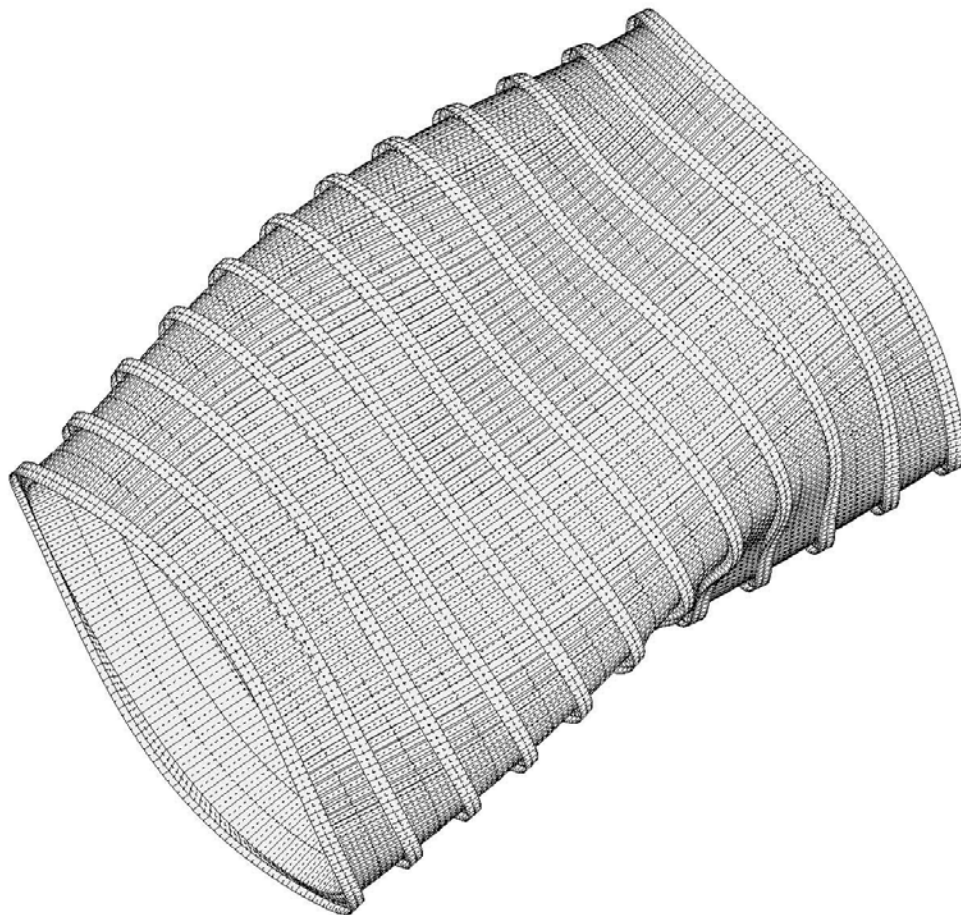


FIG. 11 Radius-inches; bigbosor4 model generated with use of PANEL2



STAGS model generated by STAGSUNIT processor; rings and stringers are shell branches

mode 1, pcr = 0.16491E+01; Configuration is listed in Table 2

Θ_x -35.84

Θ_y -13.14

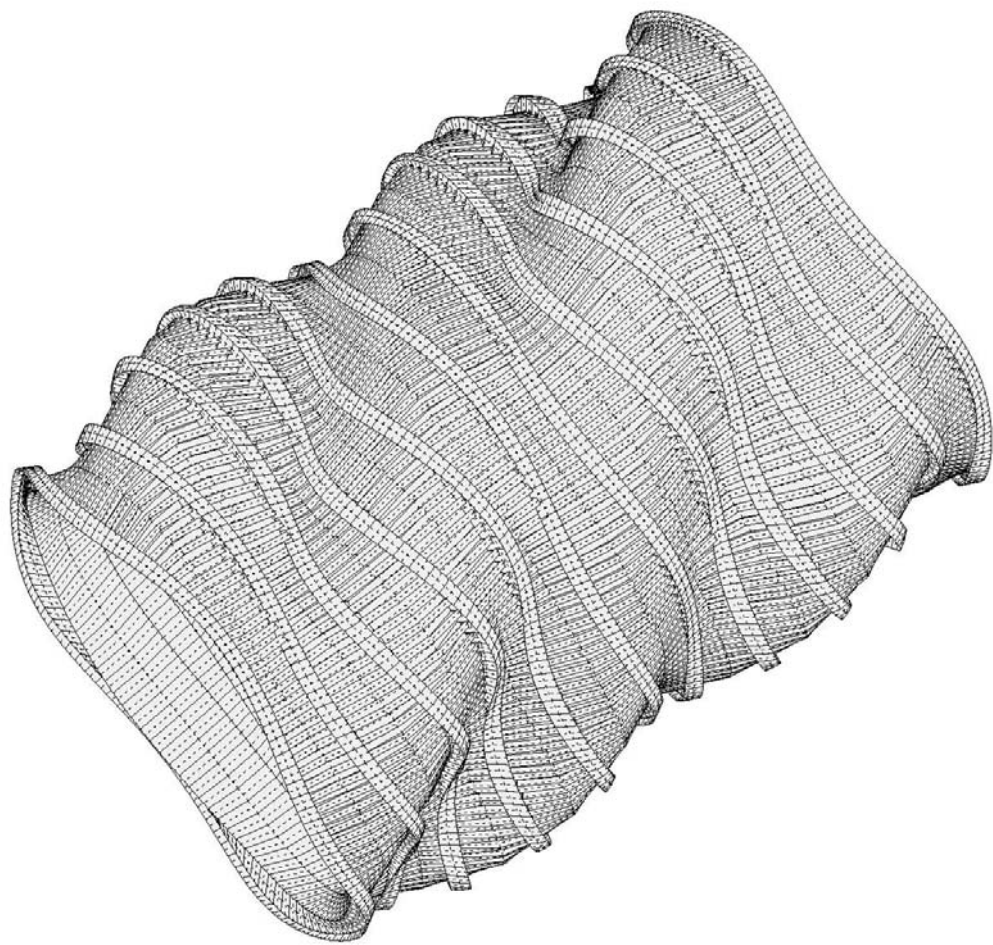
Θ_z 35.63

y z x
↙ ↘ ↗

step 0 eigenvector; 480 finite element; general buckling, n=3 circ. waves

FIG. 12 linear buckling of perfect shell; Configuration is listed in Table 2

| 6.247E+01 |



STAGS model generated by STAGSUNIT processor; rings and stringers are shell branches

mode 336, pcr = 0.19098E+01; Configuration listed in Table 2

step 0 eigenvector; 480 element; general buckling; 5 circ. waves

FIG. 13 linear buckling of perfect shell

Θ_x -35.84

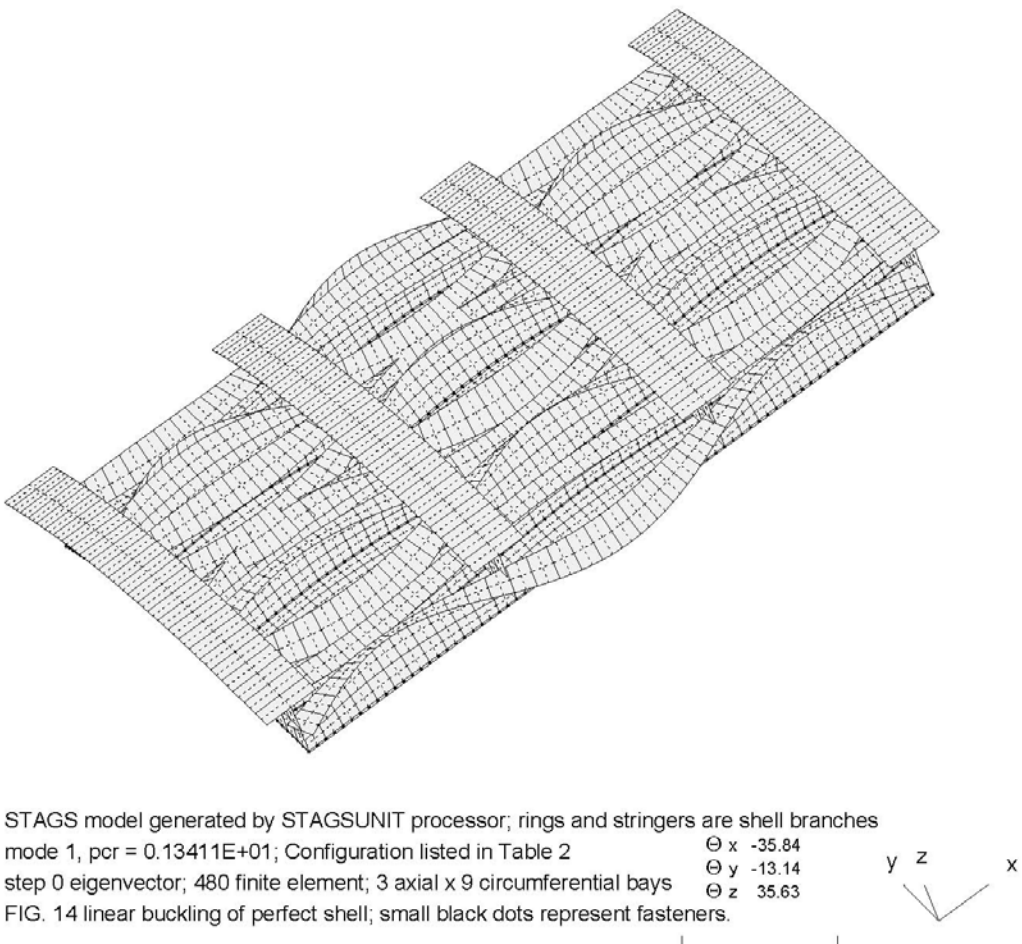
Θ_y -13.14

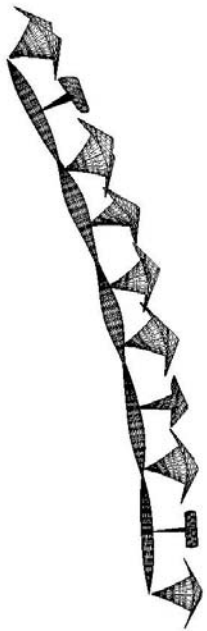
Θ_z 35.63

y z



| - 6.247E+01 - |





End view of STAGS model with rings removed so that skin-stringer buckling shows
mode 1, pcr = 0.13411E+01; Configuration listed in Table 2

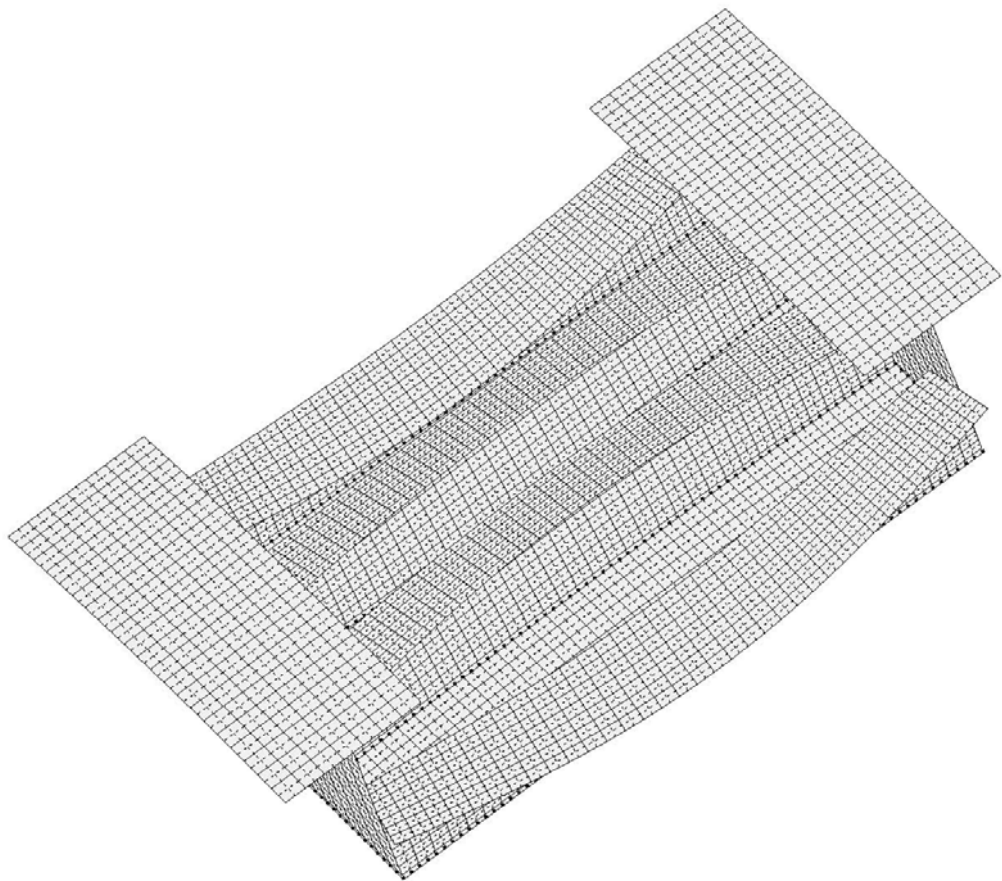
Θ_x 0.00
 Θ_y 90.00
 Θ_z 0.00

step 0 eigenvector; 480 finite element; 3 axial x 9 circumferential bays

FIG. 15 end view of linear buckling of perfect shell

y
|
x z

| 1.364E+01 |



STAGS model generated by STAGSUNIT processor; rings and stringers are shell branches

mode 1, pcr = 0.13072E+01; Configuration listed in Table 2

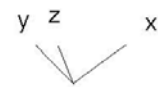
Θ_x -35.84

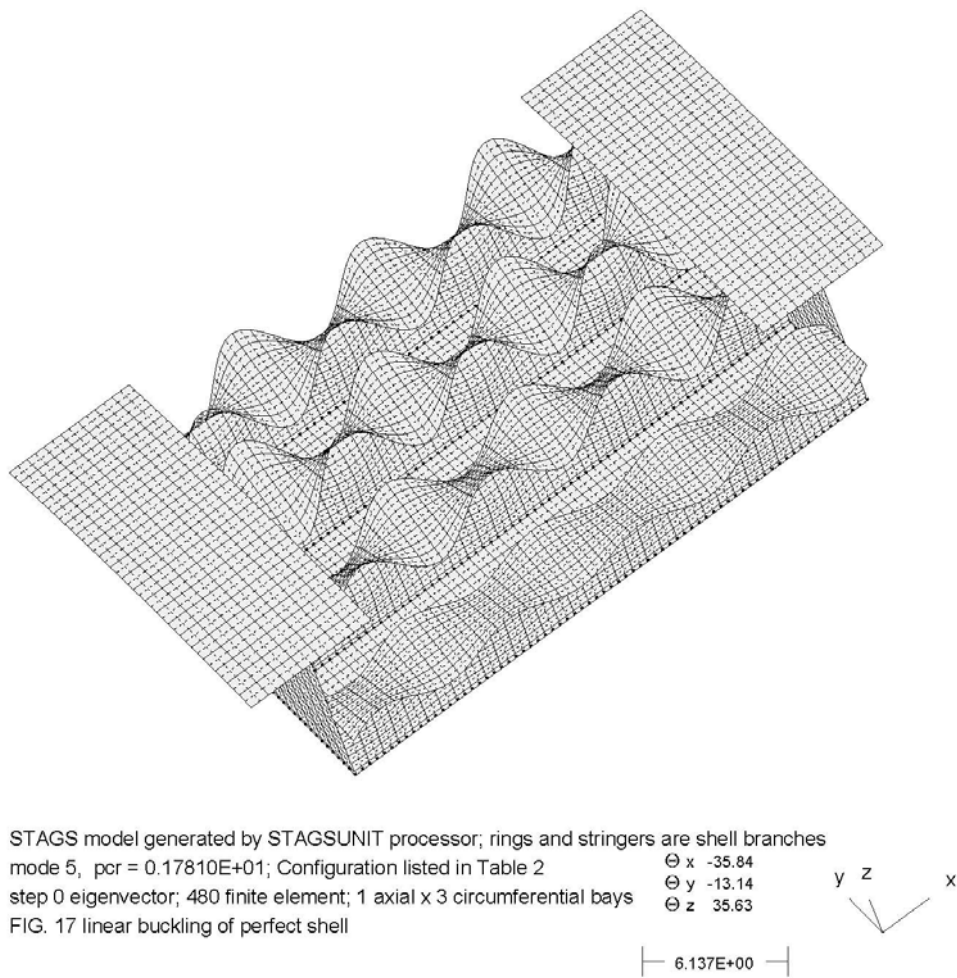
step 0 eigenvector; 480 finite element; 1 axial x 3 circumferential bays

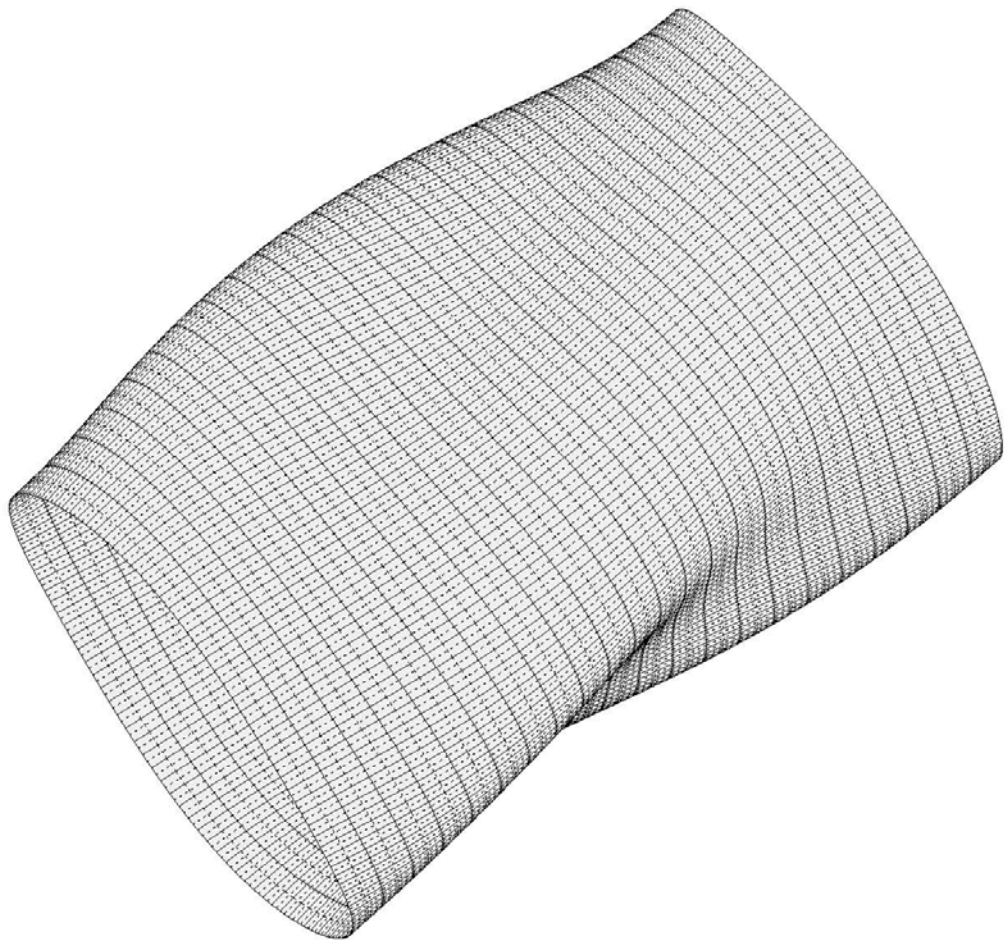
Θ_y -13.14

Θ_z 35.63

FIG. 16 linear buckling of perfect shell; small black dots represent fasteners.







STAGS model generated by STAGSUNIT processor; "smeared" rings and stringers

mode 1, pcr = 0.18240E+01; entire shell

Θ_x -35.84

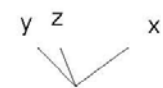
step 0 eigenvector; 480 element, general buckling, n = 3 circ. waves

Θ_y -13.14

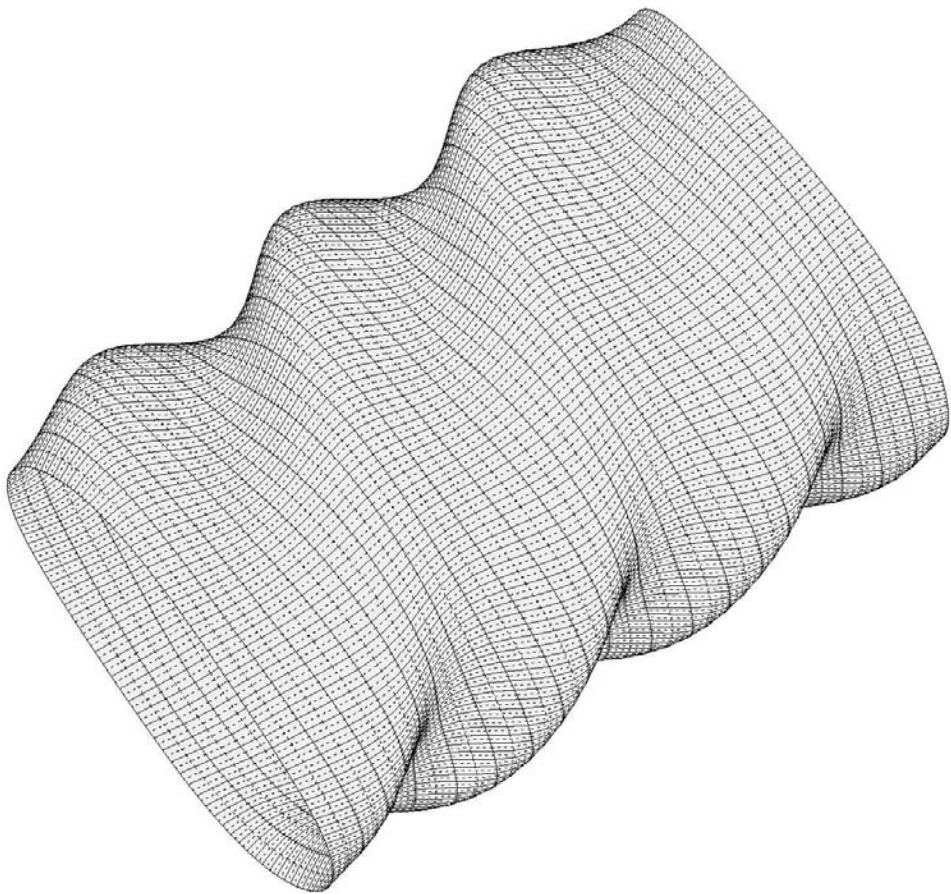
Θ_z 35.63

Θ_z 35.63

FIG. 18 linear buckling of perfect shell: Configuration is listed in Table 2



— 5.995E+01 —



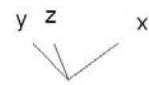
general buckling with $n = 0$ circ. waves; configuration is listed in Table 2

mode 9, $p_{cr} = 0.21841E+01$; entire shell

step 0 eigenvector; 480 element; "smeared" stringers and rings

FIG. 19 linear buckling of perfect shell; high-axial-wave mode

$\Theta_x -35.84$
 $\Theta_y -13.14$
 $\Theta_z 35.63$



- 1.1.1 Local buckling: discrete model
- 2.1.1 Bending-torsion buckling
- △ 3.1.1 m=? lateral-torsional buckling
- + 4.1.1 Ring flange buckling,discrete model
- ×
- 5.1.1 Lo-n Ring sidesway, discrete model
- ◊ 6.1.1 buckling: stringer seg.3 . MIDLENGTH
- ▽ 7.1.1 buckling: stringer seg.4 . MIDLENGTH
- ⊗ 8.1.1 buckling: stringer lsegs.3+4. MIDLENGTH
- × 9.1.1 buckling: stringer lseg 4 as beam on foundation. MIDLENGTH
- ◊ 10.1.1 buckling: ring lseg 4 as beam on foundation. MIDLENGTH
- ⊕ 11.1.1 buck(SAND)simp-support inter-ring; MIDLENGTH;(1.00*altsol)
- ⊗ 12.1.1 buck(SAND)simp-support general buck; MIDLENGTH
- 田 13.1.1 buck(SAND)simp-support general buck; MIDLENGTH;(0.85*altsol)
- ⊗ 14.1.1 buck(SAND)rolling only of stringers; MIDLENGTH
- ⊗ 15.1.1 buck(SAND)hiwave roll. of stringers; MIDLENGTH
- 16.1.1 buck(SAND) STRINGERS: web buckling; MIDLENGTH
- 20.1.1 Long-axial-wave bending-torsion buckling

testax3: PANDA2 not allowed to change imperfection amplitudes; Wimp=+1.

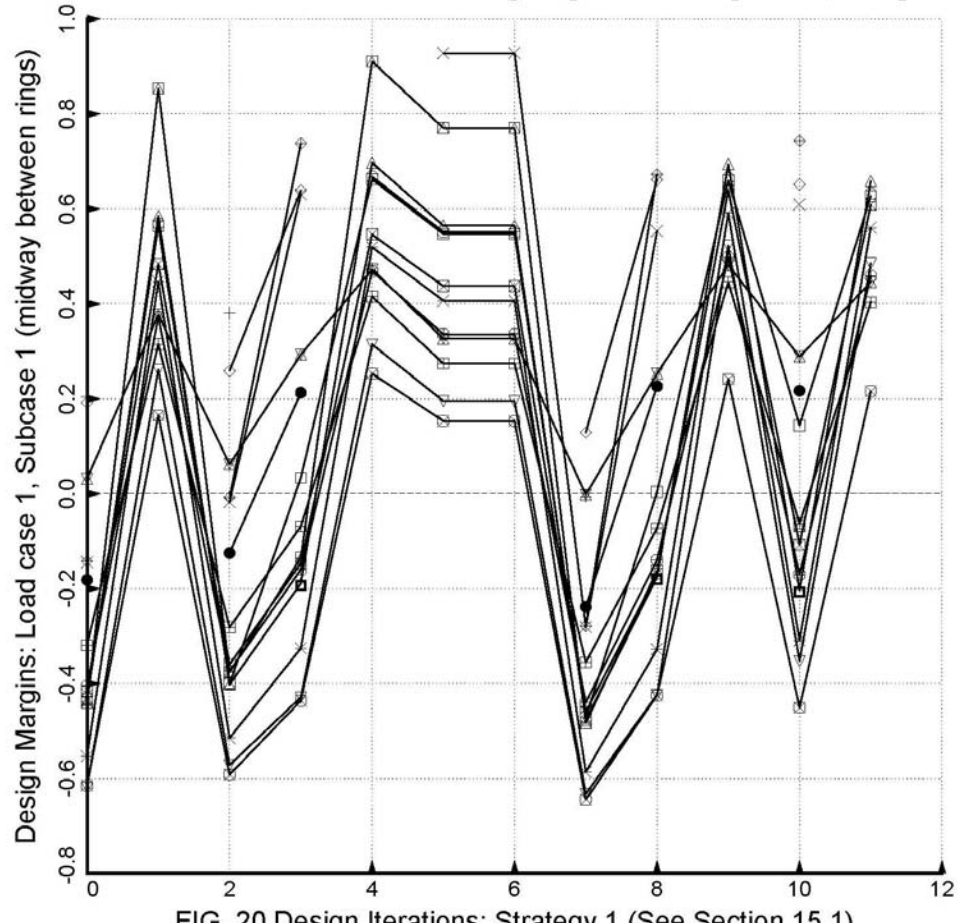


FIG. 20 Design Iterations; Strategy 1 (See Section 15.1)

- 1.1.1 Local buckling: discrete model
- 2.1.1 Bending-torsion buckling
- 3.1.1 m=? lateral-torsional buckling
- 4.1.1 Ring flange buckling,discrete model
- 5.1.1 Lo-n Ring sidesway, discrete model
- 6.1.1 buckling: stringer seg.4 . MIDLENGTH
- 7.1.1 buckling: stringer Isegs.3+4. MIDLENGTH
- 8.1.1 buckling: stringer Iseg 4 as beam on foundation. MIDLENGTH
- 9.1.1 buckling: ring Iseg 4 as beam on foundation. MIDLENGTH
- 10.1.1 buck(SAND)simp-support local buck.; MIDLENGTH;(0.95*altsol)
- 11.1.1 buck(SAND)simp-support inter-ring; MIDLENGTH;(1.00*altsol)
- 12.1.1 buck(SAND)simp-support general buck; MIDLENGTH
- 13.1.1 buck(SAND)simp-support general buck; MIDLENGTH;(0.85*altsol)
- 14.1.1 buck(SAND)rolling only of stringers; MIDLENGTH
- 15.1.1 buck(SAND)hiwave roll. of stringers; MIDLENGTH
- 16.1.1 -V(3)^1+20.V(6)^1-1
- 17.1.1 -V(10)^1+20.V(12)^1-1
- 18.1.1 buck(SAND) STRINGERS: web buckling; MIDLENGTH
- 19.1.1 buckling: stringer seg.3 . MIDLENGTH

testax3: PANDA2 is allowed to change imperfection amplitudes; Wimp=+1.

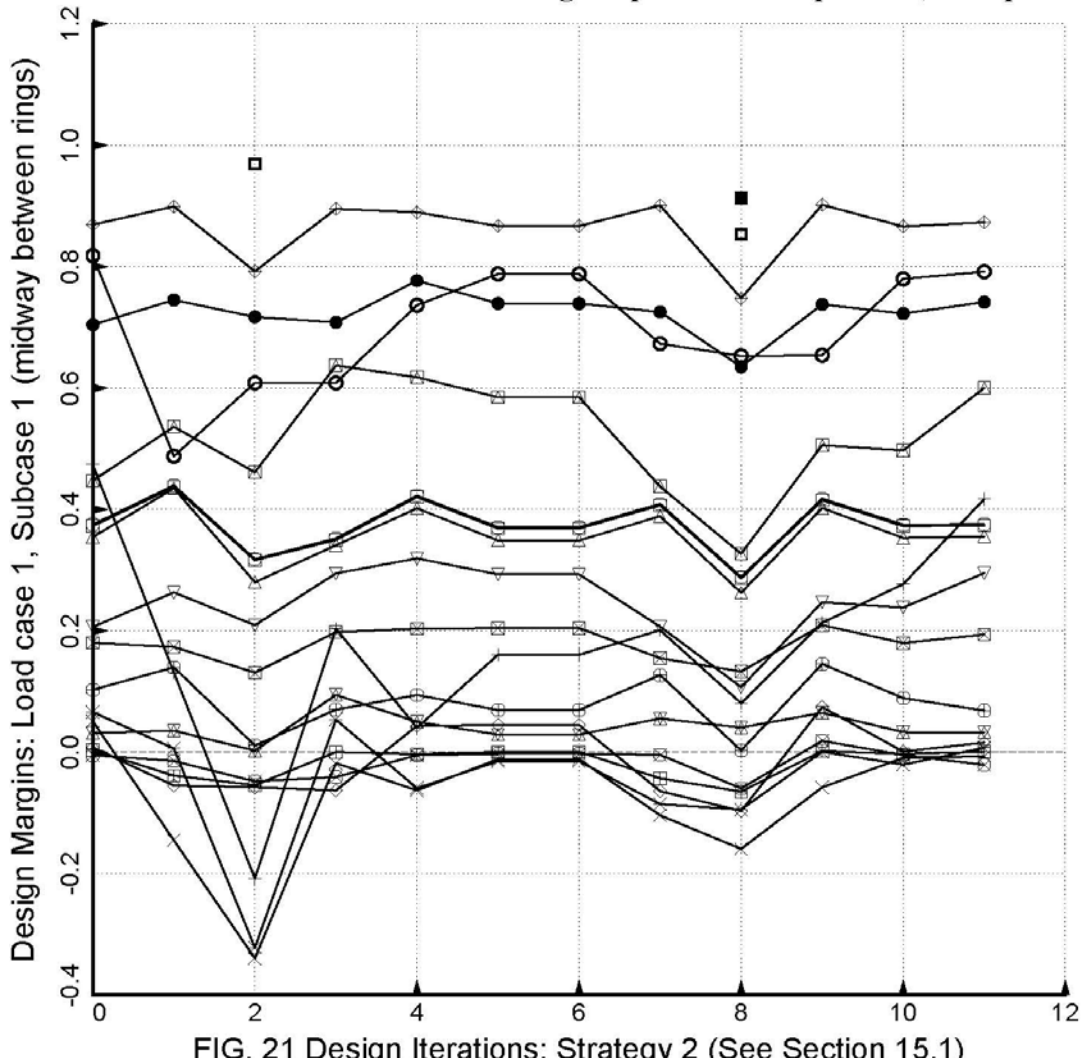
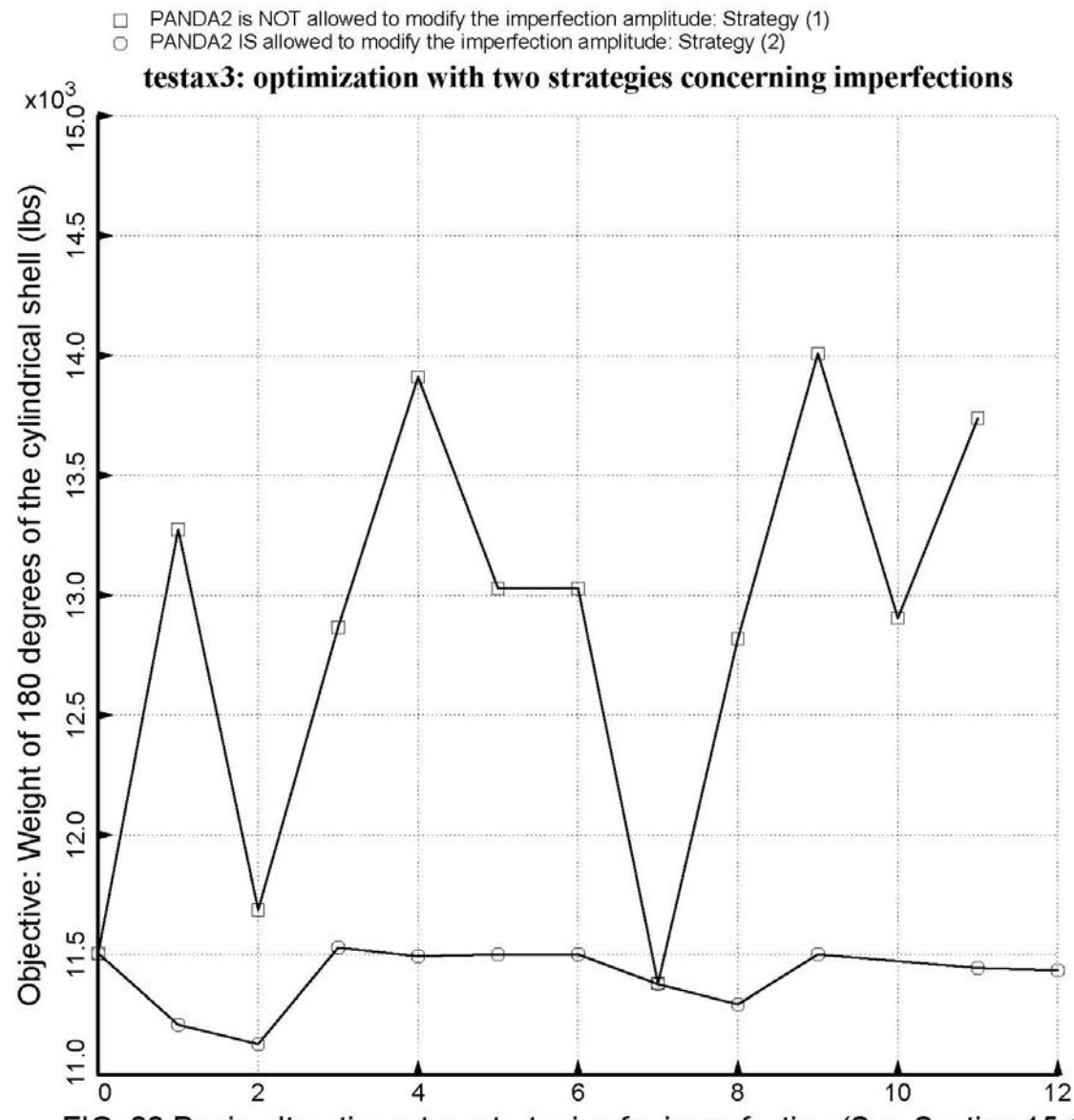


FIG. 21 Design Iterations; Strategy 2 (See Section 15.1)



□ Buckling load factors for m=1,n=3 halfwaves: Shell dimensions are listed in Tables 1 and 2

Buckling load factor vs. slope of the buckling nodal lines for design in Table 2

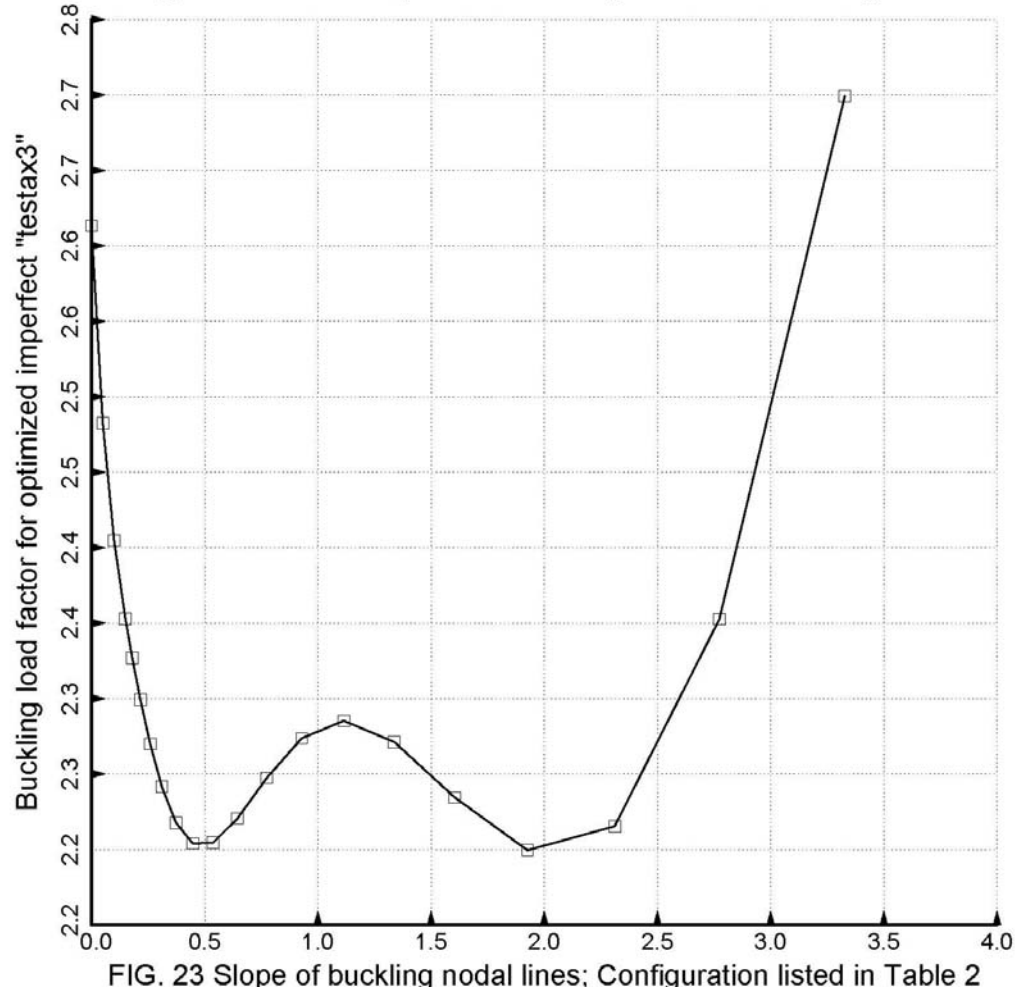


FIG. 23 Slope of buckling nodal lines; Configuration listed in Table 2

- 1.1.1 Local buckling; discrete model
- 2.1.1 Bending-torsion buckling
- △ 4.1.1 m=? lateral-torsional buckling
- + 5.1.1 Ring flange buckling,discrete model
- × 6.1.1 Lo-n Ring sidesway, discrete model
- ◊ 9.1.1 buckling: stringer seg.4 . MIDLENGTH
- ▽ 10.1.1 buckling: stringer Isegs.3+4. MIDLENGTH
- ▣ 11.1.1 buckling: stringer Iseg 4 as beam on foundation. MIDLENGTH
- × 13.1.1 buckling: ring Iseg 4 as beam on foundation. MIDLENGTH
- ⊕ 14.1.1 buck(SAND)simp-support local buck.; MIDLENGTH;(0.95*altsol)
- ⊖ 15.1.1 buck(SAND)simp-support inter-ring; MIDLENGTH;(1.00*altsol)
- ⊗ 16.1.1 buck(SAND)simp-support general buck; MIDLENGTH
- 17.1.1 buck(SAND)simp-support general buck; MIDLENGTH;(0.85*altsol)
- ⊗ 19.1.1 buck(SAND)rolling only of stringers; MIDLENGTH
- ⊗ 20.1.1 buck(SAND)hiwave roll. of stringers; MIDLENGTH
- 27.1.1 Hi-n Ring flng buck.,discrete model
- 28.1.1 Long-axial-wave bending-torsion buckling
- 30.1.1 Inter-ring buckling, discrete model

testax3: including slope of buckling nodal lines when computing Wxx,Wyy,Wxy

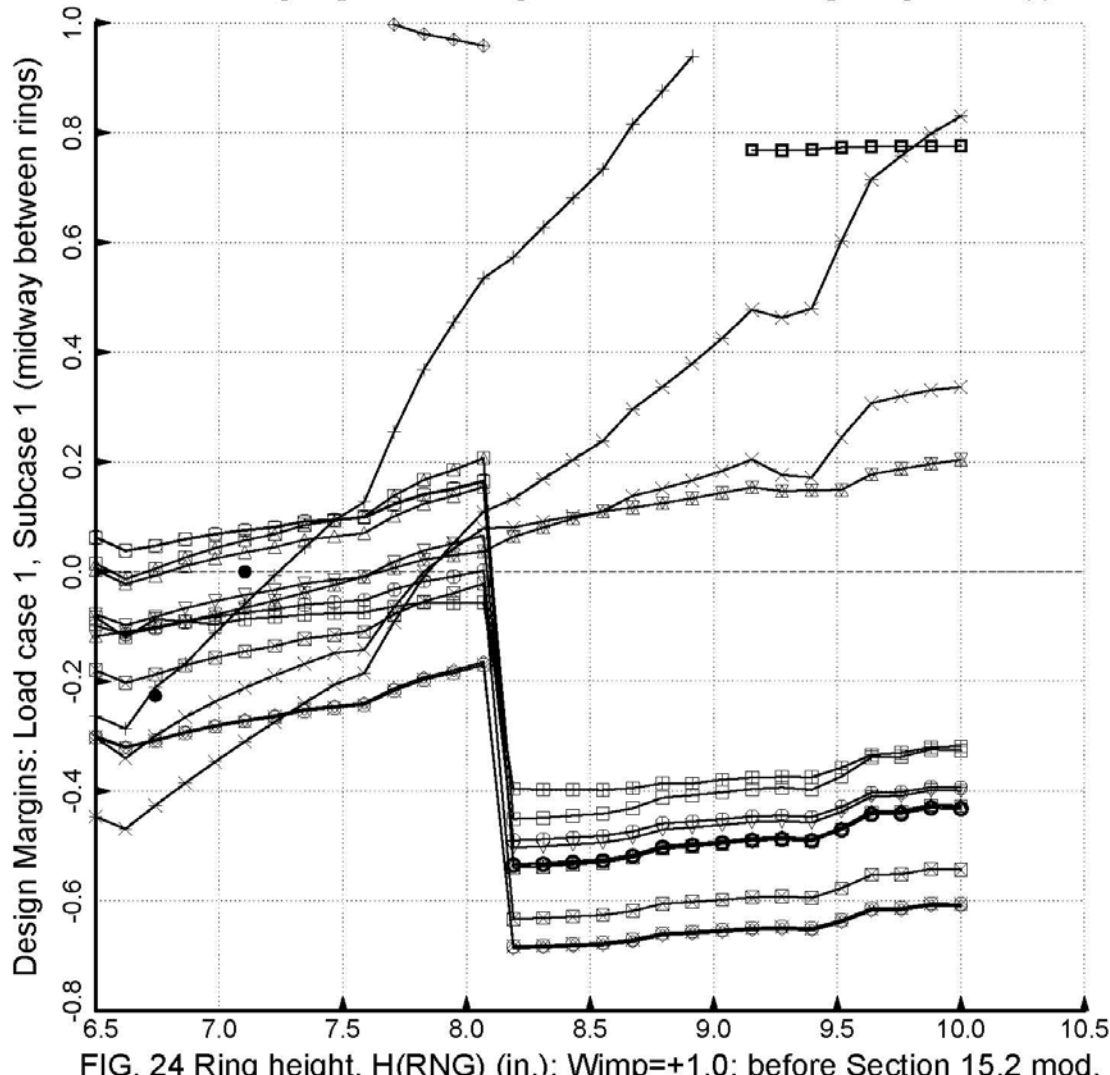


FIG. 24 Ring height, H(RNG) (in.); Wimp=+1.0; before Section 15.2 mod.

- 1.1.1 Local buckling; discrete model
- 2.1.1 Bending-torsion buckling
- △ 4.1.1 m=? lateral-torsional buckling
- + 5.1.1 Ring flange buckling,discrete model
- × 6.1.1 Lo-n Ring sidesway, discrete model
- ◇ 9.1.1 buckling: stringer seg.4 . MIDLENGTH
- ▽ 10.1.1 buckling: stringer lseg.3+4. MIDLENGTH
- ▣ 11.1.1 buckling: stringer lseg 4 as beam on foundation. MIDLENGTH
- ✗ 13.1.1 buckling: ring lseg 4 as beam on foundation. MIDLENGTH
- ◊ 14.1.1 buck(SAND)simp-support local buck.; MIDLENGTH;(0.95*altsol)
- ⊕ 15.1.1 buck(SAND)simp-support inter-ring; MIDLENGTH;(1.00*altsol)
- ⊗ 16.1.1 buck(SAND)simp-support general buck; MIDLENGTH
- 17.1.1 buck(SAND)simp-support general buck; MIDLENGTH;(0.85*altsol)
- ▢ 19.1.1 buck(SAND)rolling only of stringers; MIDLENGTH
- ▢ 20.1.1 buck(SAND)hiwave roll. of stringers; MIDLENGTH
- 27.1.1 Hi-n Ring flng buck.,discrete model
- 28.1.1 Inter-ring buckling, discrete model

testax3: neglecting slope of buckling nodal lines when computing Wxx,Wyy,Wxy

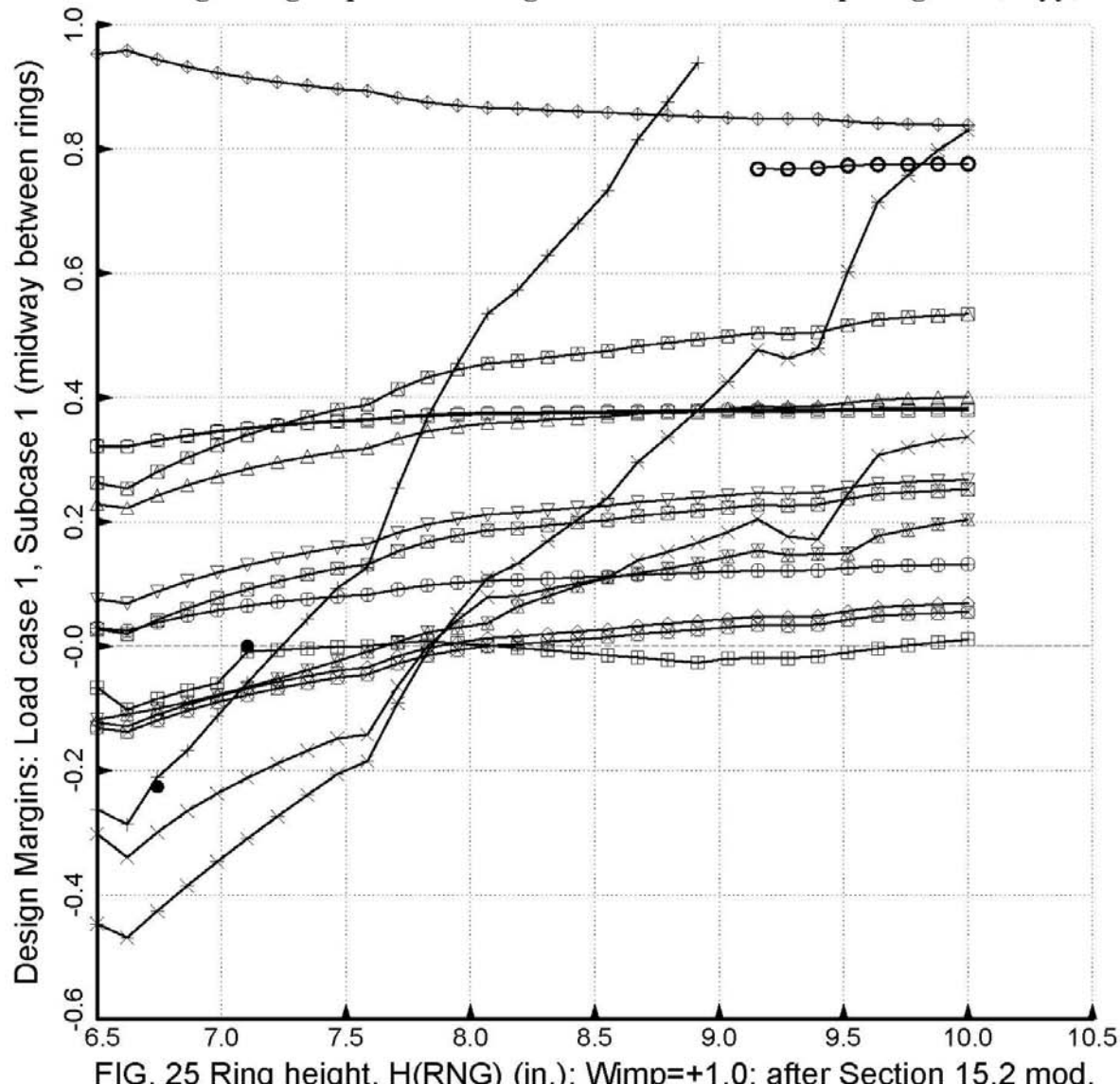


FIG. 25 Ring height, H(RNG) (in.); Wimp=+1.0; after Section 15.2 mod.

- 1. 2.1 Local buckling: discrete model
- 2. 2.1 Bending-torsion buckling
- △ 4. 2.1 m=? lateral-torsional buckling
- + 5. 2.1 Inter-ring buckling, discrete model
- ◇ 8. 2.1 buckling: stringer seg.4 . MIDLENGTH
- ▽ 9. 2.1 buckling: stringer lseg.3+4. MIDLENGTH
- ▣ 10. 2.1 buckling: stringer lseg 4 as beam on foundation. MIDLENGTH
- ◊ 12. 2.1 buckling: ring lseg 4 as beam on foundation. MIDLENGTH
- ⊕ 13. 2.1 buck(SAND)simp-support general buck; MIDLENGTH
- ⊗ 14. 2.1 buck(SAND)rolling with smear string; MIDLENGTH
- 16. 2.1 buck(SAND)rolling only of stringers; MIDLENGTH
- ⊗ 17. 2.1 buck(SAND)hiwave roll. of stringers; MIDLENGTH
- 18. 2.1 buck(SAND)rolling only of rings; MIDLENGTH
- 19. 2.1 buck(SAND)hiwave roll. of rings; MIDLENGTH
- 23. 2.1 Lo-n Inter-ring buc.,discrete model

testax3: neglecting slope of buckling nodal lines when computing Wxx,Wyy,Wxy

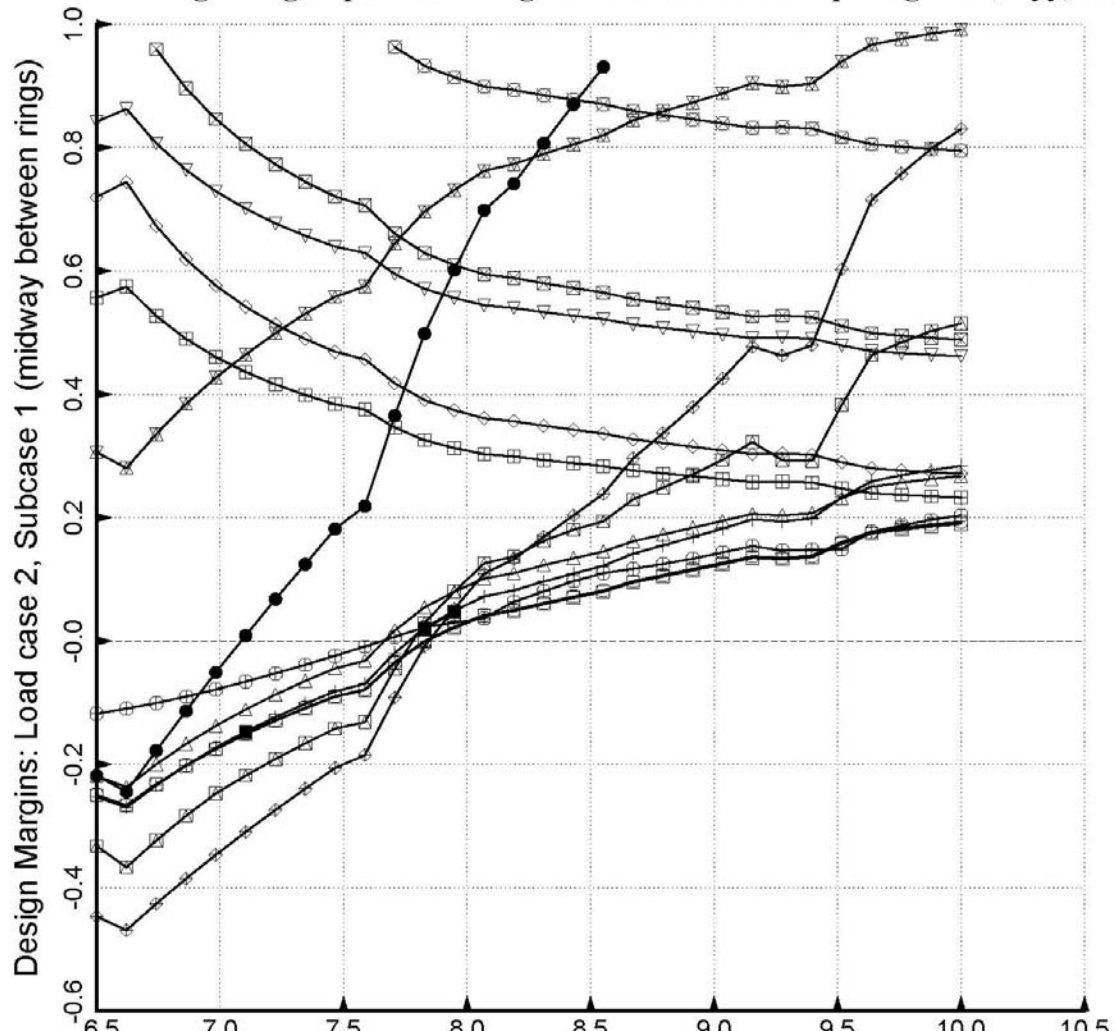


FIG. 26 Ring height, H(RNG) (in.); Wimp=-1.0; after Section 15.2 mod.



STAGS model generated by STAGSUNIT processor; rings and stringers are shell branches

mode 275, pcr= 1.8869; One of many "spurious" local buckling modes

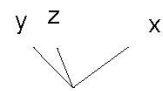
$$\Theta_x -35.84$$

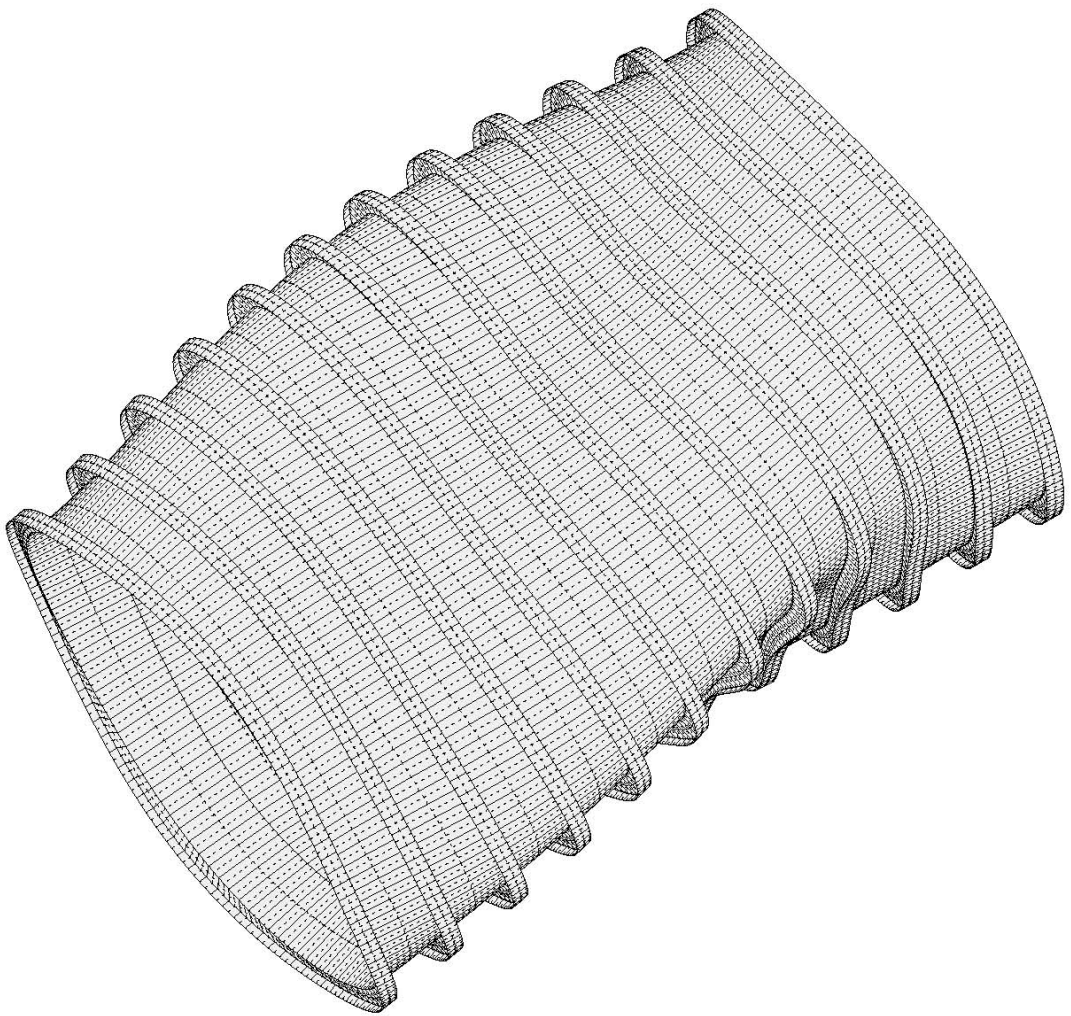
$$\Theta_y -13.14$$

$$\Theta_z 35.63$$

The general buckling modes are "hidden" among the "spurious" modes

FIG. 27 linear buckling of perfect shell; Configuration is listed in Table 2





STAGS model generated with STAGSUNIT processor; stringers smeared; rings are shell branches

mode 1, pcr = 0.16516E+01; Configuration is listed in Table 2

step 0 eigenvector; general buckling with n = 3 circ. waves

FIG. 28 linear buckling of perfect shell

Θ_x -35.84

Θ_y -13.14

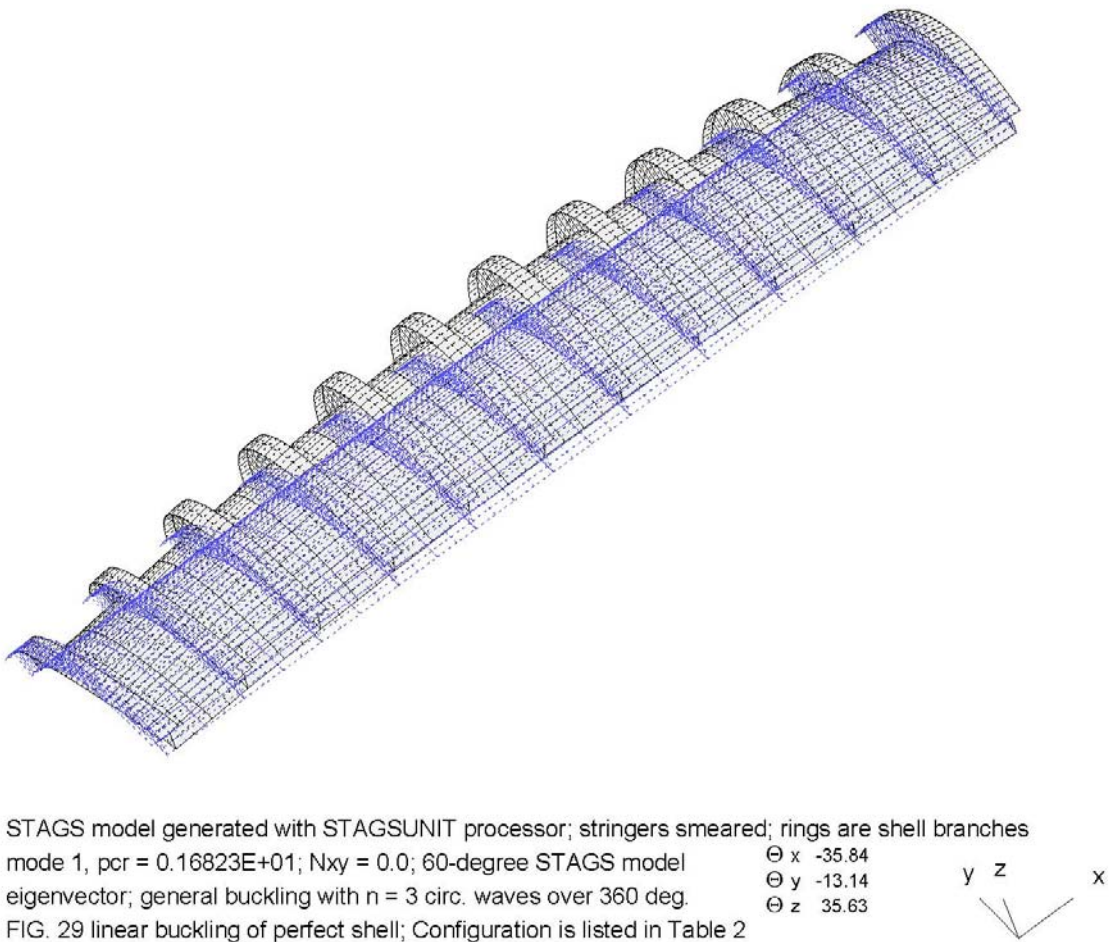
Θ_z 35.63

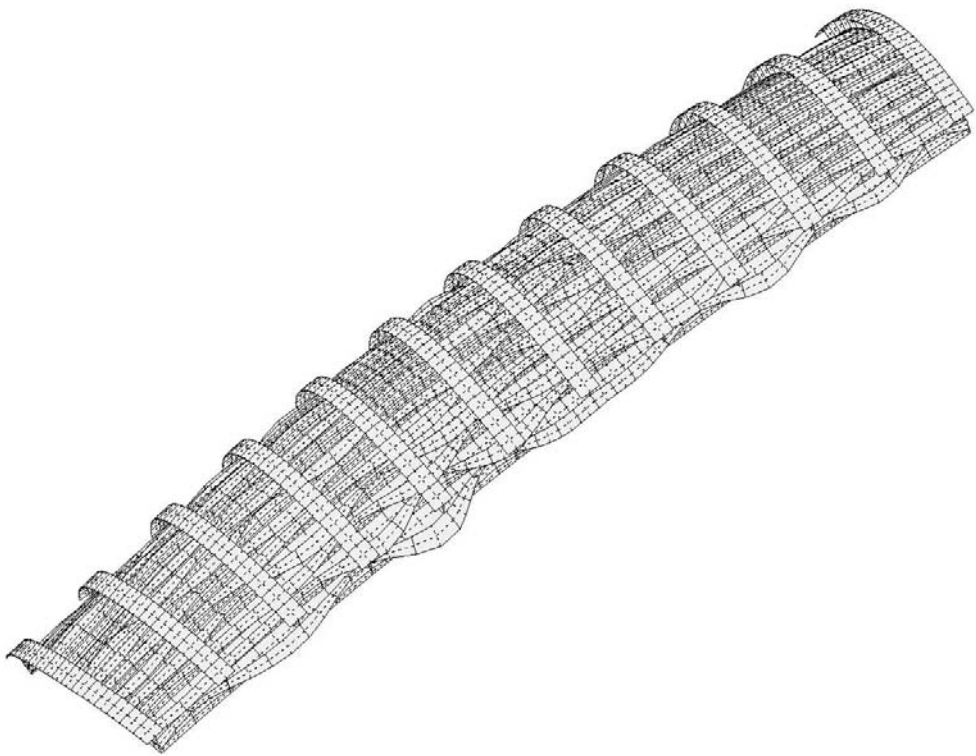
y z

x



| - 6.247E+01 - |





STAGS model generated with STAGSUNIT processor; 60-degrees of cyl. shell included

mode 58, pcr = 0.16544E+01; This mode is used for imperfection.

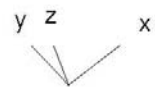
Θ_x -35.84

eigenvector; deformed geometry; general buckling, n = 3 circ. waves

Θ_y -13.14

FIG. 30 linear buckling of perfect shell; $N_{xy}=0.0$; The configuration is listed in Table 2

Θ_z 35.63



| - 4.721E+01 - |

- Displacement w; Node 1388; inward Wimp; Table 2 dimensions; 60-deg. model
- w; Node 5236; outstanding flange, stringer 7; inward Wimp; Table 2; 60-deg. model
- △ w; Node 5238; outstanding flange, stringer 7; inward Wimp; Table 2; 60-deg. model
- + w; Node 5692; outstanding flange, stringer 8; inward Wimp; Table 2; 60-deg. model
- × w; Node 5694; outstanding flange, stringer 8; inward Wimp; Table 2; 60-deg. model
- ◊ w; Node 5025; at web tip, stringer 7; inward Wimp; Table 2; 60-deg. model
- ▽ w; Node 5481; at web tip, stringer 8; inward Wimp; Table 2; 60-deg. model
- w; Node 1056; in panel skin; outward Wimp; Table 2; 60-deg. model

STAGS 60-degree models: testax3, (m,n)=(1,3) imperfection; Wimp=+,-1.0

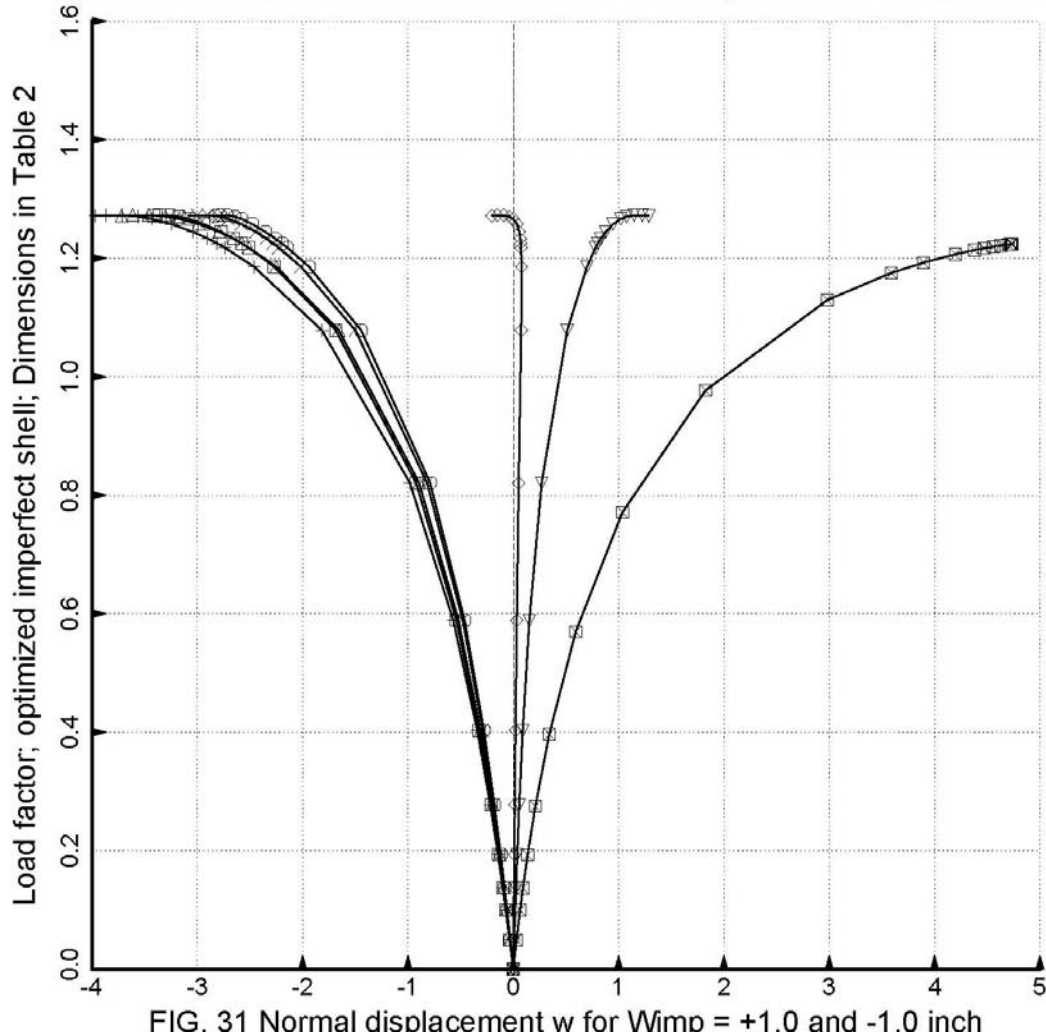
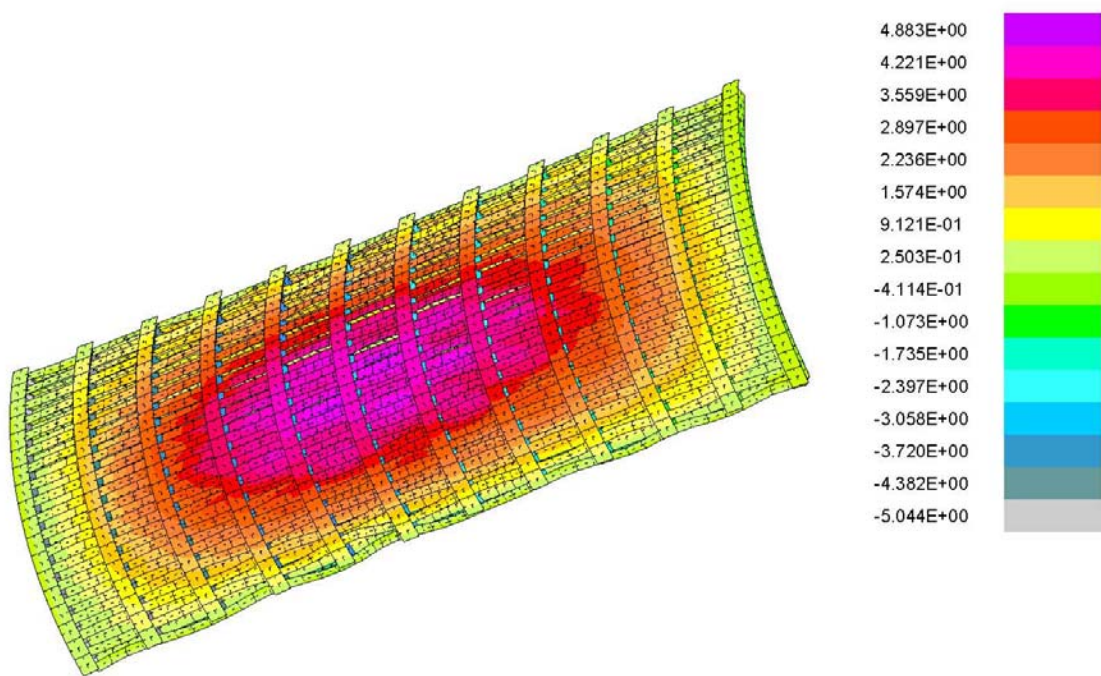


FIG. 31 Normal displacement w for $Wimp = +1.0$ and -1.0 inch



solution scale=1.0; initial imperfection shape = +1.0 x mode 58

PA= 1.22378E+00 PB= 0.00000E+00 PX= 0.00000E+00

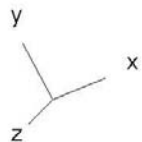
step 29 displacement w contours; Nxy=0.0

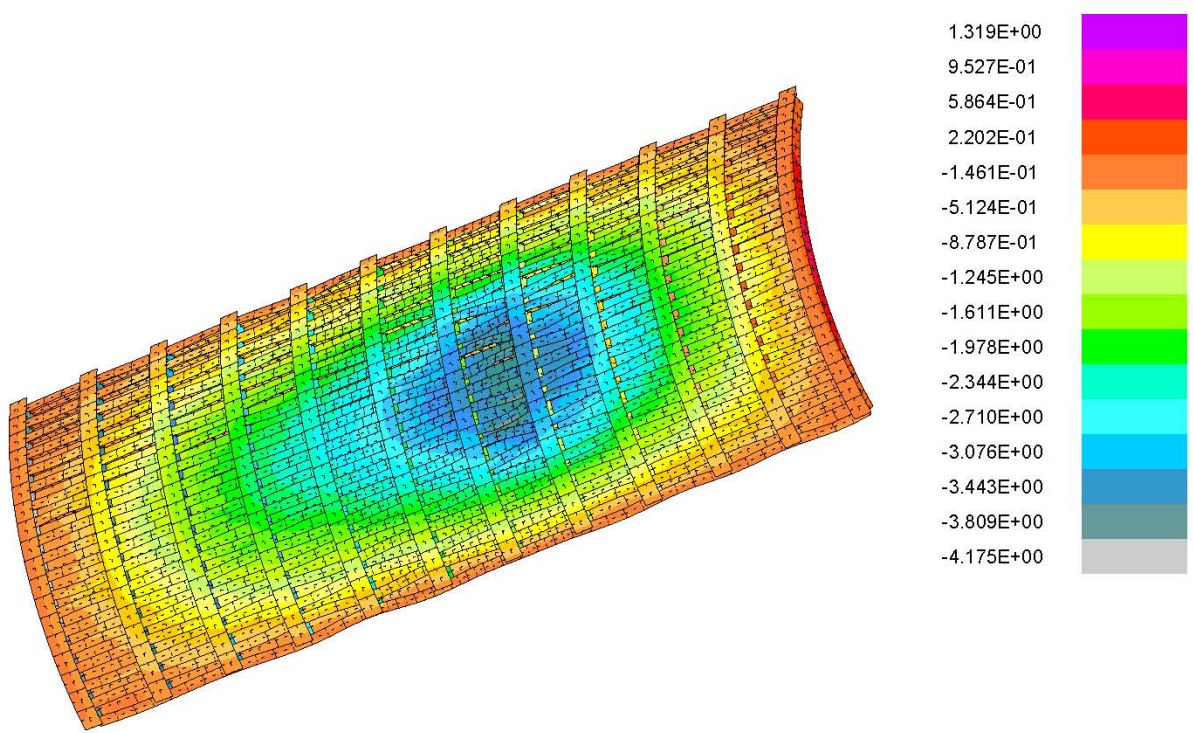
testax3: optimum design from [16], dimensions listed in Tables 1 and 2

FIG. 32 Normal displacement contours from STAGS nonlinear run

Θ_x 24.00
 Θ_y -22.00
 Θ_z 30.00

5.407E+01





solution scale=1.0; initial imperfection shape = -1.0 x mode 58

PA= 1.27168E+00 PB= 0.00000E+00 PX= 0.00000E+00

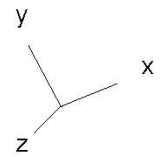
step 20 displacement w contours; Nxy=0.0

testax3: optimum design from [16], dimensions listed in Tables 1 and 2

FIG. 33 Normal displacement contours from STAGS nonlinear run

Θ_x 24.00
 Θ_y -22.00
 Θ_z 30.00

5.410E+01



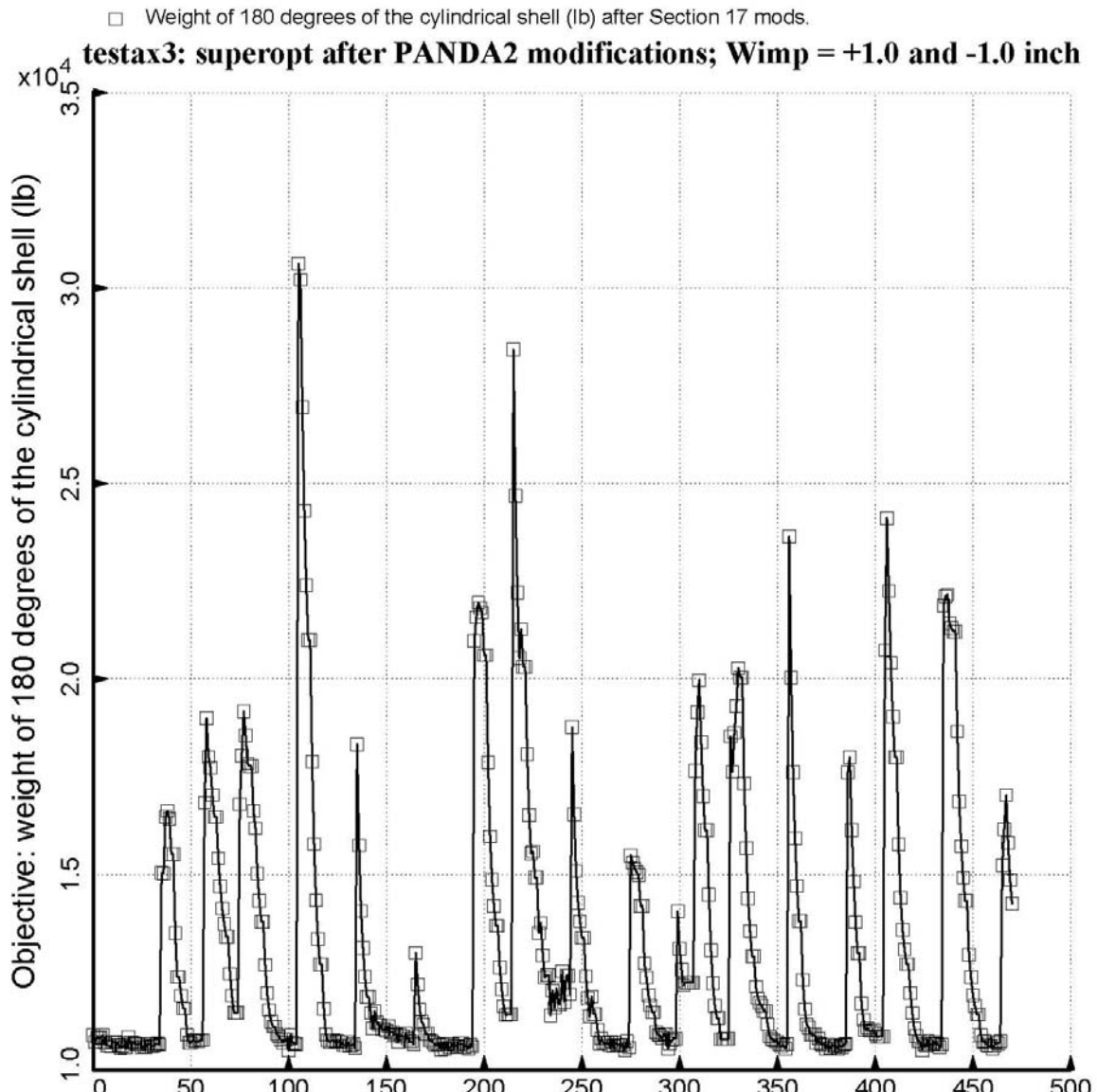


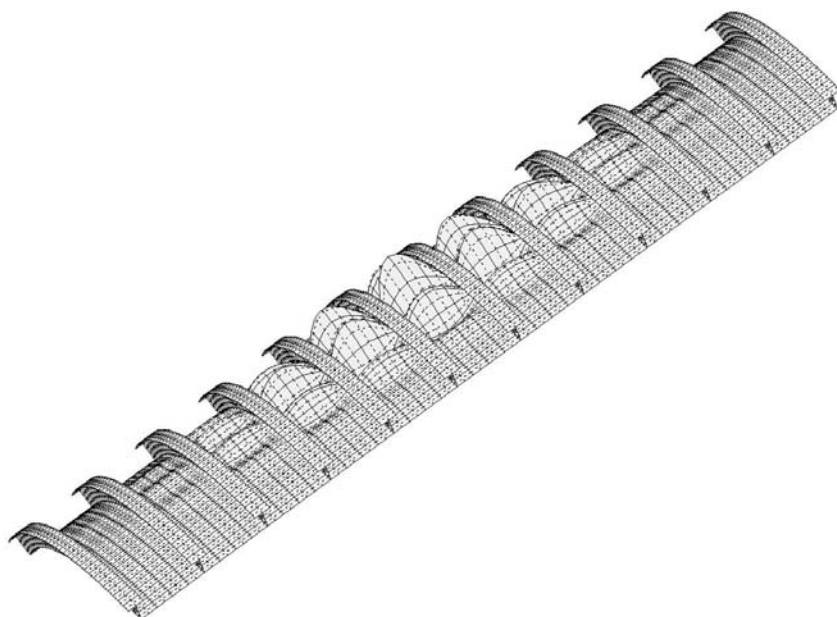
FIG. 34 Design Iterations from SUPEROPT run after PANDA2 mods.



STAGS model; 60 degrees of cyl. shell included; $N_{xy}=0.0$; smeared stringers
 mode 1, $p_{cr} = 0.13753E+01$; This mode is used for the imperfection.
 eigenvector deformed geometry; general buckling, $n = 3$ circ. waves $\Theta_x -35.84$
 $\Theta_y -13.14$ $\Theta_z 35.63$

FIG. 35 linear buckling of perfect shell; Configuration is listed in Table 14

4.720E+01

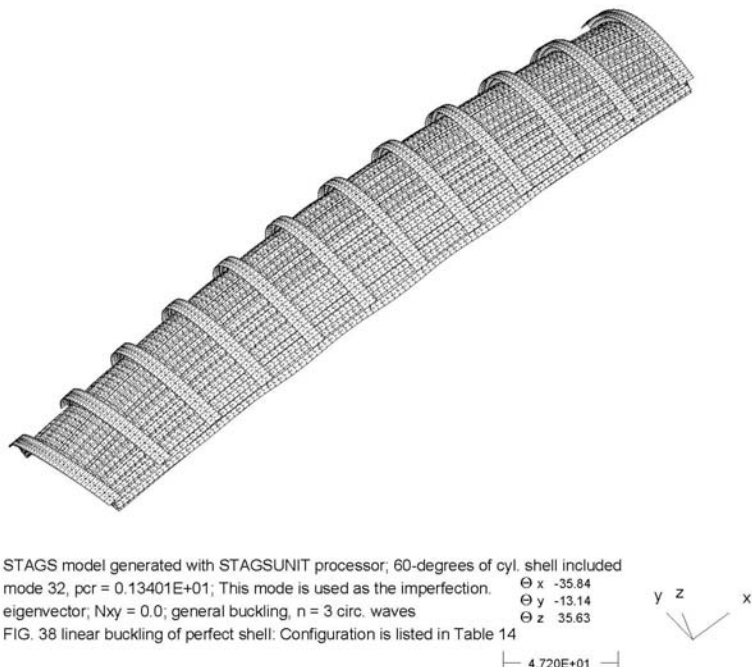
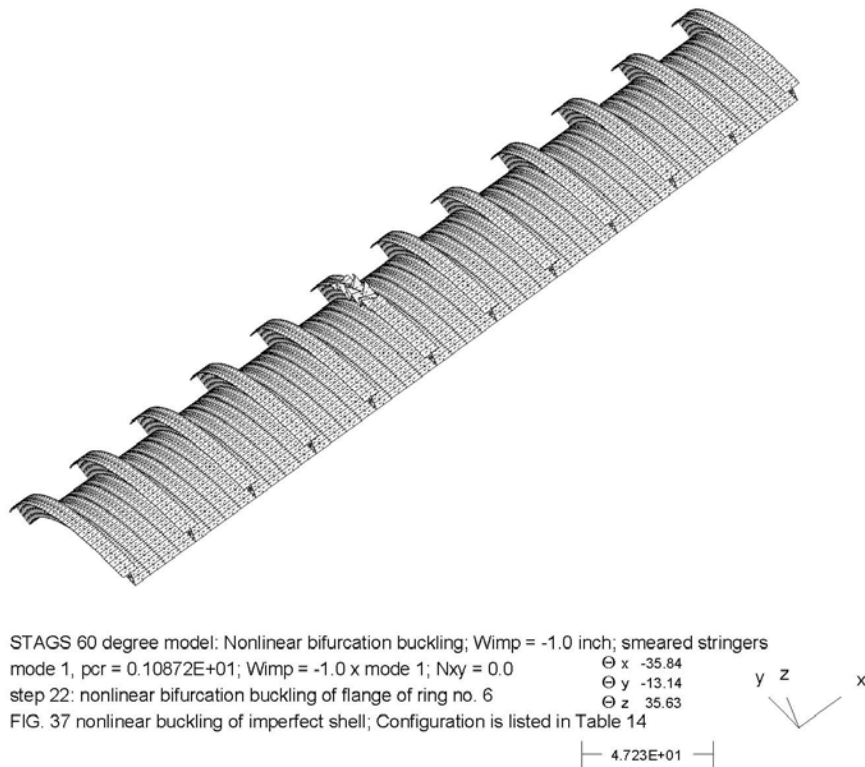


STAGS 60 degree model: Nonlinear bifurcation buckling; $W_{imp} = +1.0$ inch; smeared stringers
 mode 1, $p_{cr} = 0.11244E+01$; $N_{xy} = 0.0$; $W_{imp} = +1.0 \times$ mode 1 $\Theta_x -35.84$
 step 13 eigenvector: panel skin+smeared stringers; inter-ring buckling $\Theta_y -13.14$ $\Theta_z 35.63$

FIG. 36 nonlinear buckling of imperfect shell; Configuration is listed in Table 14

4.718E+01



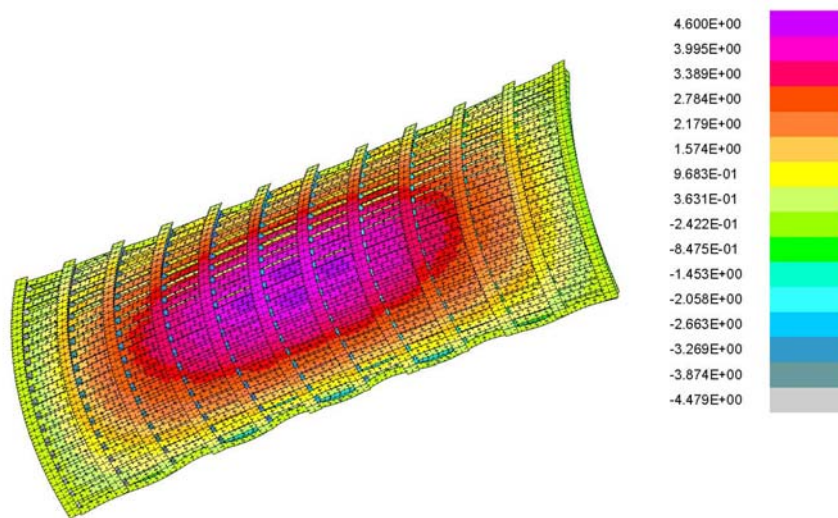




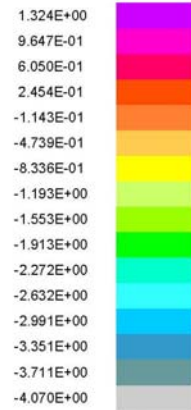
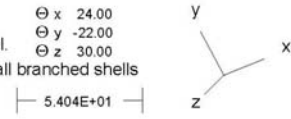
STAGS 60 degree model: Nonlinear bifurcation buckling; Wimp=+1.0 inch; all branched shells
 mode 1, pcr = 0.10495E+01; Nxy=0.0; Wimp=+1.0 x mode 32 Θ_x -35.84 Θ_y -13.14 Θ_z 35.63
 step 15 eigenvector: panel skin+stringers buckling between rings y z x
 FIG. 39 nonlinear buckling of imperfect shell: Configuration is listed in Table 14
 | 4.718E+01 |



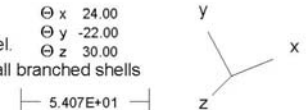
STAGS 60 degree model: Nonlinear bifurcation buckling; Wimp=-1.0 inch; all branched shells
 mode 5, pcr = 0.10460E+01; Nxy=0.0; Wimp=-1.0 x mode 32 Θ_x -35.84 Θ_y -13.14 Θ_z 35.63
 step 15 eigenvector: buckling of flange of Ring No. 6 y z x
 FIG. 40 nonlinear buckling of imperfect shell: Configuration is listed in Table 14
 | 4.723E+01 |

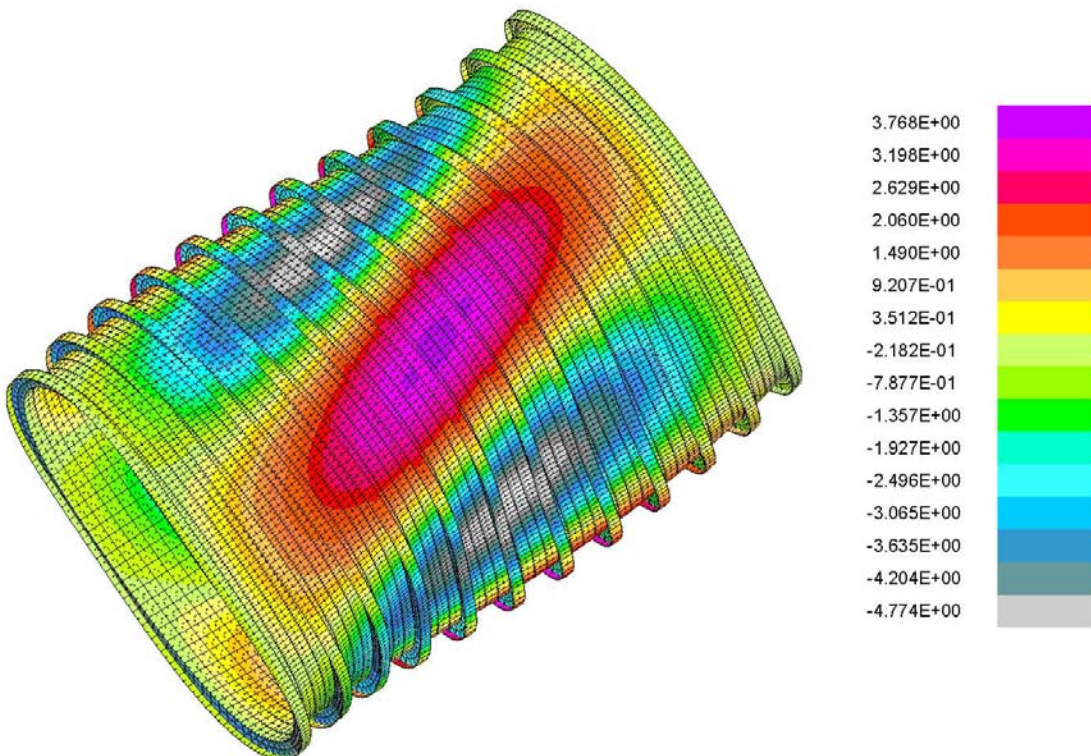


nonlinear equilibrium of imperfect shell
 $PA = 1.04299E+00 \quad PB = 0.00000E+00 \quad PX = 0.00000E+00$ $\Theta_x = 24.00 \quad \Theta_y = -22.00 \quad \Theta_z = 30.00$
 testax3: Optimum design is listed in Table 14. $N_{xy} = 0.0$ in this model.
 STAGS 60 degree model: Nonlinear equilibrium; $W_{imp} = +1.0$ inch; all branched shells
 FIG. 41 step 15 displacement w contours; imperfect shell



nonlinear equilibrium of imperfect shell
 $PA = 1.10073E+00 \quad PB = 0.00000E+00 \quad PX = 0.00000E+00$ $\Theta_x = 24.00 \quad \Theta_y = -22.00 \quad \Theta_z = 30.00$
 testax3: Optimum design is listed in Table 14. $N_{xy} = 0.0$ in this model.
 STAGS 60 degree model: Nonlinear equilibrium; $W_{imp} = -1.0$ inch; all branched shells
 FIG. 42 step 13 displacement w contours; imperfect shell





STAGS 360-degree model is generated by the STAGSUNIT processor

PA= 1.14573E+00 PB= 0.00000E+00 PX= 0.00000E+00

step 12 displacement w contours; (m,n)=(1,3) imperfection shape

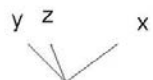
Θ_x -35.84

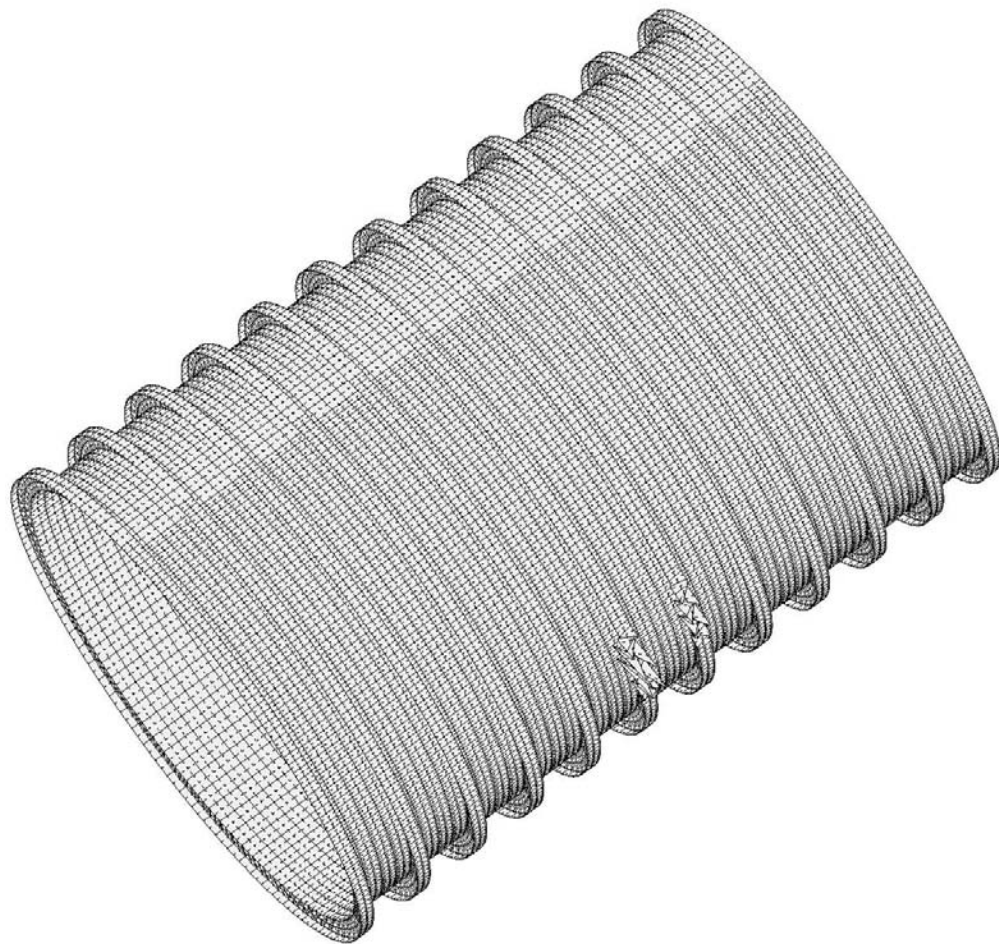
Θ_y -13.14

Θ_z 35.63

FIG. 43 Nonlinear equilibrium; Wimp = 1.0 x mode 1; Configuration is listed in Table 14

Rings are shell branches, stringers are smeared; nonuniform f.e. mesh | 7.494E+01 |





STAGS 360 degree model: Nonlinear bifurcation buckling; Wimp=1.0 inch; smeared stringers

mode 1, pcr = 0.10932E+01; Wimp = 1.0 inch x mode 1

Θ_x -35.84

Θ_y -13.14

Θ_z 35.63

step 17 eigenvector; buckling of outstanding flanges of Rings 6 and 7

y z
x

FIG. 44 nonlinear buckling of imperfect shell: Configuration is listed in Table 14

| - 6.245E+01 - |

- Wimp = -1.0 x mode 1; w; smrstr; Node 3249; panel skin; Table 14; 60 deg.model
- Wimp = +1.0 x mode 1; w; smrstr; Node 3249; panel skin; Table 14; 60 deg.model
- △ Wimp = +1.0 x mode32; w; allbranches; Node 3975 panel skin; Table 14; 60 deg.model
- + Wimp = -1.0 x mode32; w; allbranches; Node 3975 panel skin; Table 14; 60 deg.model
- × Wimp = -1.0 x mode1; w; smeared stringers; Node 10755; Table 14; 360 deg.model
- ◇ Wimp = 1.0 x mode1; w; smeared stringers; Node 10815; Table 14; 360 deg.model
- ▽ Wimp = -1.0 x (1,3)mode; w in panel skin; PANDA2 prediction; Table 14
- ⊗ Wimp=-1.0x(1,3) mode; w in stringer 11 flange, node 28379; STAGS 60-deg.model in Fig. 50
- * Wimp=+1.0x(1,3) mode; w in panel skin, midbay 6, betw. str.10 & 11; STAGS 60-deg.model, Fig. 50
- ◆ Wimp=+1.0x(1,3)mode; w, midbay 6, stringer 1 flange, rightmost edge; STAGS 60-deg.model, Fig. 50
- ⊕ Wimp=+1.0x(1,3)mode; w, midbay 6, stringer 1 flange, leftmost edge; STAGS 60-deg.model, Fig. 50
- ⊗ Wimp=+1.0x(1,3)mode; w, midbay 1, stringer 14 flange, leftmost edge; STAGS compound model, Fig. 56
- Wimp=+1.0x(1,3)mode; w, midbay 1, stringer 14 flange, rightmost edge; STAGS compound model, Fig. 56

STAGS, PANDA2 models, Table 14 dimensions: Wimp= + 1.0 and -1.0 inch

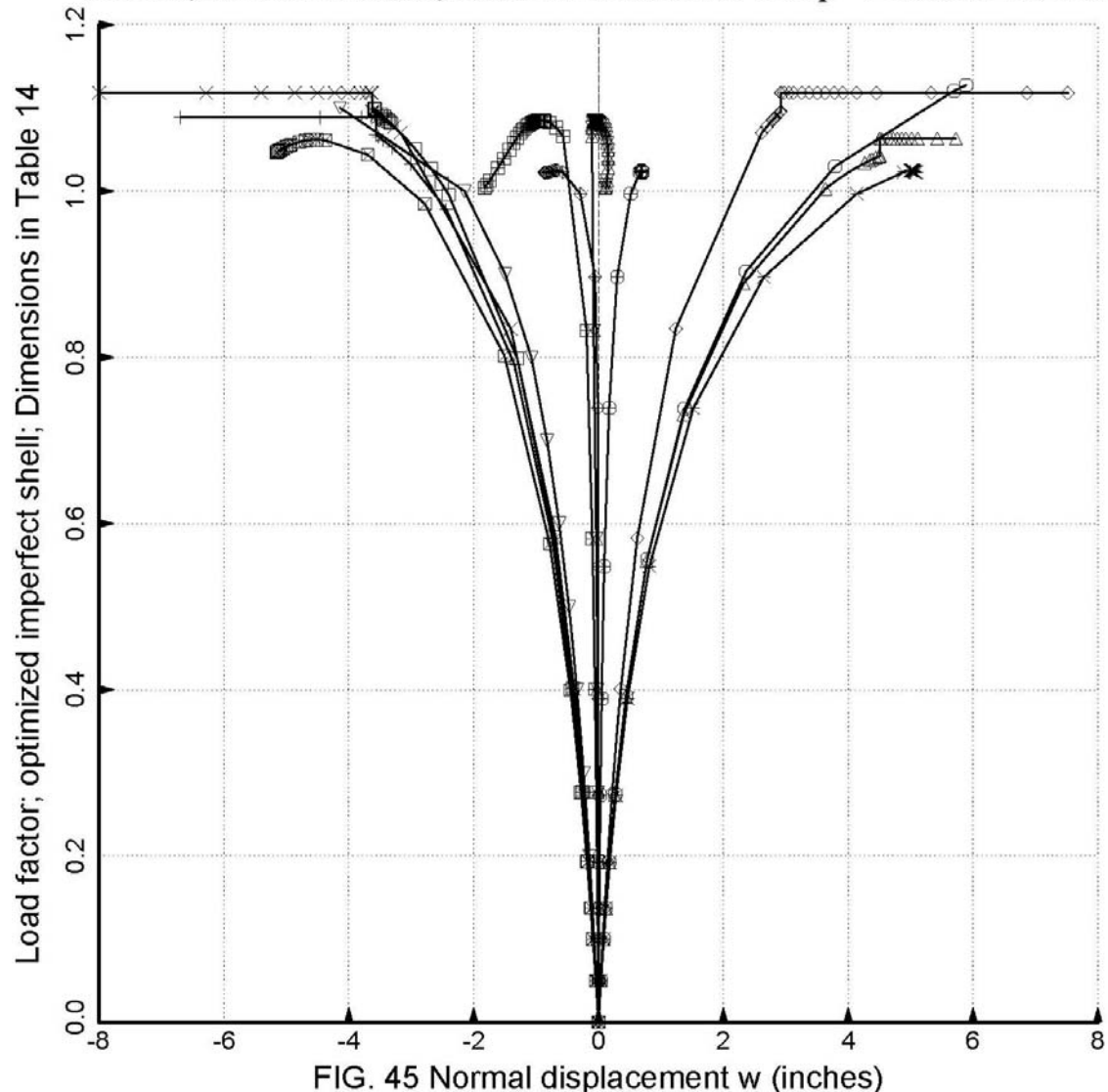


FIG. 45 Normal displacement w (inches)

- \square Wimp = -1.0 x mode 1; Nx; smearstringer; f.e.7756; Ring7 flange; Table 14; 360 deg. model
- \circ Wimp = +1.0 x mode 1; Nx; smearstringer; f.e.7786; Ring7 flange; Table 14; 360 deg. model
- \triangle Wimp = -1.0 x (1,3)mode; Nx in stringer flange; PANDA2 prediction; Table 14
- $+$ Wimp = -1.0 x (1,3)mode; Nx in ring flange; PANDA2 prediction; Table 14
- \times Wimp = +1.0 x (1,3)mode; Nx in f.e.990 panel skin; Table 14; 60 deg. model
- \diamond Wimp = +1.0 x (1,3)mode; Ny in f.e.990 panel skin; Table 14; 60 deg. model
- \triangledown Wimp = +1.0 x (1,3)mode; Nx in f.e.3603 stringer 10 flange; Table 14; 60 deg. model
- \blacksquare Wimp = +1.0 x (1,3)mode; Nx in f.e.5746 ring 6 flange; Table 14; 60 deg. model
- \ast Wimp = -1.0 x (1,3)mode; Nx in f.e.990 panel skin; Table 14; 60 deg. model
- \oplus Wimp = -1.0 x (1,3)mode; Ny in f.e.990 panel skin; Table 14; 60 deg. model
- \oplus Wimp = -1.0 x (1,3)mode; Nx in f.e.3603 stringer 10 flange; Table 14; 60 deg. model
- \boxtimes Wimp = -1.0 x (1,3)mode; Nx in f.e.5746 ring 6 flange; Table 14; 60 deg. model
- \boxplus Wimp = -1.0 x (1,3)mode; Nx in skin; PANDA2 prediction; Table 14
- \boxtimes Wimp = +1.0 x (1,3)mode; Nx in skin; PANDA2 prediction; Table 14
- \boxdot Wimp = -1.0 x (1,3)mode; Ny in skin; PANDA2 prediction; Table 14
- \bullet Wimp = +1.0 x (1,3)mode; Ny in skin; PANDA2 prediction; Table 14

STAGS,PANDA2 models, Table 14 dimensions: Wimp= +1,0 and -1.0 inch

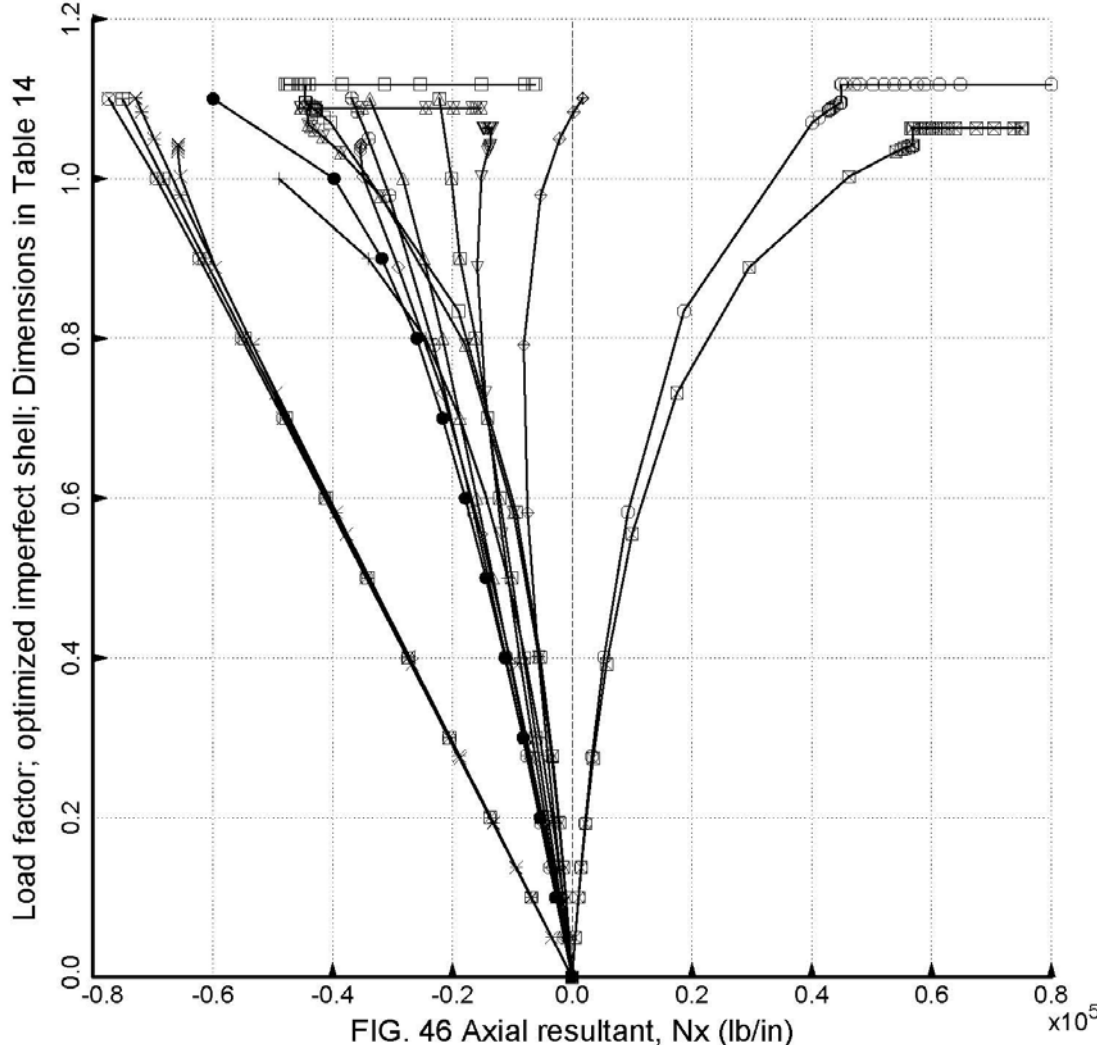
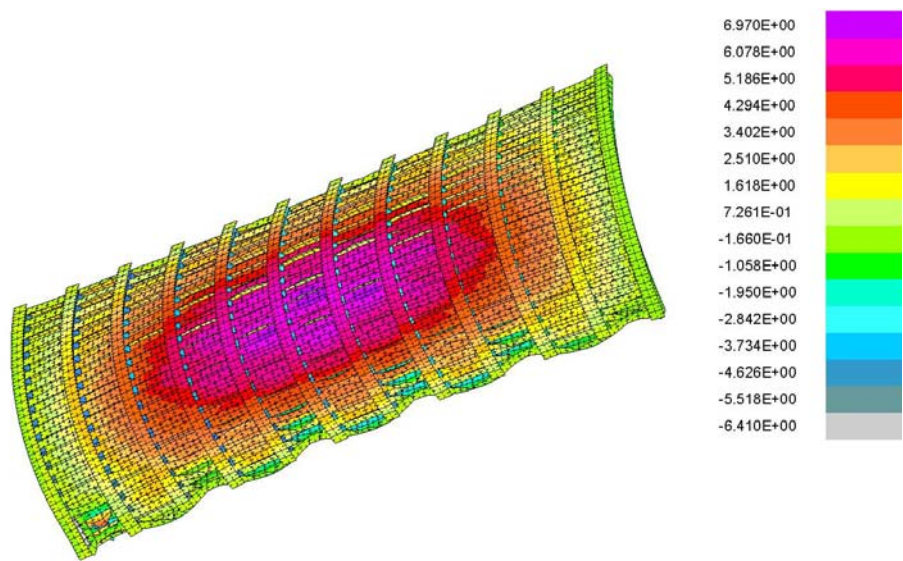


FIG. 46 Axial resultant, N_x (lb/in)



nonlinear state of imperfect shell after STAGS dynamic run (INDIC=6)

PA= 1.06300E+00 PB= 0.00000E+00 TIME= 2.07040E-02

Θ_x 24.00

testax3: Optimum design is listed in Table 14. $N_{xy} = 0.0$ in this model.

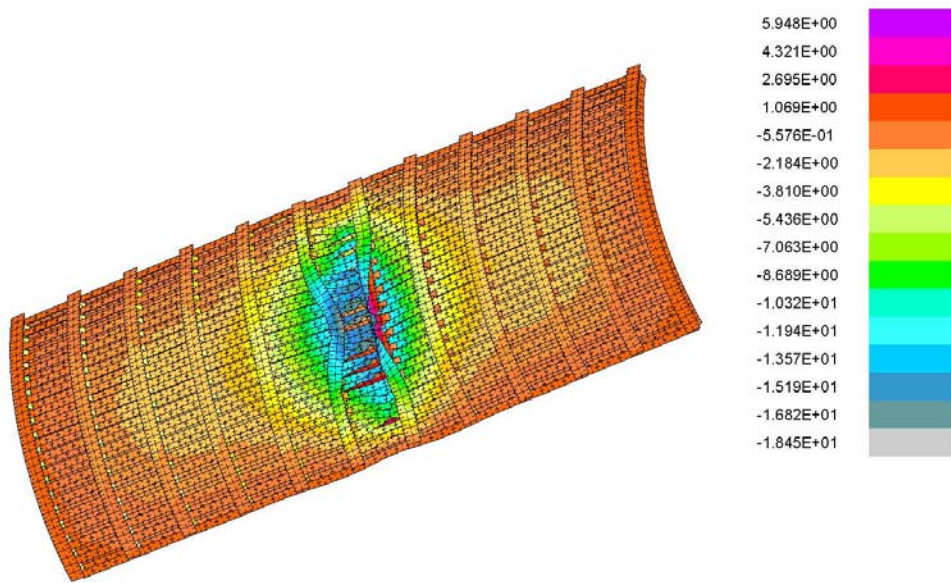
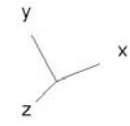
Θ_y -22.00

STAGS 60 degree model: Nonlinear state; Wimp = +1.0 inch; all branched shells

Θ_z 30.00

FIG. 47 Time step 220 displacement w contours after transient run

5.404E+01



nonlinear state of imperfect shell after STAGS dynamic run (INDIC=6)

PA= 1.08886 PB= 0.00000E+00 TIME= 2.22156E-02

Θ_x 24.00

testax3: Optimum design is listed in Table 14. $N_{xy} = 0.0$ in this model.

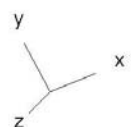
Θ_y -22.00

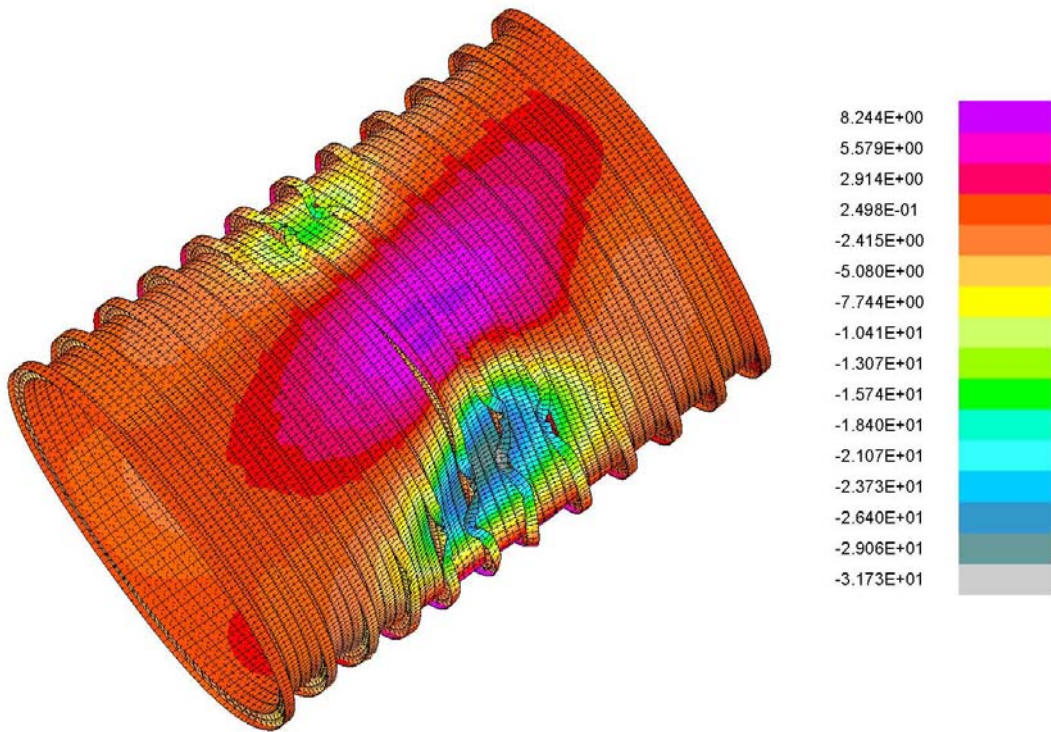
STAGS 60 degree model: Nonlinear state; Wimp = -1.0 inch; all branched shells

Θ_z 30.00

FIG. 48 Time step 200 displacement w contours after transient run

5.407E+01





nonlinear state of imperfect shell after STAGS dynamic run (INDIC=6)

PA= 1.118 PB= 0.00000E+00 TIME= 2.77500E-02

testax3: Optimum design is listed in Table 14.

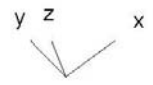
STAGS 360 degree model: Nonlinear state; Wimp = 1.0 inch; smeared stringers

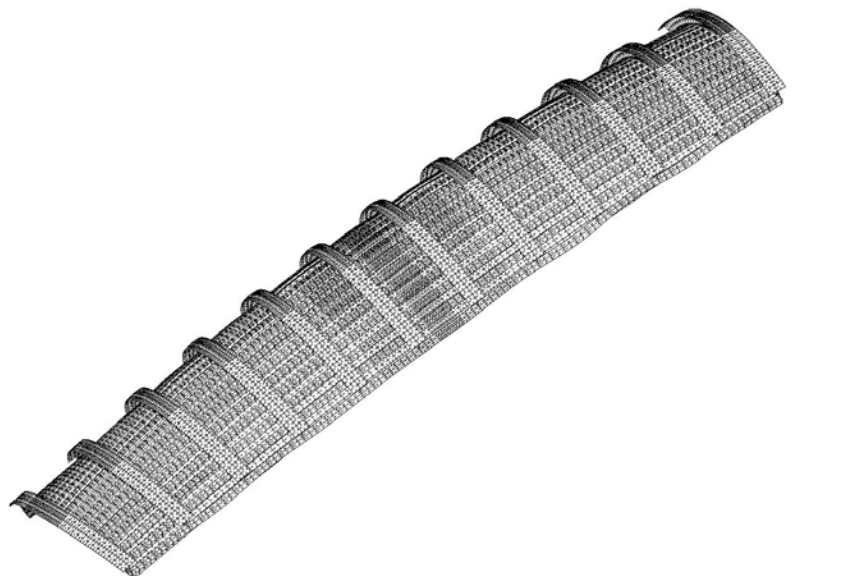
FIG. 49 Time step 180 displacement w contours after transient run

Θ_x -35.84

Θ_y -13.14

Θ_z 35.63





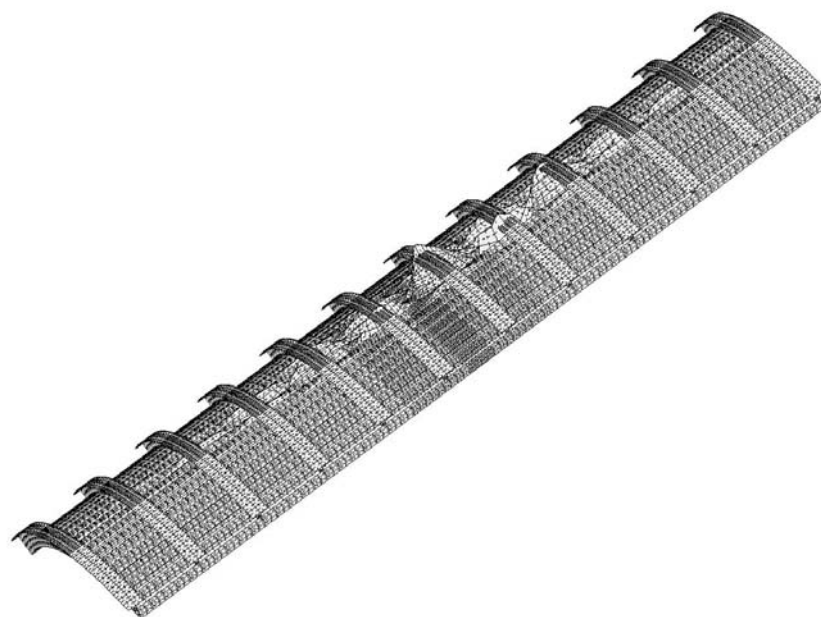
STAGS model generated with STAGSUNIT processor; 60-degrees of cyl. shell included

mode 31, pcr = 0.13283E+01; This mode is used as the imperfection.
 eigenvector; Nxy = 0.0; general buckling, n = 3 circ. waves

Θ_x -35.84
 Θ_y -13.14
 Θ_z 35.63

FIG. 50 linear buckling of perfect shell: Configuration is listed in Table 14

4.720E+01



STAGS 60 degree model: Nonlinear bifurcation buckling; Wimp=-1.0 inch; all branched shells

mode 7, pcr = 0.11294E+01; Nxy=0.0; Wimp=-1.0 x mode 31

Θ_x -35.84

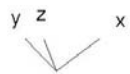
step 10, Run 2; eigenvector: rolling of stringers where the mesh is dense

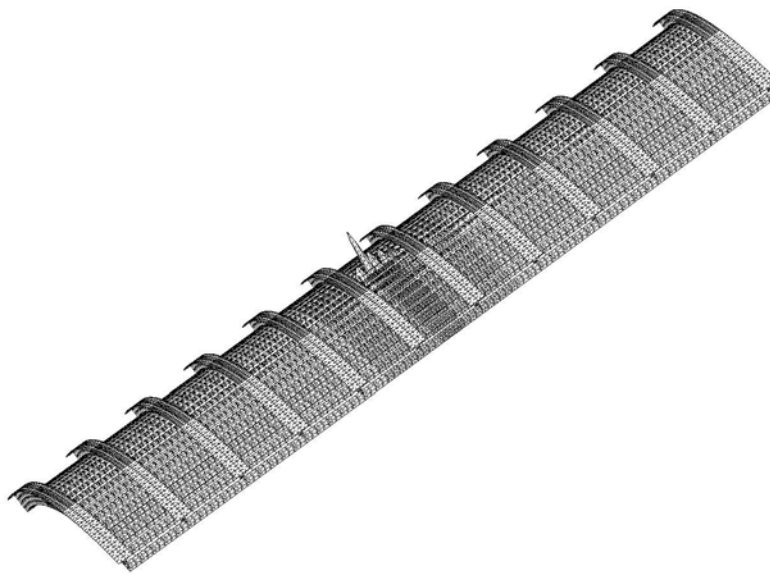
Θ_y -13.14

FIG. 51 nonlinear buckling of imperfect shell: Configuration is listed in Table 14

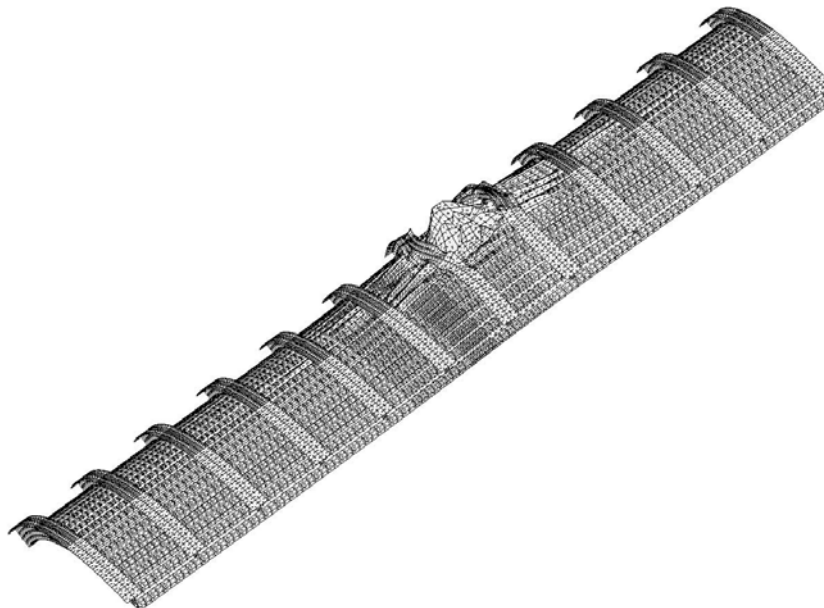
Θ_z 35.63

4.723E+01

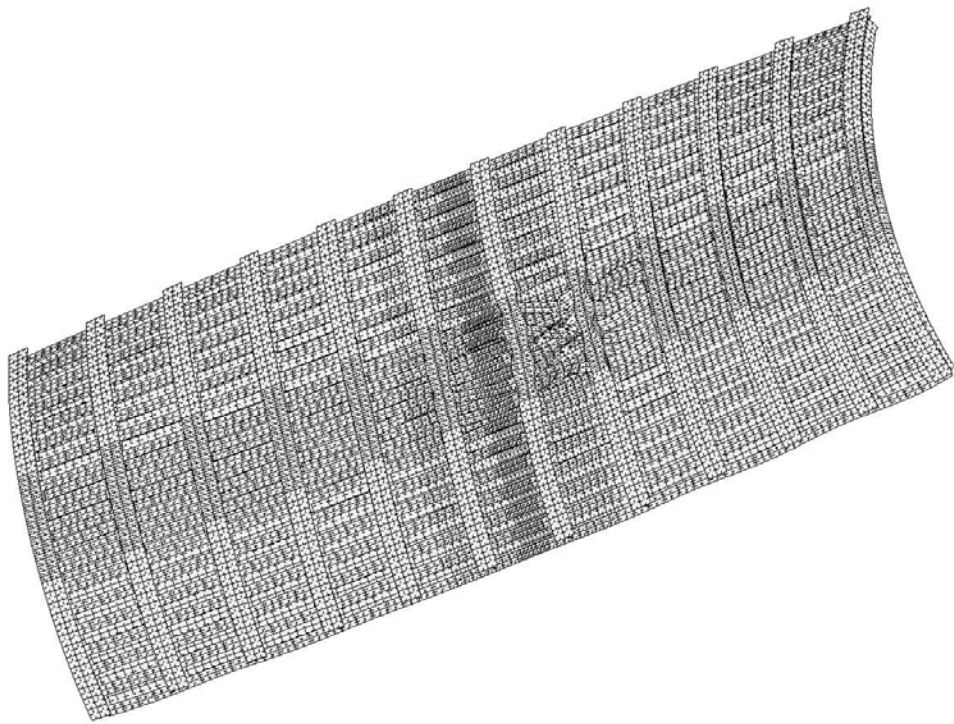




STAGS 60 degree model: Nonlinear bifurcation buckling; Wimp=-1.0 inch; all branched shells
mode 8, pcr = 0.11625E+01; Nxy=0.0; Wimp=-1.0 x mode 31 Θ_x -35.84 Θ_y -13.14 Θ_z 35.63
step 10, Run 3; eigenvector: buckling of flange of Stringer No. 11 y z x
FIG. 52 nonlinear buckling of imperfect shell: Configuration is listed in Table 14
|— 4.723E+01 —|



STAGS 60 degree model: Nonlinear bifurcation buckling; Wimp=-1.0 inch; all branched shells
mode 1, pcr = 0.10705E+01; Nxy=0.0; Wimp=-1.0 x mode 31 Θ_x -35.84 Θ_y -13.14 Θ_z 35.63
step 21, Run 6; eigenvector: buckling primarily of Bay no. 7 y z x
FIG. 53 nonlinear buckling of imperfect shell: Configuration is listed in Table 14
|— 4.723E+01 —|



STAGS 60 degree model: Nonlinear equilibrium; Wimp = -1.0 inch; all branched shells

PA= 1.04693E+00 PB= 0.00000E+00 PX= 0.00000E+00

Θ_x 24.00

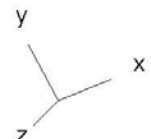
Θ_y -22.00

Θ_z 30.00

testax3: Optimum design is listed in Table 14. Nxy = 0.0 in this model.

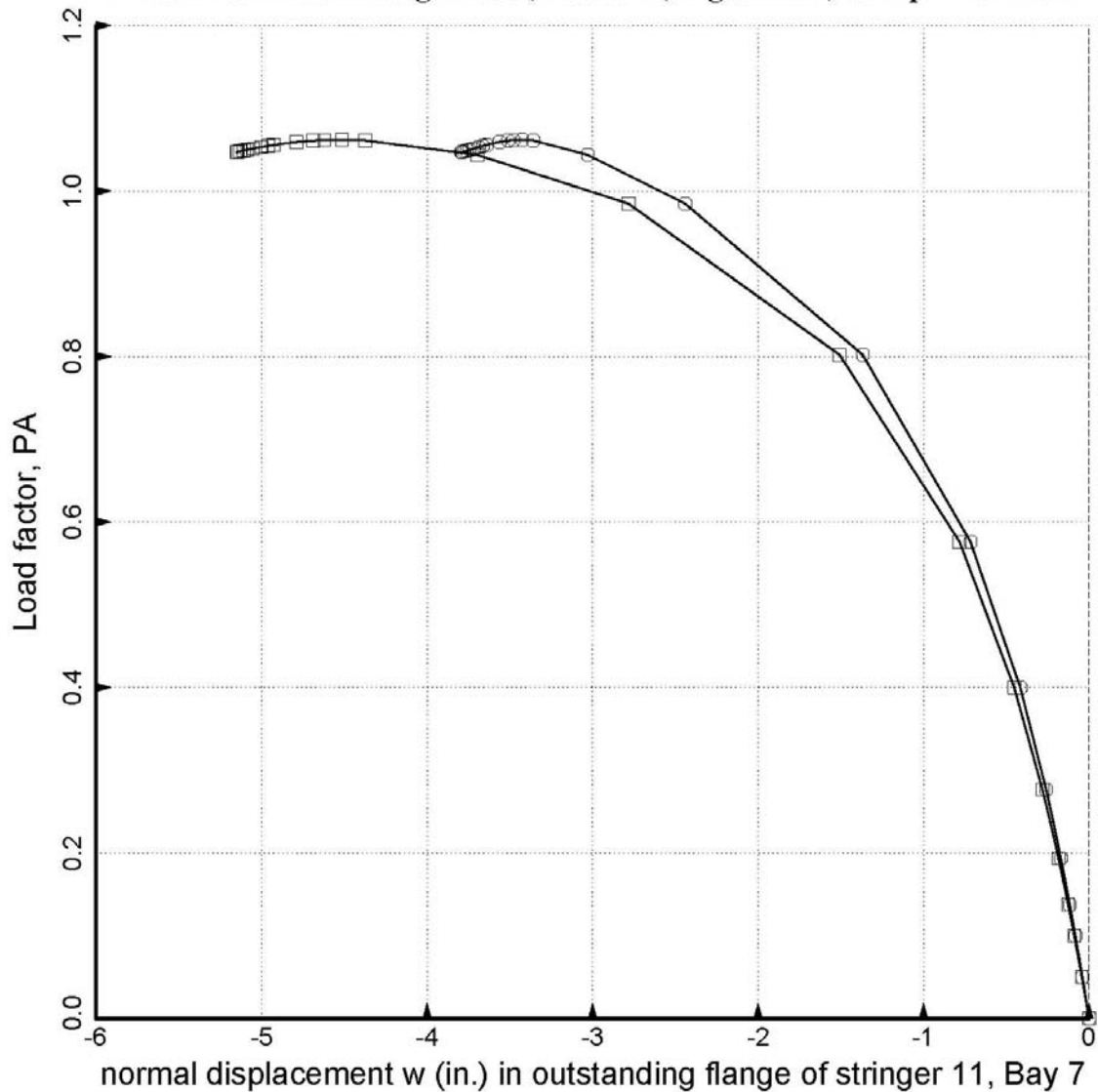
FIG. 54 step 25 deformed shell at final load step possible in the static analysis, Run 8

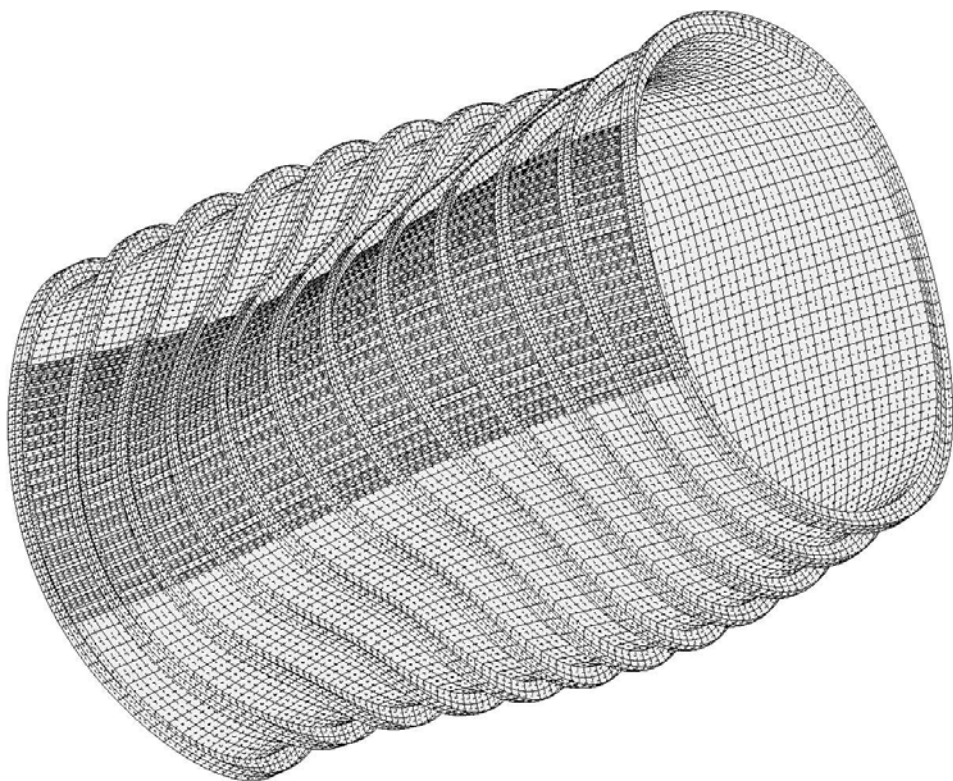
| - 4.506E+01 - |



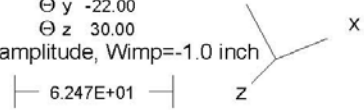
- Disp(28379,w,L) vs. load_PA: Rightmost edge of outstanding flange between F.E. 4 & F.E. 5 near Ring 7
- Disp(28383,w,L) vs. load_PA: Leftmost edge of outstanding flange between F.E. 4 & F.E. 5 near Ring 7

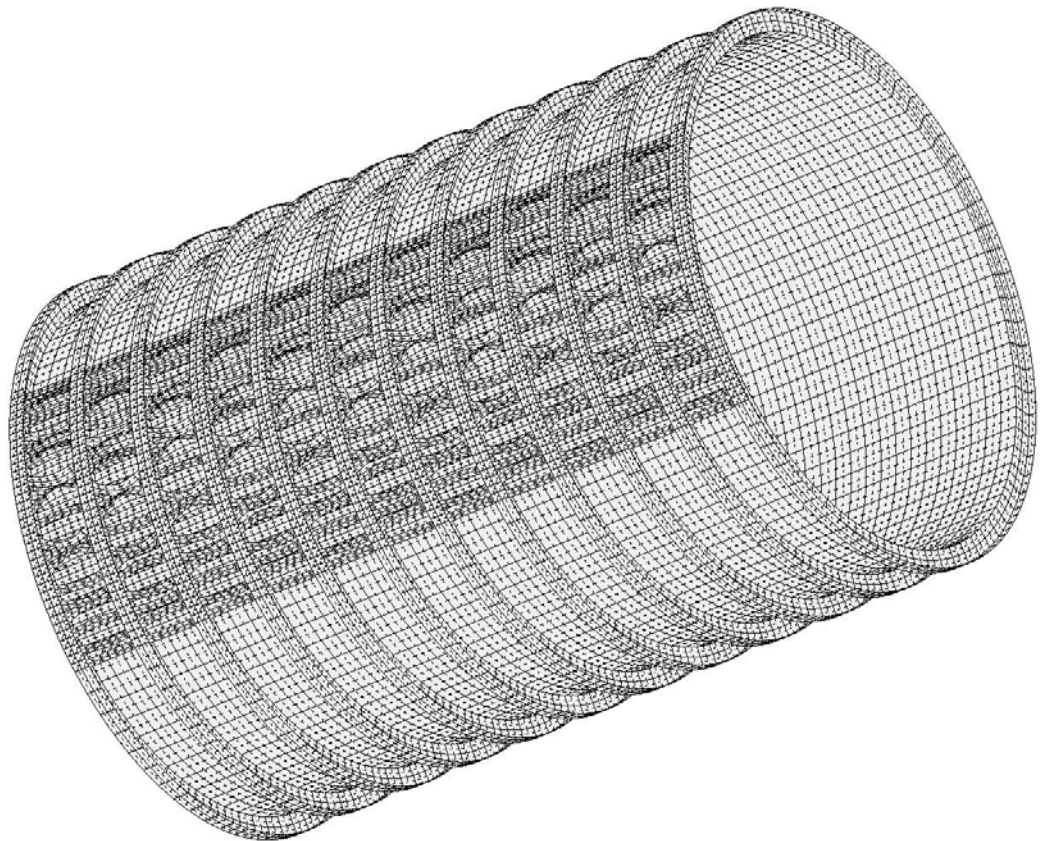
FIG. 55 STAGS 60-deg. model, Table 14, Figs. 50-53, Wimp= -1.0 inch





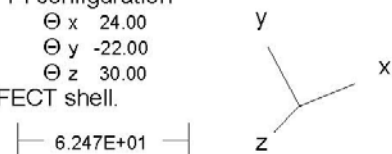
testax3: compound model, ILIN = 1, linear bifurcation buckling of the PERFECT shell
mode 19, pcr=0.14438E+01; Compare with Margins 13,14 in Table 15 Θ_x 24.00 Θ_y -22.00 Θ_z 30.00
The design dimensions are listed in Table 14.
FIG. 56 General buckling. This mode is used as an imperfection with amplitude, $W_{imp}=-1.0$ inch

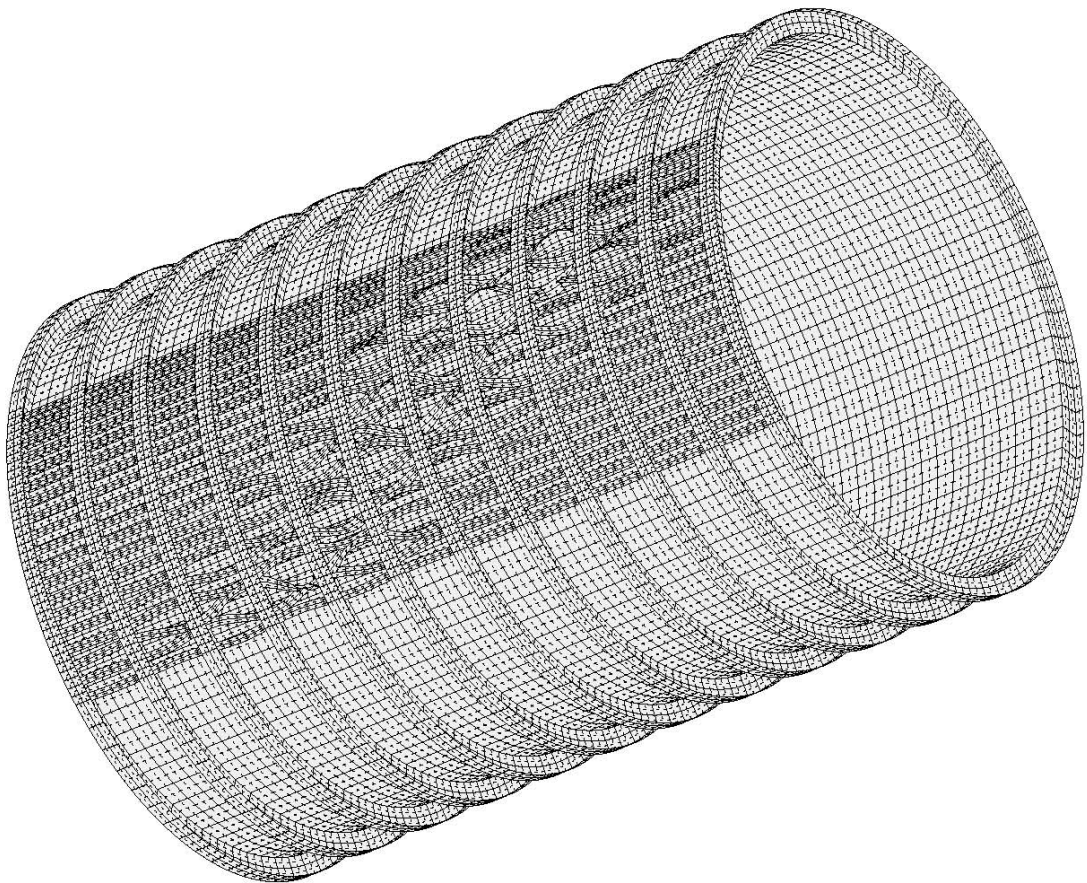




testax3: compound model, ILIN = 1, linear bifurcation buckling; Table 14 configuration
mode 1, pcr=0.13512E+01; Compare with Margins 1,2,4,5,12,16
in Table 15.

FIG. 57 Inter-ring buckling. This is the first buckling mode of the PERFECT shell.





testax3: compound model, ILIN=0, nonlinear bifurcation buckling, IMPERFECT shell, Run 2

mode 8, pcr = 0.10853E+01; This imperfection is to be used in Run 3. Θ_x 24.00

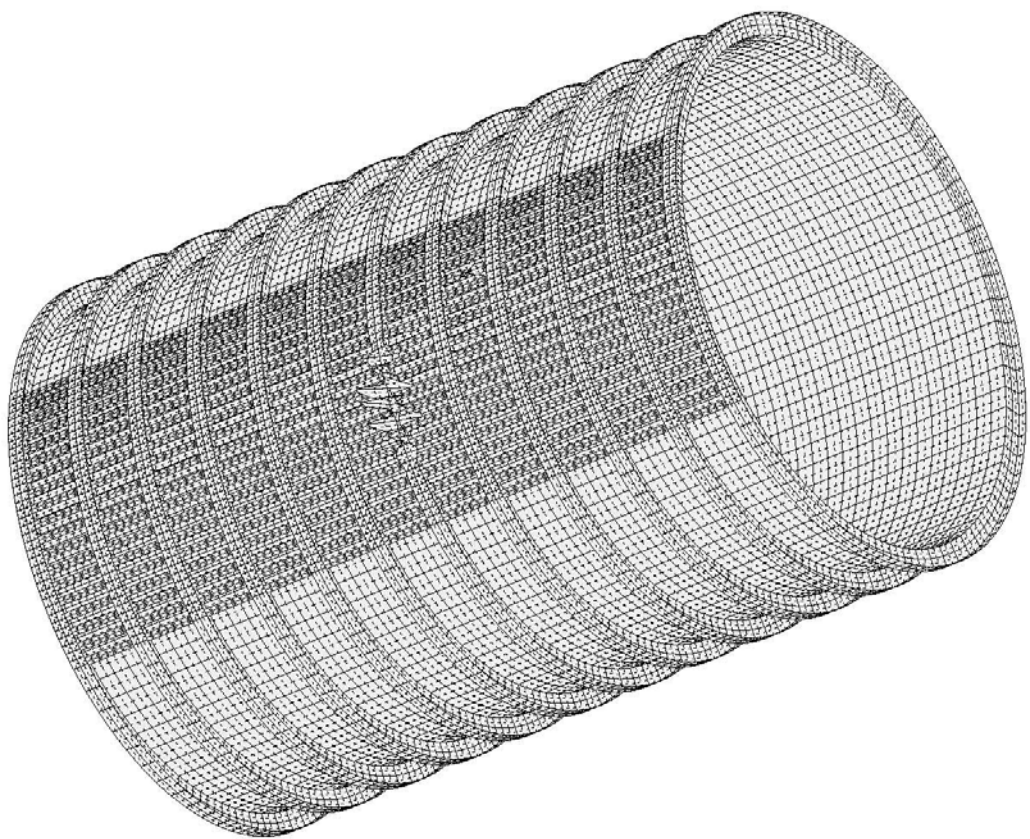
y

step 17 eigenvector deformed geometry; 2nd imperf. Wimp=0.05 Θ_y -22.00

Θ_z 30.00

FIG. 58 Stringer rolling. This mode is used as an imperfection with amplitude, Wimp=0.05 inch

|--- 6.249E+01 ---| x
z



testax3: compound model, ILIN=0, nonlinear bifurcation buckling, IMPERFECT shell, Run 3

mode 4, pcr = 0.10985E+01; buckling of Ring 7 outstanding flange

Θ_x 24.00

y

Θ_y -22.00

x

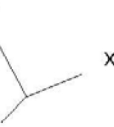
Θ_z 30.00

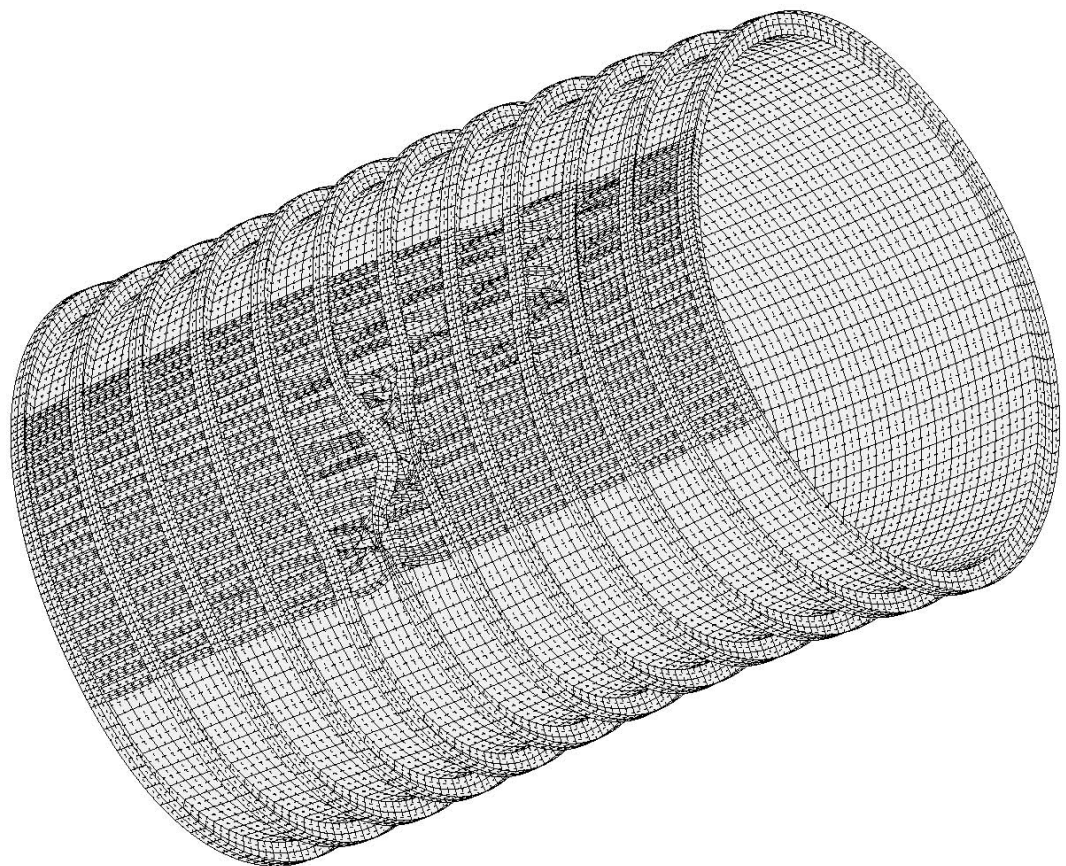
step 15, run 3 eigenvector; 3rd imperfection amplitude, Wimp=0.01

FIG. 59 Ring 7 flange. This mode is used as an imperfection with amplitude, Wimp=0.01 inch

| 6.249E+01 |

z





Nonlinear state of imperfect shell. Wimp= -1.0 inch; 60-deg. sector with stringers as shell units.

PA= 1.100; PB= 0.00; TIME= 1.24750E-02 seconds;

Θ x 24.00 y

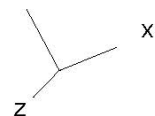
Θ y -22.00

Θ z 30.00

STAGS 360-degree compound model; Table 14 optimum design

FIG. 60 Time step 110 displacement w after STAGS transient run.

| 6.249E+01 |





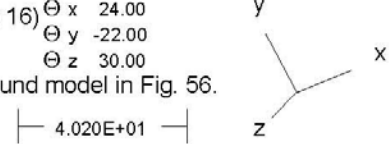
Stringer 14 from imperfect compound STAGS model with general buckling imperfection $W_{imp} = +1.0$ inch.

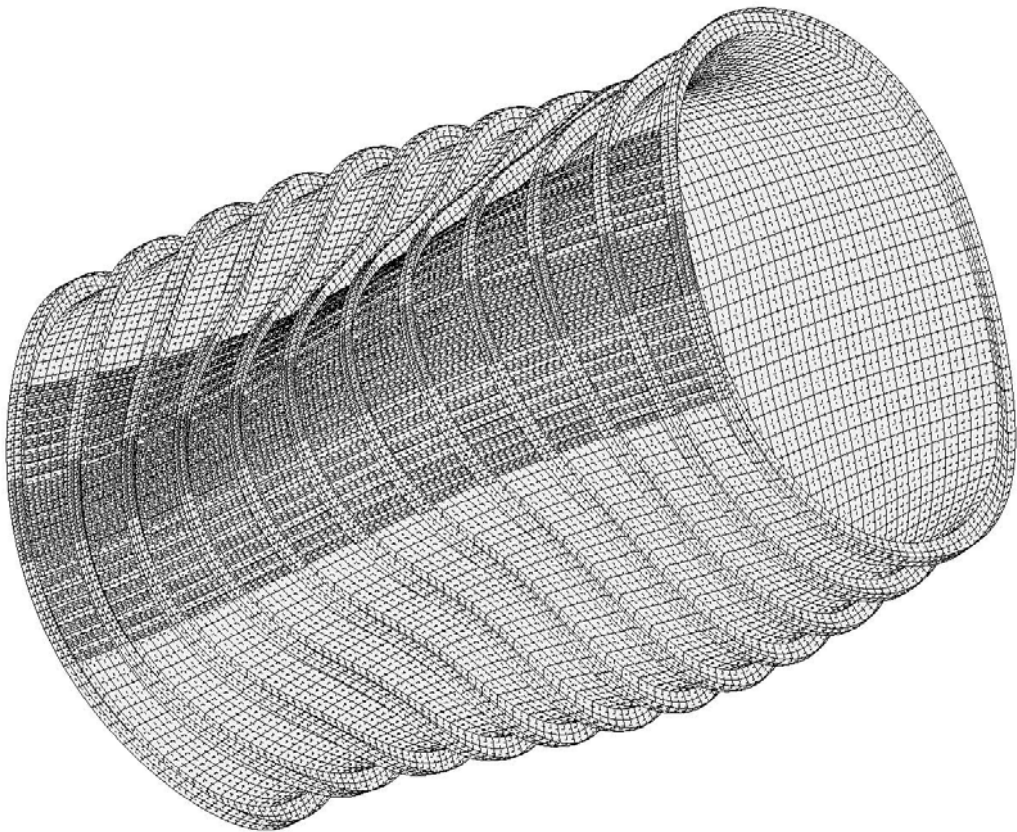
$PA = 1.00367E+00$ (after reaching a maximum of $PA = 1.0852$ at step 16) $\Theta_x = 24.00$

$\Theta_y = -22.00$

$\Theta_z = 30.00$

STAGS 360-degree compound model; Table 14 optimum design
FIG. 61 Deformed shape of Stringer 14 after static collapse of compound model in Fig. 56.





testax3: Linear buckling with ILIN = 1. This mode is used as an initial imperfection shape.

mode 28, pcr = 0.14429E+01; Model generated as described in Item 643 [17]

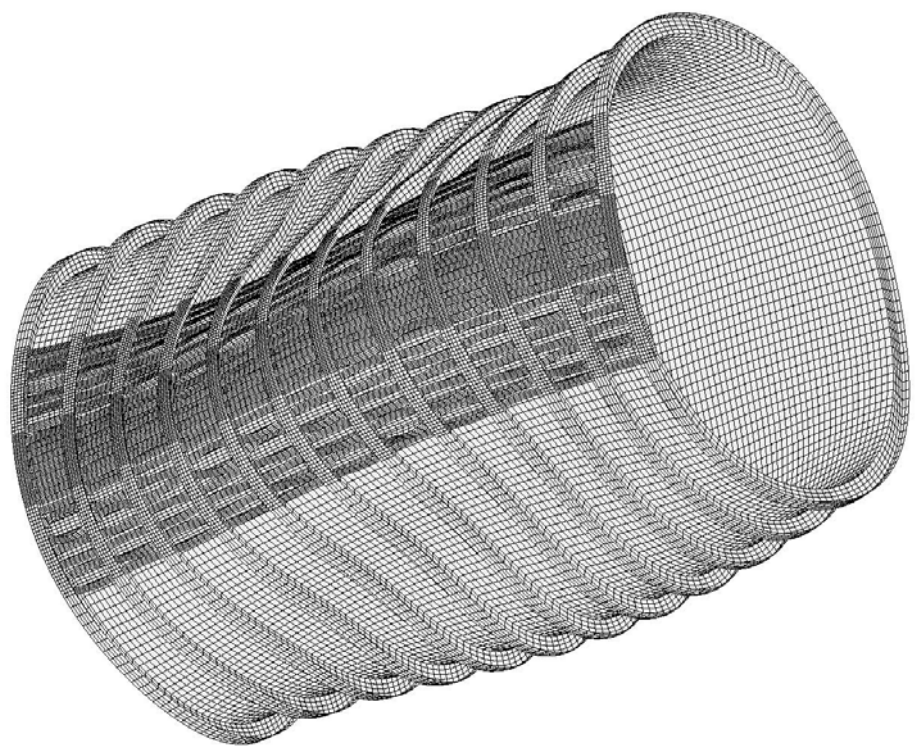
y

Θ_y -22.00

General buckling mode with 3 circumferential waves. Table 14 design Θ_z 30.00

FIG. 62 STAGS compound model with circumferentially varying mesh density in the 60-degree sector

| - 6.247E+01 - | z



testax3: Linear buckling with ILIN = 1. This mode is used as an initial imperfection shape.

mode 39, pcr=1.4269; Model created as described in Item 643 of [17]

Θ_x 24.00

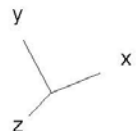
Θ_y -22.00

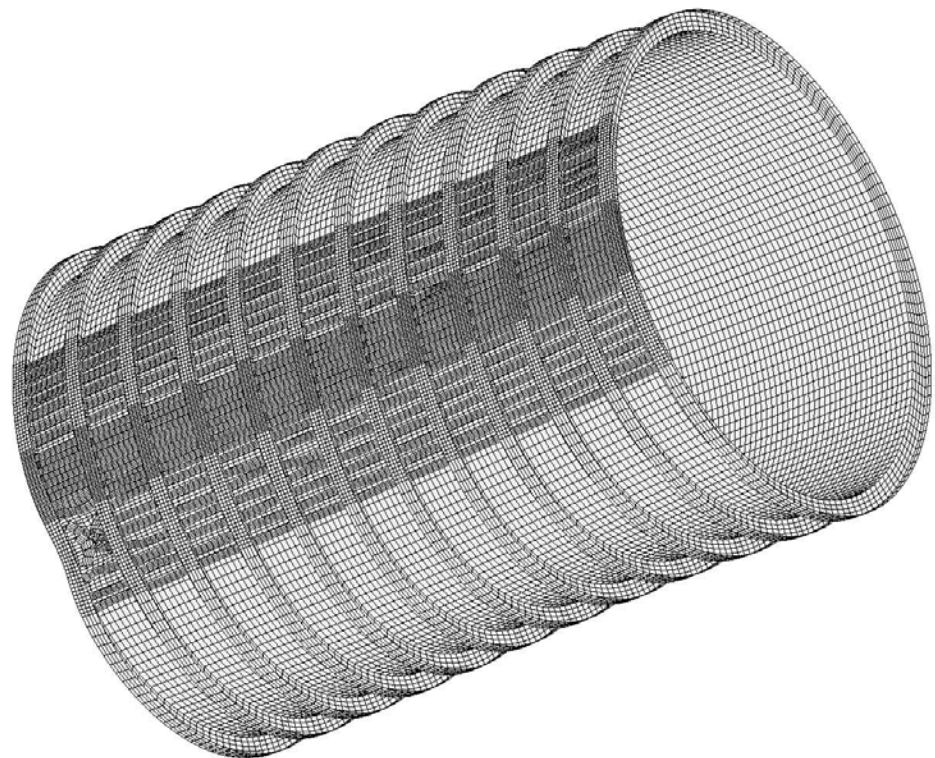
Θ_z 30.00

General buckling mode with 3 circumferential waves. table 14 design.

FIG. 63 STAGS compound model as in previous figure, but with use of 410 finite elements.

|--- 6.247E+01 ---|





"Early" collapse because of "noisy" general buckling imperfection shape (Fig. 63).

PA=0.95; TIME = 8.95000E-03 seconds; Wimp = -1.0 inch

Θ_x 24.00

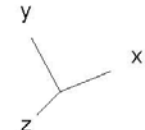
Θ_y -22.00

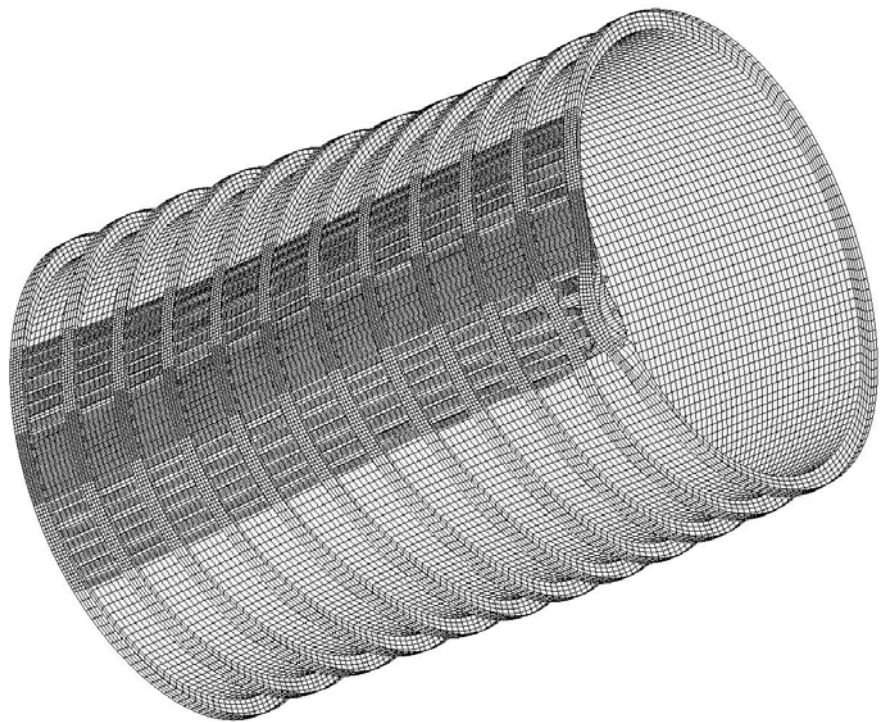
Θ_z 30.00

STAGS 360-degree compound model with use of 410 elements.

FIG. 64 Deformed shell after STAGS transient run at load factor, PA = 0.95 (time step 120)

| - 6.248E+01 - |





"Early" collapse because of "noisy" general buckling modal imperfection shape (Fig. 63)

PA = 1.00; TIME= 4.78437E-03 seconds; Wimp = +1.0 inch.

Θ x 24.00

y

Θ y -22.00

x

Θ z 30.00

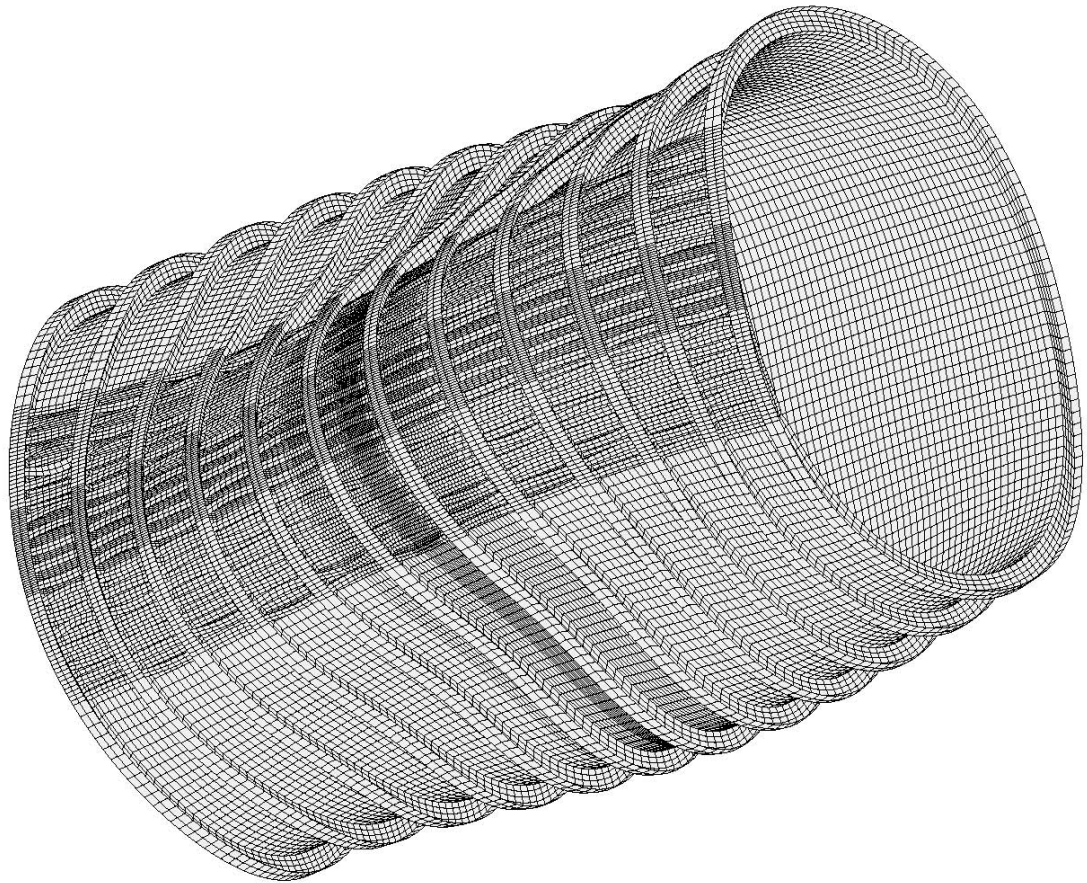
z

STAGS 360-degree compound model with use of 410 elements.

FIG. 65 Deformed shell after STAGS transient run at load factor, PA = 1.00 (time step 120)

| 6.245E+01 |

x
y
z



testax3: Linear buckling with ILIN = 1. This mode is used as an initial imperfection shape.

mode 34, pcr=1.4275; Model created as described in Item 643 of [17]

Θ_x 24.00

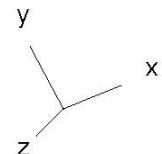
Θ_y -22.00

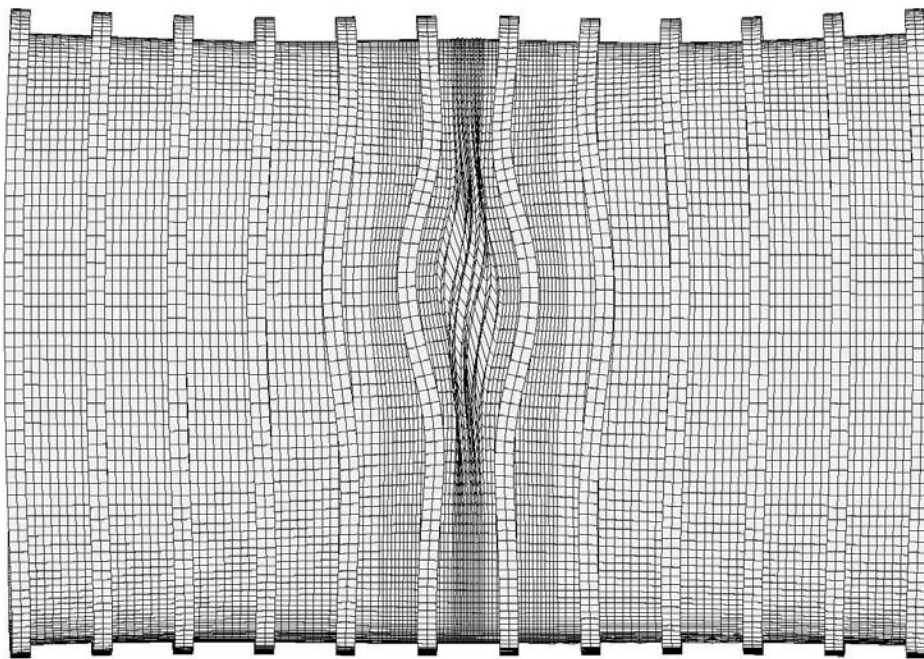
Θ_z 30.00

General buckling mode with 3 circumferential waves. Table 14 design.

FIG. 66 STAGS compound model with mesh density variation in both x and y directions.

6.247E+01





testax3: Nonlinear buckling with ILIN=0; Spurious mode in most dense region between Rings 6 and 7
mode 39, pcr=1.0205; Ring rolling with spurious inter-ring buckling.

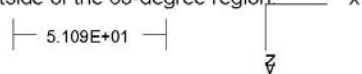
Θ_x 140.00

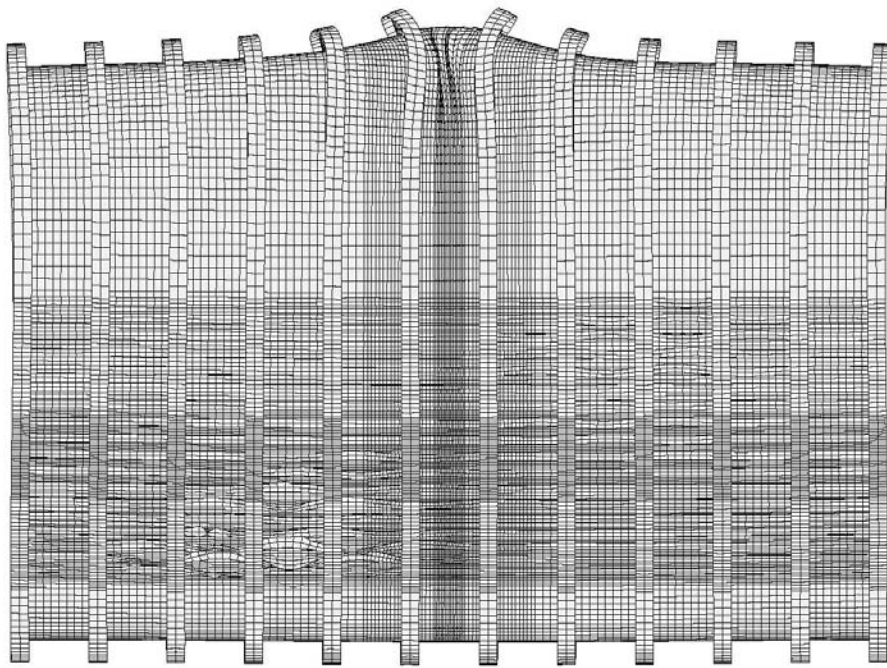
Θ_y 0.00

Θ_z -0.00

Nonlinear buckling, Run 2, Step 23; Table 14 design.

FIG. 67 STAGS compound model. Buckling occurs at inward lobe, outside of the 60-degree region





testax3: Nonlinear buckling with ILIN = 0. Same spurious mode as that shown in previous figure.

mode 39, pcr=1.0205; Ring rolling with interring buckling.

Θ_x 50.00

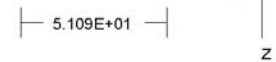
y

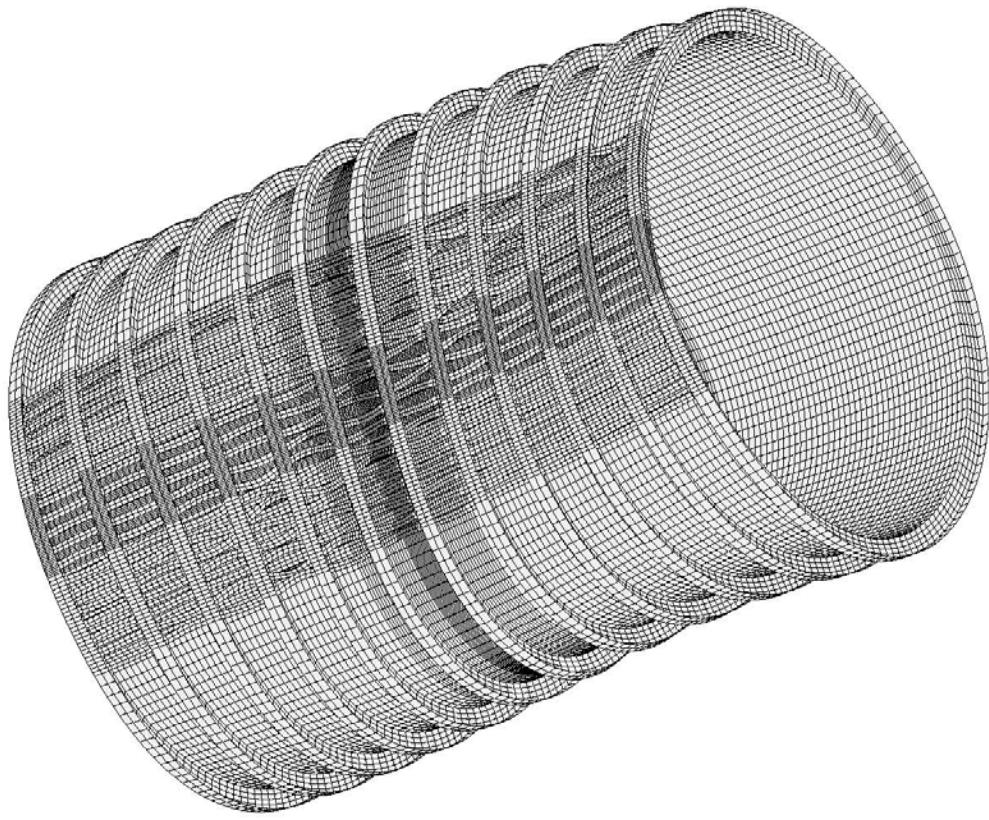
Θ_y 0.00

Θ_z -0.00

Nonlinear buckling, Step 23, Run 2; Table 14 design.

FIG. 68 STAGS compound model. Same nonlinear buckling mode as that shown in previous figure.





"Early" collapse because of "noisy" general buckling modal imperfection shape (Fig. 66)

PA=1.018; TIME= 2.38750E-03 seconds; Wimp = -1.0 inch.

Θ_x 24.00

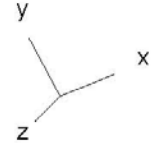
Θ_y -22.00

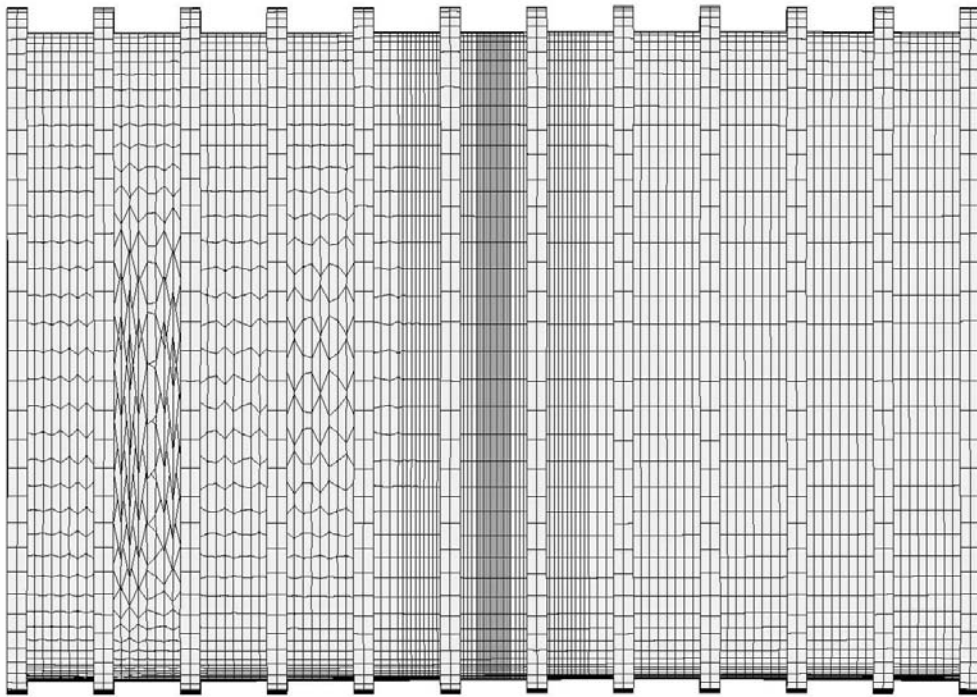
Θ_z 30.00

STAGS 360-degree compound model with use of 410 elements.

FIG. 69 Deformed shell after STAGS transient run at load factor, PA = 1.018 (time step 50)

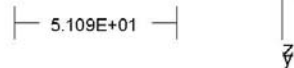
| - 6.248E+01 - |

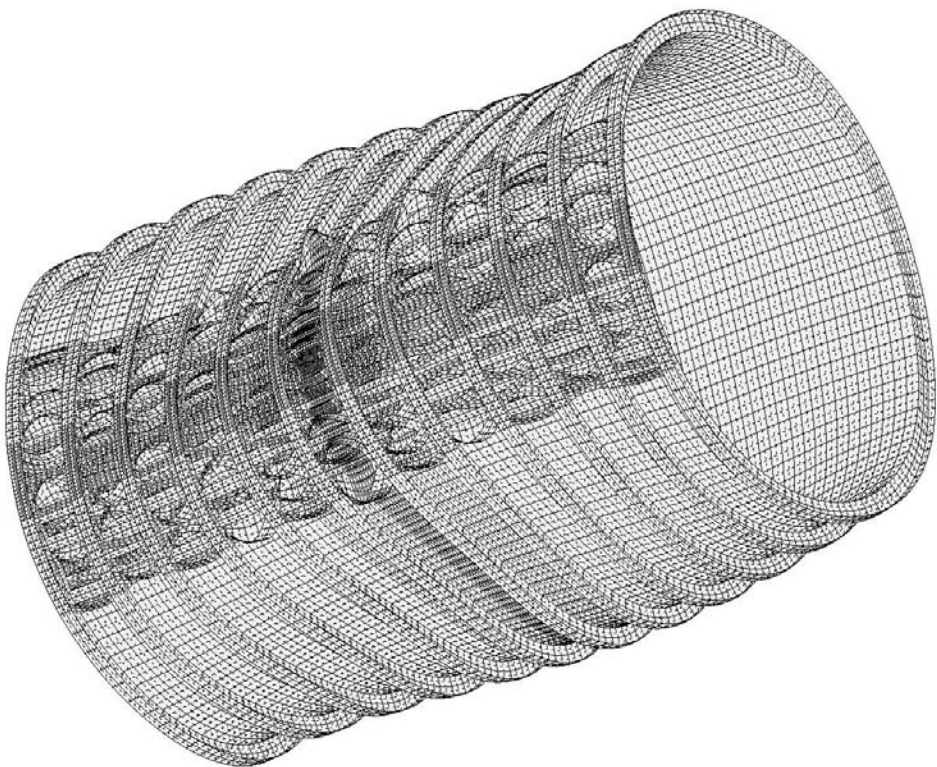




testax3: Nonlinear bifurcation buckling with ILIN = 0. This buckling mode is spurious.
mode 597, pcr = 0.71653E+00; Design listed in Table 14
Spurious nonlinear bifurcation buckling at load step 30.

FIG. 70 STAGS compound model showing "hourglass" buckling in 410 elements with smeared stringers. x





testax3: Linear buckling with ILIN = 1. This is a very "noisy" general buckling mode shape.
mode 30, pcr=1.442; The 480 finite element is used.
A "noisy" general buckling mode with 3 circumferential waves.
FIG. 71 STAGS compound model with mesh density variation in both x and y directions.

